NUREG/CR-6731

Scaling Analysis for the OSU APEX-CE Integral System Test Facility

U.S. Nuclear Regulatory Commission
Office of Nuclear Regulatory Research
Washington, DC 20555-0001

AVAILABILITY OF REFERENCE MATERIALS IN NRC PUBLICATIONS

NRC Reference Material

As of November 1999, you may electronically access NUREG-series publications and other NRC records at NRC's Public Electronic Reading Room at http://www.nrc.gov/reading-rm.html.

Publicly released records include, to name a few, NUREG-series publications; *Federal Register* notices; applicant, licensee, and vendor documents and correspondence; NRC correspondence and internal memoranda; bulletins and information notices; inspection and investigative reports; licensee event reports; and Commission papers and their attachments.

NRC publications in the NUREG series, NRC regulations, and Title 10, Energy, in the *Code of Federal Regulations* may also be purchased from one of these two sources:

1. The Superintendent of Documents
   U.S. Government Printing Office
   Mail Stop SSOP
   Washington, DC 20402–0001
   Internet: bookstore.gpo.gov
   Telephone: 202-512-1800
   Fax: 202-512-2250
2. The National Technical Information Service
   Springfield, VA 22161–0002
   www.ntis.gov
   1–800–553–6847 or, locally, 703–605–6000

A single copy of each NRC draft report for comment is available free, to the extent of supply, upon written request as follows:

Address: Office of the Chief Information Officer
Reproduction and Distribution
Services Section
U.S. Nuclear Regulatory Commission
Washington, DC 20555-0001
Email: DISTRIBUTION@nrc.gov
Facsimile: 301–415–2289

Some publications in the NUREG series that are posted at NRC's Web site address http://www.nrc.gov/reading-rm/doc-collections/nuregs are updated periodically and may differ from the last printed version. Although references to material found on a Web site bear the date the material was accessed, the material available on the date cited may subsequently be removed from the site.

Non-NRC Reference Material

Documents available from public and special technical libraries include all open literature items, such as books, journal articles, and transactions, *Federal Register* notices, Federal and State legislation, and Congressional reports. Such documents as theses, dissertations, foreign reports and translations, and non-NRC conference proceedings may be purchased from their sponsoring organization.

Copies of industry codes and standards used in a substantive manner in the NRC regulatory process are maintained at—

The NRC Technical Library
Two White Flint North
11545 Rockville Pike
Rockville, MD 20852–2738

These standards are available in the library for reference use by the public. Codes and standards are usually copyrighted and may be purchased from the originating organization or, if they are American National Standards, from—

American National Standards Institute
11 West 42nd Street
New York, NY 10036–8002
www.ansi.org
212–642–4900

Legally binding regulatory requirements are stated only in laws; NRC regulations; licenses, including technical specifications; or orders, not in NUREG-series publications. The views expressed in contractor-prepared publications in this series are not necessarily those of the NRC.

The NUREG series comprises (1) technical and administrative reports and books prepared by the staff (NUREG–XXXX) or agency contractors (NUREG/CR–XXXX), (2) proceedings of conferences (NUREG/CP–XXXX), (3) reports resulting from international agreements (NUREG/IA–XXXX), (4) brochures (NUREG/BR–XXXX), and (5) compilations of legal decisions and orders of the Commission and Atomic and Safety Licensing Boards and of Directors' decisions under Section 2.206 of NRC's regulations (NUREG–0750).

NUREG/CR-6731

Scaling Analysis for the OSU APEX-CE Integral System Test Facility

Manuscript Completed: October 2001
Date Published:

Prepared by:
J.N. Reyes, Jr.

Department of Nuclear Engineering
Oregon State University
116 Radiation Center
Corvallis, OR 97331-5902

David Bessette and Gene Rhee, NRC Project Managers

Prepared for:
Division of Systems Analysis and Regulatory Effectiveness
Office of Nuclear Regulatory Research
U.S. Nuclear Regulatory Commission
Washington, DC 20555-0001

ABSTRACT

This report presents the results of the scaling analysis performed for the Oregon State University (OSU) Advanced Plant Experiment (APEX) for a typical Combustion Engineering (CE) geometry. This research program was sponsored by the U.S. Nuclear Regulatory Commission's (NRC) through Contract NRC-04-99-040. The focus of the OSU PTS research program is to obtain integral system and separate effects test data in support of NRC's effort to assess the Pressurized Thermal Shock (PTS) rule (10 CFR 50.61) and Regulatory Guide 1.154. The primary use of the OSU data will be to assess the predictive capability of current thermal hydraulic systems analysis codes and CFD codes. The purpose of this report is to describe the scaling basis for the APEX-CE test facility. The CE nuclear plant considered in this study is the Palisades Nuclear Plant. The thermal hydraulic phenomena of interest includes, the onset of loop stagnation, the degree of thermal stratification in the cold legs, and mixing and heat transfer in the downcomer during primary and secondary side transients. This scaling anaysis has been used to guide the modifications to the existing APEX facililty.

FOREWORD

The reactor pressure vessel is exposed to neutron radiation during normal operation. Over time, the vessel steel becomes progressively more brittle in the region adjacent to the core. If a vessel had a preexisting flaw of critical size *and* certain severe system transients occurred, this flaw could propagate rapidly through the vessel, resulting in a through-wall crack. The severe transients of concern, known as pressurized thermal shock (PTS), are characterized by rapid cooling (i.e., thermal shock) of the internal reactor pressure vessel surface that may be combined with repressurization. The simultaneous occurrence of critical-size flaws, embrittled vessel, and a severe PTS transient is a very low probability event. The current study shows that U.S. pressurized-water reactors do not approach the levels of embrittlement to make them susceptible to PTS failure, even during extended operation well beyond the original 40-year design life.

Advancements in our understanding and knowledge of materials behavior, our ability to realistically model plant systems and operational characteristics, and our ability to better evaluate PTS transients to estimate loads on vessel walls have shown that earlier analyses, performed some 20 years ago as part of the development of the PTS rule, were overly conservative, based on the tools available at the time. Consistent with the NRC's Strategic Plan to use best-estimate analyses combined with uncertainty assessments to resolve safety-related issues, the NRC's Office of Nuclear Regulatory Research undertook a project in 1999 to develop a technical basis to support a risk-informed revision of the existing PTS Rule, set forth in Title 10, Section 50.61, of the *Code of Federal Regulations* (10 CFR 50.61).

Two central features of the current research approach were a focus on the use of realistic input values and models and an *explicit* treatment of uncertainties (using currently available uncertainty analysis tools and techniques). This approach improved significantly upon that employed in the past to establish the existing 10 CFR 50.61 embrittlement limits. The previous approach included unquantified conservatisms in many aspects of the analysis, and uncertainties were treated *implicitly* by incorporating them into the models.

This report is one of a series of 21 reports that provide the technical basis that the staff will consider in a potential revision of 10 CFR 50.61. The risk from PTS was determined from the integrated results of the Fifth Version of the Reactor Excursion and Leak Analysis Program (RELAP5) thermal-hydraulic analyses, fracture mechanics analyses, and probabilistic risk assessment. This report presents the geometric similarities between the Oregon State University Advanced Plant Experiment – Combustion Engineering test facility and the Palisades nuclear power plant. In addition, this report uses the hierarchical two-tiered scaling (H2TS) method to perform top-down and bottom-up scaling analyses for important processes. The results of the scaling analyses are used to interpret test results.

Brian W. Sheron, Director
Office of Nuclear Regulatory Research
U.S. Nuclear Regulatory Commission

TABLE OF CONTENTS

1.0 Introduction 1-1

2.0 Scaling Analysis Methodology 2-1
2.1 Geometric Similarity 2.3
2.2 Experiment Objectives 2-3
2.3 PTS Phenomena Identification and Ranking Table (PIRT) 2-4
2.4 Hierarchical Two-Tiered Scaling (H2TS) Analysis Method 2-6
2.4.1 Time Ratios 2-10

3.0 Geometric Similarity 3-1
3.1 Description of the Palisades Nuclear Plant 3-1
3.2 Description of the APEX-CE Test Facility 3-3
3.2.1 Primary Coolant System 3-4
3.2.2 Safety Systems 3-6
3.2.3 Break Measurement System (BAMS) 3-7
3.2.4 APEX-CE Testing Capabilities 3-8
3.3 Physical Dimensions and Geometric Scaling Ratios 3-8
3.4 Conclusions 3-8

4.0 Primary Loop Natural Circulation 4-1
4.1 Primary Loop Single-Phase Natural Circulation 4-1
4.1.1 Top-Down Scaling Analysis for Single-Phase Primary Loop Natural Circulation 4-2
4.1.2 Bottom-Up Natural Circulation Scaling Analysis 4-10
4.1.2.1 Primary Loop Resistance 4-10
4.1.2.2 Core Decay Power 4-11
4.1.2.3 Single-Phase Loop Flow Stagnation 4-12
4.1.3 Comparison of APEX-CE and Palisades Single-Phase Natural Circulation Flow Rates 4-13
4.2 Primary Loop Two-Phase Natural Circulation 4-14
4.2.1 Top-Down Scaling Analysis for Two-Phase Primary Loop Natural Circulation 4-15
4.2.1.1 Primary Loop Similarity Criteria 4-18
4.2.2 Bottom-Up Scaling of Two-Phase Natural Circulation Processes 4-24
4.2.2.1 Scaling Two-Phase Friction and Loss Coefficients 4-24
4.2.2.2 Scaling Two Phase Flow Pattern Transitions 4-25
4.2.2.3 Two-Phase Loop Stagnation 4-28
4.3 Summary 4-35

5.0 Scaling of Cold Leg and Downcomer Fluid Mixing Phenomena 5-1
5.1 Top-Down Scaling Analysis for Thermal Fluid Mixing 5-2
5.1.1 Diabatic Mixing (Heterogeneous Approximation) 5-3
5.1.2 Dimensionless Equations for Downcomer Mixing 5-6
5.2 Bottom-Up Scaling Analysis for Thermal Fluid Mixing 5-8
5.2.1 HPSI Flow Rate 5-9
5.2.2 Bottom-Up Scaling Analysis for the Onset of Backflow at the HPSI Nozzle . 5-10
5.2.3 The Onset of Cold Leg Thermal Stratification 5-12
5.2.3.1 Hydraulic Jump Leading to Perfect Mixing 5-13
5.2.4 HPSI Plume Entrainment and Temperature Decay 5-23
5.2.4.1 Top-Entry HPSI Plumes (Axisymmetric Forced Plumes 5-23

5.2.4.2 Side-Entry HPSI Plumes 5-35
5.2.4.3 Injection Flow Turbulence 5-35
5.2.5 Downcomer Plume Mixing (Planar Plumes) 5-37
5.2.5.1 Plume Velocity and Plume Residence Time 5-44
5.2.5.2 Assessment of Planar Plume Similarity Criteria 5-45
5.2.6 Downcomer Wall Heat Transfer 5-46
5.2.6.1 Plume Convection Heat Transfer Coefficient 5-49
5.2.6.2 Assessment of Downcomer Heat Transfer Similarity 5-50
5.2.6.3 Summary of Downcomer Heat Transfer 5-50
5.2.7 REMIX Calculations 5-51

6.0 Reactor Coolant System Depressurization Scaling Analysis 6-1
6.1 Governing Equations for RCS Two-Phase Fluid Depressurization 6-3
6.2 Top-Down Reactor Coolant System Depressurization Scaling Analysis 6-6
6.2.1 Similarity of Pressure Trajectories in Dimensionless Phase Space 6-9
6.3 Bottom-Up Scaling Depressurization Scaling Analysis 6-10
6.3.1 Self-Similarity of Fluid Properties in Phase Equilibria (P_{sat} Scaling) 6-10
6.3.2 Equations of State for Saturated Pressure and Temperature (T_{sat} Scaling) . 6-14
6.3.3 Dilation Property Group for Saturated Liquid-Vapor Blowdowns 6-17
6.4 RCS depressurization and Inventory Scaling Criteria 6-25
6.4.1 Saturated Vapor Breaks 6-25
6.4.2 Saturated Liquid Breaks 6-26
6.4.3 Numerical Values of the Scaling Ratios and Initial Conditions 6-27
6.5 Summary and Conclusions 6-29

7.0 Steam Generator Depressurization/RCS Cooldown Scaling Analysis 7-1
7.1 Governing Equations for Steam Generator Blowdown and RCS Cooldown 7-2
7.2 Top-Down MSLB Scaling Analysis 7-3
7.3 Bottom-Up MSLB Scaling Analysis 7-5
7.3.1 SG Fluid Properties 7-8
7.3.2 Steam Generator Critical Flow Model 7-9
7.4 Scaling Criteria 7-10
7.4.1 Numerical Values of the Scaling Ratios and Initial Conditions 7-10
7.5 Summary and Conclusions 7-15

8.0 Summary and Conclusions 7-1
8.1 Geometric Similarity 8-1
8.2 Scaling Basis for Important Thermal Hydraulic Phenomena 8-2
8.2.1 Single-Phase Fluid Natural Circulation 8-2
8.2.2 Two-Phase Fluid Natural Circulation 8-3
8.2.3 Cold Leg and Downcomer Thermal Fluid Mixing and Wall Heat Transfer . . . 8-3
8.2.4 RCS Depressurization and Cooldown Scaling Analysis 8-4
8.2.5 SG Depressurization/RCS Cooldown Scaling Analysis 8-8
8.3 Assessment of Scaling Analysis Results Relative to the PTS PIRT Tables 8-8

9.0 References 8-11

TABLES

Table 2.1 Preliminary Ranking of PTS Phenomena for a Small Hot Leg Break Transient in the Palisades Plant 2-5
Table 2.2 Preliminary Ranking of PTS Phenomena for a Main Steam Line Break Transient in the Palisades Plant 2-6

Table 3.1 Comparison of Palisades and APEX Components 3-9
Table 3.2 Comparison of Palisades and APEX Safety Injection Systems 3-11
Table 3.3 Comparison of Palisades and APEX Primary Loop Volumes 3-11
Table 3.4 Comparison of Palisades and APEX Primary Loop Lengths 3-12
Table 3.5 Comparison of Palisades and APEX Primary Loop Flow Areas 3-12
Table 3.6 Summary of Palisades and APEX Scale Ratios 3-12

Table 4.1 Π_F for Palisades and APEX-CE Loop Components 4-10
Table 4.2 Data used to Assess Onset of Loop Stagnation in Palisades and APEX-CE 4-33

Table 5.1 Conditions for Remix Comparisons 5-51

Table 6.1 Scaling Ratios for APEX-CE SBLOCAs 6-28
Table 6.2 Time Constants and Π Groups for APEX-CE SBLOCAs 6-28
Table 6.3 Numerical Values for APEX-CE SBLOCA Initial Conditions 6-29

Table 7.1. Scaling Ratios For APEX-CE Hot Zero Power MSLBs 7-12
Table 7.2 Time Constants and Π Groups for Hot Zero Power MSLBs 7-12
Table 7.3 Numerical Values for Initial Conditions for the Hot Zero Power MSLBs 7-14
Table 7.4 Scaling Ratios for APEX-CE Full Power MSLBs 7-14
Table 7.5 Time Constants and Π Groups for Full Power MSLBs 7-15
Table 7.6 Numerical Values for Initial Conditions for the Full Power MSLBs 7-15

Table 8.1 Summary of the APEX to Palisades Scale Ratios 8-2
Table 8.2 Method Used to Preserve Isochronicity in APEX-CE (*Fluid Property Similitude*) 8-3
Table 8.3 APEX-CE Scaling Analysis for PTS SBLOCA Phenomena 8-10
Table 8.4 APEX-CE Scaling Assessment for PTS MSLB Phenomena 8-11

FIGURES

Figure 1.1 OSU PTS Research Flow Chart 1-3

Figure 2.1 General Scaling Methodology for the APEX-CE Test Facility 2-2
Figure 2.2 Flow Diagram for the Hierarchical, Two-Tiered Scaling Analysis (NUREG/CR5809). 2-8
Figure 2.3 CE 2x4 Reactor Coolant System Breakdown and Hierarchy (Process) 2-9

Figure 3.1 Schematic of the Palisades 2x4 NSSS (Top View) 3-2
Figure 3.2 Schematic of the Palisades NSSS (Side View) 3-2
Figure 3.3 Illustration of the APEX-CE Test Facility 3-4
Figure 3.4 Schematic of the APEX-CE 2x4 Loop (Top View) 3-5
Figure 3.5 Schematic of the APEX-CE Loop (Side View) 3-6

Figure 4.1 Natural Circulation Mode - Palisades Nuclear Plant Trip from 91% Power . . 4-2
Figure 4.2 Scaling Analysis Flow Diagram for Single-Phase Natural Circulation 4-3
Figure 4.3 Hot and Cold Regions of Single-Phase Natural Circulation Flow within a PWR 4-4
Figure 4.4 Decay Power Profile for the Palisades Nuclear Plant Based on ANSI/ANS-5.1.24, 1979 with G-Factor 4-11
Figure 4.5 Comparison of Decay Power Equation for the APEX-CE Test Facility and ½76 of the Palisades Decay Power 4-12
Figure 4.6 Comparison of APEX-CE to Identify Scaled Palisades Test Loop 4-13
Figure 4.7 Scaling Analysis Flow Diagram for Two-Phase Natural Circulation 4-14
Figure 4.8 Regions of Single-Phase and Two-Phase Natural Circulation within a PWR 4-15
Figure 4.9 Semiscale Stepped-Inventory Reduction Test Data Showing Onset of Loop Stagnation 4-29
Figure 4.10 Comparison of APEX-CE and Palisades Void Fraction Profiles for 3% Decay Power 4-34

Figure 5.1. Scaling Analysis Flow Diagram for Cold Leg and Downcomer Thermal Fluid Mixing 5-1
Figure 5.2. Control Volume for Top-Down Scaling Analysis Balance Equations 5-2
Figure 5.3 Comparison of the Heterogeneous Mixture Time Constant to CREARE 1/2-Scale Data 5-7
Figure 5.4 Comparison of Equation (5.17) to CREARE 1/2-Scale Data 5-8
Figure 5.5 HPSI Flow Rates as a Function of Normalized Pressure for Palisades 5-9
Figure 5.6 HPSI Flow Rates as a Function of Normalized Pressure for APEX-CE 5-10
Figure 5.7 Buoyant Backflow into the Horizontal HPSI Line 5-11
Figure 5.8 Comparison of Fr_{HPI} for Palisades and APEX-CE 5-12
Figure 5.9 Hydraulic Jump Leading to Perfect Mixing 5-14
Figure 5.10 Comparison of Thermal Stratification Criteria with CREARE ½ Scale Mixing Data 5-19
Figure 5.11 Assessment of Cold Leg Thermal Stratification During Forced Flow Conditions for Palisades HPSI 5-19
Figure 5.12 Comparison of the Onset of Cold Leg Thermal Stratification During Natural Circulation Conditions in Palisades and APEX-CE (2.5% Decay Power) . . . 5-21

Figure 5.13 Comparison of the Onset of Cold Leg Thermal Stratification During Natural Circulation Conditions in Palisades and APEX-CE (1.0% Decay Power) . . . 5-22
Figure 5.14 Comparison of the Onset of Cold Leg Thermal Stratification During Natural Circulation Conditions in Palisades and APEX-CE (0.5% Decay Power) . . . 5-22
Figure 5.15 Thermally Stratified Conditions for the Top-Entry HPSI 5-23
Figure 5.16 Velocity Distributions Measured in a Planar Jet (1934)[36] 5-25
Figure 5.17 Velocity Distributions in a Planar Jet Plotted in Dimensionless Coordinates[32] and Compared to a Gaussian Profile (1934) 5-26
Figure 5.18 Gaussian Profiles in Forced Plumes 5-27
Figure 5.19 Comparison of Entrainment Correlation to Data of Davis, et. al. (1978)[36] . . 5-33
Figure 5.20 Thermally Stratified Conditions for the Side-Entry Palisades HPSI 5-35
Figure 5.21 Comparison of APEX-CE and Palisades HPSI Reynolds Numbers 5-37
Figure 5.22 Downcomer Plume Interactions as Observed in IVO 2/5 Scale Transparent Test Loop (IVO Mixing Test #115) 5-38
Figure 5.23 Schematic of a Single Planar Plume in the RPV Downcomer 5-39
Figure 5.24 Comparisons of Kotsovinos Equation to CREARE 1/2-Scale Data 5-45
Figure 5.25 Schematic of Geometry for Downcomer Wall Heat Transfer 5-47
Figure 5.26 Comparison of Dittus-Boelter Correlation to CREARE ½-Scale Convective Heat Transfer Data 5-50
Figure 5.27 Plot of Dimensionless Plume Temperatures as a Function of Downcomer Axial Location and Dimensionless Time (Case 1 at Cold Leg Centerline) 5-52
Figure 5.28 Plot of Dimensionless Plume Temperatures as a Function of Downcomer Axial Location and Dimensionless Time (Case 1 at 3 Cold Leg Diameters) 5-52
Figure 5.29 Plot of Dimensionless Plume Temperatures as a Function of Downcomer Axial Location and Dimensionless Time (Case 1 at 6 Cold Leg Diameters) 5-53
Figure 5.30 Plot of Dimensionless Plume Temperatures as a Function of Downcomer Axial Location and Dimensionless Time (Case 1 at 6 Cold Leg Diameters) 5-53
Figure 5.31 Plot of Dimensionless Plume Temperatures as a Function of Downcomer Axial Location and Dimensionless Time (Case 2 at Cold Leg Centerline) 5-54
Figure 5.32 Plot of Dimensionless Plume Temperatures as a Function of Downcomer Axial Location and Dimensionless Time (Case 2 at 3 Cold Leg Diameter) 5-54

Figure 6.1 Flow Chart of the Primary Side Depressurization Scaling Analysis 6-2
Figure 6.2 RCS Control Volume for SBLOCA Analysis 6-3
Figure 6.3 Scaling Relationship Between Palisades and APEX-CE Saturation Pressure 6-10
Figure 6.4 Power Law for Pv_{fg}/h_{fg} as a Function of Pressure 6-12
Figure 6.5 Power Law for s_f as a Function of Pressure 6-12
Figure 6.6 Power Law for v_g as a Function of Pressure 6-13
Figure 6.7 Power Law for v_{fg} as a Function of Pressure 6-13
Figure 6.8 Comparison of Equation (6.42) to Steam Tables 6-15
Figure 6.9 Scaling Relationship Between Palisades and APEX-CE Saturation Temperature 6-17
Figure 6.10 Plot of Dimensionless Mixture Specific Energy as a Function of Dimensionless Pressure 6-20
Figure 6.11 Critical Mass Flux for Saturated Liquid Breaks as Predicted by the Henry-Fauske Model (x_{Brk} = 0.03) 6-24

Figure 7.1 Flow Chart of the Secondary Side Depressurization Scaling Analysis 7-1
Figure 7.2 Steam Generator and RCS Control Volumes Used for MSLB Scaling 7-2

EXECUTIVE SUMMARY

The purpose of the PTS research being conducted at OSU is to sue the APEX-CE test facility to obtain integral system and separate effects test data for transients of potential PTS concern. This data will be used to assess the existing thermal hydraulic computer codes and any new CFD codes that might be implemented in an improved PTS thermal hydraulic analysis methodology that results from NRC's re-evaluation of the PTS rule, (10 CFR 50.61), and its supporting guidance (RG 1.154).

Three thermal hydraulic phenomena are of specific interest to the OSU experimental effort:

- The onset of loop stagnation
- The onset of thermal stratification in the cold legs, and
- Thermal fluid mixing in the downcomer

These three phenomena have been examined for various primary and secondary side transients in the APEX-CE facility. The three phenomena identified above are a subset of the important phenomena identified by the PTS Phenomena Identification and Ranking Table.

The purpose of this scaling analysis report is to establish the areas of similarity between the APEX-CE test facility and the Palisades Nuclear Plant which has been chosen as the prototype for this investigation. The results of this scaling analysis have been used to guide modifications to the existing APEX test facility and to establish the operating conditions for the OSU PTS testing.

Specifically, this scaling analysis was performed to:

1. To identify the characteristic geometric scale ratios for the APEX-CE Test Facility and to establish the geometric similarity between APEX-CE and the Palisades Nuclear Plant.

2. To develop the scaling basis for assuring that the following PTS thermal hydraulic phenomena could be adequately simulated in APEX-CE for various primary and secondary side transients.

    - The onset of loop stagnation
    - The onset of thermal stratification in the cold legs, and
    - Thermal fluid mixing in the downcomer

3. To identify which of the phenomena listed in the PTS Phenomena Identification and Ranking Table (PIRT) would be adequately simulated in APEX-CE.

The results of this scaling analysis have been used to modify the existing APEX facility to produce the APEX-CE configuration and operating conditions.

ACKNOWLEDGEMENTS

The Oregon State University (OSU) Department of Nuclear Engineering is grateful to the U.S. Nuclear Regulatory Commission (USNRC) for funding this research through Contract 04-99-040. The APEX-CE research team is especially appreciative of David Bessette, Gene Rhee, and Sarah Colpo of the U.S. NRC for their guidance on this project. OSU acknowledges the excellent cooperation and technical information support provided by Gary Jarka, Gary Pratt, John Kneeland and George Sleeper of Consumers Energy, Palisades Nuclear Plant. We also extend our thanks to Claud Pugh and Richard Bass of the Oak Ridge National Laboratory for their suggestions on the instrumentation layout.

NOMENCLATURE

a_c	cross-sectional flow area of core = na_{sc}
a_i	cross-sectional flow area of ith component
a_{sc}	cross-sectional flow area of the heated subchannel
A_s	total rod heat transfer surface area in core = nA_{sc}
A_{sc}	surface area of a single fuel rod = $\pi d\ell$
A_x	total rod solid structure cross-sectional area in core = nA_{xc}
A_{xc}	cross-sectional area of a single rod = πR^2
b	wall thickness
<Bi>	average Biot number
$C_{p\ell}$	liquid specific heat at constant pressure
$C_{v\ell}$	liquid specific heat at constant volume
C_{vs}	solid specific heat
d	fuel rod diameter
d_h	hydraulic diameter of the heated subchannel ($d_h = 4a_{sc}/\xi$)
D	pipe diameter
f	Darcy friction factor
F	thermal coupling factor for the heated slab and fluid
g	gravitational acceleration
<h>	average heat transfer coefficient
$h_{\ell g}$	is the latent heat of vaporization
h_f	is the fluid mixture enthalpy
h_p	plume heat transfer coefficient
H	average convective heat transfer coefficient over the heated length
I	normalized mass inventory (M/Mo)
j_k	superficial velocity of phase "k"
k_s	solid thermal conductivity
K	loss coefficient for the heated subchannel
ℓ	length of the heated subchannel
L_{th}	distance between heat source and heat sink thermal centers
M	Mass inventory
n	number of rods or subchannels
q_s	core heat generation rate
Q_ℓ	volumetric flow rate
R	fuel rod radius
T	temperature
$<T_s>$	volume averaged fuel rod temperature
T_w	heater rod/fuel surface temperature
T_w-T_ℓ	average rod surface to liquid temperature difference
u	velocity
U	overall heat transfer coefficient
v_{gj}	is the drift flux velocity, which is related to the relative velocity between the gas and liquid as $v_{gj} = (1-\alpha)(u_g-u_\ell)$.
V	volume
V_ℓ	liquid control volume

GREEK SYMBOLS

α	vapor volume fraction
$(1-\alpha)$	liquid volume fraction
α_E	entrainment constant
α_s	thermal diffusivity
β_T	coefficient of volume expansion
δ	conduction depth ($\delta = A_{xc}/\xi$)
ξ	wetted perimeter of the heated subchannel
ρ_ℓ	liquid density
$\Delta\rho$	density difference $\Delta\rho = (\rho_{\ell s} - \rho_{gs})$
ρ_{gs}	saturated vapor density
$\rho_{\ell s}$	saturated liquid density
ρ_f	two-phase fluid mixture density
ΔT	axial fluid temperature difference across the length of the core
Π	characteristic time ratio or dimensionless group
τ	residence time constant
γ	ratio of specific heat
$\langle\varphi\rangle$	volume averaged parameter = $\frac{1}{V}\int \varphi dv$

1.0 INTRODUCTION

The purpose of the U.S. Nuclear Regulatory Commission (USNRC) Pressurized Thermal Shock (PTS) research conducted at Oregon State University (OSU) was to obtain integral system and separate effects test data for transients of potential PTS significance using the Advanced Plant Experiment-Combustion Engineering (APEX-CE) Test Facility. This data can be used to assess the existing thermal hydraulic computer codes and any new CFD codes that might be implemented in an improved PTS thermal hydraulic analysis methodology. The purpose of this report is to provide the results of the NRC PTS thermal hydraulic research performed at OSU.

The thermal hydraulic phenomena of specific interest to the OSU experimental effort are the onset of loop stagnation, the onset of thermal stratification in the cold legs, and thermal fluid mixing and heat transfer in the downcomer. These phenomena have been examined for Main Steam Line Break (MSLB) and Small Break Loss-of-Coolant-Accident (SBLOCA) transients in the APEX-CE facility. The three phenomena identified above are a subset of the important phenomena identified by the PTS Phenomena Identification and Ranking Table (PIRT) presented in the Scaling Analysis for the OSU APEX-CE Integral System Test Facility.[1]

Figure 1.1 is a flow chart for the OSU PTS Research Program and serves as a outline to this report. As illustrated on the chart, the first step in the research program was a review of past PTS thermal hydraulic research. This review, presented in Chapter 2, was used to identify new areas of research that would be beneficial to the NRC's PTS Rule re-evaluation project. The second step was to perform a detailed scaling analysis that was used to design the modifications to the existing APEX facility. A PTS Scaling Analysis report has been issued separately.[1] The modifications made to the APEX facility to produce the APEX-CE configuration are described in Chapter 3.

A series of separate effects tests were performed to investigate the local mixing behavior in the APEX-CE cold legs and downcomer. This included a parametric study of cold leg stratification at natural circulation flow rates and multi-loop safety injection interactions. Further investigations were deemed necessary to characterize the unique injection geometry of the Palisades Plant. Therefore, flow visualizations tests matching the conditions examined in APEX-CE were performed in a PVC test section. The results of the separate effects testing are presented in Chapter 3.

One of the primary goals of the OSU PTS research was the investigation of MSLB and SBLOCA transients that can lead to reactor vessel overcooling. Integral system overcooling tests had never been performed to investigate cold leg and downcomer cooling phenomena. In particular, the onset of loop stagnation is an integral system effect that could only be characterized in this manner. The Emergency Operating Procedures (EOPs) for the Palisades nuclear plant were used to more realistically model the key operator and automatic system responses during a MSLB or SBLOCA transient. An overview of the Palisades plant operations is provided in Chapter 4 and results of the integral system and separate effects testing are presented in Chapter 5.

The integral system behaviors of the APEX-CE overcooling transients have also been analyzed using the RELAP5 systems code. Comparisons of the code's calculations to the APEX-CE MSLB and SBLOCA measured data and the ability to predict the onset of loop stagnation has been assessed for these transients and are presented in Chapter 6.

The separate effects test data has also been compared to calculations done in STAR-CD, a computational fluid dynamics code (CFD) and REMIX, a control volume fluid mixing code. These

results are presented in Chapter 7. Of particular interest to these analyses is the ability of CFD codes to predict the behavior associated with multi-loop plume interactions.

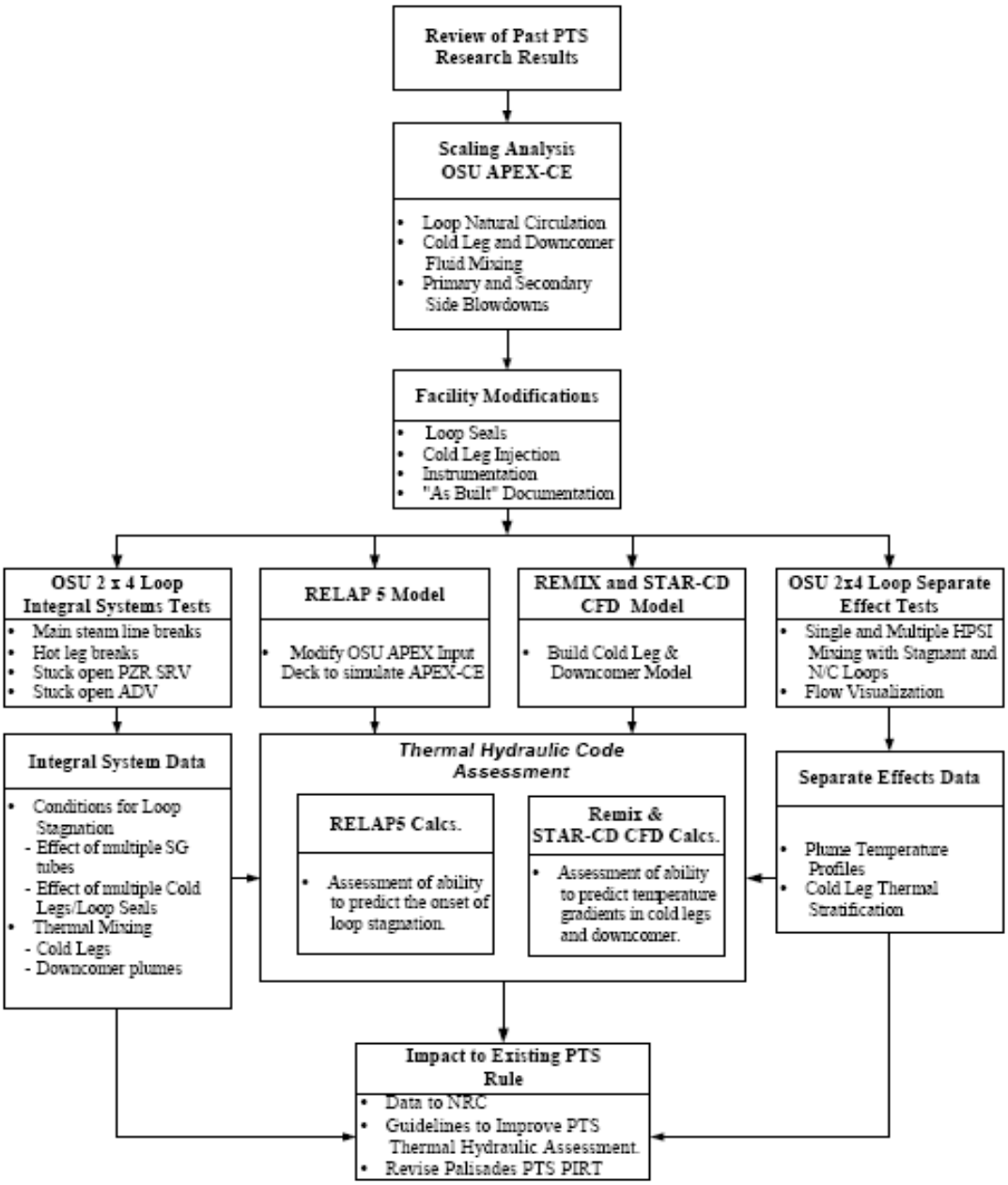

Figure 1.1 OSU PTS Research Flow Chart

2.0 SCALING ANALYSIS METHODOLOGY

This scaling analysis had the following objectives:

1. To identify the characteristic geometric scale ratios for the APEX-CE Test Facility and to establish the geometric similarity between APEX-CE and the Palisades Nuclear Plant.

2. To develop the scaling basis for assuring that the following thermal hydraulic phenomena could be adequately simulated in APEX-CE for various primary and secondary side transients:
   - The onset of loop stagnation
   - The onset of thermal stratification in the cold legs, and
   - Thermal fluid mixing in the cold legs and downcomer

3. To identify which of the phenomena listed in the PTS Phenomena Identification and Ranking Table (PIRT) would be adequately simulated in APEX-CE.

The results of this scaling analysis have been used to guide the modifications to the existing OSU-APEX Test Facility to produce the new APEX-CE facility.

To properly model PTS transient behavior in the APEX-CE Test Facility, the following specific objectives were met for each mode of the CE 2x4 operation of interest:

- The similarity groups which should be preserved between the APEX-CE Test Facility and the full-scale prototype were obtained,
- The priorities for preserving the similarity groups were established,
- The important processes were identified and addressed,
- The specifications for the APEX facility modifications were provided, and
- The biases due to scaling distortions were identified.

Different sets of similarity criteria were obtained for the different modes of operation. The similarity criteria depend on the geometry of the components, the scaling level required to address the transport phenomena of interest, and the initial and boundary conditions for each particular mode of operation.

To meet the scaling objectives in an organized and clearly traceable manner, a general scaling methodology (GSM) for the OSU APEX-CE Test Facility was developed. The model for this scaling methodology was partly drawn from the USNRC's Severe Accident Scaling Methodology (SASM) presented in NUREG/CR-5809.3 A flow diagram describing the GSM is presented in Figure 2-1. The following sections present a description of each of the tasks listed in the GSM.

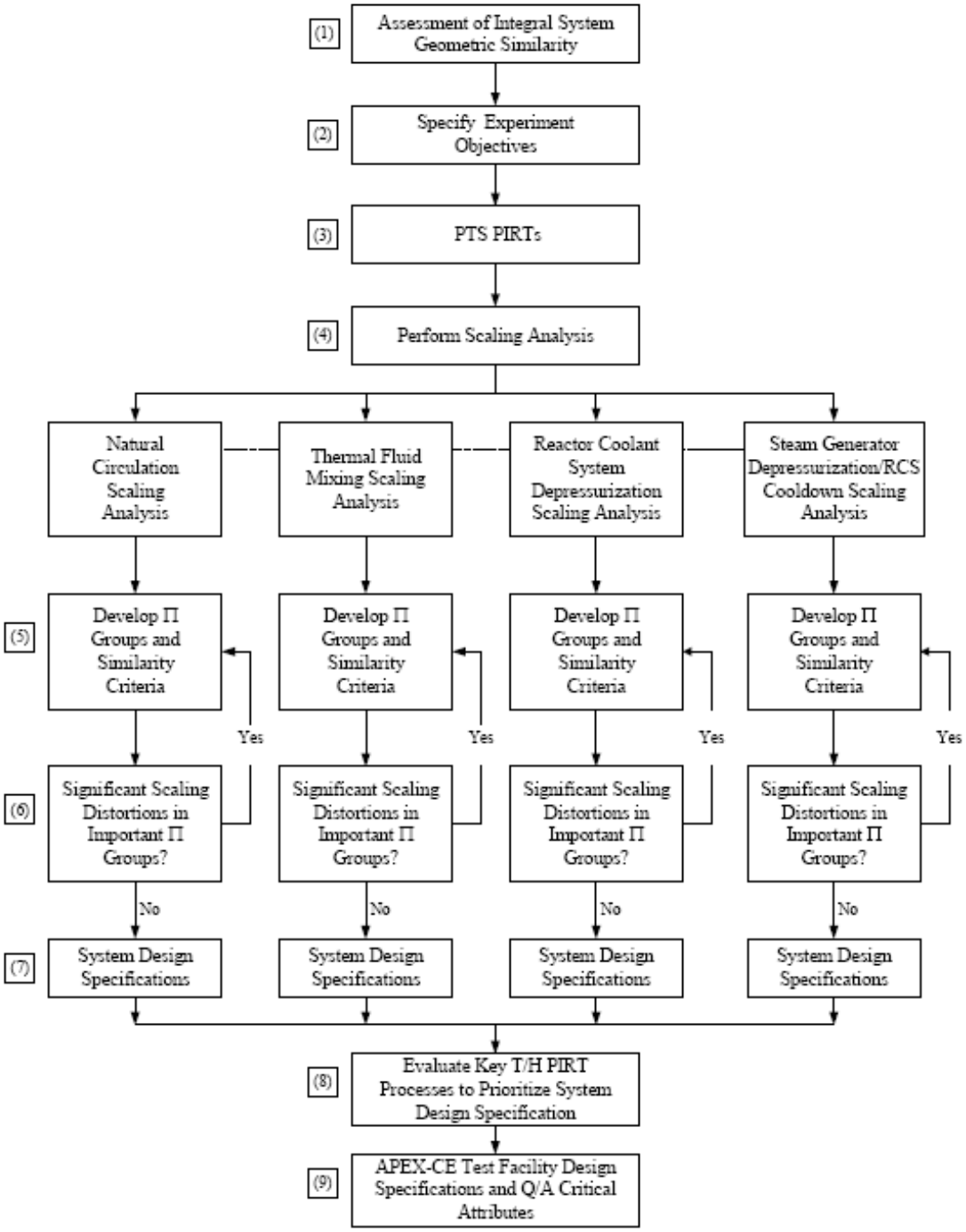

Figure 2.1 General Scaling Methodology for the APEX-CE Test Facility

2.1 Geometric Similarity

When working with an existing test facility, it is important to establish that the integral loop geometry for the test facility is similar to the prototype being investigated. It has been determined that the APEX-CE facility is geometrically similar to the Palisades nuclear plant because:

1. There is a one to one correspondence of primary loop components; arranged in the same sequence.

2. A comparison of the ratios of component lengths, diameters, elevations, flow areas and volumes, revealed that the geometric scale factors for each of the components were essentially constant throughout the loop.

Chapter 3 presents the detailed results of the assessment of geometric similarity.

2.2 Experiment Objectives

The experimental objectives define the types of tests that will be performed to respond to specific licensing, design, and data needs. These objectives determine the general modes of operation that should be simulated in the APEX-CE facility.

The objective of the test program is to characterize the onset of loop stagnation, the onset of thermal stratification in the cold legs, thermal fluid mixing in the downcomer and other important PTS PIRT phenomena during various primary side and secondary side transients.

The Integral System Tests to be performed include:

- *Hot Leg Breaks*. Using cold leg injection, a spectrum of hot leg breaks (i.e., break energy approximately equal to decay power) will be performed. The conditions leading to primary loop stagnation and the detailed temperature measurements and cooldown rates in the downcomer will be obtained.

- *Main Steam Line Breaks*. A series of Main Steam Line Breaks (MSLBs) shall be performed to identify the conditions leading to primary loop stagnation. This will include asymmetric MSL breaks to determine if stagnation in two of four loops would occur. The conditions leading to primary loop stagnation and the detailed temperature measurements and cooldown rates in the downcomer will be obtained.The Separate Effects Tests to be performed include:

- Thermal Fluid Mixing. A series of steady-state High Pressure Safety Injection tests will be performed to study thermal stratification in the cold legs and plume development and interaction in the downcomer.

Based on the Integral System Test requirements, the following modes of CE 2x4 plant operation must be simulated in the APEX-CE facility:

- Closed System Natural Circulation (single-phase and two-phase)
- Open System Depressurization
- Thermal Fluid Mixing during High Pressure Safety Injection

Each mode of operation required a separate scaling analysis as shown in the GSM.

2.3 PTS Phenomena Identification and Ranking Table (PIRT)

The next task outlined by the GSM is the development of a PTS Phenomena Identification and Ranking Table (PIRT). The nature of scaling forbids exact similitude between all thermal hydraulic processes in the CE 2x4 and the reduced scale APEX-CE test facility. As a result, the design modifications and operation of the test facility have been based on simulating the processes most important to PTS. The function of the PIRT was to identify the key thermal hydraulic phenomena that should be scaled in the context of PTS transients.

PTS PIRTs have been developed for the H.B. Robinson Unit 2 Plant[4] and the Yankee Rowe Plant[5]. The objective of the PIRTs was to identify and rank all of the thermal hydraulic phenomena of importance to PTS that could arise during the course of a small break Loss-of-Cooling-Accident (SBLOCA) or a Main Steam Line Break (MSLB). The Yankee Rowe PTS Plant also examined Steam Generator Tube Ruptures (SGTR). The Robinson PTS PIRT committee consisted of seven thermal hydraulic experts convened to determine which phenomena most affects the fluid temperature in the downcomer, the coolant cooldown rate in the downcomer, the fluid to vessel wall heat transfer coefficient and the system pressure. The temperature gradients at the beltline welds of the core region were of particular interest.

For purposes of this scaling analysis, the H.B. Robinson and Yankee Rowe results were consulted to develop SBLOCA and MSLB PTS phenomena PIRTs for the Palisades plant. The Palisades SBLOCA PTS PIRT is presented in Table 2.1 and the MSLB PTS PIRT is presented in Table 2.2.

Note that essentially the same phenomena appear in both Tables; however in different order. The scaling analyses presented herein were aimed at determining if these phenomena could be simulated in APEX-CE. The section of the report which addresses each specific phenomena has been identified in the PIRT Tables.

Table 2.1 Preliminary Ranking of PTS Phenomena for a Small Hot Leg Break Transient in the Palisades Plant

Rank	PTS Related Phenomena	Report Section
1	High Pressure Safety Injection (HPSI) Flow Rate	5
2	Reactor Vessel Wall Heat Conduction	5
3	Flow Distribution in Downcomer	5
4	HPSI Water Source Temperature	5
5	Break Flow Rate	6
6	HPSI Mixing in Cold Leg and Downcomer	5
7	Decay Heat	5
8	Surface Heat Transfer Coefficient on Reactor Vessel Wall	5
9	Loop Flow Upstream of Safety Injection Connection	5
10	Loop Temperature Upstream of Safety Injection Connection	5
11	Downcomer to Core Inlet Bypass	3
12	Downcomer to Upper Plenum Bypass	3
13	Upper Head Heat Transfer Coefficient under Voided Conditions	6
14	Liquid/Steam Interface in the Upper Part of the Downcomer	6
15	Feedwater Temperature	6
16	Feedwater Control	6
17	Steam Generator Energy Exchange	6
18	Timing of Manual RCP trips	6
19	Loop Flow Resistance	4

Table 2.2 Preliminary Ranking of PTS Phenomena for a Main Steam Line Break Transient in the Palisades Plant

Rank	PTS Related Phenomena	Report Section
1	Timing of manual RCP trips	7
2	Feedwater Temperature	7
3	Feedwater Control	7
4	Steam Generator Energy Exchange	7
5	Steam Generator Pressure Control	7
6	Steam Line Break Flow Rate (or Break Size)	7
7	Decay Heat	5
8	High Pressure Safety Injection (HPSI) Flow Rate	5
9	HPSI Water Source Temperature	5
10	Surface Heat Transfer Coefficient on Reactor Vessel Wall	5
11	Loop Flow Resistance	4
12	Reactor Vessel Wall Heat Conduction	5
13	Upper Head Heat Transfer Coefficient under Voided Conditions	6
14	HPSI Mixing in the Cold Legs and Downcomer	5
15	Downcomer Upper Plenum Bypass	3
16	Flow Distribution in Downcomer	5
17	HPSI Buoyant Backflow Mixing	5
18	Fluid Mixing in Downcomer	5

2.4 Hierarchical Two-Tiered Scaling (H2TS) Analysis Method

The third step in the GSM was to perform a scaling analysis for each of the modes of operation specified by the experimental objectives and further defined by the PTS PIRT. The Hierarchical Two-Tiered Scaling (H2TS) method was used to develop the similarity criteria necessary to scale the CE 2x4 systems and processes of importance to a hot leg break PTS transient. The H2TS method was developed by the USNRC and is fully described in Appendix D of NUREG/CR-5809[3]. This is the same method that was used to develop the similarity criteria for the original APEX facility.

Figure 2.2 is taken from NUREG/CR-5809. It presents the four basic elements of the H2TS analysis method. The first element consists of subdividing the plant into a hierarchy of systems. Each system was subdivided into interacting subsystems which were further subdivided into

interacting modules which were further subdivided into interacting constituents (materials) which were further subdivided into interacting phases (liquid, vapor or solid). Each phase could be characterized by one or more geometrical configurations and each geometrical configuration could be described by three field equations (mass, energy and momentum conservation equations). Each field equation could be characterized by several processes.

After identifying and subdividing the system of interest, the next step was to identify the scaling level at which the similarity criteria should be developed. This was determined by examining the phenomena being considered. For example, if the phenomenon being considered involved mass, momentum or energy transport between materials such as water and solid particles, then the scaling analysis was performed at the constituent level. If the phenomenon of interest involved mass, momentum or energy transport between vapor and liquid, then the scaling analysis was performed at the phase level. Therefore identifying the scaling level depended on the phenomenon being addressed.

Figure 2.3 presents the hierarchical levels for the Reactor Coolant System. This figure served as a "road map" to the scaling analyses presented in the following chapters. It identifies the hierarchical level at which each scaling analysis was performed, (i.e., the control volume), the geometrical configuration of interest, the balance equations implemented in the analyses, and the processes that were scaled.

Thermal hydraulic phenomena involving integral reactor coolant system interactions, such as primary system depressurization or loop natural circulation, were examined at the "system" level. Thermal hydraulic phenomena, such as steam generator heat transfer, were examined at the "subsystem" level. Specific interactions between the steam-liquid mixture and the stainless steel structure were examined at the "constituent" level.

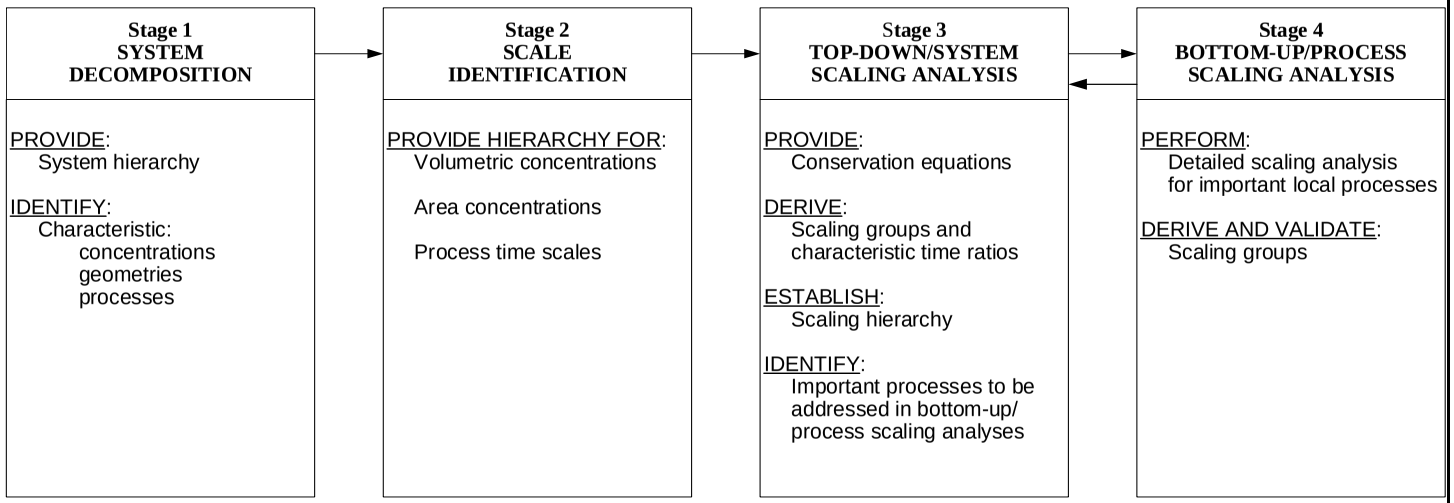

Figure 2.2 Flow Diagram for the Hierarchical, Two-Tiered Scaling Analysis (NUREG/CR5809).

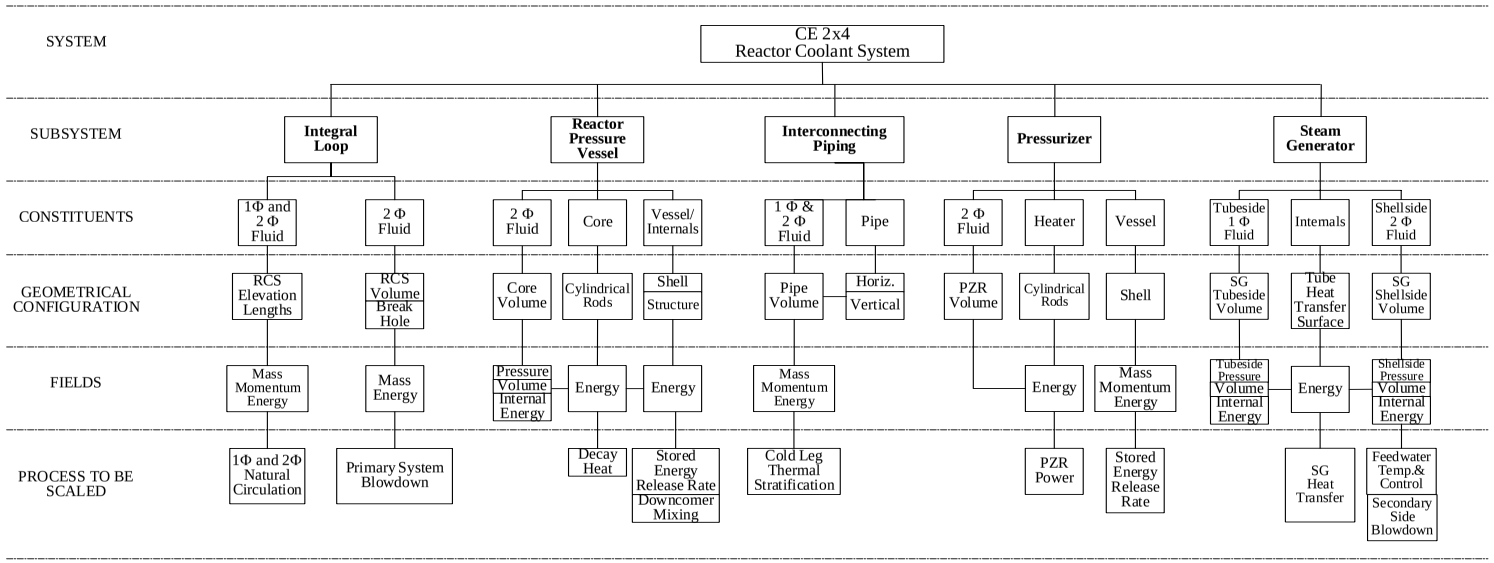

Figure 2.3 CE 2x4 Reactor Coolant System Breakdown and Hierarchy (Process)

Chapters 4 through 7 present the scaling analyses that were performed for the different modes of operation. Each chapter identifies the thermal hydraulic phenomena of interest, the system level (i.e., control volume) at which the analysis was performed, the geometrical configuration, the applicable balance equations and the processes important to the thermal hydraulic phenomena of interest.

The third element of the H2TS method required performing a "Top-Down" (system) scaling analysis. The top-down scaling analysis examined the synergistic effects on the system caused by complex interactions between the constituents which are deemed important by the PIRT. Its purpose was to use the conservation equations at a given scaling level to obtain characteristic time ratios and similarity criteria. It also identified the important processes to be addressed in the bottom-up scaling analysis.

The fourth element of the H2TS method required performing a "Bottom-Up" (process) scaling analysis. This analysis developed similarity criteria for specific processes such as flow pattern transitions and flow dependent heat transfer. The focus of the bottom-up scaling analysis was to develop similarity criteria to scale individual processes of importance to system behavior as identified by the PIRT.

2.4.1 Time Ratios

The basic objective of the H2TS method was to develop sets of characteristic time ratios for the transfer processes of interest. This was done by writing the control volume balance equations for each constituent "k" as follows:

$$\frac{dV_k\psi_k}{dt} = \Delta\left[Q_k\psi_k\right] \pm \Sigma\left(j_{kn}A_{kn}\right) + S_k \qquad \textbf{(2.1)}$$

where

$$\Delta\left[Q_k\psi_k\right] = \left[Q_k\psi_k\right]_{in} - \left[Q_k\psi_k\right]_{out} \qquad \textbf{(2.2)}$$

In equation (2.1) the ψ_k term represents the conserved property; $\psi_k = \rho$, ρu or $\rho\epsilon$ (mass, momentum or energy per unit volume), V_k is the control volume, Q_k is the volumetric flow rate, j_{kn} is the flux of property ψ_k transferred from constituent "k" to "n" across the transfer area A_{kn}. Hence, $\Delta[Q_k\psi_k]$ represents the usual mass, momentum, or energy convection terms, and $\Sigma j_{kn}A_{kn}$ represents transport process terms such as condensation and S_k represents the distributed sources, such as decay power or body forces acting internal to the control volume.

Equation (2.1) can be put in dimensionless form by specifying the following dimensionless groups in terms of the constant initial and boundary conditions:

$$V_k^+ = \frac{V_k}{V_{k,0}}\ ,\ \psi_k^+ = \frac{\psi_k}{\psi_{k,0}}\ ,\ Q_k^+ = \frac{Q_k}{Q_{k,0}}\ ,\ j_{kn}^+ = \frac{j_{kn}}{j_{kn,0}}\ ,\ A_{kn}^+ = \frac{A_{kn}}{A_{kn,0}}\ ,\ S_k^+ = \frac{S_k}{S_{k,0}} \qquad \textbf{(2.3)}$$

Substituting these groups into equation (3.1) yields:

$$V_{k,0}\psi_{k,0}\frac{dV_k^+\psi_k^+}{dt} = Q_{k,0}\psi_{k,0}\Delta\left[Q_k^+\psi_k^+\right] \pm \Sigma\left(j_{kn,0}A_{kn,0}\right)j_{kn}^+A_{kn}^+ + S_{k,0}S_k^+ \qquad \textbf{(2.4)}$$

Dividing both sides of this equation by $Q_{k,0}\ \psi_{k,0}$ yields:

$$\tau_k\frac{dV_k^+\psi_k^+}{dt} = \Delta\left[Q_k^+\psi_k^+\right] \pm \Sigma\Pi_{kn}j_{kn}^+A_{kn}^+ + \Pi_{sk}S_k^+ \qquad \textbf{(2.5)}$$

where the <u>residence time</u> of constituent "k" is

$$\tau_k = \frac{V_{k,0}}{Q_{k,0}} \qquad \textbf{(2.6)}$$

and the <u>characteristic time ratio</u> for a transfer process between constituents "k" and "n" is given by:

$$\Pi_{kn} = \frac{j_{kn,0}A_{kn,0}}{Q_{k,0}\psi_{k,0}} \qquad \textbf{(2.7)}$$

The characteristic time ratio for the distributed source term within the control volume is given by:

$$\Pi_{sk} = \frac{S_{k,0}}{Q_{k,0}\psi_{k,0}} \qquad \textbf{(2.8)}$$

Because each transfer process has a characteristic time ratio, it is possible to rank the importance of each process by comparing the time ratios. If a specific transfer process is to have the same effect in the prototype and the model, then the characteristic time ratios must be preserved.

Let us define M[$(P_{i,j})$, $(P_{i+1,j})$,...$(P_{Ni,Nj})$] as the set of time ratios that characterize all of the individual processes that occur during the evolution of a transient. The subscripts I, j, N_i,N_j identify the specific process, the hierarchical level, the total number of specific processes and the total number of hierarchical levels respectively.

$$M_p \neq M_m \qquad \textbf{(2.9)}$$

Because of differences in geometrical scale and fluid properties, it is impossible to exactly duplicate the "time ratio set" for the full-scale prototype, M_p, in a reduced scale model. That is, exact similitude for all processes cannot be preserved; therefore:

The subscript, p, refers to the full-scale prototype and the subscript, m, refers to the reduced scale model.

It is possible to design a reduced scale test facility that preserves the similitude of a subset of time ratios T [$\Pi_{i,j}$], that characterize the processes of greatest importance to the transient. This optimizes the model design to investigate the important processes while distorting the less important processes.

To determine which processes govern the overall evolution of a transient, numerical estimates of the characteristic time ratios for the prototype and the model must be obtained for each hierarchical level of interest. Physically, each characteristic time ratio, Π_i, is composed of a specific frequency, ω_i, which is an attribute of the specific process, and the residence time constant, τ_{cv}, for the control volume. That is:

$$\Pi_i = \omega_i \tau_{cv} \tag{2.10}$$

The specific frequency defines the mass, momentum or energy transfer rate for a particular process. The residence time defines the total time available for the transfer process to occur within the control volume. A numerical value of:

$$\Pi_i \ll 1 \tag{2.11}$$

means that only a small amount of the conserved property would be transferred in the limited time available for the specific process to evolve. As a result, the specific process would not be important to the overall transient. Numerical values of:

$$\Pi_i \gtrsim 1 \tag{2.12}$$

means that the specific process evolves at a high enough rate to permit significant amounts of the conserved property to be transferred during the time period, τ_{cv}. Such processes would be important to the overall transient behavior.

The fourth step in the GSM was to use the scaling analysis results to develop a set of characteristic time ratios (dimensionless Π groups) and similarity criteria for each mode of operation. Because it is impossible to identically satisfy all of the similarity criteria simultaneously, the set only includes those criteria which must be satisfied in order to scale the most important phenomena identified by the PIRT.

$$T\left\{\Pi_i\right\}_m = T\left\{\Pi_i\right\}_p \tag{2.13}$$

Scaling criteria were developed by requiring that the characteristic time ratios for a subset of specific processes in the prototype (usually those of greatest importance) are matched in the model at each hierarchical level. That is,
These criteria were satisfied by adjusting the physical geometry, fluid properties and operating conditions of the model; thus optimizing the model design for the specific process of interest.

Step five of the GSM was an evaluation of the scaling criteria to determine if the scale model geometry, boundary conditions or operating conditions would introduce significant scaling distortions. Distortions were also evaluated relative to other modes of operation.

The effect of a distortion in the model for a specific process can be quantified as follows:

$$DF = \frac{\left[\Pi_i\right]_p - \left[\Pi_i\right]_m}{\left[\Pi_i\right]_p} \tag{2.14}$$

The distortion factor, DF, physically represents the fractional difference in the amount of conserved property transferred through the evolution of a specific process in the prototype to the amount of conserved property transferred through the same process in the model during their respective residence times. A distortion factor of zero would indicate that the model ideally simulates the specific process. A distortion factor of +0.05 would indicate that the specific process in the model transfers 5 percent less of the conserved property (on a scaled basis) than the same process in the prototype. The distortion factor can also be written as:

$$DF = 1 - \left[\omega_i\right]_R \left[\tau_{cv}\right]_R \tag{2.15}$$

or

$$DF = 1 - \left[\Pi_i\right]_R \tag{2.16}$$

The degree to which a specific transfer process could impact a particular transient can be determined by comparing the *maximum* characteristic time ratio for each of the transfer processes that arise during the transient. The reader is encouraged to examine the details of the H2TS analysis method presented in NUREG/CR-5809[3].

Upon satisfying the important scaling criteria, step six of the GSM provided the specific component geometries and operating conditions for each mode of operation in the APEX-CE test facility. Step seven was an evaluation of the key thermal hydraulic PIRT processes to prioritize the system design specifications. Step eight served to integrate all of the design requirements for the OSU APEX-CE test facility.

The remaining chapters of this report present the scaling results obtained by executing the general scaling methodology.

3.0 GEOMETRIC SIMILARITY

Geometric similarity is the minimum requirement for adequately simulating the PTS thermal hydraulic processes of interest to the Palisades Nuclear Plant. The draining and refilling of loop seals, the interruption of natural circulation in the primary loops, the driving head for natural circulation, and fluid mixing in the cold legs and downcomer all depend on preserving geometric similarity in APEX-CE. This chapter presents a brief description of the Palisades Nuclear Plant and the APEX-CE test facility. It also includes the key physical dimensions for both systems and their scale ratios.

3.1 Description of the Palisades Nuclear Plant

The Palisades Nuclear plant, located near Covert, Michigan, went into commercial operation on December 31, 1971. It is a Pressurized Water Reactor (PWR) with a Combustion Engineering Nuclear Steam Supply System (NSSS). The core and pumps produce 2530 MW(t) of thermal power and the turbine-generators have an electric power output of 798 MW(e).

Palisades is a basic 2x4 primary loop design as shown in Figure 3.1. That is, a single reactor vessel, housing the nuclear core, feeds water through two hot legs to two steam generators. The cooled water returns to the vessel via four cold legs. The reactor coolant pumps are connected to the steam generators by a loop seal which is designed to prevent pump cavitation. Figure 3.2 shows a side view of the Palisades NSSS with the loop seals.

The Emergency Core Cooling System for the Palisades plant consists of a High Pressure Safety Injection (HPSI) system, a Low Pressure Safety Injection (LPSI) system, a set of four Safety Injection Tanks (SIT) (i.e., also called Accumulators), and a Residual Heat Removal (RHR) system. The HPSI and LPSI systems draw borated water from the Refueling Water Storage Tank (RWST) and inject coolant through the large diameter SIT lines which connect to each of the four cold legs. With regard to fluid mixing in the cold legs, it is important to note that the safety injection nozzles are located on the side of each cold leg.

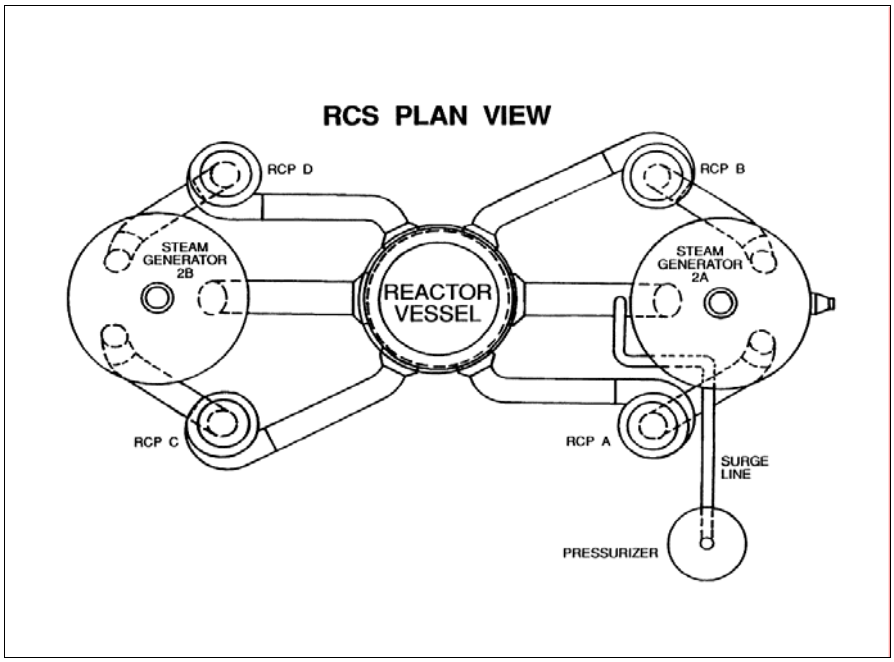

Figure 3.1 Schematic of the Palisades 2x4 NSSS (Top View)

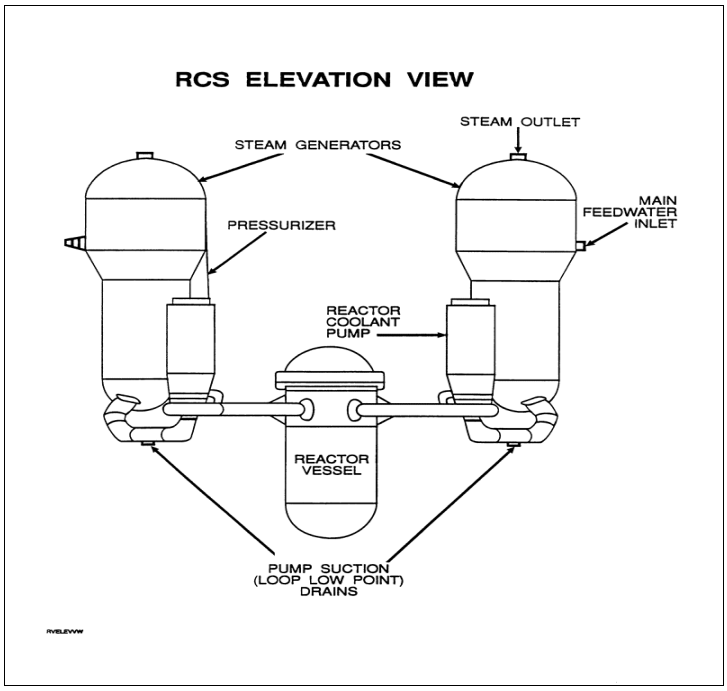

Figure 3.2 Schematic of the Palisades NSSS (Side View)

3.2 Description of the APEX-CE Test Facility

The OSU APEX-CE test facility is roughly a one-fourth height integral system model of the Palisades plant. The facility would be operated at reduced pressure and on a one to one time scale. The design of the original APEX test facility was based on the Westinghouse AP600. A description of the APEX facility and a summary of the non-proprietary results of the OSU AP600 research effort have been documented in NUREG/CR-6641.

Many features of the APEX test facility were geometrically similar to the Palisades NSSS. The basic APEX configuration was a 2x4 loop system with two inverted U-Tube steam generators, four reactor coolant pumps and a pressurizer. Thus it was a straightforward process to modify APEX to simulate the geometry of the Palisades plant. The modified version of the APEX facility has been titled ***APEX-CE***.

The modifications made to APEX to produce the APEX-CE facility include the addition of:

- Four cold leg loop seals
- Four cold leg , horizontally mounted Safety Injection Nozzles
- A HPSI system
- Approximately 50 thermocouples in the downcomer

A schematic of the APEX-CE facility is shown in Figure 3.3. Each cold leg includes a weir wall that limits backflow of HPI fluid towards the loop seals to simulate the backflow and loop draining behavior of the Palisades cold legs.

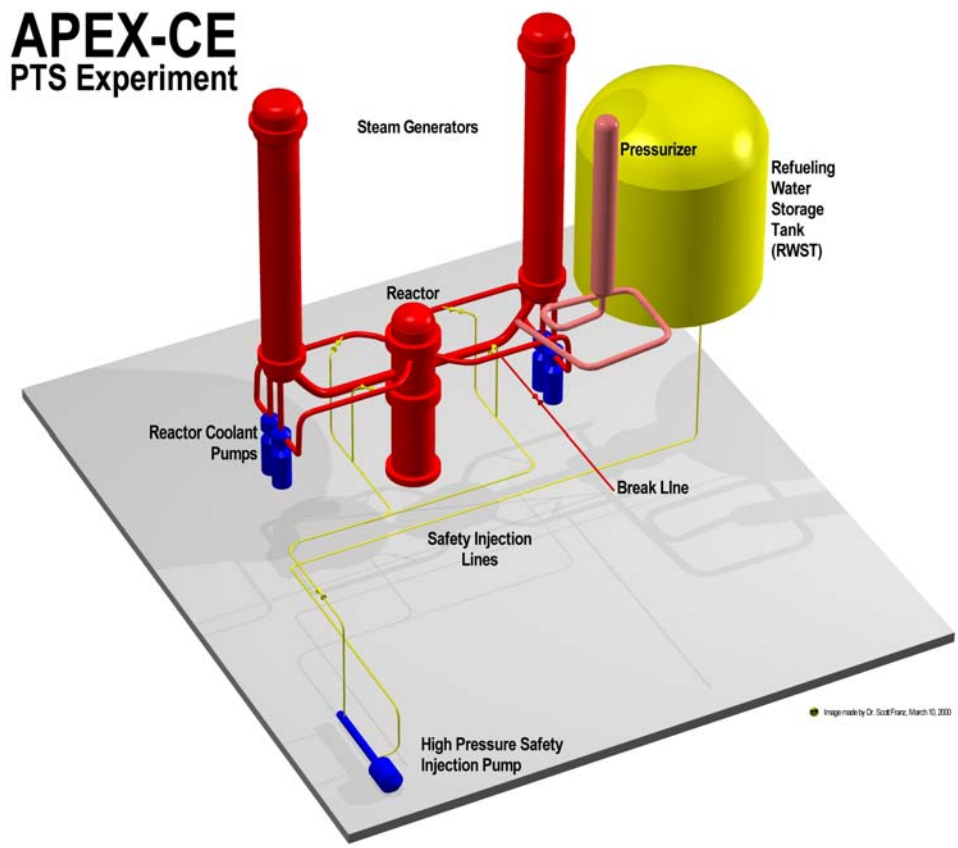

Figure 3.3 Illustration of the APEX-CE Test Facility

3.2.1 Primary Coolant System

All of the primary system components are fabricated of stainless steel and are capable of prolonged operation at 400 psia (2.76 MPa) and saturation conditions. The APEX-CE primary system includes the following components:

- A *Reactor Pressure Vessel* (*RPV)* that models the upper and lower reactor internals, the core barrel, the downcomer, and the core. Connections for the hot and cold legs and DVI lines are provided. The RPV houses 48 electric heater rods each having a 1 inch (2.54 cm) diameter and a heated length of 36 inches (91.44 cm). The maximum core power is 650 kW.

- *Reactor coolant loop piping* that models two primary loops, each consisting of one hot leg and two cold legs. Break spool pieces have been installed on both the hot and cold legs to simulate pipe breaks. The discharge from these valves vent to the Break Measurement System (BAMS) to separate and measure break flow rates.

- Two *Steam Generators (SGs)*, one on each loop, each having 133 U-tubes.
- Four *Reactor Coolant Pumps (RCPs)*, one attached to each cold leg loop seal.
- A *Pressurizer* with internal heaters capable of controlling pressure and minimizing pressure spikes in the RCS.

Figures 3.4 and 3.5 are schematics of the APEX-CE primary loop. Note the geometric similarity to the Palisades plant.

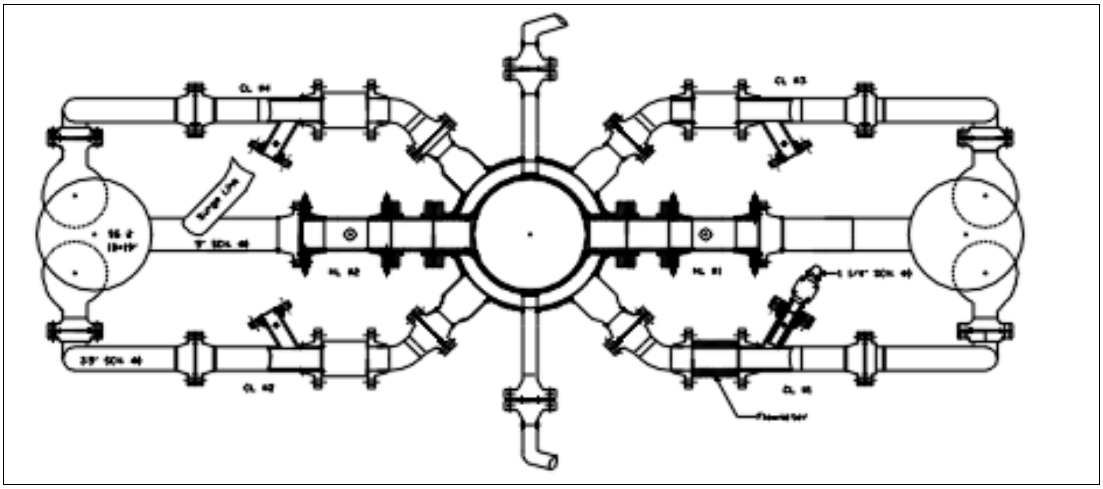

Figure 3.4 Schematic of the APEX-CE 2x4 Loop (Top View)

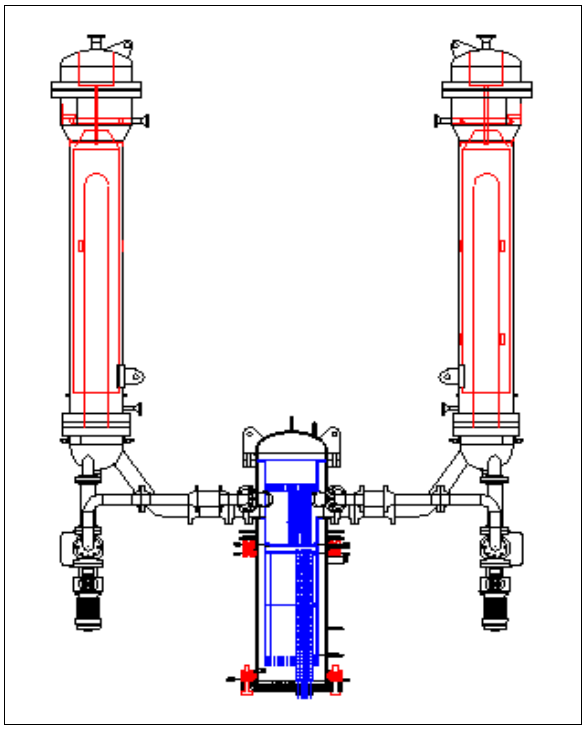

Figure 3.5 Schematic of the APEX-CE Loop (Side View)

3.2.2 Safety Systems

The APEX-CE facility includes the following passive safety systems:

- A *High Pressure Safety Injection (HPSI)* capable of injecting coolant at system pressure into each of the four cold legs.
- A *Refueling Water Storage Tank (RWST)* that connects to the HPSI. The RWST is capable of being pressurized to 80 psia (0.55 MPa) to simulate containment backpressure.

Potential Future Modifications:

- Four *Accumulators* pressurized with nitrogen to provide safety injection during depressurization events.
- A *Low Pressure Safety Injection System (LPSI)* capable of injecting coolant at reduced system pressure into each of the four cold legs.

3.2.3 Break Measurement System (BAMS)

The BAMS is used to measure two-phase flows from breaks. The two-phase flow is directed to a separator where the flow is separated into liquid and vapor. The liquid flow is measured and directed to the Primary Sump. The vapor flow is measured and vented from the test facility. Electrical strip heaters are used to maintain boundary conditions at approximately 212°F (100°C). The system is capable of being pressurized to 80 psia (0.55 MPA) to simulate containment backpressure.

The BAMS contains the following components:

- The *Primary and Secondary Sumps* - These tanks serve as catch tanks for the break flow and are capable of being pressurized to 80 psia (0.55 MPa) to simulate containment backpressure.

- *Four Moisture Separators* - Three small break separators and one large break separator sized based on the maximum flow rates. Separation is primarily accomplished by the use of gravity and a swirl vane moisture separator element. Each separator is provided with a loop seal line on the liquid discharge to ensure vapor flow does not bypass the separator.

APEX-CE includes the following types of instruments:

• *Thermocouples (TF/TFM/TH/TW - 495 total)* are used to measure fluid core heater rod temperatures. Premium grade thermocouples have been used and connected to the DAS through controlled purity thermocouple wire.

• *Magnetic Flowmeters (FMM - 28 total)* are used to measure all single-phase liquid flow rates.

• *Pressure Transducers (PT - 41 total)* are used to measure the static pressures within the tanks and piping.

• *Differential Pressure (DP - 50 total)* transducers are used to measure liquid levels in tanks and piping and to determine pressure drops.

• *Vortex Flowmeters (FVM - 17 total)* are used to measure all steam flow rates.

• *Heated Phase Switches (HPS - 12 total)* are used to determine the fluid phase at various points inside system piping. Each HPS measures: 1) fluid temperature, 2) ΔT between the fluid and the heater, and 3) a relative heat transfer coefficient.

• *Load Cells (LC - 3 total)* are used to measure the weight of liquid inside the RWST, the Primary Sump, and the Secondary Sump.

Ambient air temperature and barometric pressure are also recorded. All of the instruments are monitored and recorded by the DAS. Additionally, a sequence-of-events program is used to monitor the status of pumps and valves.

3.2.4 APEX-CE Testing Capabilities

The following types of tests can be performed in the APEX-CE facility:

- Cold leg breaks (top and bottom)
- Hot leg breaks (top and bottom)
- Main Steam Line Breaks
- Partial loss of Safety Injection signal, and
- Parametric core uncovering.

All testing in the APEX-CE facility meets the applicable sections of ASME NQA-1 as incorporated into the OSU APEX Quality Plan. This includes requirements for instrument calibration, test conduct and records.

3.3 Physical Dimensions and Geometric Scaling Ratios

The physical dimensions and nominal operating conditions for the Palisades plant and the APEX-CE test facility are listed in Table 3.1 and Table 3.2. Tables 3.3 through 3.5 are the ratios for the loop volumes, lengths and flow areas, respectively. A review of the geometric ratios for the reactor coolant system reveals that the primary loop component volume, area, and length scale ratios are not exactly identical from component to component. This is to be expected because the original basis for the test facility design was not the Palisades plant. In general, the volumes of components scale as ½76, the flow areas as 1/73, the diameters as 1/8.5, the horizontal lengths as 1/4 and the elevations as 1/3.5. Assuming “isochronicity,”that is, a one to one time scale, the core power and natural circulation mass flow rates would scale as the volume (i.e., ½76). The method for achieving isochronicity is explained in Chapter 4.

Table 3.6 presents the characteristic geometric scale ratios that will be used in this study. The components which deviated most from these values were the reactor vessel downcomer, which has a volume scale ratio of approximately 1/95. This signifies that the APEX-CE downcomer volume is too large on a scaled basis. The desired volume scale is ½76. Because the downcomer serves as the mixing volume for plumes generated by coolant injection into the cold leg, mixing calculations have been made using the REMIX code to assess the impact of this distortion. These calculations are presented in Chapter 5. Although the volume scale ratio for the downcomer is distorted, the aspect ratio is well modeled having a scale ratio close to unity.

A minor area of concern is the SG/Core thermal center distance which scales as 1/3.2. This means that the APEX-CE facility is somewhat taller than the desired elevation scale ratio of 1/3.67. This is of particular interest because the thermal center elevation is an integral part of the natural circulation driving head term. It is shown in Chapter 4 that this small elevation distortion is easily compensated for by the density difference and loop resistance terms that also comprise the driving head term.

3.4 Conclusions

In conclusion, a comparison of the geometry of the Palisades and APEX-CE geometries indicates that the scale ratios for the piping lengths, volumes, flow areas and elevations are relatively constant around the loop. Thus the minimum scaling requirement of geometric similarity for the test facility has been established. The only significant geometric distortion identified in APEX-CE is the

downcomer fluid volume. Additional analysis is provided in Chapter 5 to assess the impact of this distortion.

Table 3.1 Comparison of Palisades and APEX Components

Components		Palisades	APEX-CE
a.	***RCS Nominal Operating Conditions***		
	Core Power, MWt	2530	0.7
	Pressurizer Pressure, psia	2060	385
	Cold Leg Temperature, F	537.3	420
	Core Mass Flow Rate, lbm/hr	1.41×10^8	538.6
	Total RCS Volume including PZR, ft^3	10900	39.4
b.	***RCS Natural Circulation (2.5% Decay Power)***		
	Decay Power, MWt	63.25	0.23
	Loop Flow Rate, lbm/hr	5.1×10^6	1.85×10^4
	Core DT, F	30	30
	SG/Core Thermal Center Distance, ft	31.39	9.69
c.	***Reactor Vessel***		
	Active Core Flow Area, ft^2	56.72	0.77
	Active Core Length, ft	11.0	3.0
	Reactor Vessel Minimum Wall Thickness, in	8.5	0.5
	Reactor Vessel Nominal Clad Thickness, in	0.25	N/A
	Reactor Vessel ID, in	172	25
	Core Barrel, OD, in	152.75	20
	Downcomer Gap, in	9.625	2.5
	Downcomer Length (Below Cold Leg), in	207.7	60.5
	Downcomer Volume (Below Cold Leg), ft^3	590.1	6.19
	Downcomer Aspect Ratio (Gap/Length)	½1.6	½4.2

†Control Blades Inserted

Table 3.1 Comparison of Palisades and APEX Components (Continued)

Components	Palisades	APEX-CE
d. Interconnecting Piping/Reactor Coolant Pumps		
Hot Leg ID, in	42	5.047
Hot Leg Length, ft	21.4	5.09
Hot Leg Volume, ft^3	209.4	0.707
Crossover Leg ID, in	30	3.54
Crossover Leg Length, ft (Including RCP Length)	28.1	5.29
Crossover Leg Volume, ft^3	123.7	0.350
RCP Volume, ft^3	74.8	0.288
Cold Leg ID, in	30	3.54
Cold Leg Length, ft	19.1	5.81
Cold Leg Volume, ft^3	93.8	0.397
Active Cold Leg/Loop Seal Mixing Volume, ft^3	223.1	0.818
e. Pressurizer		
Internal Volume, ft^3	1500	6.77
HFP Normal Water Volume, ft^3	800	2.9
PZR Power (Proportional & Backup), MWt	1.5	0.013
Pressurizer Surge Line ID, in	12	3.54
f. Steam Generators		
HFP Pressure, psia	770	300
Tube ID, in	0.666	0.607
Tube OD, in	0.75	0.687
Number of Tubes per SG	8219	133
Total Tube Outside Surface Area, ft^2	70,663	414
Total Tube Volume per SG, ft^3 (Above Tubesheet)	870.64	4.62

Table 3.2 Comparison of Palisades and APEX Safety Injection Systems

Components	Palisades	APEX-CE
Safety Injection Nozzle ID, in	11.375	1.33
Safety Injection Tank Internal Volume, ft^3	2011	10.42
Safety Injection Tank Liquid Volume, ft^3	1040	3.77
Safety Injection Actuation Pressure, psia	240	240
Maximum HPSI Flow Rate (14.7 psia), gpm	1459.2	5.29
RWST Minimum Liquid Volume, ft^3	33420.	121.1

Table 3.3 Comparison of Palisades and APEX Primary Loop Volumes

Components	Palisades	APEX-CE	*Ratio
Total RCS Volume including PZR, ft^3	10900	39.4	½76.6
Active Cold Leg/Loop Seal Mixing Volume, ft^3	223.1	0.818	½72.7
Pressurizer Internal Volume, ft^3	1500	6.77	½21.6
Downcomer Volume (Below Cold Leg), ft^3	590.1	6.19	1/95.4
Hot Leg Volume, ft^3	209.4	0.707	½95.5
PZR HFP Normal Water Volume, ft^3	800	2.9	½76
Crossover/Cold Leg/RCP Volume, ft^3	292.3	1.035	½82.4
Safety Injection Tank Internal Volume, ft^3	2011	10.42	1/193
Safety Injection Tank Liquid Volume, ft^3	1040	3.77	½76
RWST Minimum Liquid Volume, ft^3	33420.	121.1	½76

Table 3.4 Comparison of Palisades and APEX Primary Loop Lengths

Components	Palisades	APEX-CE	*Ratio
Hot Leg Length, ft	21.4	5.09	1/4.2
SG/Core Thermal Center Distance, ft	31.39	9.69	1/3.24
Crossover/Cold Leg Length, ft (Including RCP)	47.2	11.1	1/4.3
Active Core Length, ft	11.0	3.0	1/3.67
Downcomer Length (Below Cold Leg), ft	17.31	5.04	1/3.43
Total Loop Transport Length, ft (Uses average SG Tube Length)	176.5	48.27	1/3.66

*APEX-CE to Palisades Ratio

Table 3.5 Comparison of Palisades and APEX Primary Loop Flow Areas

Components	Palisades	APEX-CE	*Ratio
Active Core Flow Area, ft^2 (Control Blades Inserted)	56.72	0.77	1/73.7
Hot Leg Flow Area, ft^2	9.62	0.1389	1/69.3
Cold Leg/Crossover Leg Flow Area, ft^2	4.91	0.0683	1/71.8
Steam Generator Flow Tube Flow Area, ft^2	19.88	0.267	1/74.4

*APEX-CE to Palisades Ratio

Table 3.6 Summary of Palisades and APEX Scale Ratios

Geometric Parameter	APEX-CE to Palisades Scale Ratios
Flow Areas	~1/70
Piping Lengths	~1/4
Volumes	~1/276
Elevations	~1/3.45
Operating Parameters	
Power	½76
Natural Circulation Mass Flow Rates	~1/276
Fluid Velocities	~1/3.66
Total RCS Power/Volume	1/1

4.0 PRIMARY LOOP NATURAL CIRCULATION

This chapter examines the degree of similarity between primary loop natural circulation in APEX-CE and Palisades for single-phase and two-phase fluid flow conditions. The results of this chapter were used to select the core power and loop resistance values in APEX-CE that would best simulate the primary loop natural circulation phenomena in Palisades.

Top-down and bottom-up scaling analyses were performed for both the single-phase and two-phase natural circulation modes. Single-phase natural circulation in the primary loop will be encountered during the Main Steam Line Break (MSLB) transients proposed for APEX-CE. Two-phase natural circulation in the primary loop will be encountered during the Small Break Loss-of-Coolant Accident (SBLOCA) scenarios.

4.1 Primary Loop Single-Phase Natural Circulation

Figure 4.1 depicts data from a manual reactor trip that occurred at the Palisades Nuclear Plant on July 14, 1987.[7] The plant was initially operating at 91 percent power (2302 MW_{th}) with a steady-state core flow rate of 137.1 x 10^6 lbm/hr (62.2 x 10^6 kg/hr). The cold leg and hot leg fluid temperatures differed by 45°F &.22 °C). Subsequent to the reactor trip, the reactor coolant pumps coasted down and the primary loop flow transitioned from forced flow to a single-phase liquid natural circulation mode. Approximately 15 minutes after the reactor trip, the core was at 2.5 percent of normal full power with a single phase natural circulation flow rate of approximately 5.1x10^6 lbm/hr (2.31 x 10^6 kg/hr). The temperature difference across the reactor vessel cold and hot legs settled to approximately 30°F (-1.11 °C). This data provides a valuable benchmark for establishing the steady-state single-phase natural circulation flow rates and core temperature rise in APEX-CE.

The PTS phenomena of interest to the natural circulation mode of operation have been specified in PIRT Table 2.1. Figure 4.2 provides a flow diagram which describes the scaling analysis process for this operational mode.

First, a top-down scaling analysis was performed. This included an analysis at the system level (integrated loop behavior) for transient conditions. The objective of the top-down scaling analysis was to scale the primary loop mass flow rates and to scale the natural circulation steam generator energy exchange rate. Following the top-down scaling analysis, a bottom-up/process scaling analysis was performed to develop similarity criteria to scale specific PTS phenomena.

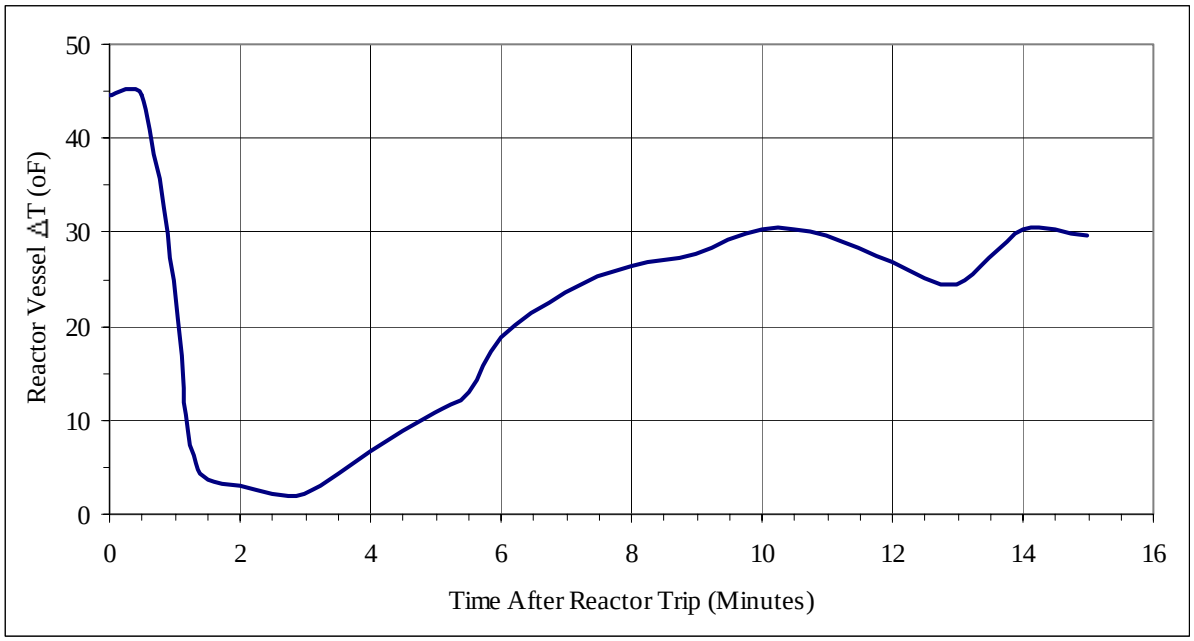

Figure 4.1 Natural Circulation Mode - Palisades Nuclear Plant Trip from 91% Power.

4.1.1 Top-Down Scaling Analysis for Single-Phase Primary Loop Natural Circulation

The loop being considered consists of the core, which serves as a heat source, the steam generator which serves as the heat sink and the insulated interconnecting piping. A simple sketch is presented in Figure 4.3. As shown in this figure, the primary loop is divided into a hot fluid side having an average temperature T_H and a cold fluid side having an average temperature T_C.

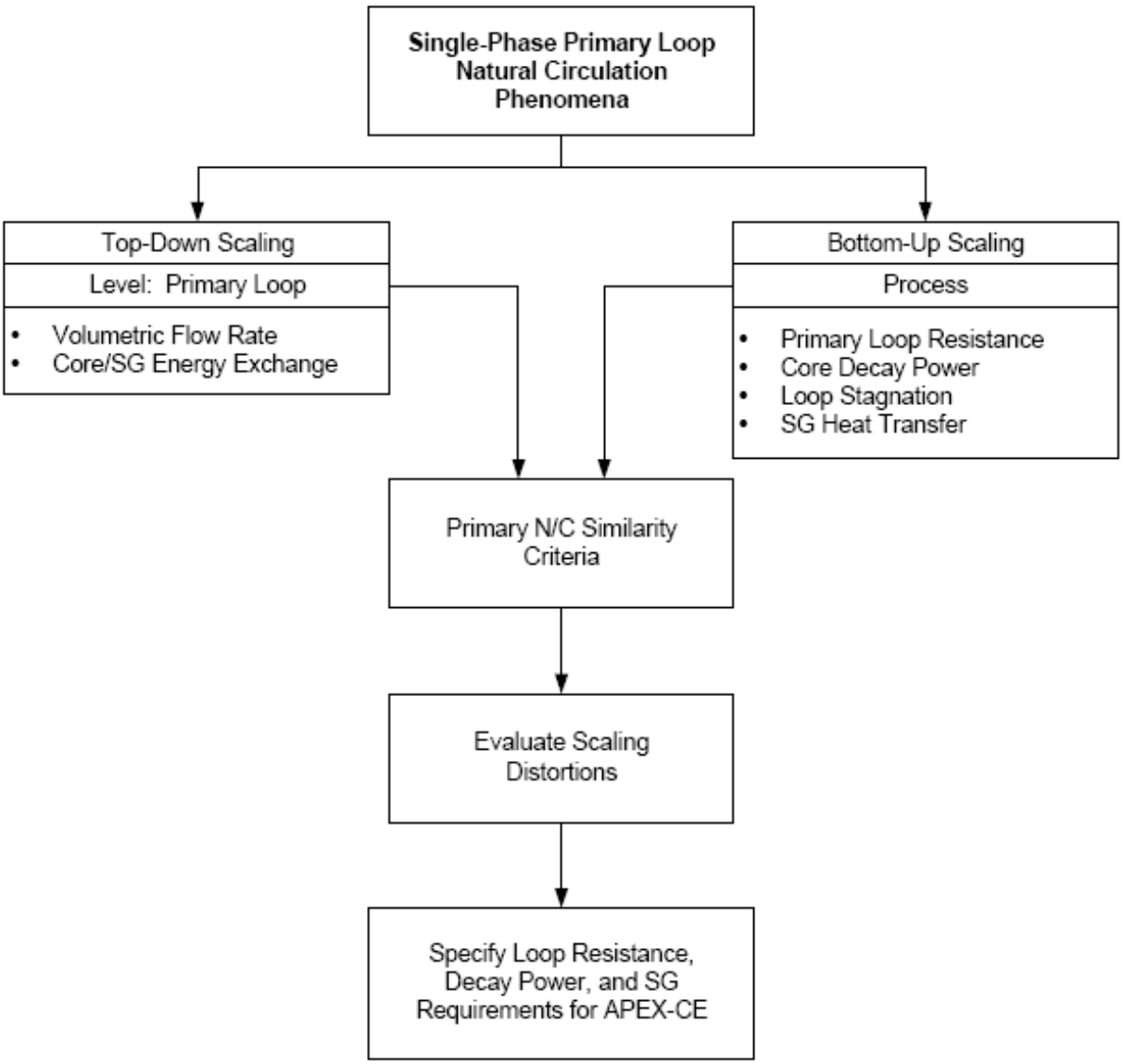

Figure 4.2 Scaling Analysis Flow Diagram for Single-Phase Natural Circulation

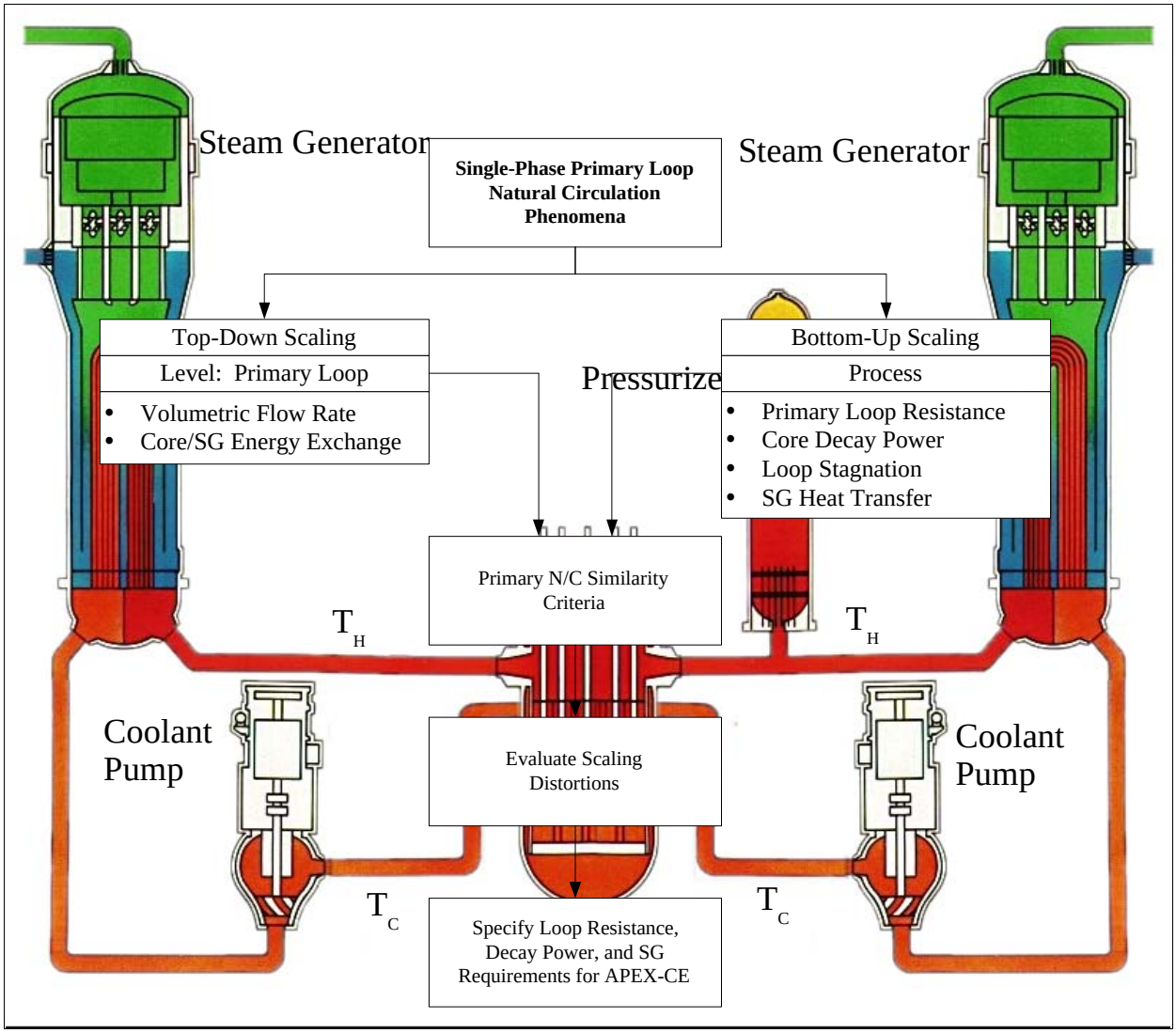

Figure 4.3 Hot and Cold Regions of Single-Phase Natural Circulation Flow within a PWR

Control Volume Balance Equations

Control volume balance equations for mass, momentum and energy conservation for *each component "I"* of the loop were written as follows:

Mass Conservation:

$$\frac{d}{dt}\left(\rho_\ell V_\ell\right)_i = \Delta\left[\rho_\ell Q_\ell\right]_i \qquad \textbf{(4.1)}$$

Momentum Conservation:

$$\frac{d}{dt}\left(\rho_\ell u_\ell \ell\right)_i = \Delta\left[\rho_\ell u_\ell u_\ell\right]_i + \left[\beta_T g \rho_\ell \Delta T \ell_z\right]_i - \frac{\left(\rho_\ell u_\ell u_\ell\right)_i}{2}\left(\frac{f\ell}{d_h} + K\right)_i \tag{4.2}$$

Energy Conservation (Heat Sink or Heat Source):

$$\frac{d}{dt}\left(\rho_\ell C_{v\ell}\left\langle T_\ell \right\rangle V_\ell\right)_i = \Delta\left[\rho_\ell C_{P\ell} T_\ell Q_\ell\right]_i + q_i \tag{4.3}$$

The nomenclature for these equations is provided at the beginning of the report. For purposes of our study, the following analysis assumptions were made:

1. The flow was one-dimensional along the loop axis, therefore fluid properties were uniform at every cross-section.

2. The Boussinesq approximation was applicable.

3. The fluid was incompressible.

By implementing the Boussinesq approximation, all of the fluid densities in the loop were assumed equal to an average fluid density except for those that comprise the buoyancy term. The fact that the components of the loop remain liquid filled during the natural circulation mode of operation coupled with the third assumption eliminates the time dependence in the component mass

$$\dot{m} = n_i \rho_i u_i a_i = \rho_\ell u_\ell a_c = \text{constant} \tag{4.4}$$

conservation equation. Applying these assumptions to the governing equations presented above and integrating the momentum equation over the entire loop, resulted in the following equations for fluid transport around the loop:

Fluid Mass Balance Equation (at every cross-section):
where n_i is the number of parallel paths or loops for the component. The fluid momentum equation for a system of parallel loops with “N” components in each loop is given by:

Fluid Momentum Balance Equation for Parallel Loops:

$$\left[\sum_{i=1}^{N} \ell_i\left(\frac{a_c}{n_i a_i}\right)\right]\rho_\ell \frac{du_c}{dt} = \beta_T g \rho_\ell \left(T_H - T_c\right) L_{th} - \frac{\rho_\ell u_c^2}{2}\sum_{i=1}^{N}\left(f\frac{\ell}{d_h} + K\right)_i\left(\frac{a_c}{n_i a_i}\right)^2 \tag{4.5}$$

Fluid Energy Balance Equation for Loop:

$$C_{v\ell}M_{sys}\frac{d\langle T_\ell\rangle}{dt} = \dot{m}C_p\left(T_H - T_C\right) - \left(UA\Delta T\right)_{SG} - q_{loss} \tag{4.6}$$

where the core energy transport equation was given by:

$$q_{Core} = \dot{m}C_p\left(T_H - T_C\right) \tag{4.7}$$

and the steam generator energy transport equation was given by:

$$q_{SG} = \left(UA\Delta T\right)_{SG} \tag{4.8}$$

Dimensionless Balance Equations

The control volume balance equations presented above were used to identify the dimensionless groups that govern the single phase natural circulation process. This was done by making the equations dimensionless using the following definitions which were based on the initial conditions of the problem.

$$\dot{m} = \dot{m}_o \dot{m}^+ \tag{4.9}$$

$$\langle T_\ell\rangle = \left(T_H - T_c\right)_o \langle T_\ell\rangle^+ \tag{4.10}$$

$$\left(T_H - T_c\right) = \left(T_H - T_c\right)_o \left(T_H - T_c\right)^+ \tag{4.11}$$

$$U_{SG} = U_{SG_o} U_{SG}^+ \tag{4.12}$$

$$\Delta T_{SG} = \left(T_H - T_c\right)_o \Delta T_{SG}^+ \tag{4.13}$$

$$q_{Loss} = q_{Loss_o} q_{Loss}^+ \tag{4.14}$$

In these equations, the superscripted "+" indicates a dimensionless term. Substituting the dimensionless initial conditions into the momentum control volume balance equations produced:

$$\tau_{loop}\frac{du_c^+}{dt} = \varepsilon_{nc}\left[\left(T_H - T_c\right)^+ \Pi_{Ri} - \frac{\left(u_c\right)^+}{2}\Pi_{F1}\right] \tag{4.15}$$

where the characteristic time constant for a single loop is the fluid transport time around the loop given by:

$$\tau_{loop} = \sum_{i=1}^{N} \frac{\ell_i}{u_i} = \sum_{i=1}^{N} \tau_i = \frac{M_{sys}}{\dot{m}} \tag{4.16}$$

The ratio of the loop transport time to an area averaged loop transport time was given by:

$$\epsilon_{nc} = \frac{\sum_{i=1}^{N} \tau_i}{\sum_{i=1}^{N} \tau_i \left(\frac{a_c}{n_i a_i} \right)^2} \tag{4.17}$$

The dimensionless group characterizing the total loop resistance due to friction and form losses was given by:

$$\Pi_{F1} = \sum_{i=1}^{N} \left(\frac{f\ell}{d_h} + K \right) \left(\frac{a_c}{n_i a_i} \right)^2 \tag{4.18}$$

The dimensionless equations also yielded a loop Richardson Number defined as:

$$\Pi_{Ri} = \frac{u_{co}^{\ 2}}{\beta_T g \left(T_H - T_C \right)_o L_{th}} \tag{4.19}$$

Applying the dimensionless initial conditions to the energy control volume equation yielded the following dimensionless energy balance equation:

$$\frac{\tau_{loop}}{\gamma} \frac{d\left\langle T_\ell \right\rangle^+}{dt} = \dot{m}^+ \left(T_H - T_C \right)^+ - \Pi_{SG} U_{SG}^+ \Delta T_{SG}^+ - \Pi_{loss} q_{loss}^+ \tag{4.20}$$

where the time constant is the fluid transport time around a single loop as defined previously. One property group and two dimensionless groups appeared in the dimensionless energy balance equation. The fluid property group is the ratio of specific heats given by:

$$\gamma = \frac{c_p}{c_v} \tag{4.21}$$

which is unity for ideal liquids. The first dimensionless Π group characterized the primary side steam generator heat transport.

$$\Pi_{SG} = \frac{U_{SG,o} A_{SG} \Delta T_{SG,o}}{q_{core,o}} \tag{4.22}$$

The last dimensionless Π group characterized the heat loss around the loop.

$$\Pi_{Loss} = \frac{q_{loss,o}}{C_v \langle T_{\ell,o} \rangle} \tag{4.23}$$

Steady-State Approximation

To provide closure to the dimensionless groups, it was necessary to obtain an expression for the loop natural circulation flow rate. This was done by assuming that the du_c/dt term in the loop momentum balance equation is very small even under transient conditions. That is, loop natural circulation is essentially described by the balance of the buoyancy and the frictional/form pressure loss terms as shown below:

$$\beta_T g \left(T_H - T_c\right) L_{th} = \frac{u_c^2}{2} \sum_{i=1}^{N} \left(f \frac{\ell}{d_h} + K \right)_i \left(\frac{a_c}{n_i a_i} \right)^2 \tag{4.24}$$

Expressing $(T_H - T_C)$ in terms of the core power in this equation and rearranging yields the well known solution for steady-state single phase natural circulation flow in terms of the fluid velocity at the core inlet. That is,

$$u_\ell = \left(\frac{2 \beta_T q_{core} L_{th} g}{a_c C_{P\ell} \rho_\ell \Pi_{F1}} \right)^{1/3} \tag{4.25}$$

Having developed a steady-state solution for the liquid velocity at the core inlet based on the conservation of mass and momentum, a set of similarity criteria can be developed for each of the loop components. The component fluid velocity scaling ratio can be found using equation (4.4).

$$u_{\ell i,R} = \left(\frac{\beta_T q L_{th}}{a_c C_p \rho_\ell \Pi_{F1}} \right)_R^{1/3} \left(\frac{a_c}{a_i} \right)_R \tag{4.26}$$

where the ratio of the number of loops $n_{i,R}$ is unity, ρ_ℓ is the average loop fluid density and "R" denotes an APEX-CE to Palisades ratio.

The assessment of geometric similarity presented in Chapter 2, indicates that kinematic similarity will be preserved because the area ratios are essentially constant throughout the loop at ~ 1/69. Thus similitude between flow area ratios are maintained. That is:

$$\left(\frac{a_c}{a_i}\right)_R \approx 1 \qquad \textbf{(4.27)}$$

thus $(a_c)_R = (a_i)_R = a_R$. Furthermore, the length ratios throughout the loop are also approximately preserved. That is:

$$\left(L_{th}\right)_R \approx \ell_R \qquad \textbf{(4.28)}$$

where the subscript, I, has been dropped to indicate its validity for the entire loop. Applying the requirements of equations (4.27) and (4.28) to equation (4.26) yields the loop fluid velocity scaling ratio:

$$u_R = \left(\frac{\beta_T}{\rho_\ell C_p}\right)_R^{1/3} \left(\frac{q_{core}\ell}{a_C \Pi_{F1}}\right)_R^{1/3} \qquad \textbf{(4.29)}$$

The fluid residence time scaling ratio can be obtained by dividing the length scaling ratio, ℓ_R, by the loop fluid velocity scaling ratio. That is:

$$\tau_R = \frac{\ell_R}{u_R} \qquad \textbf{(4.30)}$$

or:

$$\tau_R = \left(\frac{\rho_\ell C_P a_c \ell^2 \Pi_{F1}}{\beta_T q_{core}}\right)_R^{1/3} \qquad \textbf{(4.31)}$$

The following chapter indicates that one-to-one time scale tests will be performed in APEX-CE to preserve the onset of cold leg thermal stratification behavior. That is, the time required for a fluid element to travel around the APEX loop would be the same as in the full scale CE prototype. This can be assured by requiring that:

$$\frac{\tau_{APEX}}{\tau_{CE}} = \tau_R = 1 \qquad \textbf{(4.32)}$$

Substituting this requirement into equation (4.30) yields:

$$u_R = \ell_R \tag{4.33}$$

Substituting this result into equation (4.31) and rearranging yields the following requirement for the loop resistance:

$$\Pi_{F1} = \left(\frac{\beta_T}{\rho_\ell C_p}\right)_R \left(\frac{q_{core}}{a_c \ell^2}\right)_R \tag{4.34}$$

This dimensionless group has been used to scale the primary loop resistance.

4.1.2 Bottom-Up Natural Circulation Scaling Analysis

This section presents the process scaling analysis that was performed to provide closure to the dimensionless groups developed as part of the top-down natural circulation scaling analysis. The results of the analysis include scaling equations for primary loop resistance, core decay power, and single-phase loop flow stagnation.

4.1.2.1 Primary Loop Resistance

Preserving the single-phase natural circulation behavior required carefully matching the loss coefficients in APEX-CE and Palisades. As indicated in the previous section, equation (4.34) was used to obtain the APEX-CE loop resistance that would properly simulate one-to-one time scale loop transport behavior.

Table 4.1 lists the component Π_{F1} terms for APEX-CE and Palisades. As shown in the table, additional resistance needed to be added to the current configuration of APEX to obtain the desired one-to-one time scale behavior. This was easily accomplished with slotted orifices.

Table 4.1 Π_F for Palisades and APEX-CE Loop Components

Component	**Palisades**	**APEX-CE (1/1 Time Scale)**
	Π_{F1}	Π_{F1}
Steam Generator	36.8	147.2
Reactor Vessel and Loops	33.7	134.8
All Loop Components	70.5	282.0

4.1.2.2 Core Decay Power

Figure 4.4 presents the predicted decay power for the Palisades nuclear plant based on the "American National Standard for Decay Heat Power in Light Water Reactors (ANSI/ANS-5.1.24, 1979). The power curve includes a G-factor which takes into account the transient decay of heavy elements. Because APEX-CE is modeled on a 1:1 time scale, the power ratio is equal to the volume ratio. Thus:

$$(q_{core})_R = \frac{1}{276} \tag{4.35}$$

Figure 4.5 presents the decay power required for the APEX-CE facility assuming fluid property similitude. This figure shows that the desired scaled power can be achieved using the programmed decay power for the APEX-CE facility which is given by:

$$P = \frac{P_o}{(1 + \omega_D t)^c} \tag{4.36}$$

where the initial power, P_o, in APEX-CE is 610 kW, the decay time constant, ω_D is 0.2338 s^{-1} and the exponent, c, is 0.2316.

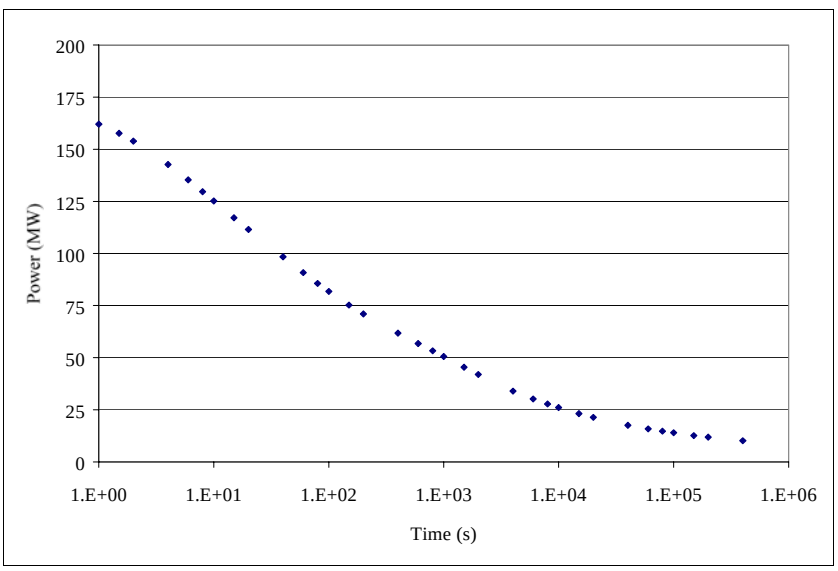

Figure 4.4 Decay Power Profile for the Palisades Nuclear Plant Based on ANSI/ANS-5.1.24, 1979 with G-Factor.

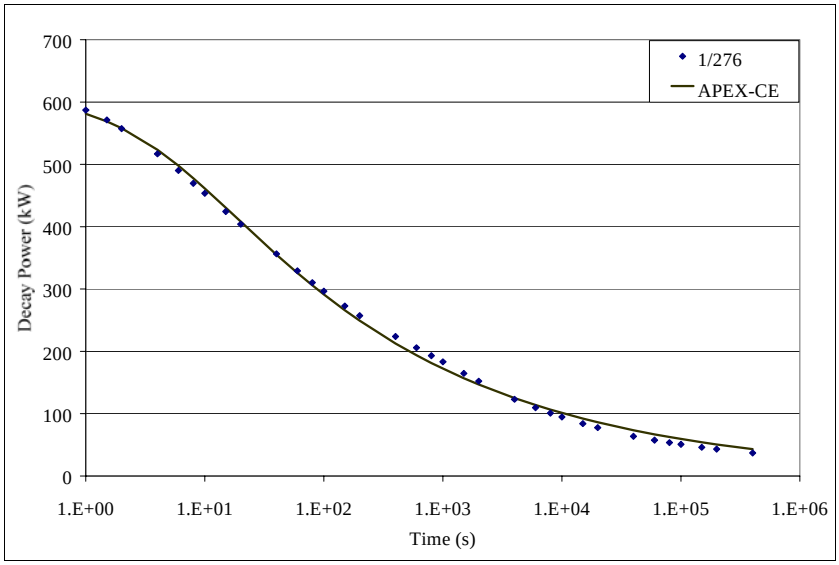

Figure 4.5 Comparison of Decay Power Equation for the APEX-CE Test Facility and ½76 of the Palisades Decay Power.

4.1.2.3 Single-Phase Loop Flow Stagnation

The onset of loop flow stagnation is of particular interest to this PTS study if it occurs during HPSI operation. The loss of loop flow would result in thermal stratification of the cold leg fluid and the development of cold plumes in the reactor vessel downcomer. Depending on the downcomer mixing behavior, these plumes could possibly come in contact with the beltline welds. This section briefly examines the mechanisms leading to single-phase loop flow stagnation for conditions of interest to PTS.

Single-phase loop natural circulation will persist while both the heat source and heat sink remain active within the primary loop. Subsequent to reactor shutdown, core power will continue to decay as predicted in the previous section. Therefore the heat source will remain active for prolonged periods of time. Thus the only mechanism that will lead to single-phase loop flow stagnation in one or more of the cold legs would be the loss of one or both steam generators as a heat sink. In addition, for this event to be of significance to PTS, the primary loop pressure must have dropped below the HPSI actuation setpoint. Main Steam Line Break (MSLB) scenarios have the potential for achieving these conditions.

A large MSLB in one steam generator will result in a rapid cooldown of the primary system as the steam generator liquid flashes and boils to steam. If the unaffected steam generator is isolated, the primary loop temperature will eventually drop below the fluid temperature in the unaffected steam generator. The result is a loss of heat sink in the unaffected steam generator which causes stagnation in the corresponding loop. Depending on the size of the MSLB and the core power, primary system pressure may drop below the HPSI actuation setpoint. Therefore, the conditions would be established to generate cold plumes in the downcomer. This will be one of the scenarios examined in APEX-CE.

Boiling heat transfer is a very efficient process because of the large values of convective heat transfer coefficient. The greatest resistance to tube heat transfer is due to conduction through the tube wall and any surface containment (i.e., tube fouling that may have built up over time). A cursory look at equation (4.22) reveals that under steady-state conditions:

$$\Pi_{SG} = 1 \tag{4.37}$$

This is true because the loop surface area and the values for the overall heat transfer coefficient, U_{SG}, are capable of removing all of the core heat during normal operation. That is, one should expect Π_{SG} to be very close to unity in both APEX-CE and Palisades if heat losses are reasonable (i.e., < 5%).

Steam generator energy removal during transient blowdowns, such as MSLBs, will be examined in Chapter 7.

4.1.3 Comparison of APEX-CE and Palisades Single-Phase Natural Circulation Flow Rates

Figure 4.6 compares the APEX-CE natural circulation flow rates to the ideally scaled Palisades (i.e., 1/276) natural circulation flow rates based on equation 4.25. As illustrated by this figure, APEX-CE should provide an excellent simulation of Palisades single-phase natural circulation flow.

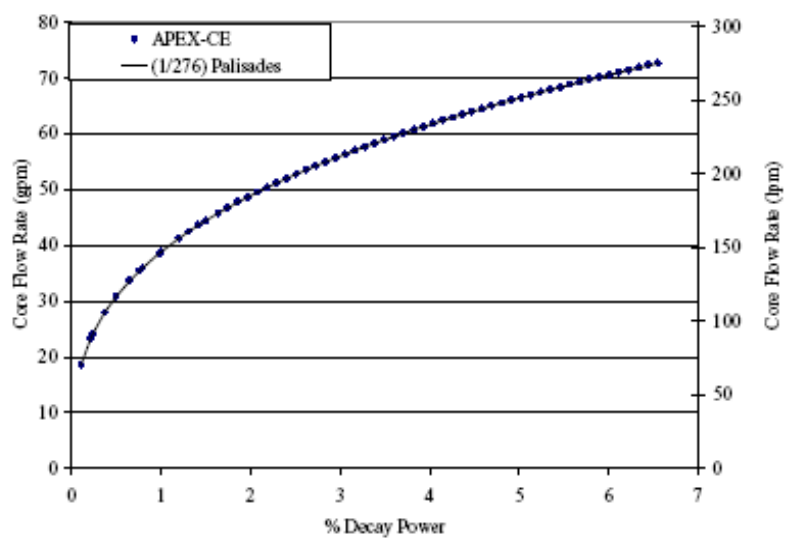

Figure 4.6 Comparison of APEX-CE to Identify Scaled Palisades Test Loop

4.2 Primary Loop Two-Phase Natural Circulation

This section presents the scaling analysis performed to assess the degree of similarity between primary loop natural circulation in APEX-CE and Palisades for two-phase natural circulation conditions. Figure 4.7 provides a flow diagram which describes the scaling analysis process for this operational mode.

First a top-down integral system scaling analysis was performed. The primary objective of the top-down scaling analysis was to scale the primary loop mass flow rates. Following the top-down scaling analysis, a bottom-up scaling analysis was performed to scale the loop resistance for two-phase flow conditions and to assess the degree of similarity between flow pattern transitions in APEX-CE and in Palisades. The mechanisms for the interruption of two-phase natural circulation are also discussed.

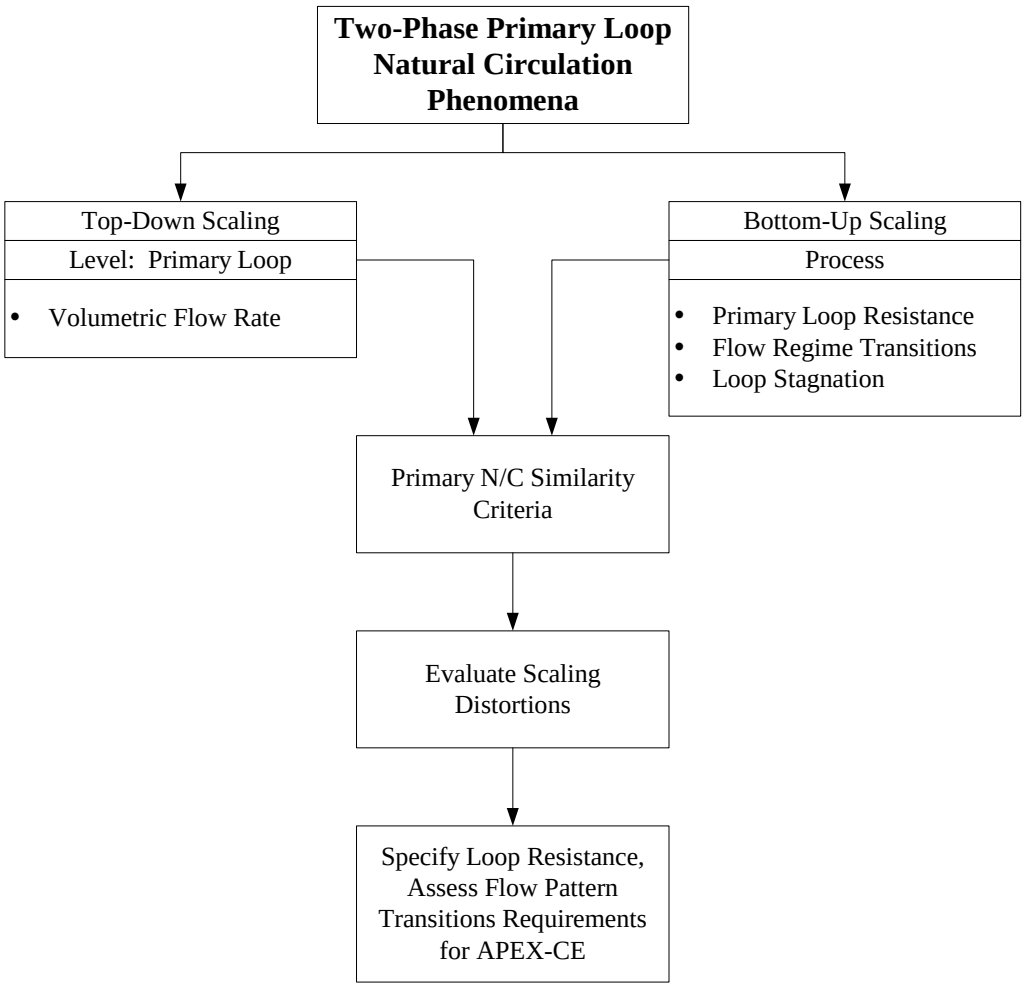

Figure 4.7 Scaling Analysis Flow Diagram for Two-Phase Natural Circulation

4.2.1 Top-Down Scaling Analysis for Two-Phase Primary Loop Natural Circulation

This section presents an analysis that describes how the two-phase natural circulation flow rate (two-phase fluid velocity and mass flow rate) in APEX-CE would compare to Palisades. This analysis results in an analytical expression for the two-phase fluid velocity. Figure 4.8 depicts the loop geometry considered for this analysis. The loop is divided into two regions; a two-phase region with a fluid density ρ_{TP} and a single-phase region with a fluid density ρ_{ℓ}. The simplifying integral analysis assumptions are as follows:

1. Steady-state flow,
2. One dimensional flow along the loop axis,
3. Uniform fluid properties at every cross-section,
4. Homogeneous flow,
5. Chemical Equilibrium – no chemical reactions,
6. Thermal Equilibrium – both phases at the same temperature,
7. The sum of convective accelerations due to vaporization and condensation are negligible,
8. Viscous effects included in determination of form losses only.

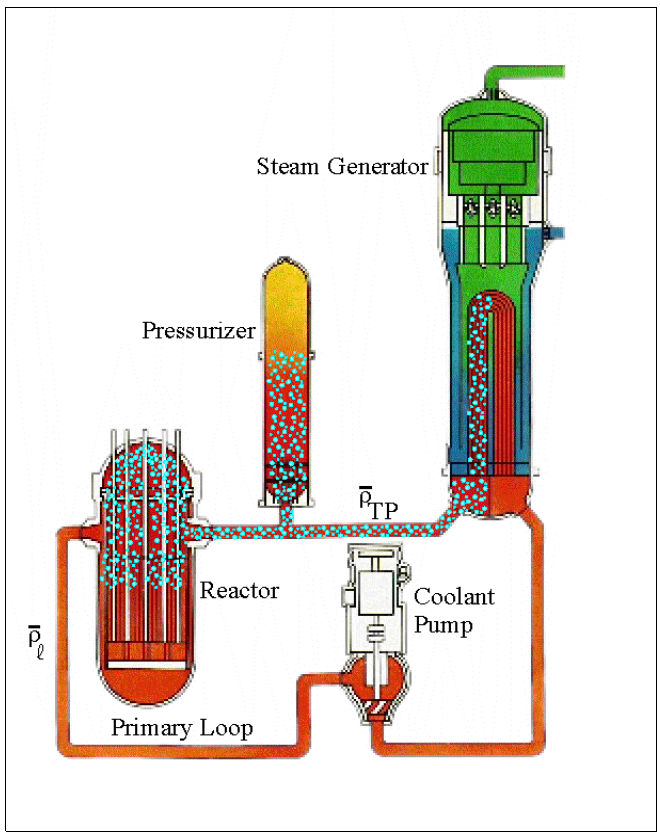

Figure 4.8 Regions of Single-Phase and Two-Phase Natural Circulation within a PWR

The assumptions listed above were applied to the mass, momentum, and energy equations for each component in the loop to obtain a simplified set of conservation equations. The equations were then integrated over their respective single-phase and two-phase regions to obtain the loop balance equations. These equations were used to obtain an analytical expression for the fluid velocity at the core entrance. The coefficients of the fluid velocity equation were scaled to obtain a two-phase fluid velocity scaling ratio, a two-phase power density scaling ratio and a two-phase time scaling ratio.

Loop Mass Conservation Equation

For steady-state, one-dimensional flow, the mass conservation equation at every flow cross section along the loop is written as:

$$\dot{m} = \rho_i u_i a_i = \text{constant} \tag{4.38}$$

where $\dot{m}$ is a constant mass flow rate for the system, ρ_i and u_i are the fluid density and fluid velocity within the ith component respectively, and a_i is the flow cross-sectional area of the ith component. Steady-state conditions require that:

$$\rho_i u_i a_i = \rho_c u_c a_c \tag{4.39}$$

where ρ_c, u_c, and a_c are the fluid density, fluid velocity, and flow-cross-sectional area at the core entrance respectively.

Loop Momentum Conservation Equation

Applying the assumptions stated previously, the steady-state momentum balance equation is integrated over the single and two-phase regions to obtain a general force balance relating the pressure drop due to friction and form losses to the buoyancy forces. That is:

$$\sum_{i=1}^{N} \frac{\rho_i u_i^2}{2}\left(f\frac{\ell}{d_h} + K\right)_i = \left(\overline{\rho_\ell} - \overline{\rho_{TP}}\right)L_{th}\, g \tag{4.40}$$

Using equation (4.39), equation (4.40) is re-written in terms of single and two-phase regions as follows:

$$\frac{\rho_c^2 u_c^2}{2}\left[\frac{1}{\overline{\rho_{TP}}}\sum_{TP}\left(f\frac{\ell}{d_h} + K\right)_i\left(\frac{a_c}{a_i}\right)^2 + \frac{1}{\overline{\rho_\ell}}\sum_{SP}\left(f\frac{\ell}{d_h} + K\right)_i\left(\frac{a_c}{a_i}\right)^2\right] = \left(\overline{\rho_\ell} - \overline{\rho_{TP}}\right)L_{th}\, g \tag{4.41}$$

For this analysis, $\overline{\rho_{TP}}$ is the average two-phase fluid density given by the following definition for a two-phase fluid under homogeneous equilibrium conditions.

$$\overline{\rho_{TP}} = \frac{\rho_{\ell s}}{1 + x_e\left(\frac{\Delta\rho}{\rho_{gs}}\right)} \tag{4.42}$$

Loop Energy Conservation Equation

Under steady-state conditions, the energy balance for the core, that governs the rate of energy transport into the system is given by:

$$\rho_c u_c a_c \left(h_{TP} - h_\ell\right) = q_{core} \tag{4.43}$$

where q_{core} is the core heat generation rate less heat losses from the core. The equilibrium vapor quality used in equation (4.42) is defined as follows:

$$x_e = \frac{h_{TP} - h_{\ell s}}{h_{\ell g}} \tag{4.44}$$

Substituting the energy equations (4.43) into (4.44) yields:

$$x_e = \frac{q_{core} - \rho_c u_c a_c h_{sub}}{\rho_c u_c a_c h_{\ell g}} \tag{4.45}$$

where the subcooling enthalpy, $h_{sub} = h_{\ell s} - h_\ell$, and the latent heat of vaporization, $h_{\ell g} = h_{gs} - h_{\ell s}$.

Fluid Velocity Equation

Substituting equation (4.45) into equation (4.42) yields:

$$\overline{\rho_{TP}} = \frac{\rho_{\ell s}}{1 + \left(\frac{q_{core} - \rho_c u_c a_c h_{sub}}{\rho_c u_c a_c h_{\ell g}}\right)\left(\frac{\Delta\rho}{\rho_{gs}}\right)} \tag{4.46}$$

Substituting equation (4.46) into equation (4.41), applying the Boussinesq approximation such that $\rho_c \approx \rho_{\ell s}$, and performing a significant amount of algebra, yields the following cubic equation for fluid velocity:

$$u_c^3 + \phi_a u_c^2 + \phi_b u_c - \phi_c = 0 \tag{4.47}$$

where:

$$\phi_a = \frac{q_{core}\Delta\rho}{a_c \rho_{\ell s}} \left(\frac{\left(\Pi_F + \Pi_{F2}\right)\rho_{gs} h_{\ell g} - 2\Delta\rho \Pi_{F2} h_{sub}}{\Pi_F \rho_{gs}^2 h_{\ell g}^2 - \left(\Pi_F + \Pi_{F2}\right)\rho_{gs} h_{\ell g} h_{sub} \Delta\rho + \Pi_{F2}\left(\Delta\rho\right)^2 h_{sub}^2} \right) \tag{4.48}$$

$$\phi_b = \frac{\Delta\rho}{a_c^2 \rho_{\ell s}^2} \left(\frac{\Delta\rho \Pi_{F2} q_{core}^2 + 2 L_{th} g \rho_c^2 a_c^2 h_{sub} \rho_{gs} h_{\ell g}}{\Pi_F \rho_{gs}^2 h_{\ell g}^2 - \left(\Pi_F + \Pi_{F2}\right)\rho_{gs} h_{\ell g} h_{sub} \Delta\rho + \Pi_{F2}\left(\Delta\rho\right)^2 h_{sub}^2} \right) \tag{4.49}$$

$$\phi_c = \frac{1}{a_c \rho_{\ell s}} \left(\frac{2 L_{th} g q_{core} \Delta\rho \rho_{gs} h_{\ell g}}{\Pi_F \rho_{gs}^2 h_{\ell g}^2 - \left(\Pi_F + \Pi_{F2}\right)\rho_{gs} h_{\ell g} h_{sub} \Delta\rho + \Pi_{F2}\left(\Delta\rho\right)^2 h_{sub}^2} \right) \tag{4.50}$$

and

$$\Pi_{F1} = \sum_{SP} \left(f \frac{\ell}{d_h} + K \right)_i \left(\frac{a_c}{a_i} \right)^2 \tag{4.51}$$

$$\Pi_{F2} = \sum_{TP} \left(f \frac{\ell}{d_h} + K \right)_i \left(\frac{a_c}{a_i} \right)^2 \tag{4.52}$$

$$\Pi_F = \Pi_{F1} + \Pi_{F2} \tag{4.53}$$

4.2.1.1 Primary Loop Similarity Criteria

To simulate the same fluid velocity behavior in APEX-CE as in Palisades, the coefficients of equation (4.47) must be scaled properly. It is interesting to note that Schroeder (1991) examines the mathematical basis for scaling equations similar to (4.47) in his text titled *Fractals, Chaos, Power Laws*[8].

A set of two-phase, natural circulation similarity criteria were obtained by scaling the coefficients ϕ_a, ϕ_b, ϕ_c of equation (4.47) such that the following transformation was possible:

$$\beta^3 \left(u_m^3 + \phi_{am} u_m^2 + \phi_{bm} u_m - \phi_{cm} \right) = u_p^3 + \phi_{ap} u_p^2 + \phi_{bp} u_p - \phi_{cp} \tag{4.54}$$

where, β^3 is a constant factor and the subscripts m and p represent values for the model and the prototype respectively. Reyes (1994) demonstrates that equation (4.47) is a constraint catastrophe function whose coefficients can be scaled as follows[9]:

$$\beta\, u_m = u_p \tag{4.55}$$

$$\beta\, \phi_{am} = \phi_{ap} \tag{4.56}$$

$$\beta^2 \phi_{bm} = \phi_{bp} \tag{4.57}$$

$$\beta^3 \phi_{cm} = \phi_{cp} \tag{4.58}$$

Rearranging these equations in terms of scaling ratios yields:

$$u_r = \frac{1}{\beta} \tag{4.59}$$

$$\phi_{aR} = \frac{1}{\beta} \tag{4.60}$$

$$\phi_{bR} = \frac{1}{\beta^2} \tag{4.61}$$

$$\phi_{cR} = \frac{1}{\beta^3} \tag{4.62}$$

were the subscript R represents a ratio of APEX-CE parameters to Palisades parameters.

<u>Two-Phase Similarity Criteria at Saturated Conditions</u>

For the special case of saturated conditions, the value of h_{sub} is zero. Furthermore, as shown in Chapter 3 similitude between APEX-CE and Palisades flow areas is generally preserved. Therefore, kinematic similarity will be preserved. That is:

$$\left(\frac{a_c}{a_i}\right)_R \approx 1 \tag{4.63}$$

In addition, efforts were made such that the ratios of single-phase and two-phase friction number (Π_{F1} and Π_{F2}) would be constant. That is:

$$\left(\Pi_{F1}\right)_R \approx 4 \tag{4.64}$$

$$\left(\Pi_{F2}\right)_R \approx 4 \tag{4.65}$$

$$\left(\Pi_{F}\right)_R \approx 4 \tag{4.66}$$

Setting h_{sub} to zero and applying the requirements presented in equations (4.63) through (4.66) to the coefficients of equations (4.47) and taking the ratio of the APEX-CE values to the Palisades values yields:

$$\phi_{aR} = \left(\frac{q_{core}}{a_c}\right)_R \left(\frac{\Delta\rho}{\rho_{\ell s}\rho_{gs}h_{\ell g}}\right)_R \tag{4.67}$$

$$\phi_{bR} = \left(\frac{q_{core}}{a_c}\right)^2_R \left(\frac{\Delta\rho}{\rho_{\ell s}\rho_{gs}h_{\ell g}}\right)^2_R \tag{4.68}$$

$$\phi_{cR} = \left(\frac{q_{core}L_{th}}{a_c}\right)_R \left(\frac{\Delta\rho}{\rho_{\ell s}\rho_{gs}h_{\ell g}}\right)_R \left(\frac{1}{\Pi_F}\right)_R \tag{4.69}$$

The scaling criteria for saturated conditions were obtained by substituting equations (4.67) through

$$\frac{1}{\beta} = \left(\frac{q_{core}}{a_c}\right)_R \left(\frac{\Delta\rho}{\rho_{\ell s}\rho_{gs}h_{\ell g}}\right)_R \tag{4.70}$$

(4.69) into equations (4.59) through (4.62). Substituting equation (4.67) into (4.60) yields: Setting equation (4.70) equal to (4.59) yields:

$$\left(\frac{q_{core}}{u_c a_c}\right)_R \left(\frac{\Delta\rho}{\rho_{\ell s}\rho_{gs}h_{\ell g}}\right)_R = 1 \tag{4.71}$$

The requirement of (4.71) has implications on the vapor quality. For saturation conditions, the vapor quality, as defined in equation (4.45), is simplified as follows:

$$x_e = \frac{q_{core}}{\rho_{\ell s} u_c a_c h_{\ell g}} \tag{4.72}$$

Substituting equation (4.72) into (4.71) yields:

$$x_R \left(\frac{\Delta\rho}{\rho_{gs}} \right)_R = 1 \tag{4.73}$$

The two-phase power scaling ratio is obtained by substituting equations (4.70) and (4.69) into (4.62). This yields:

$$q_R = a_R \left(\frac{\rho_{\ell s} \rho_{gs} h_{\ell g}}{\Delta\rho} \right)_R \left(\frac{L_{th}}{\Pi_F} \right)_R^{\frac{1}{2}} \tag{4.74}$$

Combining equations (4.71) and (4.74) yields the fluid velocity scaling ratio:

$$u_R = \left(\frac{L_{th}}{\Pi_F} \right)_R^{\frac{1}{2}} \tag{4.75}$$

The time scaling ratio is obtained by dividing the system length scaling ratio by the velocity scaling ratio given by equation (4.76). Thus:

$$\tau_R = \ell_R \left(\frac{\Pi_F}{L_{th}} \right)_R^{\frac{1}{2}} \tag{4.76}$$

The mass flow rate scaling ratio is obtained by:

$$\dot{m}_R = \left(\rho_{\ell s} \right)_R a_R \left(\frac{L_{th}}{\Pi_F} \right)_R^{\frac{1}{2}} \tag{4.77}$$

For the case of APEX-CE and Palisades:

$$\left(L_{th} \right)_R \approx \ell_R \tag{4.78}$$

The scaling ratios then become identical to those developed by Ishii and Kataoka (1983)[10]. Equations (4.74) through (4.77) are expressed in terms of L_{th}, the distance between the thermal centers of the heat source (core) and the heat sink (steam generator).

Transition from single-phase loop natural circulation

During a SBLOCA, the primary loop flow will transition from subcooled single-phase natural circulation as depicted in Figure 4.3 to two-phase natural circulation as depicted in Figure 4.8. As a result, it is important that the transition from single-phase flow to two-phase loop natural circulation be scaled properly. This section addresses that concern and presents a unified set of scaling criteria for the transition. The velocity ratio for steady-state, single-phase natural circulation flow, given by equation (4.26), is:

$$u_{R,sp} = \left(\frac{\beta_{To}}{\rho_{\ell o} C_{p\ell o} \Pi_{F1}} \right)_R^{1/3} \left(\frac{q_{core} \ell}{a_c} \right)_R^{1/3} \tag{4.79}$$

The fluid residence time scaling ratio for steady-state single-phase natural circulation flow was given by equation (4.31):

To assure that the single to two-phase loop natural circulation transition is scaled properly in APEX-

$$\tau_{R,sp} = \left[\frac{\rho_{\ell o} C_{p\ell o} a_c \ell^2 \Pi_{F1}}{\beta_{To} q_{core}} \right]_R^{1/3} \tag{4.80}$$

CE, the two-phase power scaling ratio equation (4.74) was set equal to the single-phase power scaling ratio. By substituting the two-phase power scaling ratio into equation (4.79), while assuming geometric similarity, the following single-phase velocity scaling ratio was obtained:

It has been assumed that $(\Pi_{F1})_R$ equals $(\Pi_F)_R$. Similarly, the single-phase residence time scaling

$$u_{R,sp} = \left(\frac{\ell}{\Pi_F} \right)_R^{1/2} \left(\frac{\beta_T \rho_{gs} h_{\ell g}}{\Delta\rho C_p} \right)_R^{1/3} \tag{4.81}$$

ratio is:

With respect to integral system flow behavior and single to two-phase flow transitions; requiring the same power scale resulted in unifying the single and two-phase scaling ratios. Therefore the

$$\tau_{R,sp} = (\Pi_F)_R^{1/2} \ell_R^{1/2} \left(\frac{\beta_T \rho_{gs} h_{\ell g}}{\Delta\rho C_p} \right)_R^{-1/3} \tag{4.82}$$

system scaling ratios for steady-state natural circulation with single-phase and two-phase flow regions, material property similitude and a fixed length scale are given by:

Power Scaling Ratio:
Fluid Velocity Scaling Ratio:
Fluid Residence Time Scaling Ratio:

$$q_{R,sp} = q_{R,tp} = a_R \left(\frac{\ell}{\Pi_F} \right)_R^{1/2} \left(\frac{\rho_{\ell s} \rho_{gs} h_{\ell g}}{\Delta\rho} \right)_R \tag{4.83}$$

The scaling ratios presented above are identical to those developed by Kocamustafaogullari and

$$u_{R,sp} = u_{R,tp} \left(\frac{\beta \rho_{gs} h_{\ell g}}{\Delta\rho C_p} \right)_R^{1/3} \tag{4.84}$$

$$\tau_{R,sp} = \tau_{R,tp} \left(\frac{\beta \rho_{gs} h_{\ell g}}{\Delta\rho C_p} \right)_R^{-1/3} \tag{4.85}$$

Ishii (1986) for the case of material property similitude.[11]

The scaling ratios presented above are functions of pressure suggesting that aspects of high pressure natural circulation can be simulated in a low pressure test facility. However, when the same working fluid is used in the model and the prototype, time scaling and velocity scaling distortions arise in the single phase region because of fluid property differences associated with pressure differences.

4.2.2 Bottom-Up Scaling of Two-Phase Natural Circulation Processes

As shown in Figure 4.7, bottom-up scaling analyses are needed to scale important processes in the core, the hot leg and other components. This section presents scaling analyses for:

1. Two-phase friction and loss coefficients,
2. Flow regime transitions, and
3. Two-phase loop stagnation.

4.2.2.1 Scaling Two-Phase Friction and Loss Coefficients

As identified in the top-down scaling analysis, it is important that the friction number for the two-phase region of APEX-CE be modeled appropriately to preserve a one-to-one time scale. This requires a closer examination of two-phase friction factors and loss coefficients.

Dividing the two-phase friction number, as defined by equation (4.52) into a friction factor component and a loss coefficient component, a two-phase friction multiplier and loss coefficient multiplier is obtained as follows (Ishii and Kataoka, 1983).

$$\Pi_{F2} = \sum_{TP} N_{fi} + \sum_{TP} N_{ki} \tag{4.86}$$

where

$$N_{fi} = \frac{f\ell}{d_h}\left(\frac{1+\left(\Delta\rho\, x/\rho_{gs}\right)}{\left(1+\Delta\mu\, x/\mu_{gs}\right)^{1/4}}\right)\left(\frac{a_c}{a_i}\right)^2 \tag{4.87}$$

and

$$N_{ki} = K\left(1+\frac{\Delta\rho x^{3/2}}{\rho_{gs}}\right)\left(\frac{a_c}{a_i}\right)^2 \tag{4.88}$$

where f is the darcy friction factor for liquid and K is the loss coefficient. For the range of fluid velocities encountered in natural circulation flows, the dominant losses will be due to form losses rather than friction. Because proper flow scaling requires scaling the total resistance in the two-phase region rather than in each individual component, it was possible to satisfy this criterion through the careful use of flow orifices and assuming fluid property similitude at low pressure.

4.2.2.2 Scaling Two Phase Flow Pattern Transitions

Transitions in two phase flow patterns significantly impact the integral behavior of the system. Therefore an assessment was made for each component in the system to determine which two phase flow pattern transitions may be delayed or entirely missed. In their paper, Schwartzbeck and Kocamustafaogullari (1989) catalogued the applicable flow pattern transition criteria.[12] These criteria were used to determine if two phase flow pattern transitions would be properly scaled in the horizontal and vertical sections of APEX-CE. The following equations summarize the flow transition scaling criteria that was implemented.

<u>Horizontal Pipes</u>:

• Stratified-Smooth to Stratified Wavy:

$$\ell_R^{3/4} = \alpha_R \left(\frac{(1-\alpha)_R}{(1-x)_R} \right)^{1/2} \left(\frac{\Delta\rho^3 \upsilon_f}{\rho_f^2 \rho_g} \right)_R^{1/2} \tag{4.89}$$

• Stratified to Intermittent or Annular-Dispersed Liquid (Taitel and Dukler, 1976)13:

$$u_R = D_R^{1/2} \left(\frac{\Delta\rho}{\rho_f} \right)_R^{1/2} \tag{4.90}$$

• Intermittent or Dispersed Bubbly to Annular-Dispersed:

$$\alpha_R = \left(\frac{\rho_f}{\Delta\rho} \right)_R \tag{4.91}$$

• Intermittent to Dispersed Bubbly:

$$\ell_R^{0.45} = \frac{f_T(\alpha_R) a_R^{0.3}}{\upsilon_{fR}^{0.1} (\rho_f / \Delta\rho)_R^{0.5} (1-x)_R^{0.9}} \tag{4.92}$$

<u>Vertical Pipes</u>:

• Bubbly to Slug Flow:

$$\alpha_R = \left(\frac{\rho_f}{\Delta\rho}\right)_R \tag{4.93}$$

• Slug to Churn Flow:

$$\ell_R = a_R^{1/2} f_T(x, \rho) \tag{4.94}$$

• Slug/Churn to Annular Flow:

$$u_R \left(\frac{\rho_g^2}{\sigma\Delta\rho}\right)_R^{1/4} = 1 \tag{4.95}$$

These flow pattern transition scaling criteria simplify with fluid property similarity. It was impossible to satisfy all of these criteria in the scaled APEX-CE model. Therefore, emphasis was given to the important flow pattern transitions identified for various components.

<u>Hot and Cold Leg Transitions from Stratified Flow</u>

Under two-phase natural circulation conditions, the flow behavior in the hot legs and cold legs can undergo transitions from stratified flow to either intermittent-slug flow or annular-dispersed flow. This was an important feature of the FLECHT-SEASET experiments in which the hot leg diameter was increased to a maximum in an attempt to model these transitions as closely as possible (Hochreiter, 1985).[14]

The type of flow pattern in the horizontal loop piping greatly influences the loop flow rate. For example, a transition from an intermittent-slug flow to a stratified flow in the hot leg will cause a significant change in the mode of heat transfer removal in the steam generators. Therefore it was important to assure that this flow pattern transition would occur at the same relative liquid level (h/d)

in the APEX-CE hot leg as in the Palisades. This type of flow transition can occur in any of the horizontal piping that may be in a "drain-down" situation. Therefore, special attention was given to the reactor coolant loop hot and cold legs.

Based on Taitel and Dukler's work (1976)[13], appropriate scaling of the hot legs required satisfying the modified Froude number ratio. The modified Froude number is given by:

$$Fr = \frac{j_g}{\left[gD \frac{\Delta\rho}{\rho} \right]^{1/2}} \tag{4.96}$$

where D denotes the diameter of the horizontal pipe. Thus, to preserve the transition from stratified

$$(Fr)_R = 1 \tag{4.97}$$

two-phase fluid conditions, it is required that:

It is noted that the superficial velocity in the horizontal piping is bound by the results of the top-down

$$(j_g)_R \approx \left(\frac{Q}{a} \right)_R \tag{4.98}$$

scaling analysis. For the case of fluid property similitude;

where the volumetric flow rate ratio has been fixed by loop resistance versus buoyancy. That is:

Writing equation (4.96) as a scaling ratio and substituting equation (4.98) yields:
where fluid property similitude has been assumed. Thus, for the APEX-CE and Palisades hot legs

$$(Fr_{HL})_R \approx \frac{1}{1.4} \tag{4.101}$$

we find:

$$(Fr_{CL})_R \approx \frac{1}{1.3} \tag{4.102}$$

For the APEX-CE cold legs relative to the Palisades cold legs we find:

Thus, the transitions from stratified two-phase conditions in the hot legs and cold legs will be reasonably simulated, particularly when fluid property similitude exists.

4.2.2.3 Two-Phase Loop Stagnation

During a SBLOCA, the primary loop will undergo several modes of operation. First, there will be a period of subcooled blowdown during which the loss of inventory will likely be observed in the pressurizer depending on the break location. As primary system pressure drops, saturation conditions are reached in the primary loop, a vapor bubble forms in the reactor vessel head and two-phase natural circulation is established upon tripping the reactor coolant pumps. Depending on the break size, pressure may remain relatively constant for a prolonged period. Two-phase natural circulation will persist under these conditions provided that the steam generators are still available to remove heat and the steam generator tubes have not voided.

It is of particular interest in APEX-CE to observe the conditions required to interrupt two-phase natural circulation. Earlier APEX tests have demonstrated that even when the long tubes of the steam generator have stopped flowing, the short tubes will continue to provide primary loop flow.

$$(Q)_R = \frac{1}{276} \tag{4.99}$$

Because HPSI actuation conditions would be reached during a SBLOCA, the potential exists for the formation of cold plumes in the downcomer as a result of very low primary loop flows.

$$(Fr)_R = \frac{Q_R}{D_R^{5/2}} \tag{4.100}$$

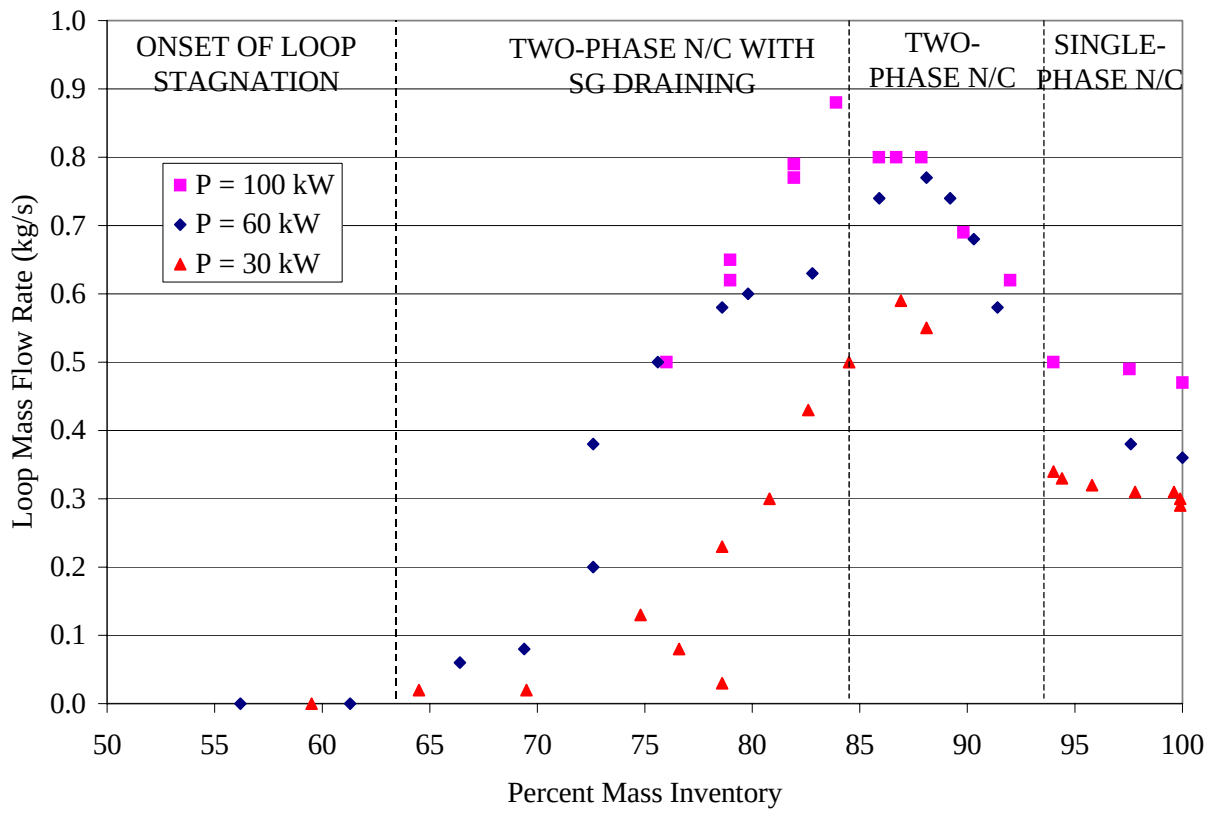

Figure 4.9 Semiscale Stepped-Inventory Reduction Test Data Showing Onset of Loop Stagnation

The USNRC has supported extensive studies of natural circulation cooling in U.S. pressurized water reactors.[15] Figure 4.9 presents natural circulation flow rate measurements obtained from stepped-inventory reductions in the Semiscale MOD-2A integral system test facility.[16] This data is plotted in terms of the normalized mass inventory, I, for a fixed core power and secondary-side pressure. Initially the system is at 100% inventory with a loop flow that is driven by single-phase natural circulation. As the inventory drops below ~95%, the mass flow rate increases because of the formation of vapor bubbles in the core. This marks the transition from single-phase to two-phase natural circulation.

The maximum loop flow rate is achieved when the static differential pressure between the hot upflow side of the u-tubes and the cold down flow side of the u-tubes is a maximum. This occurs when the void fraction is as large as possible in the hot upflow side and zero in the cold downflow side. The maximum is shown to occur at ~85% inventory for the data presented in Figure 4.9. As voids form in the downflow side of the u-tubes, (i.e., longest u-tubes in the steam generators begin to drain), the driving head is reduced and a decrease in loop flow rate is observed. When the inventory reaches ~ 65% in Figure 4.9, the net loop flow rate is essentially zero. This marks the start of the “reflux condensation” mode of operation and also signifies the onset of loop stagnation.

Duffey and Sursock[17] have developed a model to predict the core mass flow rate trends illustrated in Figure 4.9. Of particular interest to our present study, is their method of determining the primary-side inventory at which total loop stagnation occurs.

The primary-side, normalized mass inventory is defined as follows:

$$I = \frac{M}{M_o} \tag{4.103}$$

where M_o is the liquid mass that initially occupies the primary system. The liquid mass in the primary loop is divided into two regions; the mass contained in the hot-side volumes, V_{HS}, and that contained in the cold-side volumes, V_{CS}. The hot-side volume consists of the core, V_{core}, the upper plenum, V_U, the hot leg, V_{HL}, and the u-tubes on the upside of the steam generator, V_{SGU}. The cold-side volume consists of the u-tubes on the downside of the steam generator, V_{SGD}, the cold leg, V_{CL}, and the downcomer, V_{DC}.

Duffey and Sursock, indicate that the onset of reflux condensation, and hence loop stagnation, occurs when the normalized mass inventory becomes:

$$I_{STG} = 1 - \alpha_{HS}\left[\frac{V_{HS} + V_{CS}}{V_T}\right] \tag{4.104}$$

where the hot-side void fraction is given by:

$$\alpha_{HS} = \frac{\{\alpha_c\}(V_{core} + V_{SGU}) + \alpha_u V_u}{V_{core} + V_{SGU} + V_u} \tag{4.105}$$

The void fraction at the core exit, α_u, was obtained using the drift-flux relationship.[18] That is, the void fraction as a function of position in the core is:

$$\alpha(z) = \frac{j_g(z)}{C_o j(z) + v_{gj}} \tag{4.106}$$

At stagnant loop conditions, j_ℓ is zero, so equation (4.106) becomes:

$$\alpha(z) = \left[C_o + \frac{V_{gj}}{j_g(z)} \right]^{-1} \tag{4.107}$$

The volumetric vapor flux, j_g, is found by:

$$j_g(z) = \frac{1}{\rho_g a_c h_{fg}} \int_{L_{NB}}^{z} q'(z)dz \tag{4.108}$$

where L_{NB} is the non-boiling height.

The void fraction at the core exit is found by evaluating equation (4.107) and (4.108) at z equal to L_c, the core heated length. These equations are easily evaluated for semiscale because of its constant axial power profile. Thus for systems implementing a constant axial power profile; equation (4.108) becomes:

$$j_g(z) = \frac{q_{core}(z - L_{NB})}{\rho_g a_c h_{fg} L_c} \tag{4.109}$$

Neither APEX-CE nor Palisades have a constant axial power profile. Thus the integration were performed numerically.

The core averaged void fraction, $<\alpha_c>$, was obtained as follows:

$$\langle \alpha_c \rangle = \frac{1}{L_c} \int_{L_{NB}}^{L_c} \alpha(z)dz \tag{4.110}$$

Substituting equations (4.107) and (4.109) into (4.110) yields the core averaged void fraction for constant axial power:

$$\langle \alpha_c \rangle = \frac{1}{C_o}\left[1 - \frac{L_c}{C_o \Pi_z (L_c - L_{NB})} \, Ln\left(1 + \frac{C_o \Pi_z (L_c - L_{NB})}{L_c}\right)\right] \qquad \textbf{(4.111)}$$

where Π_z is the Zuber number, rearranged as:

$$\Pi_z - \frac{q_{core}}{\rho_g \, v_{gj} a_c h_{fg}} \qquad \textbf{(4.112)}$$

Equation (4.110) was numerically integrated for APEX-CE and Palisades.

Duffey and Sursock[17] used the churn-turbulent drift-flux correlation to assess equation (4.107). That is,

$$v_{gj} = 1.53 \left[\frac{\sigma g \Delta\rho}{\rho_\ell^2}\right]^{1/4} \qquad \textbf{(4.113)}$$

Table 4.2 presents the pertinent values needed to estimate the loop stagnation inventory in APEX-CE and Palisades for the special case of 3% decay power and saturated liquid at the core inlet. Figure 4.10 compares the void fraction profiles in Palisades and APEX-CE for an average subchannel. The difference in void fraction profiles arises because the power profiles have different shapes.

Table 4.2 Data used to Assess Onset of Loop Stagnation in Palisades and APEX-CE

	Palisades	APEX-CE	Units
Core Flow Area (a_c) =	5.3	0.072	m^2
Total Volume (Less PZR Volume) (V_T) =	266.2	0.924	m^3
Core Volume (V_{core}) =	17.7	0.065	m^3
Hot Leg Volume (2 HL) (V_{HL}) =	11.9	0.040	m^3
Upper Plenum Volume (Top of HL) (V_u) =	12.8	0.048	m^3
2 SG Upside U-Tube Volume (V_{SGU}) =	22.9	0.131	m^3
Cold Leg Volume (4 CL) (V_{CL}) =	33.1	0.117	m^3
Downcomer Volume (below HL) (V_{DC}) =	16.7	0.175	m^3
2 SG Downside U-Tube Volume (V_{SGD}) =	22.9	0.131	m^3
$V_{HS} = V_{core} + V_{HL} + V_u + V_{SGU}$ =	65.2	0.284	m^3
$V_{CS} = V_{CL} + V_{DC} + V_{SGD}$ =	72.7	0.423	m^3
3% Decay Power with Saturated Liquid at Core Inlet			
Pressure =	142.00	26.54	bars
Power (3% Decay) =	75.90	0.28	MW
ρ_g	88.93	13.27	kg/m^3
ρ_L	617.73	830.91	kg/m^3
σ	6.076E-03	3.140E-02	kg/s^2
h_g	2362.6	2802.5	kJ/kg
h_L	1578.8	976.8	kJ/kg
C_o =	1.22	1.22	
v_{gj} =	0.15	0.21	m/s
α_u =	0.48	0.45	
$<\alpha_c>$ =	0.29	0.23	
α_{HS} =	0.31	0.28	
Predicted Stagnation Inventory =	**0.82**	**0.79**	

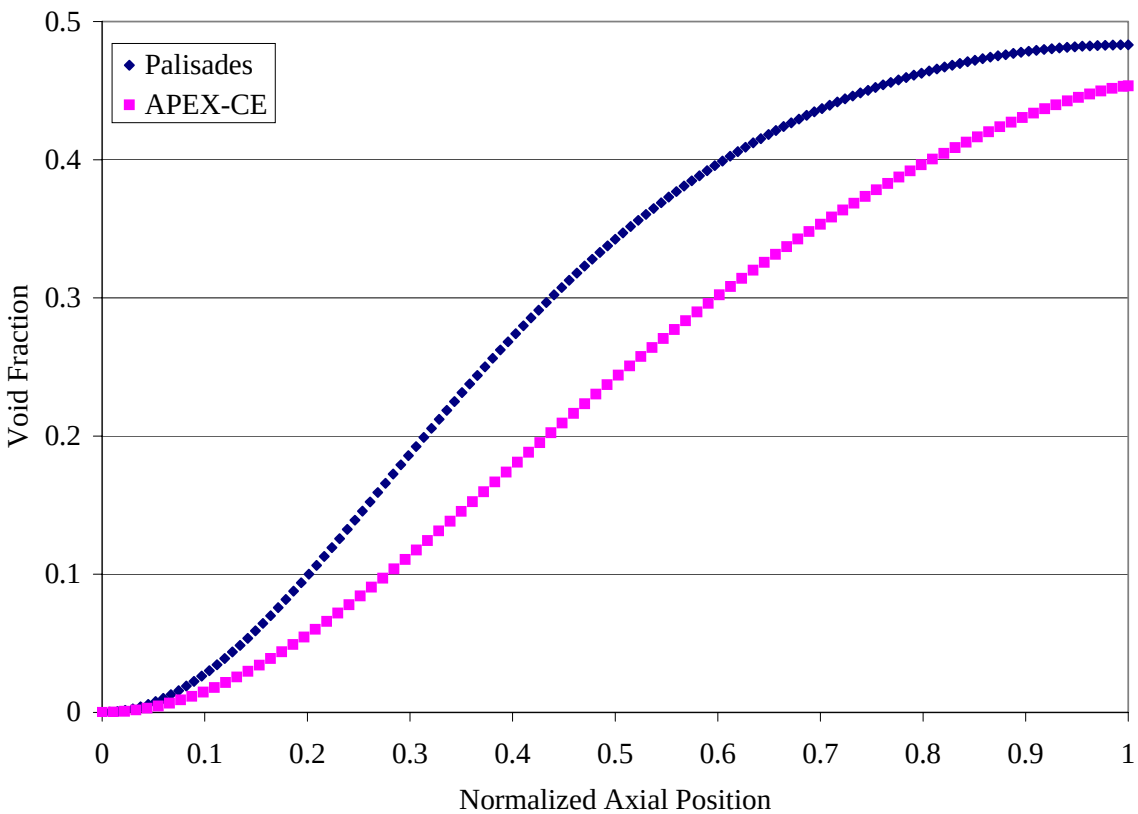

Figure 4.10 Comparison of APEX-CE and Palisades Void Fraction Profiles for 3% Decay Power

It has been assumed that Palisades has a chopped cosine axial power profile. Thus, the total power input is given by:

$$q(z) = \int_{-L_c/2}^{z} q'_c \cos\left(\frac{\Pi z}{L_c}\right) dz \qquad \textbf{(4.114)}$$

APEX-CE has a skewed power profile. Thus, the total power input is given by:

$$q(z) = \int_{o}^{Z} 3.11 q'_{avg} \left(\frac{z}{L_c}\right) \left(1 - \frac{z}{L_c}\right)^{1/3} dz \qquad \textbf{(4.115)}$$

Based on the Duffey and Sursock model, loop stagnation will occur at similar mass inventory fractions in Palisades and APEX-CE for the 3% decay power case examined.

4.3 SUMMARY

The single-phase natural circulation phenomenon of greatest importance to PTS is the primary loop volumetric flow rate which governs the onset of thermal stratification in the cold legs. The two-phase fluid natural circulation phenomena of greatest importance to PTS are the onset of primary loop stagnation during the SBLOCA and the flow regime transition from stratified flow to intermittent flow.

The single-phase fluid volumetric flow rate was scaled to preserve the onset of thermal stratification in the cold legs by requiring isochronicity. That is,

$$\tau_R = 1 \tag{4.116}$$

This resulted in a loop velocity ration and volumetric flow rate ratio of:

$$u_R = \frac{1}{4} \tag{4.117}$$

$$Q_R = \frac{1}{276} \tag{4.118}$$

Chapter 5 demonstrates how this result is used in the thermal stratification criterion to preserve the onset of thermal stratification in the cold legs.

The onset of primary loop stagnation during the SBLOCA was shown to be preserved in APEX-CE using the model developed by Duffey and Sursock.[17] this phenomena is important because primary loop stagnation reduces the mixing, and consequently the warming of the cold HPI fluid before it reaches the downcomer. Table 4.2 summarizes the results of the onset of loop stagnation analysis.

The transition from stratified two-phase fluid conditions to intermittent flow is important to PTS because the phenomenon can significantly impact mixing in the cold legs. Based on the work of Taitel and Dukler,[13] it was determined that the flow regime transition from stratified flow is preserved when the modified Froude number is identical to both systems. The scaling analysis indicates that:

$$(Fr)_R = \frac{1}{1.3} \tag{4.119}$$

and therefore this phenomenon is reasonably scaled in APEX-CE.

5.0 SCALING OF COLD LEG AND DOWNCOMER FLUID MIXING PHENOMENA

This chapter presents the scaling analysis used to assess the similarity between cold leg and downcomer thermal fluid mixing and heat transferin the APEX-CE test facility and that in the Palisades Plant. The results of this analysis were used to specify the HPSI nozzle diameter, the cold leg diameter and the HPSI fluid temperature in APEX-CE. The road map for this analysis is shown in Figure 5.1.

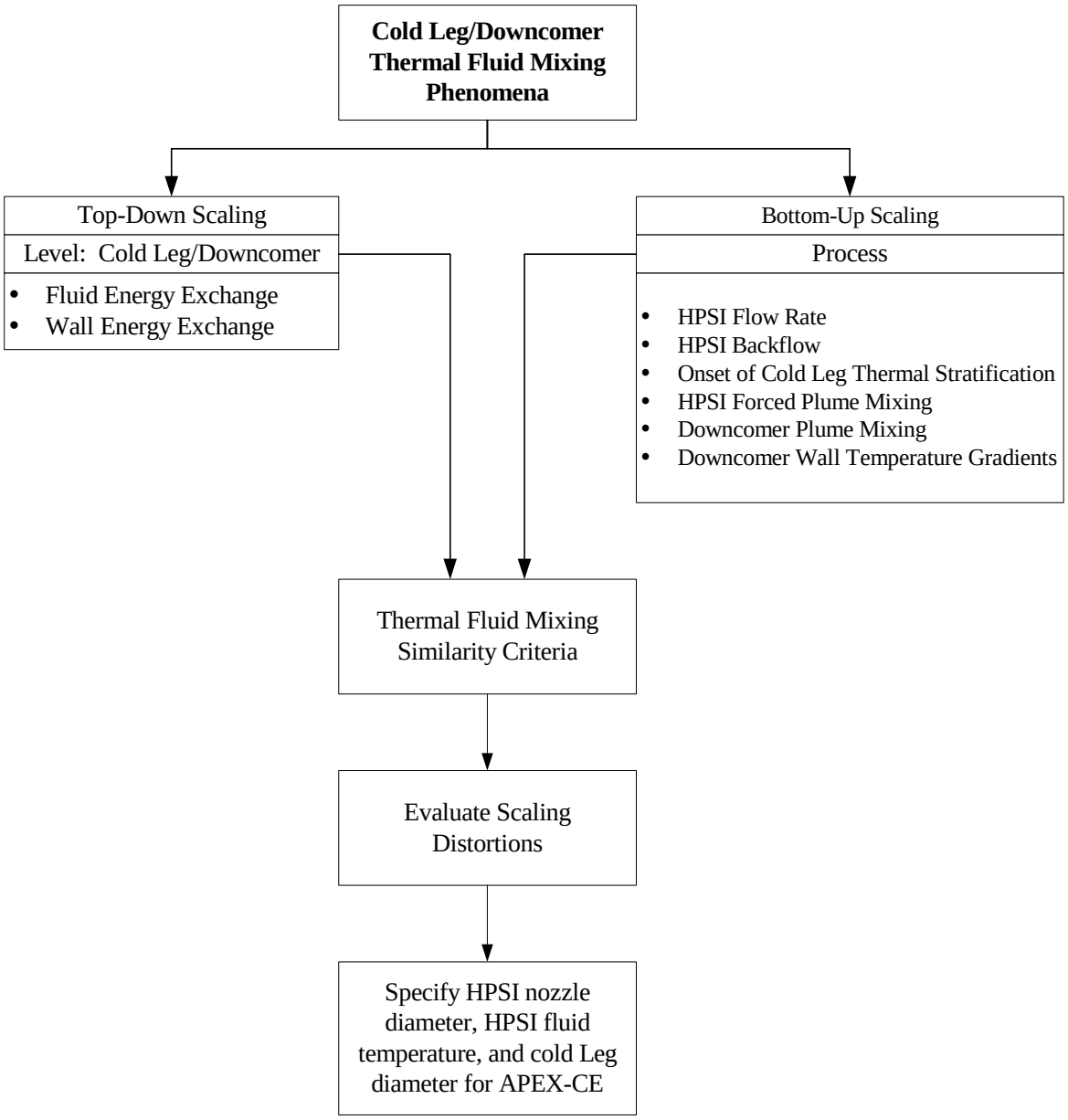

Figure 5.1. Scaling Analysis Flow Diagram for Cold Leg and Downcomer Thermal Fluid Mixing

The top down scaling analysis was performed for a control volume that consisted of the cold leg and a portion of the downcomer. This resulted in global similarity criteria which were closed using

the results of the bottom-up scaling analysis. The bottom-up scaling analysis was used to assess local phenomena such as the onset of thermal stratification in the cold legs, downcomer plume velocities and downcomer wall heat transfer.

5.1 Top-Down Scaling Analysis for Thermal Fluid Mixing

The control volume under consideration in this analysis is depicted in Figure 5.2. This control volume approach for cold leg and downcomer mixing was developed by Theofanous and Nourbakhsh and was used in the development of the REMIX computer code.[15-16] REMIX has been successfully benchmarked against fluid mixing data for systems ranging from 1/5 to full scale.[17]

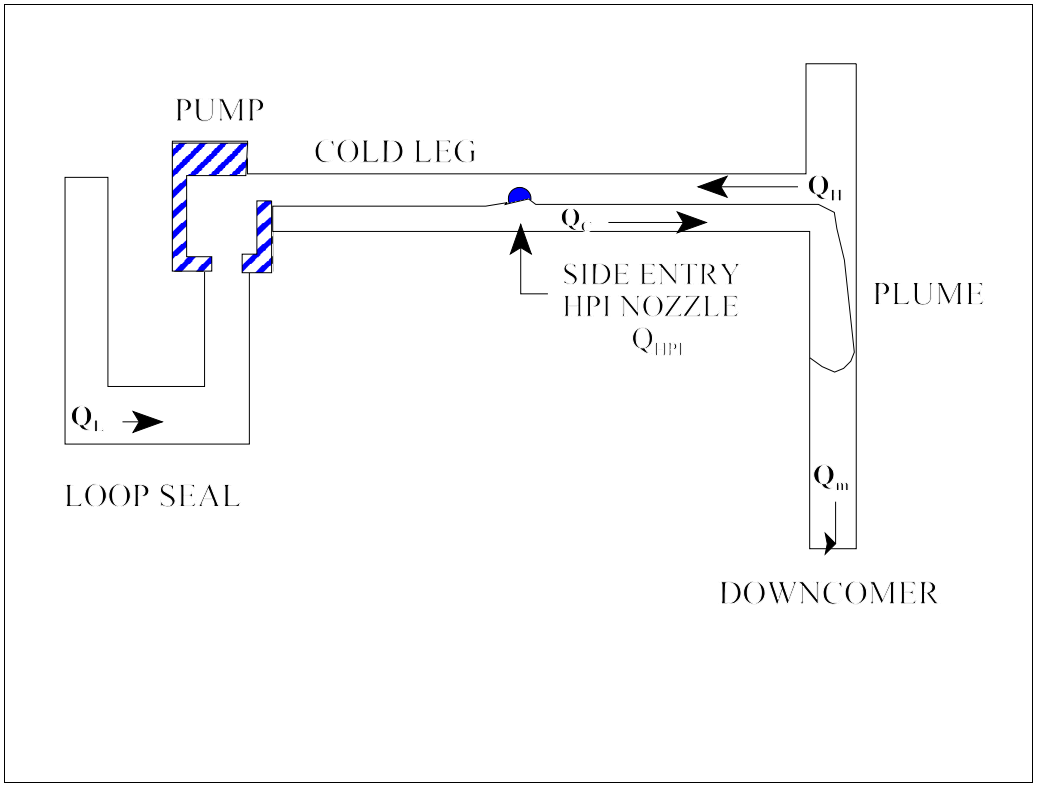

Figure 5.2. Control Volume for Top-Down Scaling Analysis Balance Equations

Cold water enters the control volume through the HPSI nozzle located at the side of the cold leg. The HPSI volumetric flow rate is given by Q_{HPI}. If the loop natural circulation rate, Q_L, is sufficiently low, the cold HPSI water falls to the bottom of the cold leg and spreads towards the loop seal and the downcomer. For the Palisades plant, the reactor coolant pump geometry limits the amount of cold water spilling into the loop seal. Hot water is entrained into the HPSI plume. The cold stream height formed by the HPSI flow is limited by the counter-current flow pattern established at the cold leg/downcomer junction. A hot stream of water from the downcomer rushes into the top of the cold leg while a cold stream of water exits from the bottom of the cold leg into the downcomer. A cold turbulent plume forms in the downcomer and mixes with the hot water as it travels downward. A thermally well mixed fluid leaves the control volume via the lower plenum at a volumetric flow rate, Q_m.

This section examines the scaling requirements for the transient cooling of fluid in the entire control volume as depicted in Figure 5.2. The control volume balance equations are formulated in terms of an average mixture temperature, T_m, for the fluid and an average temperature of the metal structure, T_s. The local heat transfer coefficients and temperature gradients in the vicinity of the plume are examined in the bottom-up scaling analysis.

The top-down mass balance equation for this control volume is as follows:

$$V\frac{d\rho_m}{dt} = Q_{HPI}\rho_{HPI} + Q_L\rho_L - Q_m\rho_m \tag{5.1}$$

The energy balance equation for this control volume in terms of enthalpies is as follows:

$$V\frac{d}{dt}\left(\rho_m h_m\right) = Q_{HPI}\rho_{HPI}h_{HPI} + Q_L\rho_L h_L - Q_m\rho_m h_m + q_{DC} \tag{5.2}$$

Expanding the left-hand side of equation 5.2 and substituting equation 5.1 yields:

$$V\rho_m\frac{dh_m}{dt} = Q_{HPI}\rho_{HPI}\left(h_{HPI} - h_m\right) + Q_L\rho_L\left(h_L - h_m\right) + q_{DC} \tag{5.3}$$

which can be written in terms of fluid temperatures as follows:

$$v\rho_m C_p\frac{dT_m}{dt} = Q_{HPI}\rho_{HPI}C_p\left(T_{HPI} - T_m\right) + Q_L\rho_L C_p\left(T_L - T_m\right) + q_{DC} \tag{5.4}$$

where T_{HPI} and T_L are constant.

The energy equation for the downcomer walls is given by:

$$-V_s\rho_s C_{ps}\frac{dT_s}{dt} = q_{DC} \tag{5.5}$$

where a decrease in the average slab temperature means heat added to the fluid. Substituting equation (5.5) into (5.4) yields:

$$V\rho_m C_p\frac{dT_m}{dt} + V_s\rho_s C_{ps}\frac{dT_s}{dt} = Q_{HPI}\rho_{HPI}C_p\left(T_{HPI} - T_M\right) + Q_L\rho_L C_p\left(T_L - T_m\right) \tag{5.6}$$

5.1.1 Diabatic Mixing (Heterogeneous Approximation)

The exchange of energy between the downcomer walls and the fluid occurs over the entire length of the interface. The actual heat transfer process is likely not to be uniform and for the condition

of cold plume intrusion, would be highly localized. However, for the global mixing conditions considered in this section, the heat transfer from the wall can be easily approximated because we are dealing with averaged fluid and wall temperatures.

The boundary condition at the downcomer wall can be expressed as:

$$\langle h \rangle \left(T_s - T_m\right) = -\frac{k_s}{b}\left(T_s - T_o\right) \tag{5.7}$$

where <h> is the average heat transfer coefficient over length of the downcomer, T_o is the temperature of the outer surface of the heated slab, and "b" is the thickness of the slab. Taking the derivative of this equation with respect to time yields:

$$\langle h \rangle \left(\frac{dT_s}{dt} - \frac{dT_m}{dt} \right) = -\frac{k_s}{b}\frac{dT_s}{dt} \tag{5.8}$$

where it has been assumed that the average heat transfer coefficient is constant. Rearranging this equation yields:

$$\frac{dT_s}{dt} = F\,\frac{dT_M}{dt} \tag{5.9}$$

where F describes the thermal coupling between the heated slab and the fluid. It is defined as:

$$F = \frac{\langle Bi \rangle}{\left[1 + \langle Bi \rangle\right]} \tag{5.10}$$

The average Biot number, <Bi>, is defined as:

$$\langle Bi \rangle = \frac{\langle h \rangle\, b}{k_s} \tag{5.11}$$

The value of F will range from zero to one as the Biot number ranges from zero to infinity. A value of F equal to one means perfect thermal coupling whereas a value of zero implies adiabatic conditions.

Substituting equation (5.9) into equation (5.6) yields:

$$\left[V \rho_m C_p + F\, V_s \rho_s C_{ps}\right] \frac{dT_m}{dt} = Q_{HPI}\rho_{HPI} C_p \left(T_{HPI} - T_m\right) + Q_L \rho_L C_p \left(T_L - T_m\right) \tag{5.12}$$

Dividing by $\rho_{HPI} C_p \left(Q_{HPI} + Q_L\right)$ and neglecting the fluid density differences yields:

$$\tau_m \frac{dT_m}{dt} = \frac{Q_{HPI}\left(T_{HPI} - T_m\right)}{\left(Q_{HPI} + Q_L\right)} + \frac{Q_L\left(T_L - T_m\right)}{\left(Q_{HPI} + Q_L\right)} \tag{5.13}$$

where the heterogeneous mixture time constant, τ_m is given by:

$$\tau_m = \frac{1}{\left(Q_{HPI} + Q_L\right)}\left[V + \frac{F\, V_s \rho_s C_{ps}}{\rho_{HPI} C_p}\right] \tag{5.14}$$

Equation (5.13) is a linear, first order, differential equation with constant coefficients (assuming T_L, T_{HPI}, Q_L, and Q_{HPI} are constant). Its solution is given by:

$$T_m(t) = T_I + \left(T_L - T_I\right) e^{\left(-\frac{t}{\tau_m}\right)} \tag{5.15}$$

where the ideally mixed fluid temperature is defined as:

$$T_I = \frac{Q_{HPI} T_{HPI} + Q_L T_L}{Q_{HPI} + Q_L} \tag{5.16}$$

Equation (5.16) is the perfect mixed mean temperature as used by Levy[18] and (Rothe and Wallis)[19] with regards to global mixing in the downcomer. For example, the case of stagnant loop conditions requires that Q_L equal zero, thus equation (5.14) becomes:

$$T_m(t) = T_{HPI} + \left(T_L - T_{HPI}\right) e^{-\left(\frac{t}{\tau_{HPI}}\right)} \tag{5.17}$$

where the time constant, τ_{HPI}, is defined as:

$$\tau_{HPI} = \frac{1}{Q_{HPI}}\left[V + \frac{F\, V_s \rho_s C_{ps}}{\rho_{HPI} C_p}\right] \tag{5.18}$$

For adiabatic conditions, F is equal to zero and equation (5.18) becomes:

$$\tau_{HPI}(F = 0) = \frac{V}{Q_{HPI}} \tag{5.19}$$

Equations (5.17) and (5.19) where used by (Fanning and Rothe) to approximate the adiabatic CREARE 1/5- scale data.[24]

The CREARE 1/2- scale tests included wall heat transfer. Assuming F equal to one in equation (5.18) yields:

$$\tau_{HPI}(F=1)=\frac{1}{Q_{HPI}}\left[V+V_s\frac{\rho_s C_{ps}}{\rho_{HPI}C_p}\right] \tag{5.20}$$

which is the time constant used by Valenzuela and Dolan to approximate the CREARE 1/2-scale data.[25]

5.1.2 Dimensionless Equations for Downcomer Mixing

Equation (5.13) is the governing equation for the mixed mean fluid temperature in the downcomer. It can be re-written in terms of the perfectly mixed fluid temperature as follows:

$$\tau_m \frac{d}{dt}\left(T_m - T_I\right) = -\left(T_m - T_I\right) \tag{5.21}$$

This equation can be made dimensionless using the following definition based on the initial conditions in the control volume:

$$\left(T_m - T_I\right) = \left(T_L - T_I\right)_o \left(T_m - T_I\right)^+ \tag{5.22}$$

Substituting into equation (5.21) yields:

$$\tau_m \frac{d}{dt}\left(T_m - T_I\right)^+ = -\left(T_m - T_I\right)^+ \tag{5.23}$$

Based on this result, the analysis of the transient cooldown of the downcomer will implement the following dimensionless time scale:

$$t^+ = \frac{t}{\tau_m} \tag{5.24}$$

and the dimensionless temperature scale:

$$\Pi_T = \frac{T_m - T_I}{T_L - T_I} \tag{5.25}$$

Figures 5.3 and 5.4 compare equations (5.17) and (5.18) to the CREARE 1/2- scale data.

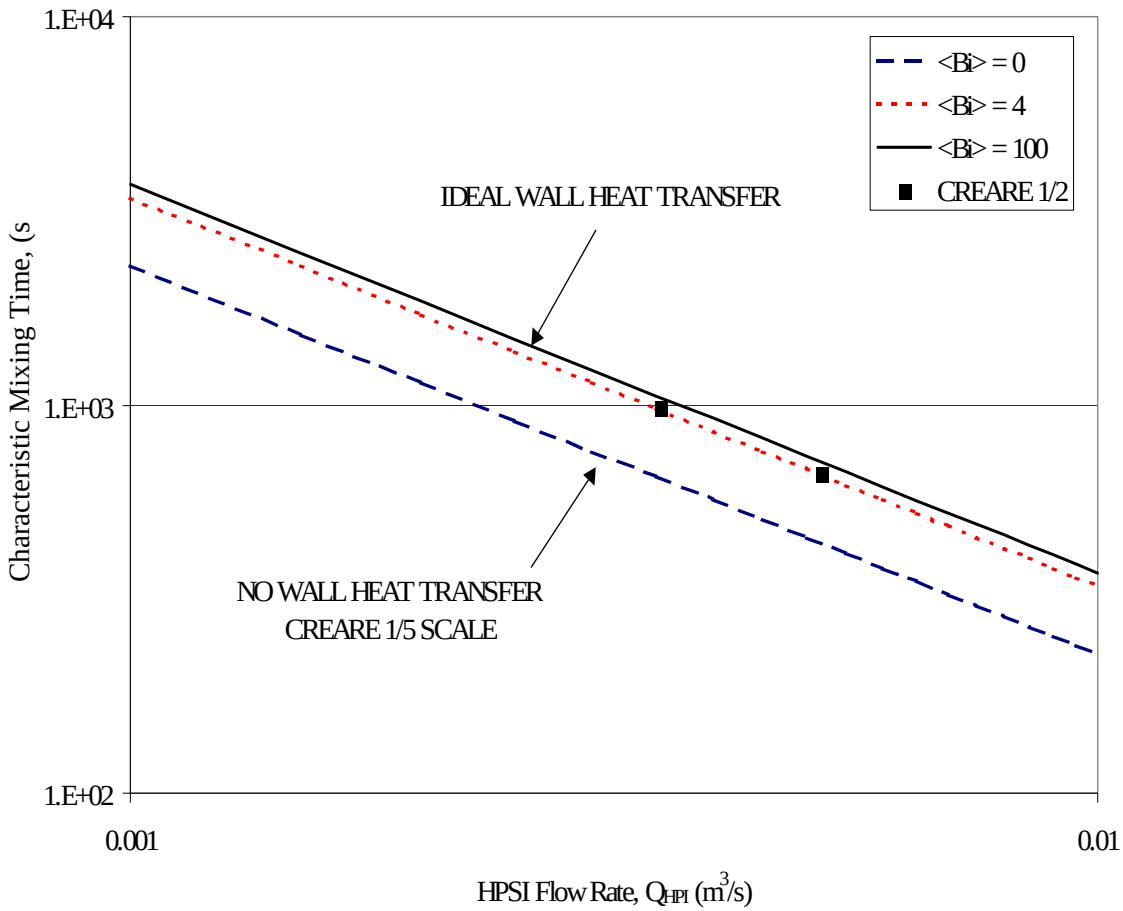

Figure 5.3 Comparison of the Heterogeneous Mixture Time Constant to CREARE 1/2-Scale Data

The time constant for the CREARE 1/2-scale data are best fit with a <Bi> of 4.

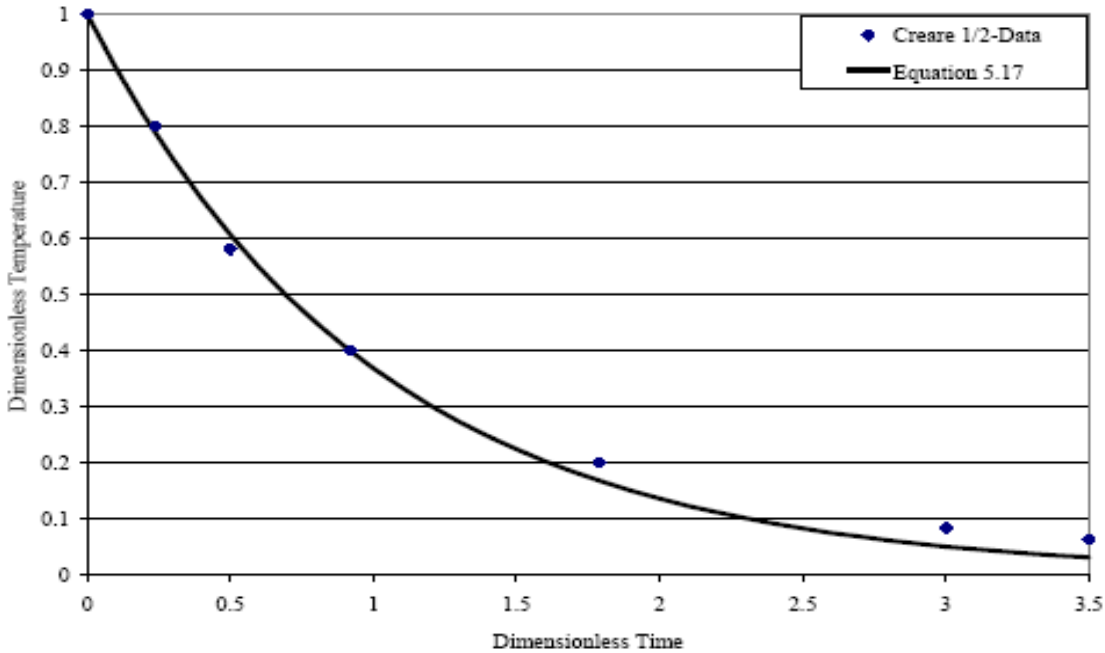

Figure 5.4 Comparison of Equation (5.17) to CREARE 1/2-Scale Data

Figure 5.4 shows that equation (5.17) is in good agreement with the CREARE 1/2-scale mixed mean temperature data.

In conclusion, the top-down scaling analysis has identified two key dimensionless parameters; a dimensionless time scale t^+ and a dimensionless temperature scale, Π_T. This Π group and time scale will be evaluated and compared for conditions in the APEX-CE test facility and the Palisades Plant.

5.2 Bottom-Up Scaling Analysis for Thermal Fluid Mixing

This section presents scaling analyses for the bottom-up processes described in the flow chart of Figure 5.1. It includes the following:

1. a description of the HPSI flow rates as a function of scaled pressures
2. a criterion for the onset of backflow in the HPSI nozzle
3. a criterion for the onset of cold leg thermal stratification
4. dimensionless equations for the HPSI forced plume mixing
5. dimensionless equations for downcomer plume mixing
6. dimensionless equations for downcomer wall heat transfer

This section includes comparisons of REMIX calculations for cold leg and downcomer thermal fluid mixing under stagnant loop conditions for comparable APEX-CE and Palisades cases.

5.2.1 HPSI Flow Rate

The Palisades high pressure safety injection system nominal flow curve has been modeled in the APEX-CE facility on a scaled basis. The reference pressure used for Palisades is 900 psia, which corresponds to the steam generator pressure maintained by the turbine bypass valves following a reactor trip. Similarly, the reference pressure for APEX-CE is 293 psia which is the saturation pressure for the nominal cold leg temperature. The relationship between Palisades and APEX-CE steam generator pressures is described in Tables 6.3, 7.3, and 7.6. Figure 5.5 presents the nominal HPSI flow curve for the Palisades plant.[22] Figure 5.6 presents the same curve for the APEX-CE plant. The basis for pressure scaling is described in Chapter 6.

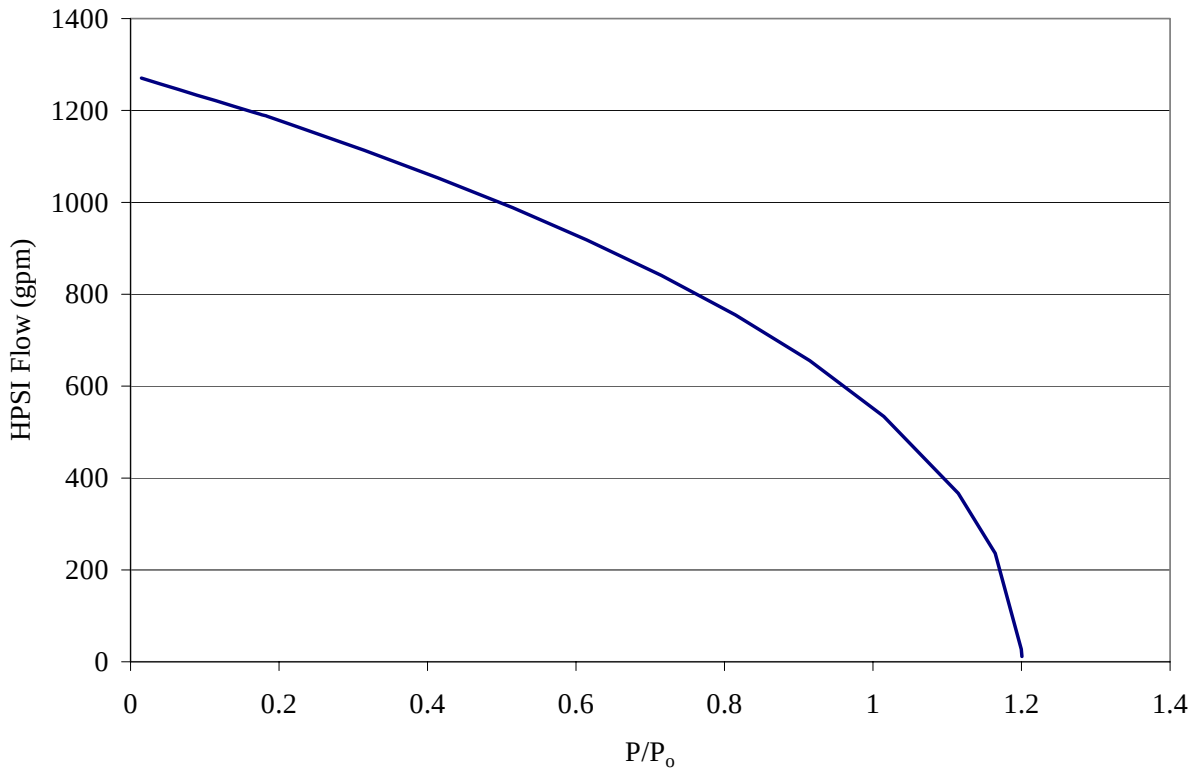

Figure 5.5 HPSI Flow Rates as a Function of Normalized Pressure for Palisades

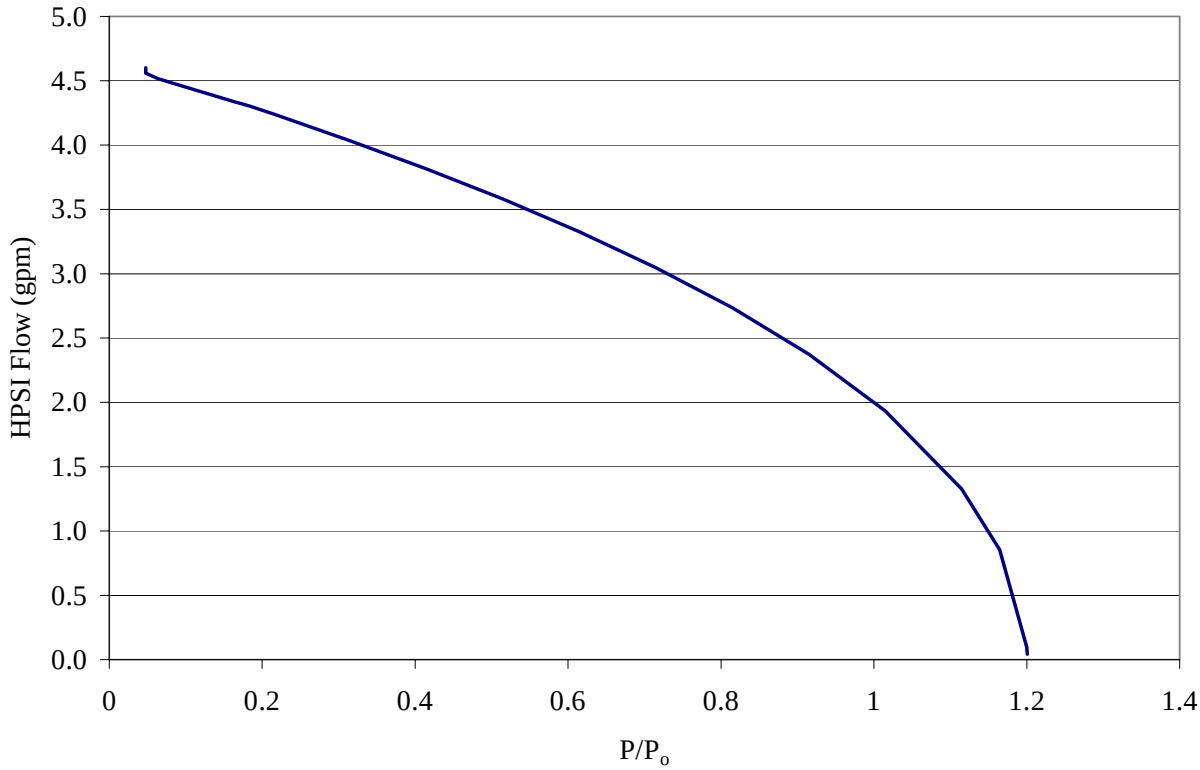

Figure 5.6 HPSI Flow Rates as a Function of Normalized Pressure for APEX-CE

5.2.2 Bottom-Up Scaling Analysis for the Onset of Backflow at the HPSI Nozzle

The relatively low flow rates through the large diameter HPSI nozzle suggests the potential for the backflow of hot water into the horizontal HPSI nozzle as depicted in Figure 5.5. Simulating this phenomena in the APEX-CE requires that the following similarity criteria be satisfied.

$$\left(Fr_{HPI}\right)_R = 1 \tag{5.26}$$

where the HPSI Froude number is defined as:

$$Fr_{HPI} = \frac{Q_{HPI}}{a_{HPI}\left[g D_{HPI} \frac{\left(\rho_{HPI} - \rho_{CL}\right)}{\rho_{HPI}}\right]^{\frac{1}{2}}} \tag{5.27}$$

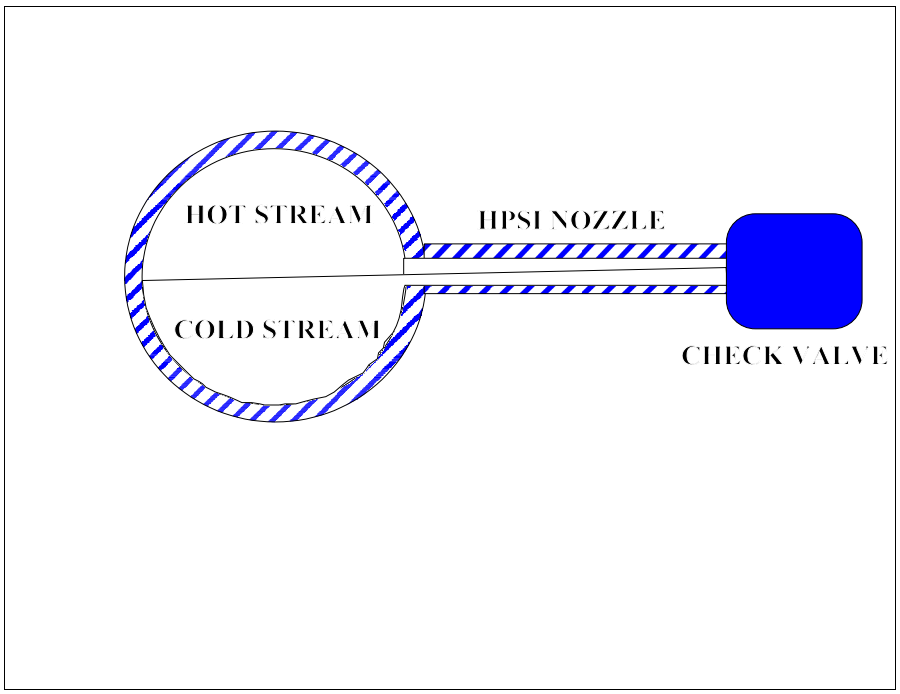

Figure 5.7 Buoyant Backflow into the Horizontal HPSI Line

Substituting equation (5.27) into (5.26) and rearranging, yields the following scaling criterion for the HPSI nozzle diameter:

$$\left(D_{HPI}\right)_R = \left(Q_{HPI}\right)_R^{\frac{2}{5}} \left(\frac{\Delta\rho}{\rho}\right)_R^{-\frac{1}{5}} \qquad \textbf{(5.28)}$$

This criterion has been used to size the APEX-CE HPSI nozzle diameter. Figure 5.8compares the calculated values of Fr_{HPI} for APEX-CE with that for Palisades for the full range of HPSI flow conditions. This figure indicates that the Fr_{HPI} for APEX-CE overlays that of Palisades almost exactly.

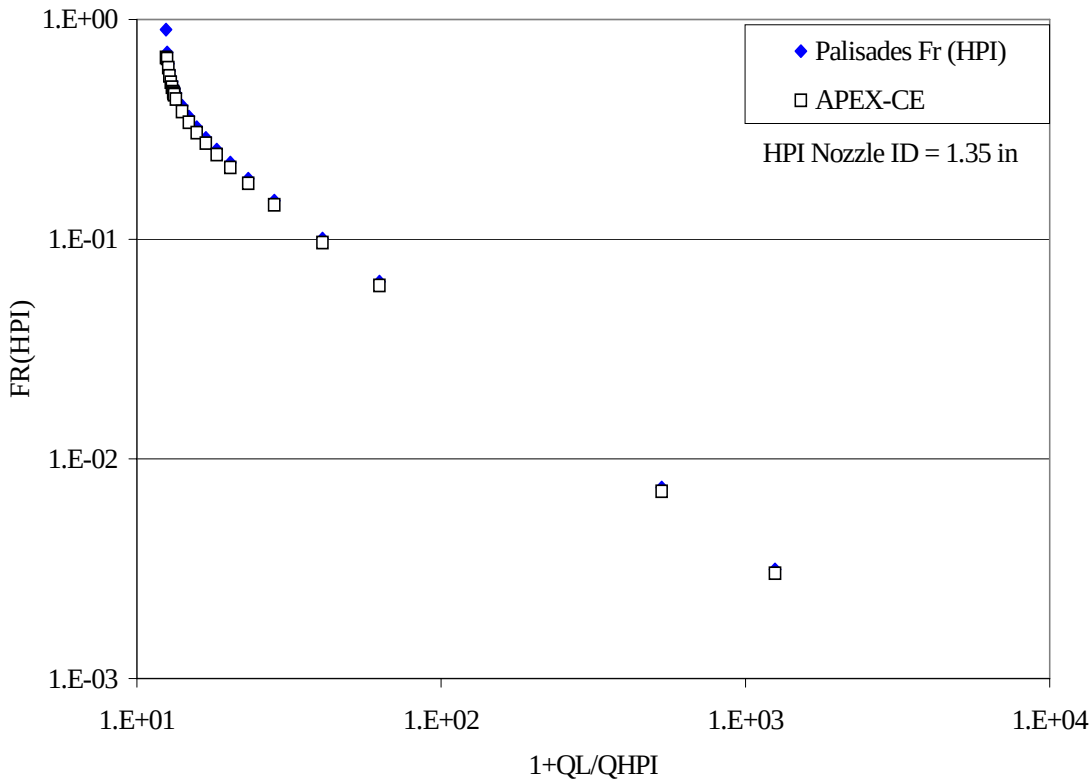

Figure 5.8 Comparison of Fr_{HPI} for Palisades and APEX-CE

5.2.3 The Onset of Cold Leg Thermal Stratification

This section presents the scaling rationale for preserving the conditions for the onset of thermal stratification in the APEX-CE cold legs. The result of this analysis is a set of scaling ratios for the cold leg diameter and the HPSI volumetric flow rate.

Theofanous, et al.,[20] successfully correlated a significant amount of cold leg thermal stratification data using the following criterion:

$$Fr_{HPI/CL} = \left[1 + \frac{Q_L}{Q_{HPI}}\right]^{-\frac{7}{5}} \tag{5.29}$$

where Q_L is the volumetric flow rate through a cold leg, Q_{HPI} is the volumetric flow rate through a single HPSI nozzle and $Fr_{HPI/CL}$ is the superficial Froude Number defined as:

$$Fr_{HPI/CL} = \frac{Q_{HPI}}{a_{CL}\left[gD_{CL}\dfrac{\rho_{HPI} - \rho_{CL}}{\rho_{HPI}}\right]^{1/2}} \tag{5.30}$$

Equation (5.29) was derived by assuming that a mixture Froude number of unity implies perfect mixing. This line of reasoning led to the following equation:

$$Fr_{HPI/CL} = \left[\frac{\beta_m}{\beta_{HPI}}\right]^{-\frac{1}{2}} \left[1 + \frac{Q_L}{Q_{HPI}}\right]^{-\frac{3}{2}} \qquad \textbf{(5.31)}$$

which was modified to obtaining equation (5.29).

Although equation (5.29) fits the data quite well, several questions arise with respect to the characteristic length scale used to predict the onset of thermal stratification. That is, it is not intuitively obvious that the cold leg diameter should serve as the characteristic length for this process. The following section presents a new analysis of the problem which yields considerably different results at low loop flow rates.

5.2.3.1 Hydraulic Jump Leading to Perfect Mixing

Consider the case of two immiscible fluids of different density flowing under stratified conditions as shown in Figure 5.9.

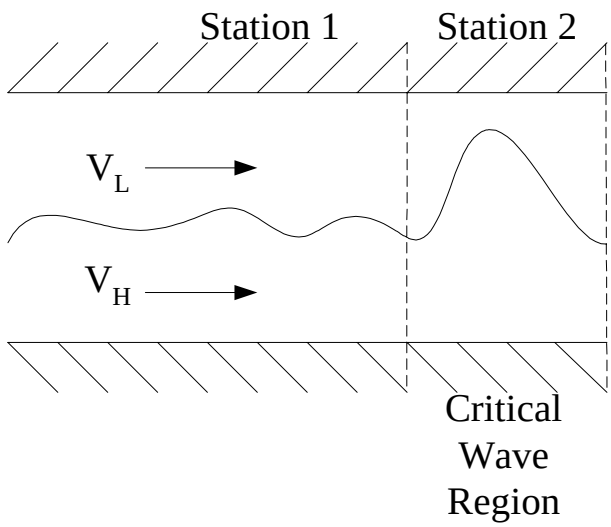

a) Critical wave height at inception of slug formation

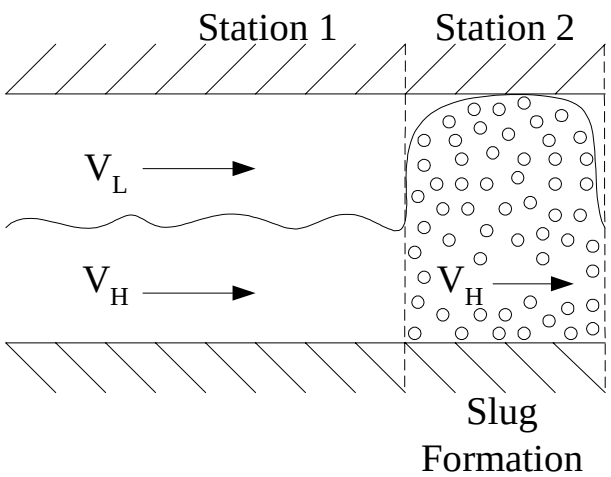

b) Equivalent fluid mixture geometry at inception

Figure 5.9 Hydraulic Jump Leading to Perfect Mixing

At station 1, the light fluid has a velocity, v_L, and flows over a heavier fluid which has a velocity, v_H. As the relative velocity of the fluids increases, the interface becomes wavy and a distribution of wave heights develops. If the height of any of the wave crests exceeds a critical value, a hydraulic jump occurs and both fluids become uniformly mixed at Station 2. The fact that there is a distribution of wave heights makes the slug formation a stochastic process. In essence, the inlet relative velocity affects the wave height distribution and the critical wave height, coupled with the local relative velocity, causes slug formation.

Analysis of this problem is straightforward if one recognizes that the critical wave height condition at the inception of slugging, as depicted in Figure 1(a), can be approximated by the fluid mixture

slug condition depicted in Figure 1(b). That is, the area fraction for the light fluid at the critical wave height equals the area fraction for the light fluid dispersed within the mixture at slug formation. Beyond station 2, the fluid mixture slug is assumed to move at a new velocity, v_m. Both fluids are assumed to be incompressible and no phase change occurs. The fluids could be oil and water or gas and liquid. An examination of the results will show that this analysis is also applicable to the fluid mixing case of interest to this study.

The following definitions will be useful. The area fraction of the light fluid at Stations 1 and 2 have been denoted by α_1 and α_2 respectively, that is:

$$\alpha_1 = \left(\frac{A_L}{A}\right)_1 \tag{5.32}$$

and

$$\alpha_2 = \left(\frac{A_L}{A}\right)_2 \tag{5.33}$$

where A is the pipe cross-sectional area. The fluid velocities have been expressed in terms of volumetric flow rates, Q, as follows:

$$v_H = \frac{Q_H}{(1 - \alpha_1)A} \tag{5.34}$$

$$v_L = \frac{Q_L}{\alpha_1 A} \tag{5.35}$$

and

$$v_m = \frac{Q_H + Q_L}{A} \tag{5.36}$$

The analysis proceeds by writing the continuity equation and Bernoulli's equation for each fluid. The continuity equation for the heavy fluid is written as follows:

$$\rho_H v_H (1 - \alpha_1) A = \rho_H v_m (1 - \alpha_2) A \tag{5.37}$$

Substituting equations (5.33) and (5.35) and rearranging yields:

$$\frac{Q_L}{Q_H} = \frac{\alpha_2}{(1 - \alpha_2)} \tag{5.38}$$

Bernoulli's equation for each fluid is written as:

Heavy Fluid:

$$P_1 + \frac{\rho_H v_H^2}{2} + \rho_H g D(1 - \alpha_1) = P_2 + \frac{\rho_H v_m^2}{2} + \rho_H g D(1 - \alpha_2) \tag{5.39}$$

Light Fluid:

$$P_1 + \frac{\rho_L v_L^2}{2} - \rho_L g D \alpha_1 = P_2 + \frac{\rho_L v_m^2}{2} - \rho_L g D \alpha_2 \tag{5.40}$$

The pressures are evaluated at the interface. Substituting equations (5.33) through (5.35) into these two equations yields the Bernoulli equations in terms of volumetric flow rates. Solving each of the two equations for ΔP and equating the results yields a single equation. Using equation (5.37) and performing significant algebra, yields the final result:

$$\frac{\rho_H Q_H^2}{g D \Delta\rho A^2 (1 - \alpha_1)^2} \left[\frac{2 - (\alpha_1 + \alpha_2)}{2(1 - \alpha_2)^2} \right] + \frac{\rho_L Q_L^2}{g D \Delta\rho A^2 \alpha_1^2} \left[\frac{(\alpha_1 + \alpha_2)}{2\alpha_2^2} \right] = 1 \tag{5.41}$$

This is the governing equation for the hydraulic jump. It shall be assumed that when the height at Station 2, exceeds some critical value, then a transition from stratified to mixed conditions will occur. That is, the transition occurs when:

$$\alpha_2 = \alpha_{critical} \tag{5.42}$$

In their studies of stratified to slug flow transitions in air-water systems, Mishima and Ishii[27], and Kordyban[28] calculated critical wave lengths for the onset of slugging based on the Kelvin-Helmholtz instability. Gardner[29] used a different approach. He used an integrated energy equation to obtain the critical condition.

The following critical conditions is consistent with the air-water data of Wallis[30] and Kordyban[28] and the fluid mixing data of CREARE[24]. This is a preliminary correlation that predicts the behavior well when and when . $\rho_H \gg \rho_L$ $\rho_H \approx \rho_L$

$$\text{For } \rho_H \approx \rho_L ; \alpha_{critical} \approx \alpha_1$$

$$\text{For } \rho_H >> \rho_L ; \alpha_{critical} \approx \frac{\phi}{4}\alpha_1 \tag{5.43}$$

ϕ is the golden mean which results from solving for the Wallis correlation.[30] For the fluid density differences applicable to this problem, equations (5.42) and (5.43) indicates that:

$$\alpha_{critical} = \alpha_2 \approx \alpha_1 \tag{5.44}$$

For the fluid density differences applicable to this problem, equation (5.43) indicates that: Substituting this critical condition into equation (5.40) will yield the flow conditions for the hydraulic jump. The result is the following equation for the critical condition:

$$\frac{\rho_H Q_H^2}{gD\Delta\rho A^2(1-\alpha_1)^3} + \frac{\rho_L Q_L^2}{gD\Delta\rho A^2 \alpha_1^3} = 1 \tag{5.45}$$

Writing this equation in terms of velocity, yields:

$$\frac{\rho_H v_H^2}{gD\Delta\rho(1-\alpha_1)} + \frac{\rho_L v_L^2}{gD\Delta\rho\alpha_1} = 1 \tag{5.46}$$

Defining the Froude number for each fluid as follows:

$$Fr_k = \frac{\rho_k v_k^2}{gD\Delta\rho(1-\alpha_1)} \tag{5.47}$$

and substituting into equation (5.45) yields the following well known equation.

$$Fr_H^2 + Fr_L^2 = 1 \tag{5.48}$$

It arises in Kelvin-Helmholtz instability studies and the classic “Lock Exchange” problem. This is the governing equation for the transition from stratified to well mixed conditions. It should be noted in equation (5.45) that the governing length scales are the respective fluid heights, $D\alpha_1$ and $D(1-\alpha_1)$

as opposed to the pipe diameter. However, equation (5.48) can be arranged into a form similar to that given by the equation (5.31). Substituting the critical condition, equation (5.44) into equation (5.37) yields the following equation:

$$\frac{Q_L}{Q_H} = \frac{\alpha_1}{(1 - \alpha_1)} \tag{5.49}$$

Substituting this result into equation (5.45) and rearranging to obtain an expression in terms of the $Fr_{HPI/CL}$ yields:

$$Fr_{HPI/CL} = \left[1 + \frac{\rho_L Q_H}{\rho_H Q_L}\right]^{-\frac{1}{2}} \left[1 + \frac{Q_L}{Q_{HPI}}\right]^{-\frac{3}{2}} \tag{5.50}$$

which is of the same form as equation (5.31).

Figure 5.10 compares equations (5.29) and (5.50) with the CREARE 1/5-scale mixing data.

It is observed that the two criteria are nearly identical at the high loop flow to injection flow ratios (i.e., $Q_L/Q_{HPI} >> 1$). The two criteria diverge significantly as Q_L/Q_{HPI} approaches 1. Fortunately for our study, the conditions of interest are at the high values of Q_L/Q_{HPI} as is shown in Figures 5.11 through 5.14.

Figure 5.11 presents the calculated values for $Fr_{HPI/CL}$ for the full range of HPSI flows during forced circulation in the Palisades plant. Under these conditions, this criterion indicates that the cold leg fluid would be well-mixed. Therefore, the focus of the bottom-up scaling will be HPSI injection during single-phase natural circulation in the primary loop.

To accurately simulate the onset of cold leg thermal stratification in the APEX-CE facility, it was required that the ratio of the superficial Froude numbers be unity. That is,

$$\left(Fr_{HPI/CL}\right)_R = 1 \tag{5.51}$$

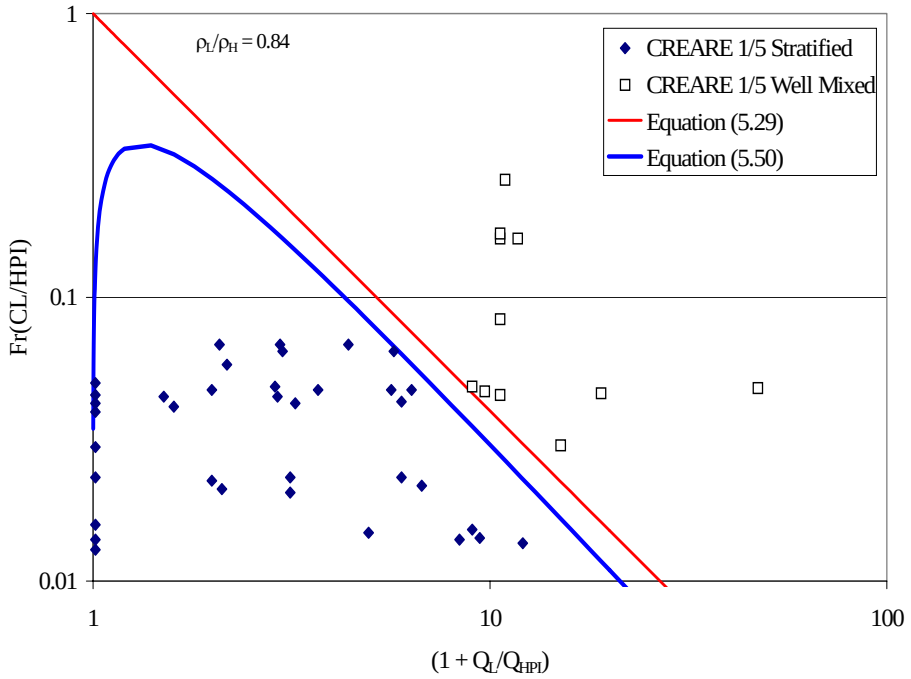

Figure 5.10 Comparison of Thermal Stratification Criteria with CREARE ½ Scale Mixing Data

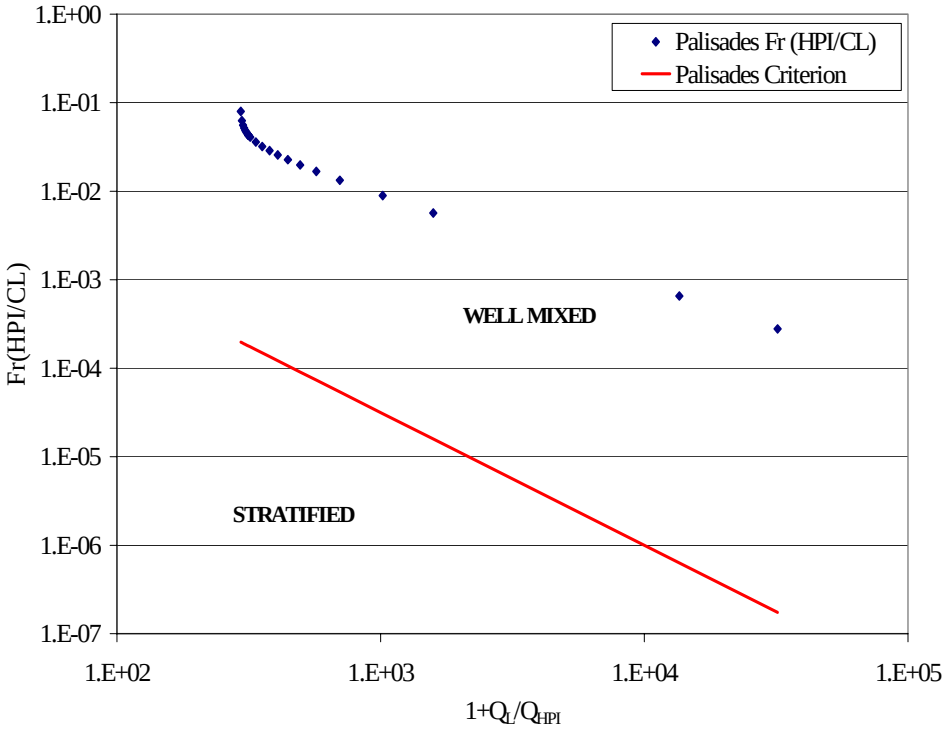

Figure 5.11 Assessment of Cold Leg Thermal Stratification During Forced Flow Conditions for Palisades HPSI

Applying this requirement to equation (5.50) yields for the region of interest:

$$\left(\frac{Q_L}{Q_{HPI}}\right)_R = 1 \tag{5.52}$$

That is, the term of $\rho_L Q_H/\rho_H Q_L$ is very small.

Applying the requirement of equation (5.51) to equation (5.30) and rearranging yields cold leg diameter scaling criterion:

$$(D_{CL}) = (Q_{HPI})_R^{\frac{2}{5}} \left(\frac{\Delta\rho}{\rho}\right)_R^{-\frac{1}{5}} \tag{5.53}$$

Here, use has been made of the fact that the area ratio is the square of the diameter ratio. This equation can be expressed in terms of the volumetric flow rate of the cold leg by substituting equation (5.52) to obtain:

$$(D_{CL})_R = (Q_L)_R^{\frac{2}{5}} \left(\frac{\Delta\rho}{\rho}\right)_R^{-\frac{1}{5}} \tag{5.54}$$

The volumetric flow rate through the loop is needed to provide closure to this similarity criterion. This is obtained from the top-down natural circulation scaling analysis. In that analysis, the volumetric flow rate ratio was determined to be:

$$(Q_L)_R = \frac{1}{276} \tag{5.55}$$

Substituting this value into equation (5.52) yields:

$$(Q_{HPI})_R = \frac{1}{276} \tag{5.56}$$

Substituting equation (5.55) into equation (5.54) yields:

$$(D_{CL})_R = \left(\frac{1}{276}\right)^{\frac{2}{5}} \left(\frac{\Delta\rho}{\rho}\right)_R^{-\frac{1}{5}} \tag{5.57}$$

Hence the scaling ratios for the HPSI volumetric flow rate and the cold leg diameter have been established. By implementing these scaling ratios, the onset of the thermal stratification in APEX-CE will be preserved. Figures 5.12 through 5.14 present the calculated values for $Fr_{HPI/CL}$ for HPSI injection during natural circulation in the Palisades plant and the equivalent conditions in the APEX-CE as configured using the scaling ratios above. The full range of HPSI flows were assessed for

natural circulation at 2.5% decay power, 1.0% decay power, and 0.5% decay power. The Palisades plant and the APEX-CE data overlay almost exactly, indicating that the facility is well scaled for this phenomena. At 2.5% decay power, it is expected that the fluid in the cold leg will be well mixed. At 1.0% decay power, the criterion suggests that the cold leg fluid would remain well mixed, although very close to the stratification boundary. At 0.5% decay power a transient period of stratification would be expected.

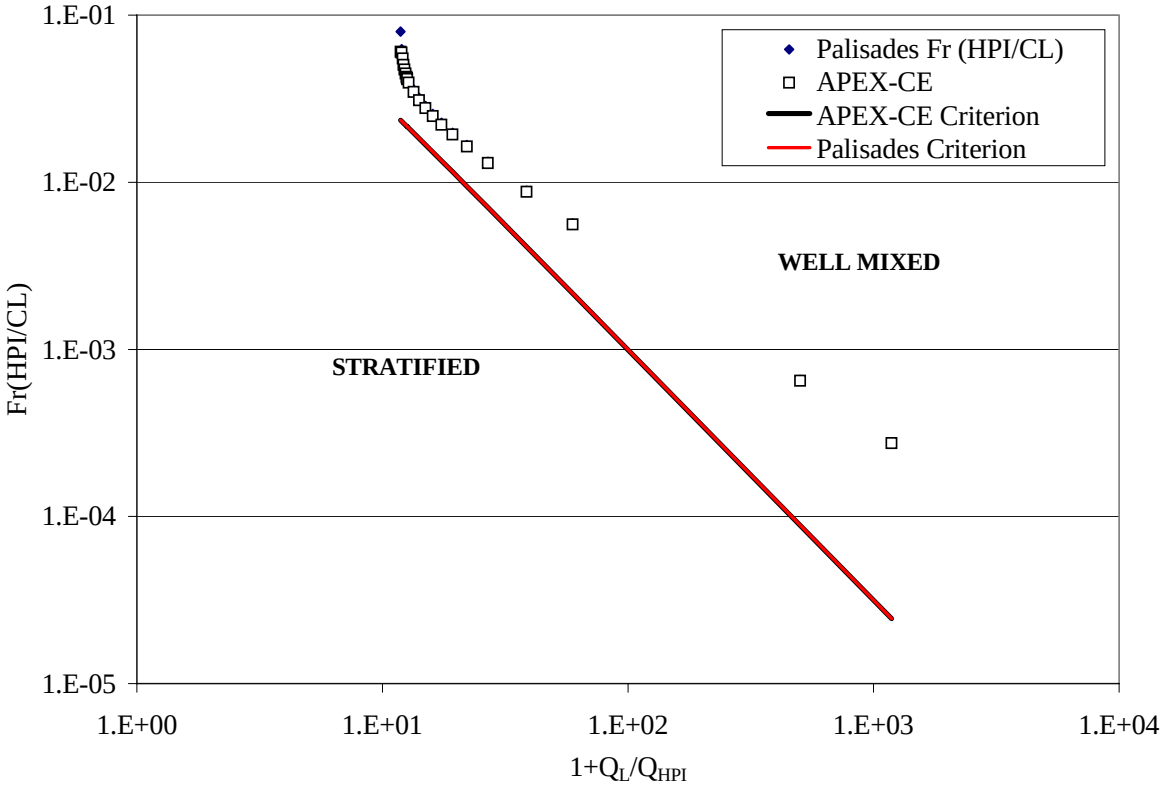

Figure 5.12 Comparison of the Onset of Cold Leg Thermal Stratification During Natural Circulation Conditions in Palisades and APEX-CE (2.5% Decay Power)

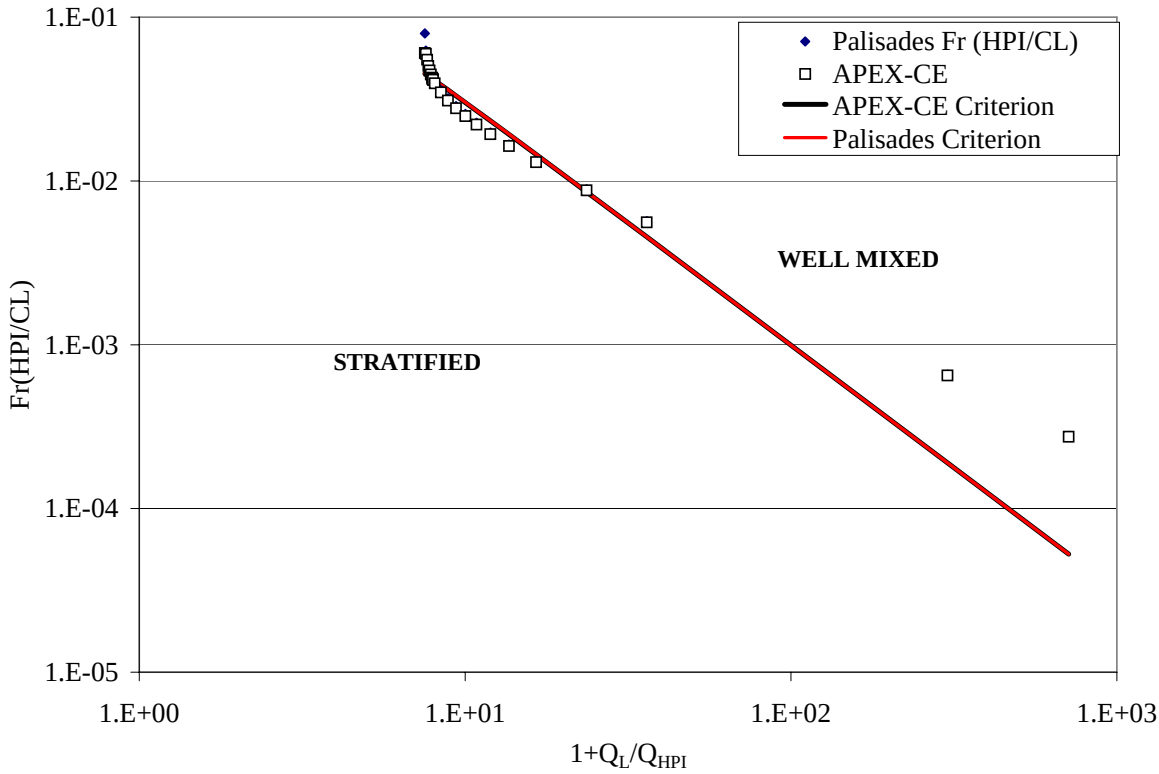

Figure 5.13 Comparison of the Onset of Cold Leg Thermal Stratification During Natural Circulation Conditions in Palisades and APEX-CE (1.0% Decay Power)

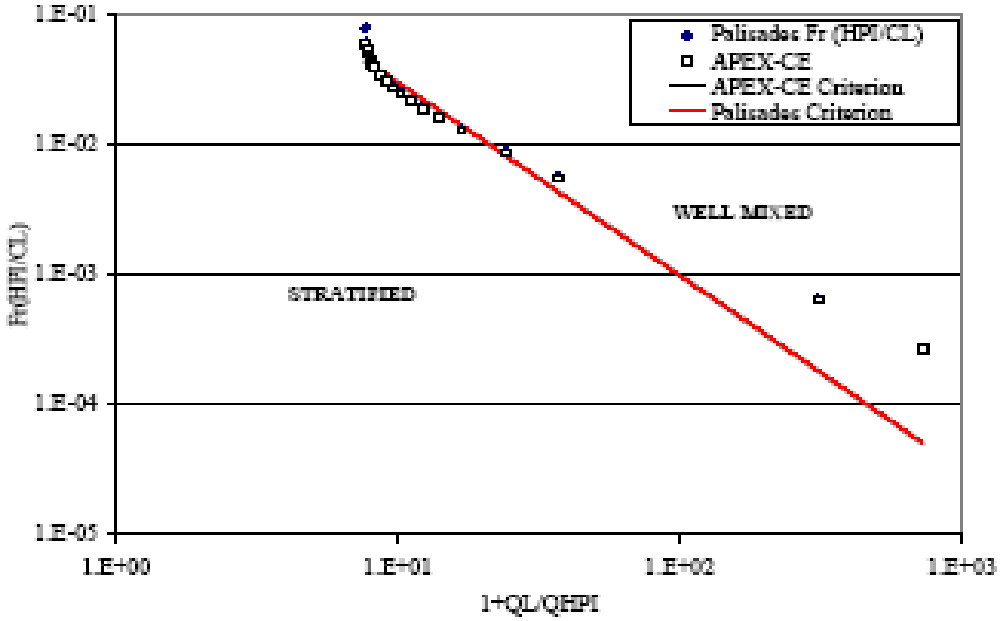

Figure 5.14 Comparison of the Onset of Cold Leg Thermal Stratification During Natural Circulation Conditions in Palisades and APEX-CE (0.5% Decay Power)

In conclusion, the onset of cold leg thermal stratification is well scaled in the APEX-CE test facility.

5.2.4 HPSI Plume Entrainment and Temperature Decay

This section provides a bottom-up scaling analysis for the HPSI plume entrainment and temperature decay phenomena. It is coupled to the top-down scaling via the primary loop natural circulation flow rate, Q_L. The objective of this analysis is to obtain the similarity criteria that must be preserved in APEX-CE to simulate the plume entrainment and plume temperature decay in the cold legs. This was done by:

1. Writing the governing mass, momentum, and thermal energy conservation equations for the appropriate conditions.

2. Assuming Gaussian velocity, buoyancy and temperature profiles inside the plume.

3. Integrating the conservation equations over the plume cross-sectional area to obtain a set of ordinary differential equations in terms of mean flow properties.

4. Non-dimensionalizing the resulting equations in terms of initial conditions to obtain the governing dimensionless Π groups.

5. Using the dimensionless Π groups to establish similarity criteria.

Two HPSI geometries are of interest to this study; the top-entry HPSI and the side-entry HPSI into horizontal cold legs of the primary loop.

5.2.4.1 Top-Entry HPSI Plumes (Axisymmetric Forced Plumes)

The injection of the cold (approximately 5°C to 20°C) fluid into a cold leg results in mixing at the boundary of the HPSI plume and at the free shear layers as illustrated in Figure 5.15.

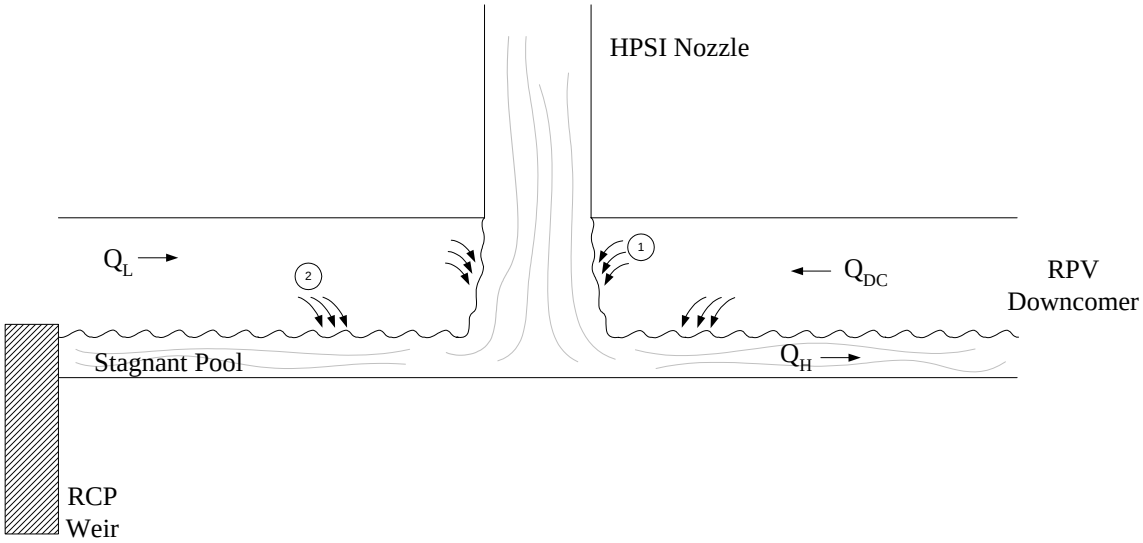

Figure 5.15 Thermally Stratified Conditions for the Top-Entry HPSI

For low, or essentially zero, primary loop flows, the cold HPSI fluid enters the top of the cold leg and falls to the bottom of the pipe. This produces a head wave which spreads the cold HPSI fluid in both directions. After the initial transient, a stagnant pool of HPSI fluid forms on the RCP side of the cold leg and all of the HPSI flow is directed towards the reactor vessel downcomer. As depicted in this figure, hot water from the loop and downcomer is entrained into the falling plume. This is shown as Region 1 of the figure. The range of HPSI Froude numbers (Fr_{HPI}) being considered is approximately 5×10^{-3} to 1.0.

Mixing also occurs at the free shear layers identified as Region 2 on the figure. Experimental evidence from the CREARE 1/5[20], CREARE ½[21] and Purdue ½[15] scale test facilities indicates that mixing at the free shear layers is negligible compared to plume entrainment mixing. This may not be true for side injection. The focus of this section will be to obtain the similarity criteria that should be used to best scale the HPSI mixing in Region 1. That is, entrainment mixing of the vertical forced plume and the resulting plume temperature decay.

A. Fundamental Assumptions

Early studies of the behavior of forced plumes relied on similarity solutions derived from the governing conservation equations. Particularly notable in this regard are the works of Rouse, Yih and Humphreys (1952)[31], Batchelor (1954)[32], Morton (1958)[33], and Turner (1979)[34].

Based on Batchelor's work, vorticity, or shearing motion, is generated inside a falling plume as a result of friction at its outer surface. This shearing motion is distributed through the plume by the downward motion along the vertical axis of the plume. The fluid outside the plume will be free from vorticity except in the thin boundary layer near the interface. The turbulent motion inside the plume will produce velocity fluctuations near the interface which will penetrate into the ambient fluid. The plume will break-up only if the inertia of the fluid within the plume is not small compared with the inertia of the fluid surrounding the plume. Therefore, turbulent entrainment of the ambient fluid into the plume, dilution (thermal or solute concentrations) of the density difference and the rate at which the plume falls depends greatly on the ambient fluid density. Further studies by Turner revealed that entrainment takes place in two stages, the engulfing of external fluid by larger eddies at the boundary, followed by rapid, smaller scale, mixing across the central core.

In Morton's analysis of forced plumes, he made three key assumptions which enabled him to obtain solutions to the governing conservation equations. These assumptions are described in the following paragraphs.

1. Taylor's Entrainment Assumption

G.I. Taylor[31] was the first to recognize that the linear spread of the plume radius with axial position implies that the mean inflow velocity across the edge of the plume is proportional to the local mean downward velocity of the plume. That is,

$$-v_E = \alpha_E u_p \qquad \textbf{(5.58)}$$

Where the ratio of the mean speed of inflow v_E at the edge of the forced plume to the mean vertical speed on the plume axis, u_p is equal to an entrainment constant, α_E, which is a value between zero and one. Taylor's assumption of a constant value of α_E is known to be true for pure plumes or pure

jets. Other correlations for α_E have been developed for forced plumes in which both the momentum flux and buoyancy flux are important.

2. Similarity of Velocity and Buoyancy Profiles

Morton assumed that the profiles of mean vertical velocity and buoyancy are each of similar form at all axial elevations. The experimental data strongly supports this assumption as shown in Figure 5.16 which is a plot of local velocity inside a planar plume. Figure 5.17 demonstrates that all of the data collapses to a single curve when plotted in dimensionless coordinates.

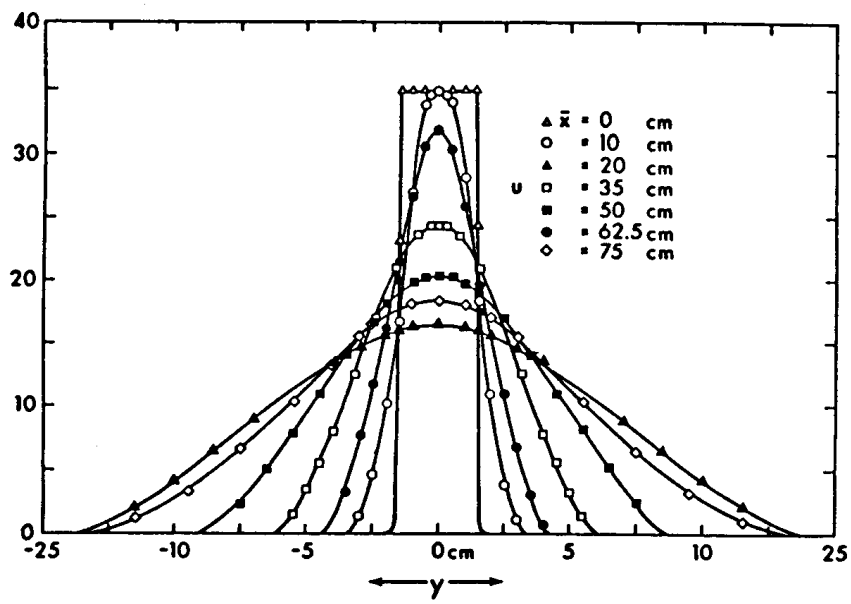

Figure 5.16 Velocity Distributions Measured in a Planar Jet (1934)[36]

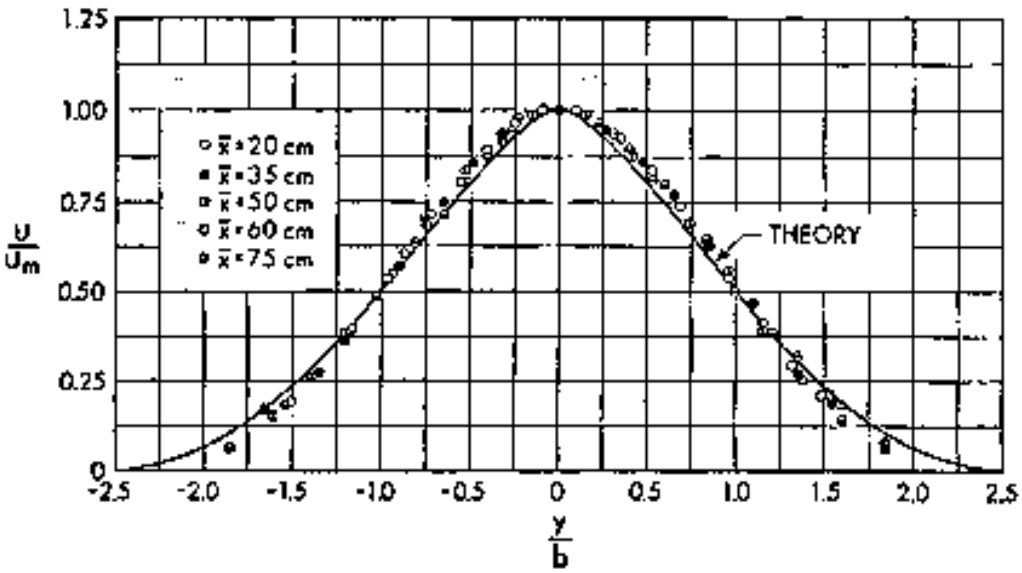

Figure 5.17 Velocity Distributions in a Planar Jet Plotted in Dimensionless Coordinates[32] and Compared to a Gaussian Profile (1934)

By assuming a particular profile shape, typically a Gaussian profile as shown in Figure 5.17, the mass and momentum fluxes can be replaced by mean value defined by integrals across the plume width. The assumption of similarity implies that the rate of spread of the plume, which is governed by the turbulence generated by its own motion, must have the same relation to the mean flow whatever the scale of motion.

3. <u>Gaussian Profile</u>

The following Gaussian profiles are typically assumed for the mean vertical velocity and mean buoyancy respectively.

$$u(r,z) = u_p(z)\exp\left(-\frac{r^2}{b_u^2}\right) \tag{5.59}$$

and

$$g\,\Delta\rho(r,z) = g\,\Delta\rho_p(z)\exp\left(-\frac{r^2}{b_g^2}\right) \tag{5.60}$$

where

$$\Delta\rho = (\rho - \rho_m) \tag{5.61}$$

In these profiles, u_p and $g\Delta\rho_p$ are the mean axial velocity and buoyancy of the forced plume. These mean values are functions of the axial position (z). The ambient fluid density is denoted by ρ_m. The profile dependence on the radial position is given by the r-coordinate found in the exponent. The length b_u characterizes the radial spread of the velocity profiles whereas the length b_g characterizes the radial spread of the buoyancy profile. Both are functions of axial position. The values of b_u and b_g are empirically determined. Figure 5.18 illustrates the profile nomenclature that has been implemented in this analysis.

The following equation of state for the fluid:

$$\left(T - T_m\right) = \frac{\left(\rho - \rho_m\right)}{\beta_o \rho_o} \tag{5.62}$$

where β_o is the reference thermal expansion coefficient and ρ_o is a reference density, can be applied to the buoyancy profile to obtain the following fluid temperature profile:

$$\left(T - T_m\right) = \left(T - T_m\right)_p \exp\left(-\frac{r^2}{b_g^2}\right) \tag{5.63}$$

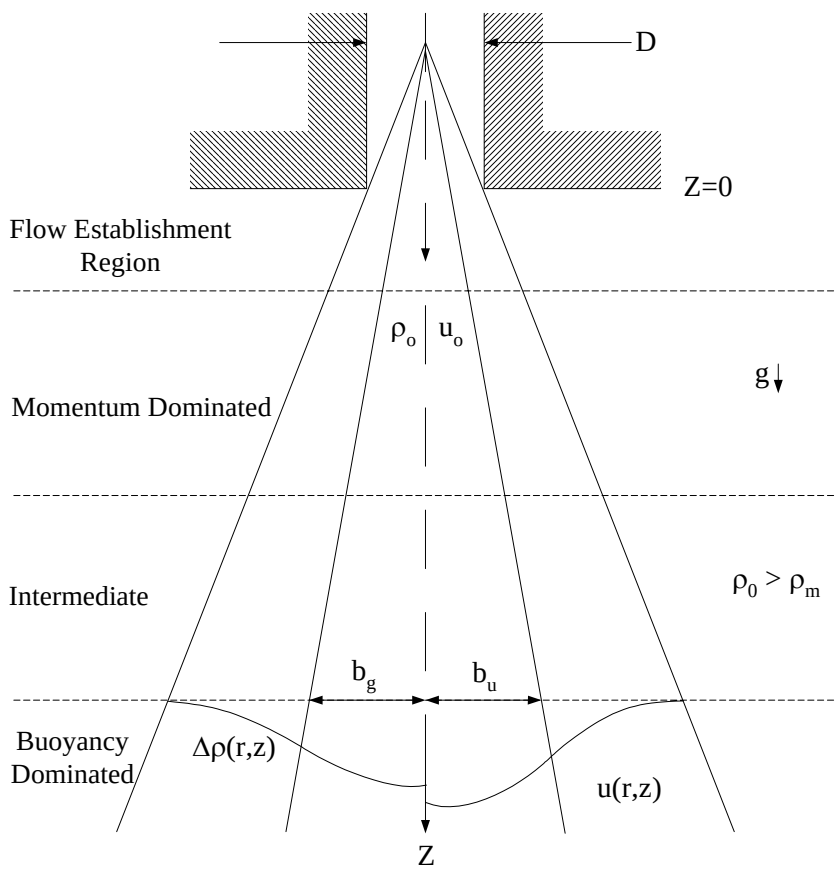

Figure 5.18 Gaussian Profiles in Forced Plumes

B. Governing Equations for Axisymmetric Forced Plumes

The governing equations for the flow quantities in an axisymmetric vertical buoyant jet, where gravity acts along the z-coordinate, are as follows (Chen and Rodi)[37]:

Mass Conservation:

$$\frac{\partial}{\partial z}(\rho u r) + \frac{\partial}{\partial r}(\rho v r) = 0 \qquad \textbf{(5.64)}$$

Momentum Conservation:

$$\frac{\partial}{\partial z}(\rho u^2 r) + \frac{\partial}{\partial r}(\rho u v r) = g(\rho - \rho_m) r - \frac{\partial}{\partial r}(r \rho u' v') \qquad \textbf{(5.65)}$$

Thermal Energy Conservation:

$$\frac{\partial}{\partial z}(\rho u T r) + \frac{\partial}{\partial r}(\rho v T r) = -\frac{\partial}{\partial r}(r \rho v' T') \qquad \textbf{(5.66)}$$

These equations were obtained by Chen and Rodi using the boundary-layer assumptions and the Boussinesq approximation assuming steady-flow conditions. The $\rho u' v'$ term represents the turbulent shear stress. The thermal energy equation can also be written in terms of a stratified ambient temperature, $T_m(z)$ as follows:

$$\frac{\partial}{\partial z}\left[\rho u r (T - T_m)\right] + \frac{\partial}{\partial r}\left[\rho v r (T - T_m)\right] = -\rho u r \frac{\partial T_m}{\partial z} - \frac{\partial}{\partial r}(r \rho v' T') \qquad \textbf{(5.67)}$$

Integrating the mass conservation equation yields the following balance equation for the plume volume flux:

$$\frac{d}{dz}\int_0^R u r \, dr = -v_E R \qquad \textbf{(5.68)}$$

Where 2π and ρ (Boussinesq approximation) were canceled from both sides of the equation. In this equation, v_E is the entrainment velocity at the plume boundary.

Integrating the momentum conservation equation yields the following balance equation for the momentum flux:

$$\frac{d}{dz}\int_0^R \rho u^2 \, dr = g\int_0^R (\rho - \rho_m) r \, dr \qquad \textbf{(5.69)}$$

A value of 2π was canceled from both sides of the equation. In arriving at this equation, it was assumed that u and ρu′v′ are close to zero at r equal to R.

Integrating the energy conservation equation yields the following balance equation for the thermal energy flux:

$$\frac{d}{dz}\int_{o}^{R} u\left(T - T_m\right) r\, dr = -\frac{d\,T_m}{dz}\int_{o}^{R} u\, r\, dr \qquad \textbf{(5.70)}$$

The terms 2π and ρ (Boussinesq approximation) were canceled from both sides of the equation. Use has also been made of the approximation that u, $\left(T - T_m\right)$ and ρ v′T′ are zero at r equal to R.

The integral volume flux, momentum flux, and thermal energy flux equations can be evaluated by substituting the Gaussian profiles presented earlier. This will yield a set of ordinary differential equations which can be made dimensionless to obtain the desired scaling groups.

Substituting equation (5.59) into (5.68) and performing the integration yields the balance equation for the volume flux:

$$\frac{d}{dz}\left(b_u^2\, u_p\right) = -2\, R\, v_E \qquad \textbf{(5.71)}$$

Use has been made of the fact that $\exp\left(-R/b_u^2\right)$ is approximately zero. Substituting equation (5.60) into (5.67) and performing the integration yields the balance equation for the momentum flux:

(5.72)

$$\frac{d}{dz}\left(\rho\, b_u^2\, u_p^2\right) = 2\, g\left(\rho - \rho_L\right)_p b_g^2$$

Substituting equation (5.63) into (5.70) and integrating yields the thermal energy flux balance equation:

$$\frac{d}{dz}\left[\frac{b_g^2\, b_u^2\, u_p\, \Delta\, T_p}{b_g^2 + b_u^2}\right] = -b_u^2\, u_p\, \frac{d\,T_m}{dz} \qquad \textbf{(5.73)}$$

Equations (5.71) through (5.73) are similar to those obtained by Rodi[34]. The integrated balance equations given by (5.71) through (5.73) can also be written in terms of volumetric flow rates, Q. The volumetric flow rate of the plume, Q_p is given by:

$$Q_p = 2\pi\int_{o}^{R} u\, r\, dr \qquad \textbf{(5.74)}$$

Substituting the Gaussian velocity profile, equation (5.57) and integrating yields:

$$Q_p = \pi b_u^2 u_m \tag{5.75}$$

The entrainment volumetric flow rate can be related to the entrainment velocity by:

$$\frac{d Q_e}{dz} = 2\pi R v_E \tag{5.76}$$

Substituting equations (5.75) and (5.76) into (5.71) through (5.73) yields:

Volume Balance:

$$\frac{d Q_p}{dz} = -\frac{d Q_E}{dz} \tag{5.77}$$

Momentum Balance:

$$\frac{d}{dz}\left[\frac{\rho Q_p^2}{b_u^2}\right] = 2\pi^2 g b_g^2 \left(\rho - \rho_L\right)_p \tag{5.78}$$

Energy Balance:

$$\frac{d}{dz}\left[\frac{Q_p \Delta T_p}{1 + \lambda^2}\right] = -Q_p \frac{d T_m}{dz} \tag{5.79}$$

where λ is equal to b_u/b_g.

C. Governing Dimensionless Groups

In this section, it is shown how the governing dimensionless groups for buoyant jets were obtained. Each term in the integrated balance equations was made dimensionless by using the conditions at the plume entrance. The following dimensionless parameters were defined:

$$Q_p = Q_{HPI}\, Q_p^+ \tag{5.80}$$

$$Q_E = Q_{E,O}\, Q_E^+ \tag{5.81}$$

$$b_u = \frac{1}{2} D_{HPI}\, b_u^+ \tag{5.82}$$

$$b_g = \frac{1}{2} D_{HPI}\, b_g^+ \tag{5.83}$$

$$\Delta T_p = \left(T_{HPI} - T_m\right) \Delta T_p^+ \tag{5.84}$$

$$\frac{d\,T_m}{dz} = \left(\frac{d\,T_m}{dz}\right)_o \left(\frac{d\,T_m}{dz}\right)^+ \tag{5.85}$$

$$\Delta \rho_p = \left(\rho_{HPI} - \rho_m\right) \Delta \rho_p^+ \tag{5.86}$$

$$z = \frac{1}{2} D_{HPI}\, z^+ \tag{5.87}$$

In these equations, Q_{HPI} is approximately Q_p, D_{HPI} is approximately 2R and ΔT_p is approximately $(T_{HPI} - T_m)$ at z equal zero.

Substituting the dimensionless parameters into the integrated volume flux equation yields the following dimensionless equation.

Dimensionless Volumetric Flux Equation:

$$\frac{d\,Q_p^+}{dz^+} = -\Pi_{QE} \frac{d\,Q_E^+}{dz^+} \tag{5.88}$$

where the dimensionless group Π_{QE} represents the ratio of the entrainment volumetric flux to the plume volumetric flux at the entrance. That is,

$$\Pi_{QE} = \left(\frac{Q_E}{Q_{HPI}} \right)_o \tag{5.89}$$

Substituting the dimensionless parameters into equation (5.78) yields:

Dimensionless Momentum Flux Equation:

$$\left(Fr_{HPI}\right)^2 \frac{d}{dz^+} \left(\frac{\rho\, Q_p}{b_u^2} \right)^+ = 2\left(b_g^2\, \Delta\rho_p\right)^+ \tag{5.90}$$

The dimensionless group, Fr_{HPI}, is the ratio of inertia to buoyancy and represents the well-known densimetric Froude number:

$$Fr_{HPI} = \frac{Q_{HPI}}{a_{HPI} \left[\frac{g\, \Delta\, \rho_{p,o}\, D_{HPI}}{\rho_{HPI}} \right]^{\frac{1}{2}}} \tag{5.91}$$

where a_{HPI} is the cross-sectional flow area of the HPI nozzle.

Substituting the dimensionless parameters into equation (5.79) yields:

Dimensionless Thermal Energy Equation:

$$\frac{d}{dz^+} \left[\frac{Q_p\, \Delta\, T_p}{1 + \lambda^2} \right]^+ = -\frac{\Pi_{DT}}{2}\, Q_p^+ \left(\frac{d\, T_m}{dz} \right)^+ \tag{5.92}$$

where Π_{DT} characterizes the degree of ambient thermal stratification. It is defined as:

$$\Pi_{DT} = \frac{D_{HPI}}{\left(T_{HPI} - T_M\right)_o} \left(\frac{dT_m}{dz} \right)_o \tag{5.93}$$

For uniform ambient fluid conditions, the ambient fluid temperature gradient, dT_m/dz, would be zero.

In conclusion, the dimensionless groups that govern the behavior of axisymmetric forced plumes in vertical flows are (D_{HPI}/z), Π_{QE}, Fr_{HPI}, and Π_{DT}.

D. Correlations for Plume Entrainment Rate and Temperature Decay

Theofanous[39] and Rodi[38] have used a k-ε-θ′ turbulence model to predict the plume volumetric flow and temperature decay. Theofanous presents the following correlations to capture the results of the more detailed analysis for a limited range of conditions:

$$\Pi_{QE} = 0.5176\left(\frac{z}{D_{HPI}}\right)^{1.236}\left(Fr_{HPI}\right)^{-0.414} \qquad \textbf{(5.94)}$$

It is noted that these same dimensionless groups arose from the present scaling analysis. Figure 5.19 is a plot of this correlation evaluated over its range of applicability. The data of Davis (1978)[40] can also be correlated by the same dimensionless groups.

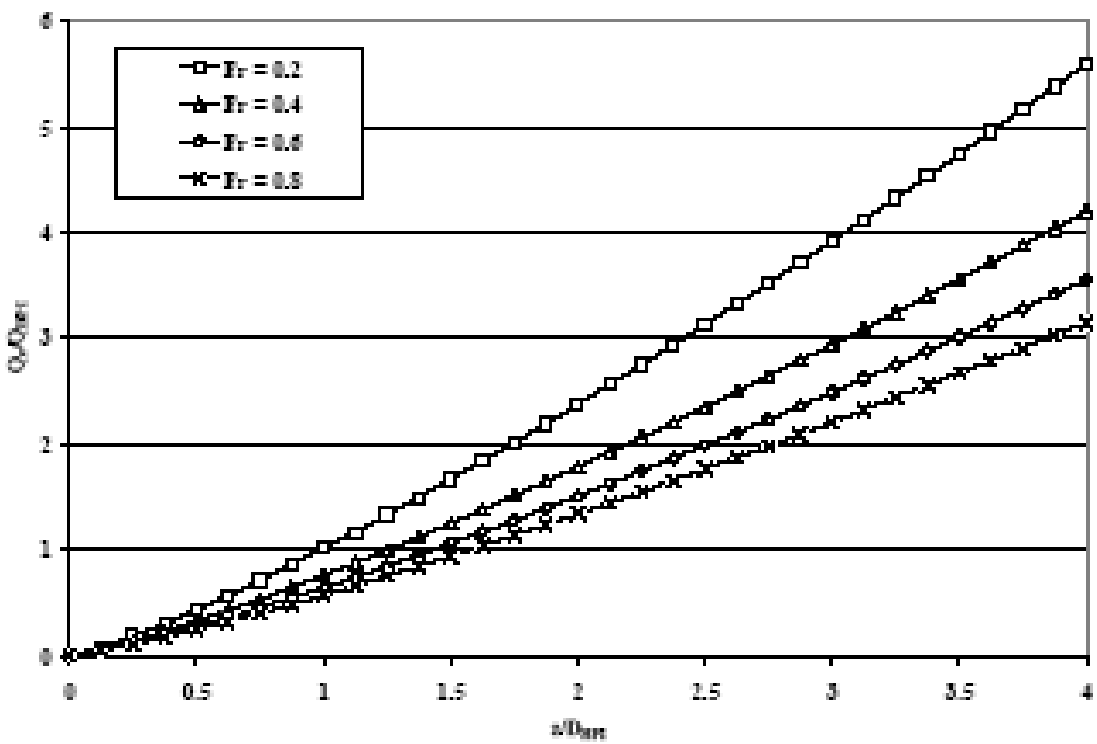

Figure 5.19 Comparison of Entrainment Correlation to Data of Davis, et. al. (1978)[36]

Similarly, Theofanous correlated the plume temperature decay by:

$$\Delta T^{+} = 1 - 0.326 \left(\frac{z}{D_{HPI}} \right)^{0.65} \left(Fr_{HPI} \right)^{-0.274} \tag{5.95}$$

which also incorporates the same dimensionless Π groups obtained in this study.

E. <u>Similarity Criteria for HPSI Plumes</u>

The following similarity criteria should be preserved in APEX-CE to properly simulate the forced plume entrainment and temperature decay:

$$\left(\Pi_{QE} \right)_R = 1 \tag{5.96}$$

and

$$\left(\Delta T^{+} \right)_R = 1 \tag{5.97}$$

Satisfying these two similarity criteria in equations (5.99) and (5.95) requires that:

$$\left(\frac{z}{D_{HPI}} \right)_R = 1 \tag{5.98}$$

and

$$\left(Fr_{HPI} \right)_R = 1 \tag{5.99}$$

In the limiting case of a plume falling from the top to the bottom of the cold leg, equation (5.98) becomes:

$$\left(\frac{D_{CL}}{D_{HPI}} \right)_R = 1 \tag{5.100}$$

For APEX-CE, the actual value of (D_{CL}/D_{HPI}) equals 2.66. For Palisades, the actual value of (D_{CL}/D_{HPI}) equals 2.64. Therefore,

$$\left(\frac{D_{CL}}{D_{HPI}} \right)_R \approx 1.0 \tag{5.101}$$

and the similarity criterion is satisfied. With respect to the Fr_{HPI} similarity criterion given by equation (5.99), it has already been shown by Figure 5.8 that the Fr_{HPI} is essentially identical in APEX-CE and Palisades for all injection conditions.

5.2.4.2 Side-Entry HPSI Plumes

The previous section developed similarity criteria for top-entry HPSI geometries. The HPSI geometry for the Palisades Plant is as depicted in Figure 5.20.

The characteristics of side-entry plume entrainment will be somewhat different than that of top-entry plume entrainment at low HPSI flow rates. In general, less entrainment is expected because the plume fall height would be shorter. Furthermore, at very low flows, the HPSI plume might look more like a water fall (i.e., a planar plume) than an axisymmetric circular plume. Thus side-entry HPSI plume entrainment would be bounded by planar plume entrainment at low flows and axisymmetric plume entrainment at high flows when the buoyant jet is capable of traversing the cold leg and impinging the wall on the other side.

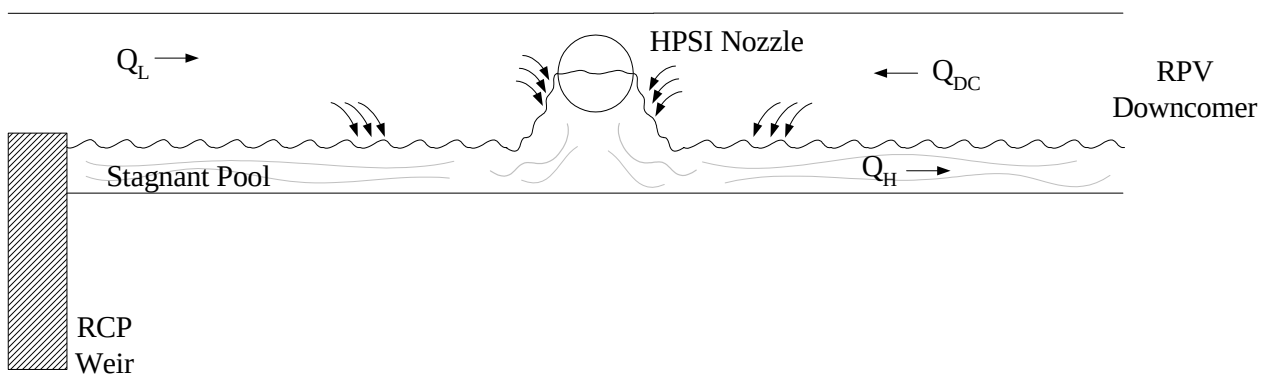

Figure 5.20 Thermally Stratified Conditions for the Side-Entry Palisades HPSI

For the low flow conditions expected in this study, the same similarity criteria will be implemented for side entry plumes as was developed for top-entry plumes; with one exception. The plume fall height scaling criterion will be defined as follows:

$$\left(\frac{z_{inj}}{D_{HPI}}\right)_R = 1 \qquad \textbf{(5.102)}$$

Thus the location of the HPSI injection nozzle is fixed. The bounding condition, planar plumes, will be discussed as part of the downcomer mixing analysis.

5.2.4.3 Injection Flow Turbulence

The top-down scaling analysis requires that the HPSI volumetric flow rate be scaled as:

$$\left(Q_{HPI}\right)_R = 1{:}276 \tag{5.103}$$

The buoyant backflow analysis and the plume entrainment analysis produced consistent results with regards to preserving the HPSI Froude number, as stated by equation (5.99). The difficulty arises in that both the HPSI Froude number and HPSI Reynolds number, which dictates the onset of turbulence in the injection flow stream cannot be simultaneously preserved.

The HPSI Reynolds number is defined as:

$$Re = \frac{v_{HPI} D_{HPI}}{\upsilon} \tag{5.104}$$

Using equation (5.103) we require that:

$$\left(v_{HPI}\right)_R \left(D_{HPI}\right)_R^2 = \frac{1}{276} \tag{5.105}$$

Using equation (5.99) and the definition of Fr_{HPI} given by equation (5.91) we also require that:

$$\frac{\left(v_{HPI}\right)_R}{\left(D_{HPI}\right)_R^{\frac{1}{2}}} = 1 \tag{5.106}$$

Substituting equation (5.106) into (5.105) yields:

$$\left(D_{HPI}\right)_R = \left(\frac{1}{276}\right)^{\frac{2}{5}} \tag{5.107}$$

and

$$\left(v_{HPI}\right)_R = \left(\frac{1}{276}\right)^{\frac{1}{5}} \tag{5.108}$$

Thus a Reynolds number ratio will yield:

$$\left(Re\right)_R = \left(\frac{1}{276}\right)^{\frac{3}{5}} \approx \frac{1}{29} \tag{5.109}$$

Figure 5.21 presents a comparison of the APEX-CE and Palisades HPSI Reynolds numbers. As shown in this figure, the APEX-CE injection flows are typically laminar whereas the Palisades injection flows are typically turbulent.

The impact of this difference in injection flow regime cannot be fully evaluated because the presence of a check valve located immediately before the HPSI nozzle/cold leg junction will induce an entrance effect that is difficult to assess analytically. The degree of turbulence introduced by the fluctuating check valve may be significantly larger than that associated with the flow regime.

Further assessments will be performed using CFD calculations.

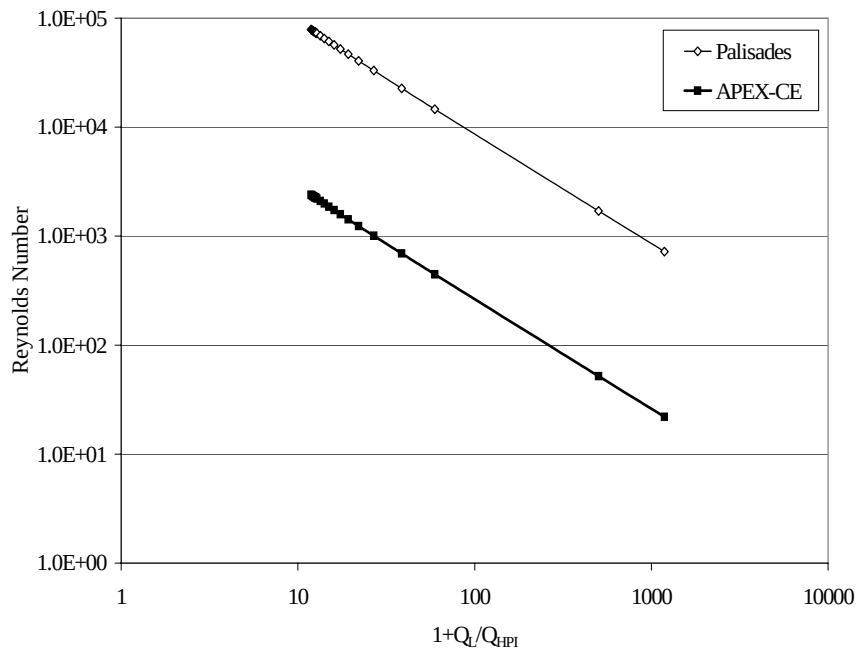

Figure 5.21 Comparison of APEX-CE and Palisades HPSI Reynolds Numbers

5.2.5 Downcomer Plume Mixing (Planar Plumes)

The objective of this analysis is to obtain the similarity criteria that must be preserved in APEX-CE to simulate the plume entrainment and plume temperature decay in the downcomer.

Figure 5.22 illustrates the downcomer plume mixing phenomena as depicted for planar plumes generated by two cold legs. This figure is based on observations obtained from the 2/5 scale, multi-loop, transparent test facility at Imatran Voima Oy (IVO) in Helsinki, Finland.[41] The complexity of the behavior, in particular the interactions between plumes, does not lend itself to simple analysis. The best starting point is the analysis of single planar plumes.

Chen and Rodi (1980)[37] have provided a valuable treatise which includes detailed discussions on planar plumes.

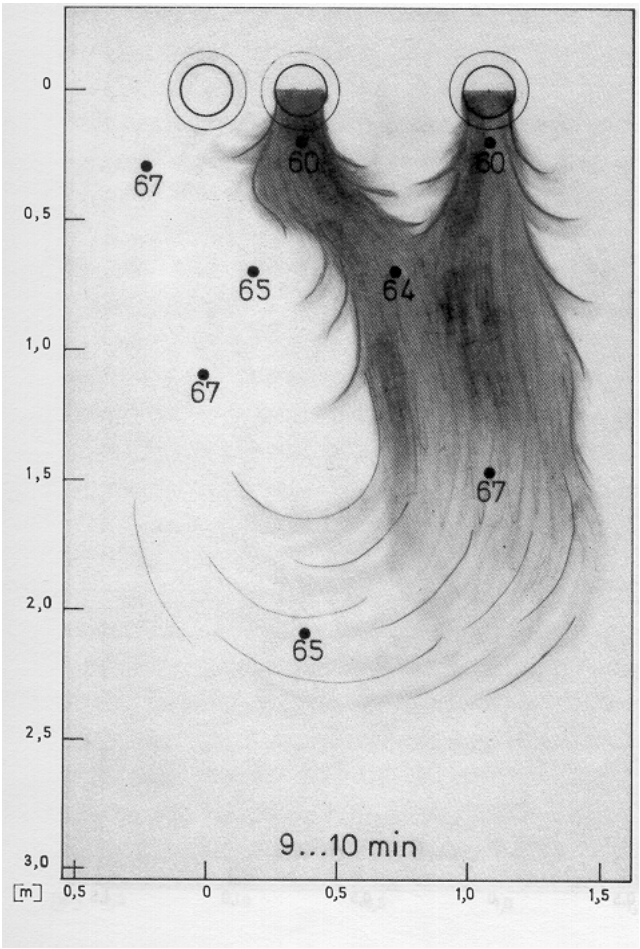

Figure 5.22 Downcomer Plume Interactions as Observed in IVO 2/5 Scale Transparent Test Loop (IVO Mixing Test #115)

The analysis for the planar plume follows that presented in Section 5.2.4.1 for the axisymmetric forced plume. The three fundamental assumptions, Taylor's entrainment assumption, the similarity of velocity and buoyancy profiles in the plume, and the Gaussian profile assumption remain applicable. Figure 5.23 illustrates the planar plume geometry.

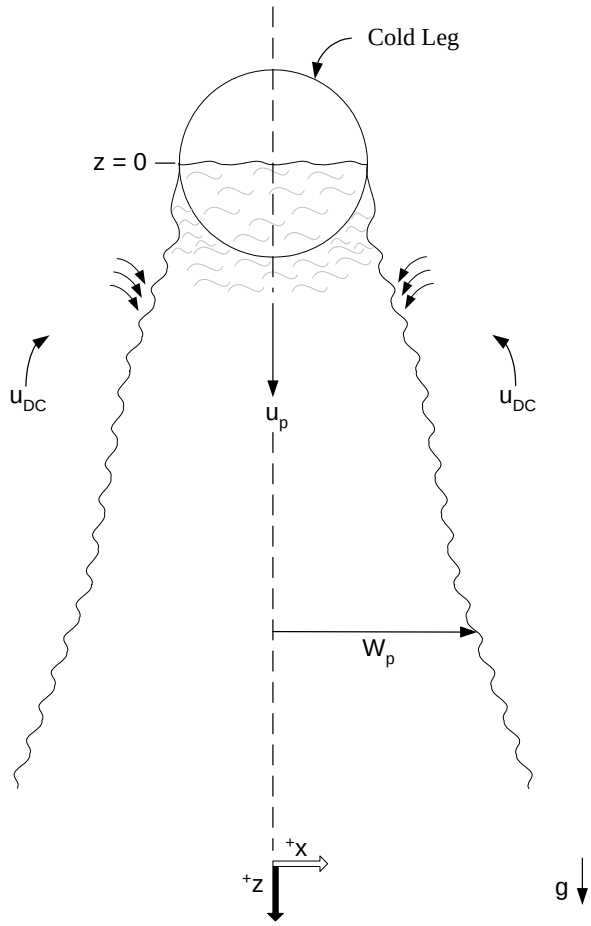

Figure 5.23 Schematic of a Single Planar Plume in the RPV Downcomer

The Gaussian profiles for the plume velocity, buoyancy and temperature are expressed as follows:

$$u(x,z) = u_p(z) \exp\left[-\frac{x^2}{b_u^2}\right] \quad \textbf{(5.110)}$$

$$g\,\Delta\rho(x,z) = g\,\Delta\rho_p(z) \exp\left[-\frac{x^2}{b_g^2}\right] \quad \textbf{(5.111)}$$

$$(T - T_m) = (T - T_m)_p \exp\left[-\frac{x^2}{b_g^2}\right] \quad \textbf{(5.112)}$$

The governing equations for the planar plume where gravity acts along the z-coordinate are (Chen and Rodi)[33]:

Mass Conservation:

$$\frac{\partial}{\partial z}(\rho u) + \frac{\partial}{\partial x}(\rho v) = 0 \qquad \textbf{(5.113)}$$

Momentum Conservation:

$$\frac{\partial}{\partial z}\left(\rho u^2\right) + \frac{\partial}{\partial x}(\rho u v) = g\left(\rho - \rho_m\right) - \frac{\partial}{\partial x}(\rho u' v') \qquad \textbf{(5.114)}$$

Thermal Energy:

$$\frac{\partial}{\partial z}\left[\rho u\left(T - T_m\right)\right] + \frac{\partial}{\partial x}\left[\rho v\left(T - T_m\right)\right] = -\rho u \frac{\partial T_m}{\partial x} - \frac{\partial}{\partial x}(\rho v' T') \qquad \textbf{(5.115)}$$

where the definitions of the terms are the same as given in Section 5.4.2.1, and the thermal energy equation has been written in terms of the stratified ambient temperature, T_m.

Integrating the equations over the cross-sectional area of the plume yields:

Volume Flux:

$$\frac{d}{dz}\int_o^{W_p} u\,dx = -v_E W_p \qquad \textbf{(5.116)}$$

Momentum Flux:

$$\frac{d}{dz}\int_o^{W_p} \rho u^2\,dx = g\int_o^{W_p}\left(\rho - \rho_m\right)dx \qquad \textbf{(5.117)}$$

Thermal Energy Flux:

$$\frac{d}{dz}\int_o^{W_p} u\left(T - T_m\right)dx = -\frac{dT_m}{dz}\int_o^{W_p} u\,dx \qquad \textbf{(5.118)}$$

where ρ (Boussinesq approximation) and a factor of 2s were canceled from both sides of each equation and the plume boundary assumptions of Section 5.4.2.1 were applied. The downcomer gap width is denoted by “s.”

Substituting the Gaussian profiles given by equations (5.110) through (5.112) into (5.116) through (5.118) respectively, yield the integral equations for the mean flow properties of the planar plume.

Volume Flux:

$$\frac{d}{dz}\left(b_u u_p\right) = -\frac{2}{\sqrt{\pi}} v_E \tag{5.119}$$

Momentum Flux:

$$\frac{d}{dz}\left(\rho b_u u_p^2\right) = 2 g \Delta\rho_p b_g \tag{5.120}$$

Thermal Energy Flux:

$$\frac{d}{dz}\left[b_u u_p \Delta T_p \left(\frac{\lambda^2}{1+\lambda^2}\right)^{\frac{1}{2}}\right] = -b_u u_p \frac{dT_m}{dz} \tag{5.121}$$

The integral balance equations can be expressed in terms of volumetric flow rates as was done in Section 5.4.2.1. The volumetric flow rate of the plume, Q_p, is given by:

$$Q_p = 2s\int_o^{W_p} u\,dx \tag{5.122}$$

Substituting the Gaussian profile and integrating yields:

$$Q_p = \sqrt{\pi}\, b_u u_p s \tag{5.123}$$

The entrainment volumetric flow rate can be related to the entrainment velocity by:

$$\frac{dQ_E}{dz} = s\, W_p\, v_E \tag{5.124}$$

Substituting equations (5.123) and (5.124) into the integrated balance equation yields:

Volume Flux:

$$\frac{dQ_p}{dz} = -\frac{dQ_E}{dz} \tag{5.125}$$

Momentum Flux:

$$\frac{d}{dz}\left(\frac{\rho Q_p^2}{b_u}\right) = 2\pi s^2 g \Delta\rho_p b_g \tag{5.126}$$

Thermal Energy Flux:

$$\frac{d}{dz}\left[\frac{Q_p \Delta T_p \lambda}{\left[1+\lambda^2\right]^{\frac{1}{2}}}\right] = -Q_p \frac{dT_m}{dz} \tag{5.127}$$

The governing dimensionless equations for the planar plume behavior were obtained by implementing the following dimensionless parameters expressed in terms of plume inlet conditions.

$$Q_p = Q_{po} Q_p^+ \tag{5.128}$$

$$Q_E = Q_{Eo} Q_E^+ \tag{5.129}$$

$$b_u = \frac{1}{2} D_{CL} b_u^+ \tag{5.130}$$

$$b_g = \frac{1}{2} D_{CL} b_g^+ \tag{5.131}$$

$$\Delta T_p = \left(T_{po} - T_m\right) \Delta T_p^+ \tag{5.132}$$

$$\frac{dT_m}{dz} = \left(\frac{dT_M}{dz}\right)_o \left(\frac{dT_m}{dz}\right)^+ \tag{5.133}$$

$$\Delta\rho_p = \left(\rho_{po} - \rho_m\right) \Delta\rho_p^+ \tag{5.134}$$

$$z = \frac{1}{2} D_{CL} z^+ \tag{5.135}$$

where the initial half plume width, W_{po}, is assumed to be one half the cold leg diameter, D_{CL}.

Substituting the dimensionless parameters into the integrated balance equations yields the following dimensionless equations:

Volume Flux:

$$\frac{dQ_p^+}{dz^+} = -\Pi_{QE}\frac{dQ_E^+}{dz^+} \tag{5.136}$$

where:

$$\Pi_{QE} = \left(\frac{Q_E}{Q_p}\right)_o \tag{5.137}$$

Momentum Flux:

$$\left(Fr_{DC}\right)^2 \frac{d}{dz^+}\left(\frac{Q_p^2}{b_u}\right)^+ = \frac{\pi}{2}\Delta\rho_p^+ b_g^+ \tag{5.138}$$

where

$$Fr_{DC} = \frac{Q_{p,o}}{a_{p,o}\left[\frac{g\,\Delta\rho_p}{\rho_{p,o}} D_{CL}\right]^{\frac{1}{2}}} \tag{5.139}$$

In this equation, the initial plume flow area, $a_{p,o}$, is defined as:

$$a_{p,o} = D_{CL}\, s \tag{5.140}$$

and hence a superficial plume velocity at the downcomer inlet is defined as:

$$j_{p,o} = \left(\frac{Q_p}{a_p} \right)_o \tag{5.141}$$

Thermal Energy:

$$\frac{d}{dz^+} \left[\frac{Q_p \Delta T_p \lambda}{\left[1 + \lambda^2\right]^{\frac{1}{2}}} \right]^+ = - \frac{\Pi_{DT}}{2} Q_p^+ \left(\frac{dT_m}{dz} \right)^+ \tag{5.142}$$

where:

$$\Pi_{DT} = \frac{D_{CL}}{\left(T_p - T_m\right)_o} \left(\frac{dT_m}{dz} \right)_o \tag{5.143}$$

For uniform ambient fluid conditions in the downcomer, the fluid temperature gradient, dT_m/dz, would be zero.

Summarizing, the dimensionless groups that govern the behavior of the planar plume in the downcomer are (D_{CL}/z), Π_{QE}, Fr_{DC}, and Π_{DT}.

5.2.5.1 Plume Velocity and Plume Residence Time

The following correlation was adapted from the work of Kotsovinos[38] to predict the mean fluid velocity at the axis of a plume:

$$u_p = 1.66 \left[\frac{Q_{p,o}\, g \left(\rho_{HPI} - \rho_m\right)}{s\ \rho_m} \right]^{\frac{1}{3}} \tag{5.144}$$

Figure 5.24 compares equation (5.144) to data from the CREARE 1/2-scale test facility. The agreement is quite good.

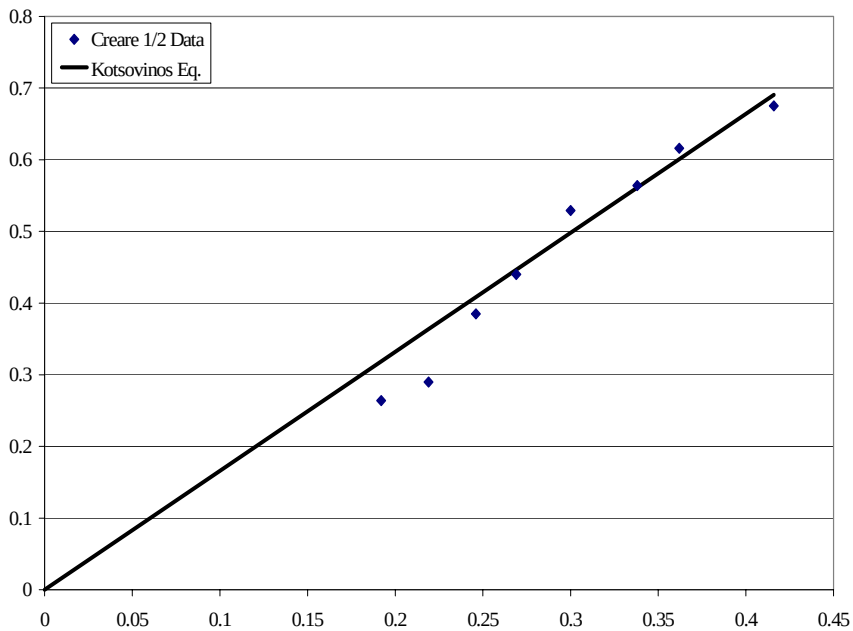

Figure 5.24 Comparisons of Kotsovinos Equation to CREARE 1/2-Scale Data

A plume residence time can be estimated from:

$$\tau_p = \frac{L_{DC}}{u_p} \tag{5.145}$$

5.2.5.2 Assessment of Planar Plume Similarity Criteria

Four similarity criteria are examined in this section for transient, integral system conditions in APEX-CE. The first is the plume residence time constant. Incorporating the actual test conditions and geometry, the ratio of the plume residence time in APEX-CE to that in Palisades is:

$$\left(\tau_p\right)_R = \left(\frac{L_{DC}}{u_p}\right)_R \approx 1 \tag{5.146}$$

where it was determined that the plume velocity ratio is approximately 1/4.

The next criterion expresses the limiting condition for a free fall of the plume over the entire length of the downcomer, $z = L_{DC}$. We find that:

$$\left(\frac{D_{CL}}{L_{DC}}\right)_R \approx \frac{1}{2} \tag{5.147}$$

This shows that the APEX-CE facility downcomer can potentially produce longer plumes on a scaled basis than is physically possible in Palisades. However, this is a limiting analysis. It is

expected that the entrainment behavior will cause the plume to completely decay well before reaching the bottom of the downcomer, possibly within 3 to 5 cold leg diameters.

The second similarity criterion is estimated for the limiting case that all of the HPSI fluid is directed towards the downcomer, hence, $Q_{p,o}$ equals Q_{HPSI}. Therefore, the similarity criterion is satisfied. That is,

$$\left(\frac{Q_{E,o}}{Q_{HPI}}\right)_R = 1 \tag{5.148}$$

Assuming the same form for the planar plume entrainment as observed for the axisymmetric plume, it is postulated that $\left(\Pi_{QE}\right)_R$ will be preserved if $\left(Fr_{DC}\right)_R$ is preserved. It is found that,

$$\left(Fr_{DC}\right)_R \approx \frac{\left(Q_{HPI}\right)_R}{\left(D_{CL}\right)^{\frac{3}{2}}\left(s\right)_R} = \frac{1}{2.9} \tag{5.149}$$

The result of this simple analysis indicates that during the transient conditions, in which $\left(Q_{HPI}\right)_R$ is held at 1:276, the downcomer plume entrainment and temperature decay will be somewhat distorted. Hence, the need for some separate effects testing to further examine plume spreading and temperature decay in the APEX-CE downcomer.

5.2.6 Downcomer Wall Heat Transfer

The evaluation of the local temperature gradient in the RPV downcomer walls is a key part of assessing a transient's potential for inducing pressurized thermal shock. This section shows how the wall heat transfer in APEX-CE compares to that in the Palisades Plant RPV.

Figure 5.25 presents a schematic of the geometry that was considered. It consists of a metal slab insulated on the exterior while the interior of the slab is in contact with a cold falling plume.

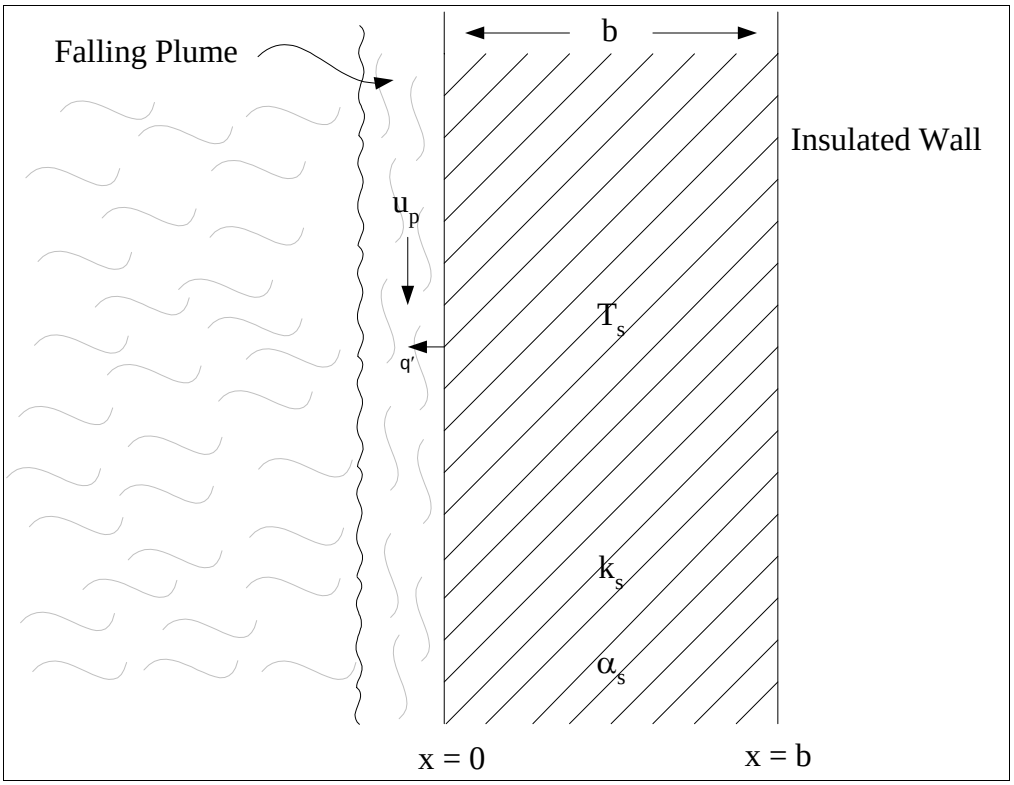

Figure 5.25 Schematic of Geometry for Downcomer Wall Heat Transfer

The general heat conduction equation for one-dimensional heat conduction through a metal slab having constant material properties is written as:

$$\frac{\partial T_s}{\partial t} = \alpha_s \frac{\partial^2 T_s}{\partial x^2} \qquad \textbf{(5.150)}$$

It is assumed that the slab is initially at a uniform temperature, $T_{s,o}$. That is,

$$T_s(x,o) = T_{s,o}$$

(5.151)

The slab is insulated on the outside and has a convection boundary condition on the inside which

$$\frac{\partial T_s}{\partial x}(b,t) = 0 \qquad \textbf{(5.152)}$$

is in contact with the cold plume. Thus the boundary conditions are expressed as:

and

$$k_s \frac{\partial T_s}{\partial x}\Big|_{x=0} = h_p\left[T_s(0,t) - T_p(t)\right] \qquad \textbf{(5.153)}$$

where h_p is the convective heat transfer coefficient in the plume and T_p is the plume temperature. These equations can be made dimensionless by normalizing each term relative to its initial condition.

That is,

$$x = bx^+ \qquad \textbf{(5.154)}$$

$$t = \tau_m t^+ \qquad \textbf{(5.155)}$$

$$\left(T_s - T_I\right) = \left(T_{s,o} - T_I\right)\left(T_s - T_I\right)^+ \qquad \textbf{(5.156)}$$

$$\left(T_s - T_p\right) = \left(T_{s,o} - T_I\right)\left(T_s - T_p\right)^+ \qquad \textbf{(5.157)}$$

where τ_m is the time constant for the fluid temperature transient and T_I is the perfectly mixed mean fluid temperature as specified in Section 5.4.2.1.

Substituting equations (5.154) through (5.157) into (5.150) and (5.153) yields:

$$\frac{\partial}{\partial t^+}\left(T_s - T_I\right) = F_o \frac{\partial^2}{\partial\left(x^+\right)^2}\left(T_s - T_I\right)^+ \qquad \textbf{(5.158)}$$

and

$$\frac{\partial}{\partial x^+}\left(T_s - T_I\right) = Bi\left[T_s - T_p\right]^+ \qquad \textbf{(5.159)}$$

where the Fourier number, F_o, is defined as:

$$F_o = \frac{\alpha_s \tau_m}{b^2} \tag{5.160}$$

and the plume Biot number, Bi, is defined as:

$$Bi = \frac{h_p b}{k_s} \tag{5.161}$$

These two dimensionless groups characterize the wall heat transfer. Equation (5.161) requires an expression for the local heat transfer coefficient in the plume. This is examined in the next section.

5.2.6.1 Plume Convection Heat Transfer Coefficient

Valenzuela and Dolan used the following correlation to predict the plume heat transfer coefficients in the CREARE 1/2-Scale test facility.[25]

$$Nu_p = C_1 \, Re_p^{0.8} \, Pr^{0.4} \tag{5.162}$$

Where the Nusselt, Reynolds and Prandtl numbers are defined as:

$$Nu_p = \frac{2 s h_p}{k_f} \tag{5.163}$$

$$Re_p = \frac{2 u_p s}{\nu_f} \tag{5.164}$$

$$Pr = \frac{c_p \mu_f}{k_f} \tag{5.165}$$

Equations (5.162) is the well-known Dittus-Boelter correlation for turbulent flow which has been expressed in terms of the plume velocity, u_p. Figure 5.26 shows the comparison of this equation to the CREARE 1/2- scale data. The data collapse quite neatly to a single line. However, it is offset by a constant factor which can be accounted for by including the entrance effect caused by the thermal shield. There is no thermal shield in APEX-CE or Palisades.

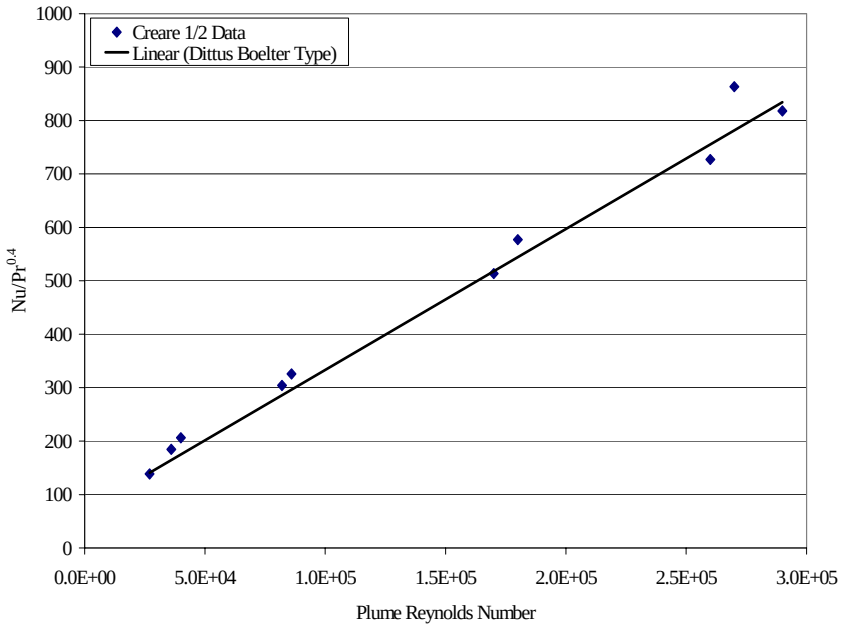

Figure 5.26 Comparison of Dittus-Boelter Correlation to CREARE ½-Scale Convective Heat Transfer Data

5.2.6.2 Assessment of Downcomer Heat Transfer Similarity

We now seek to determine the degree of similarity between wall heat transfer in APEX-CE and Palisades during integral system testing.

We find that:

$$\left(F_o\right)_R \approx \frac{1}{2.9} \tag{5.166}$$

$$\left(Bi\right)_R \approx \frac{1}{38} \tag{5.167}$$

$$\left(Nu_p\right)_R \approx \frac{1}{35} \tag{5.168}$$

5.2.6.3 Summary of Downcomer Heat Transfer

For the HPSI injection conditions required during integral system testing, the scaling analysis shows that the downcomer wall temperature gradients cannot be preserved in APEX-CE. The primary reason for this is that the APEX-CE RPV wall is very thin in comparison to the Palisades wall. As a result, the thermal penetration time will be much shorter in APEX-CE than in Palisades. Although

useful in bench marking the CFD codes, the wall temperature gradients will not be prototypical of Palisades. Based on these results, it is recommended that separate effects test also be performed in APEX-CE to obtain additional experimental data to assess the existing correlations for convection heat transfer and plume velocity in the downcomer.

5.2.7 REMIX Calculations

Because the fluid mixing behavior at the HPSI nozzle, in the cold legs, at the downcomer entrance and in the downcomer are coupled, it was deemed important to perform a global mixing assessment using the REMIX regional mixing code developed at Purdue.[43]

This section presents the results of steady-state REMIX calculations that were performed to assess the similarity of the overall cold leg and downcomer mixing behavior in the APEX-CE test facility and the Palisades plant. The two test cases chosen were at scaled flow injection conditions and stagnant loop conditions. The results have been plotted in terms of the dimensionless temperature versus the dimensionless time as developed in the top-down scaling analysis. That is,

$$\Delta T_p^+ = \frac{(T_m - T_{HPI})}{(T_{L,O} - T_{HPI})} \tag{5.169}$$

$$t^+ = \frac{t}{\tau_m} \tag{5.170}$$

The conditions for the two cases are shown in Table 5.1.

Table 5.1 Conditions for Remix Comparisons

	Pressure		Cold Leg Temperature		Injection Temperature		Injection Flow Rate	
	psia	MPa	°F	°C	°F	°C	ft^3/s	m^3/s
Case 1								
APEX-CE	90	0.6203	320	160	60	15.6	2.25×10^{-3}	6.371×10^{-5}
Palisades	315	2.1713	421.8	216.6	87	30.6	0.62	0.0176
Case 2								
APEX-CE	290	2.00	414	212.2	60	15.6	1.07×10^{-3}	3.030×10^{-5}
Palisades	1020	7.031	546.4	285.8	87	30.6	0.297	0.00841

Figures 5.27 through 5.32 show the results for the two cases. Each case represents a three hour transient. In general, the temperature decays compare reasonably well throughout the transients.

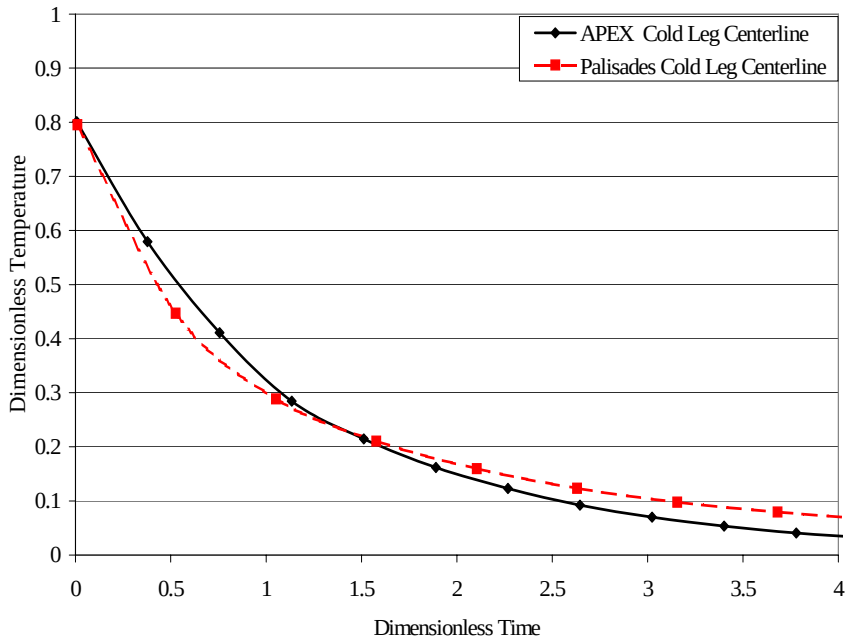

Figure 5.27 Plot of Dimensionless Plume Temperatures as a Function of Downcomer Axial Location and Dimensionless Time (Case 1 at Cold Leg Centerline)

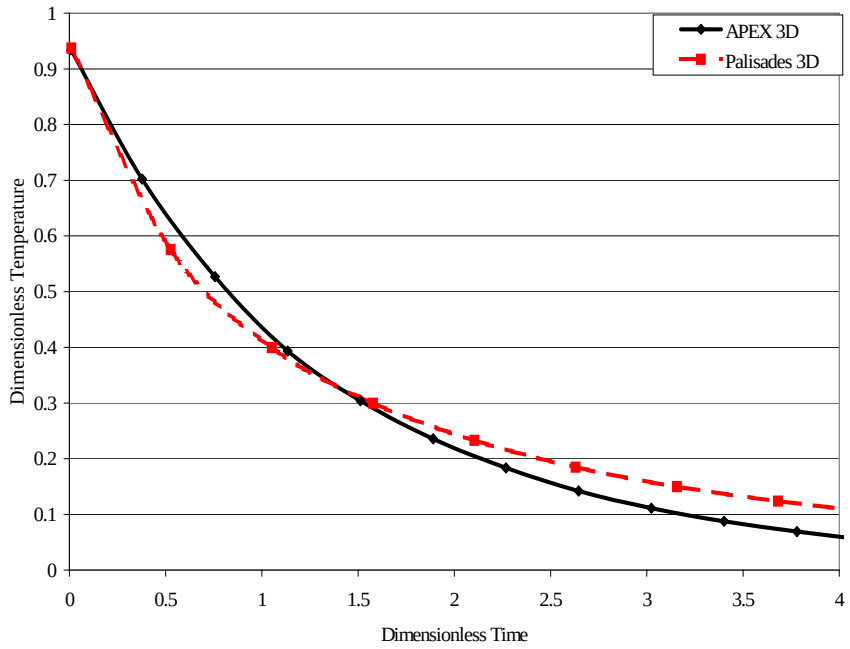

Figure 5.28 Plot of Dimensionless Plume Temperatures as a Function of Downcomer Axial Location and Dimensionless Time (Case 1 at 3 Cold Leg Diameters)

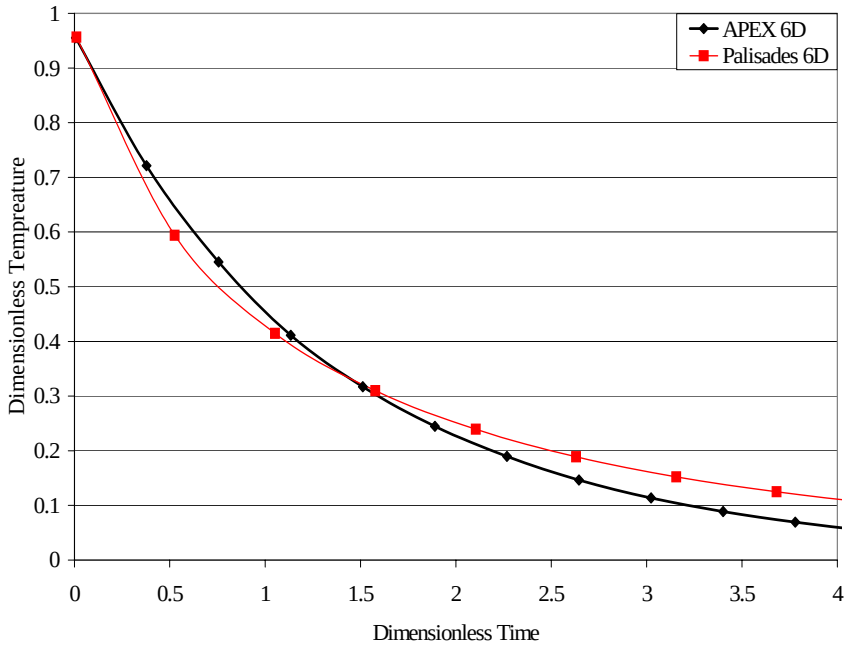

Figure 5.29 Plot of Dimensionless Plume Temperatures as a Function of Downcomer Axial Location and Dimensionless Time (Case 1 at 6 Cold Leg Diameters)

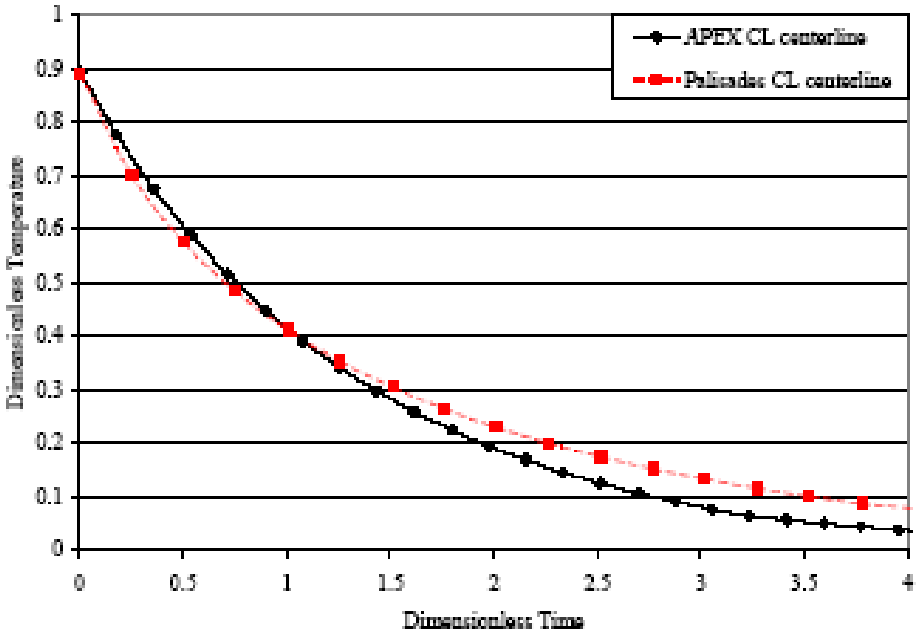

Figure 5.30 Plot of Dimensionless Plume Temperatures as a Function of Downcomer Axial Location and Dimensionless Time (Case 1 at 6 Cold Leg Diameters)

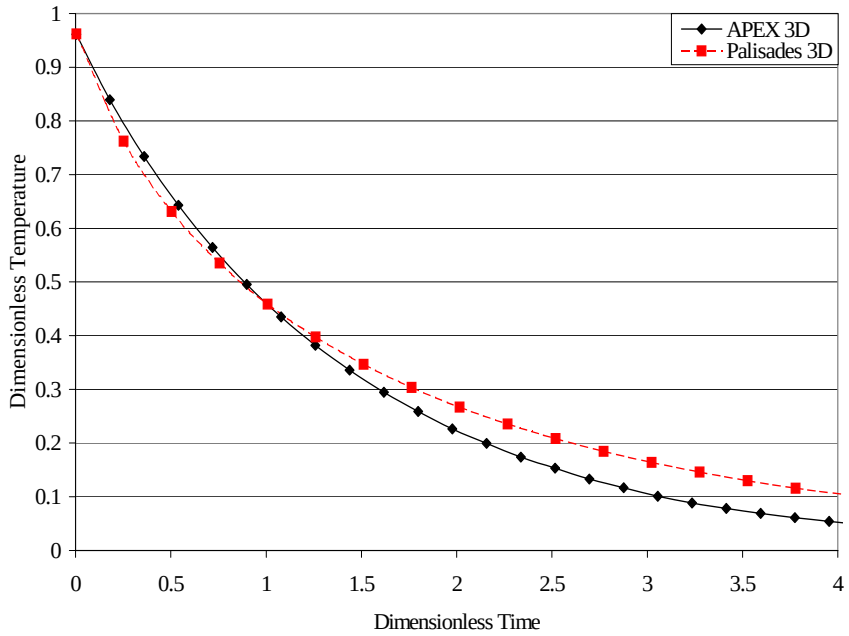

Figure 5.31 Plot of Dimensionless Plume Temperatures as a Function of Downcomer Axial Location and Dimensionless Time (Case 2 at Cold Leg Centerline)

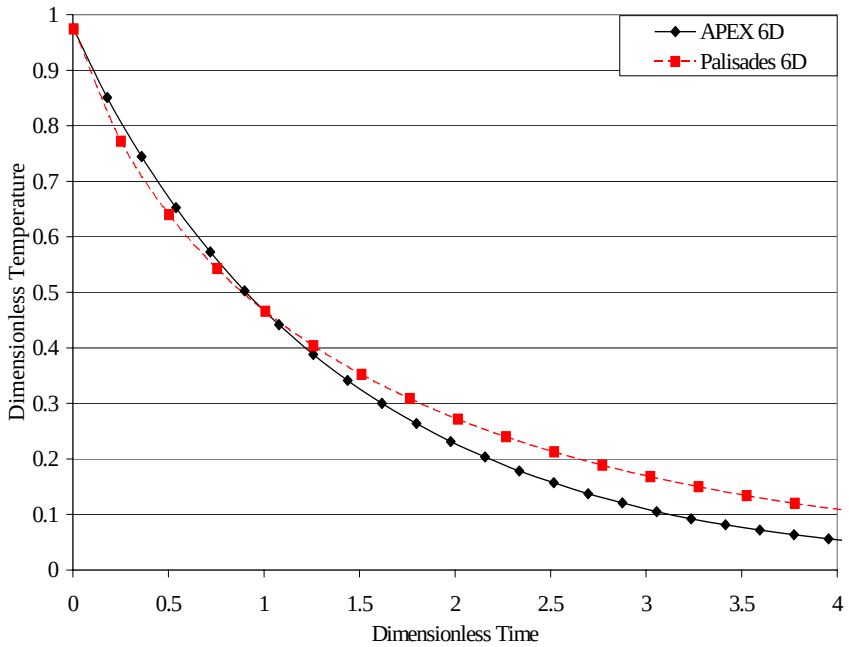

Figure 5.32 Plot of Dimensionless Plume Temperatures as a Function of Downcomer Axial Location and Dimensionless Time (Case 2 at 3 Cold Leg Diameter)

6.0 REACTOR COOLANT SYSTEM DEPRESSURIZATION SCALING ANALYSIS

The scenarios of interest to this analysis are small break loss-of-coolant-accidents (SBLOCAs). Two types of SBLOCAs are being considered; a small break on a hot leg and a stuck open pressurized Power Operated Relief Valve (PORV). The evolution of these transients are somewhat similar. After the break opens there is an initial blowdown to saturated conditions in the primary loop. The saturation pressure on the primary side corresponds to the secondary side turbine bypass valve relief pressure. For small breaks, the steam generator tubes will drain, resulting in the loss of the heat sink and consequently the loss of two-phase natural circulation in the primary loop. As primary system pressure drops, HPSI actuation will occur resulting in thermal stratification in the cold legs and the formation of cold plumes in the downcomer.

Figure 6.1 presents the scaling analysis flow diagram for primary system depressurization. First, the governing set of equations for the depressurization of a two-phase fluid system were developed. This resulted in obtaining a Depressurization Rate Equation. Next, a top-down system level scaling analysis was performed for the Reactor Coolant System (RCS) assuming multiple vent and injection paths. This included the development of scaling criteria for sizing breaks. Last, a bottom-up analysis was performed to describe the scaling of local transport processes such as the critical flow through the breaks.

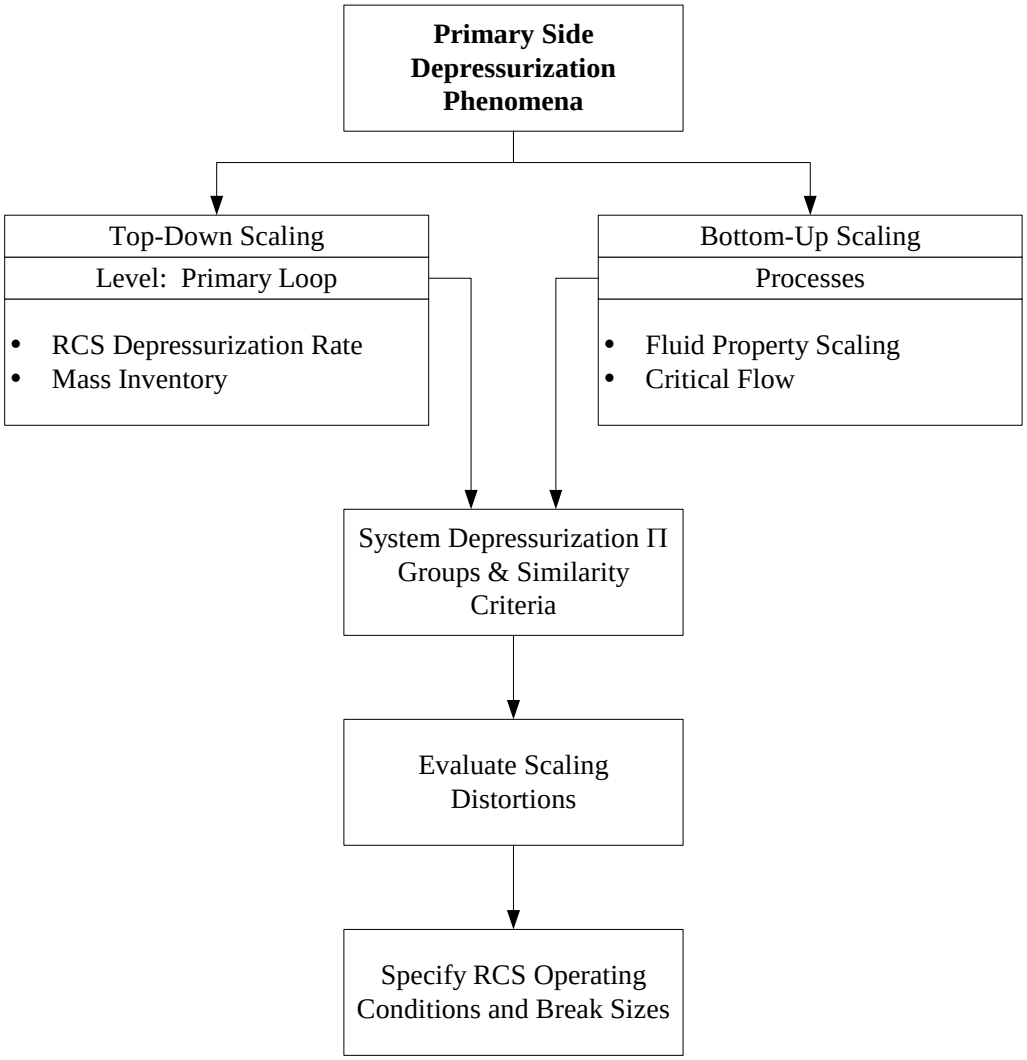

Figure 6.1 Flow Chart of the Primary Side Depressurization Scaling Analysis

Figure 6.2 describes the reactor coolant system control volume that was considered in this analysis. The break locations of interest are depicted on the sketch.

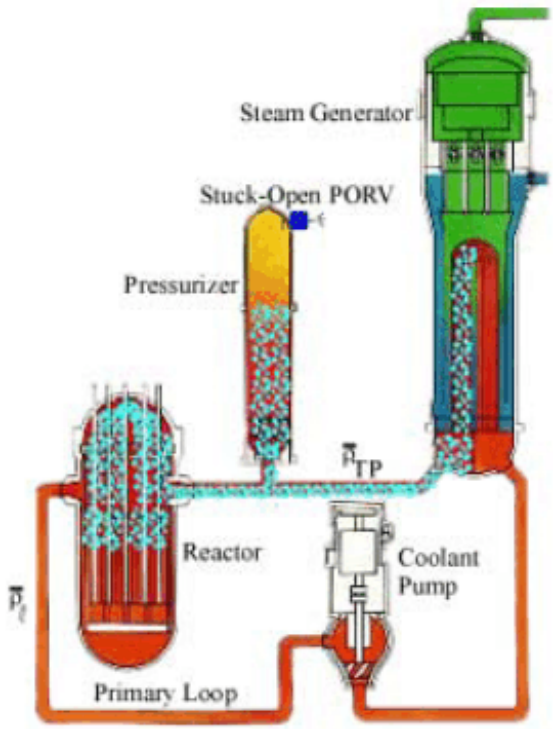

Figure 6.2 RCS Control Volume for SBLOCA Analysis

6.1 GOVERNING EQUATIONS FOR RCS TWO-PHASE FLUID DEPRESSURIZATION

The mass conservation equation for a RCS control volume undergoing a depressurization event is given by:

$$\frac{dM}{dt} = \Sigma \dot{m}_{in} - \Sigma \dot{m}_{out} \qquad \textbf{(6.1)}$$

where M is the fluid mass within the RCS and $\dot{m}$ represents the mass flow rate entering or leaving the reactor coolant system.

The energy conservation equation for the RCS fluid is expressed as follows:

$$\frac{dU}{dt} = \Sigma(\dot{m}h)_{in} - \Sigma(\dot{m}h)_{out} + q_{SG} + q_{core} + q_{loss} - P\frac{dV}{dt} \qquad \textbf{(6.2)}$$

where U is the bulk internal energy of the fluid within the RCS, h is the enthalpy of the fluid entering or leaving the RCS, q_{SG}, q_{core} and q_{loss} are the steam generator energy transfer rate, the core power and the heat loss respectively. P is the RCS pressure and V is the RCS volume.

The specific internal energy and the specific volume are defined respectively as follows:

$$e = \frac{U}{M} \tag{6.3}$$

$$v = \frac{V}{M} \tag{6.4}$$

The total change in specific internal energy is written in terms of partial differentials with respect to pressure and specific volume as follows:

$$de = \left(\frac{\partial e}{\partial p}\right)_v dP + \left(\frac{\partial e}{\partial v}\right)_p dv \tag{6.5}$$

Substituting equation (3) into (2) yields:

$$\frac{dMe}{dt} = \Sigma(\dot{m}h)_{in} - \Sigma(\dot{m}h)_{out} + q_{SG} + q_{core} + q_{loss} - P\frac{dV}{dt} \tag{6.6}$$

Expanding the term on the LHS of equation (6.6), substituting equation (6.1) and rearranging yields:

$$M\frac{de}{dt} = (\Sigma\dot{m}_{in})(h_{in} - e) - (\Sigma\dot{m}_{out})(h_{out} - e) + q_{SG} + q_{core} + q_{loss} - P\frac{dV}{dt} \tag{6.7}$$

In equation (6.7), it has been assumed that h_{in} is the same for all the injection locations and h_{out} is the same for all the vent paths. This will be true for the cases being considered. Substituting equation (6.5) into (6.7), and rearranging yields:

$$\begin{aligned} M\left(\frac{\partial e}{\partial P}\right)_v \frac{dP}{dt} &= (\Sigma\dot{m}_{in})(h_{in} - e) - (\Sigma\dot{m}_{out})(h_{out} - e) \\ &+ q_{SG} + q_{core} + q_{loss} - P\frac{dV}{dt} - M\left(\frac{\partial e}{\partial v}\right)_p \frac{dv}{dt} \end{aligned} \tag{6.8}$$

Using equation (6.4), and the mass conservation equation, the last term on the RHS of equation (6.8) is written as:

$$M\left(\frac{\partial e}{\partial v}\right)_p \frac{dv}{dt} = \left(\frac{\partial e}{dv}\right)_p \frac{dV}{dt} - v\left(\frac{\partial e}{\partial v}\right)_p \left(\Sigma\dot{m}_{in} - \Sigma\dot{m}_{out}\right) \tag{6.9}$$

Substituting back into equation (6.8) yields:

$$\begin{aligned} M\left(\frac{\partial e}{\partial P}\right)_v \frac{dP}{dt} &= \left(\Sigma\dot{m}_{in}\right)\left[h_{in} - e + v\left(\frac{\partial e}{\partial v}\right)_p\right] \\ &- \left(\Sigma\dot{m}_{out}\right)\left[h_{out} - e + v\left(\frac{\partial e}{\partial v}\right)_p\right] \\ &+ q_{SG} + q_{core} + q_{loss} - \left[P + \left(\frac{\partial e}{\partial v}\right)_p\right]\frac{dV}{dt} \end{aligned} \tag{6.10}$$

which is the "depressurization rate equation." For the RCS control volume, which has rigid boundaries, equation (6.10) becomes:

$$\begin{aligned} M\left(\frac{\partial e}{\partial P}\right)_v \frac{dP}{dt} &= \left(\Sigma\dot{m}_{in}\right)\left[h_{in} - e + v\left(\frac{\partial e}{\partial v}\right)_p\right] \\ &- \left(\Sigma\dot{m}_{out}\right)\left[h_{out} - e + v\left(\frac{\partial e}{\partial v}\right)_p\right] + q_{SG} + q_{core} + q_{loss} \end{aligned} \tag{6.11}$$

For the SBLOCA tests planned for APEX-CE, there will be four HPSI injection flows having uniform fluid properties and there will be one break location. Therefore, equation (6.11) becomes:

$$M\left(\frac{\partial e}{\partial P}\right)_v \frac{dP}{dt} = \dot{m}_{HPI}\left[h_{HPI} - e + v\left(\frac{\partial e}{\partial v}\right)_p\right] - \dot{m}_{Brk}\left[h_{Brk} - e + v\left(\frac{\partial e}{\partial v}\right)_p\right] + q_{net} \tag{6.12}$$

where the net energy transfer rate is given as:

$$q_{net} = q_{SG} + q_{core} + q_{loss} \tag{6.13}$$

Equation (6.12) is the governing equation for depressurization behavior in the RCS.

6.2 TOP-DOWN REACTOR COOLANT SYSTEM DEPRESSURIZATION SCALING ANALYSIS

The mass conservation equation, equation (6.1), is expressed in dimensionless form by dividing each term by its respective initial condition and further dividing by the mass flow rate of the fluid leaving the break. This results in the following dimensionless mass balance equation:

$$\tau_{RCS} \frac{dM^{+}}{dt} = \Pi_m \dot{m}^{+}_{HPI} - \dot{m}^{+}_{Brk} \tag{6.14}$$

where the superscript "+" indicates normalization with respect to initial conditions. The residence time constant, (τ_{rcs}), for the depressurization transient is given by:

$$\tau_{rcs} = \frac{M_o}{\dot{m}_{Brk,o}} \tag{6.15}$$

and the characteristic time ratio is given by:

$$\Pi_m = \frac{\dot{m}_{HPI,o}}{\dot{m}_{Brk,o}} \tag{6.16}$$

Π_m is the system mass flow rate ratio. For a constant injection flow rate, Π_m represents the total liquid mass injected into the RCS during the residence time (τ_{rcs}).

Equation (6.12) can be expressed in dimensionless form by dividing each term by its respective initial condition.

The normalized terms are as follows:

$$M = M_o M^+ \tag{6.17}$$

$$P = P_o P^+ \tag{6.18}$$

$$q_{net} = q_{net,o} q_{net}^+ \tag{6.19}$$

$$\dot{m}_{Brk} = \dot{m}_{Brk,o} \dot{m}_{Brk}^+ \tag{6.20}$$

$$\dot{m}_{HPI} = \dot{m}_{HPI,o} \dot{m}_{HPI}^+ \tag{6.21}$$

The temporal behavior of these normalized terms will be preserved in the model.

$$\left[h_{HPI} - e + v\left(\frac{\partial e}{\partial P}\right)_p \right] = \left[h_{HPI} - e + v\left(\frac{\partial e}{\partial P}\right)_p \right]_o \left[h_{HPI} - e + v\left(\frac{\partial e}{\partial v}\right)_p \right]^+ \tag{6.22}$$

$$\left[h_{Brk} - e + v\left(\frac{\partial e}{\partial v}\right)_p \right] = \left[h_{Brk} - e + v\left(\frac{\partial e}{\partial v}\right)_p \right]_o \left[h_{Brk} - e + v\left(\frac{\partial e}{\partial v}\right)_p \right]^+ \tag{6.23}$$

Substituting these equations into (6.12) and dividing through by $\dot{m}_{Brk,o}\left[h_{Brk} - e + v\left(\frac{\partial e}{\partial v}\right)_p\right]_o$ yields the dimensionless depressurization rate equation:

$$M^+\left(\frac{\partial e}{\partial P}\right)_v^+ \tau_{RCS}\frac{\partial P^+}{\partial t} = \frac{\Pi_h}{\Pi_\varepsilon}\dot{m}_{HPI}^+\left[h_{HPI} - e + v\left(\frac{\partial e}{\partial v}\right)_p\right]^+ - \frac{\dot{m}_{Brk}^+}{\Pi_\varepsilon}\left[h_{Brk} - e + v\left(\frac{\partial e}{\partial v}\right)_p\right]^+ + \frac{\Pi_\Gamma}{\Pi_\varepsilon}q_{net}^+ \tag{6.24}$$

where the characteristic time ratios are given by:

$$\Pi_h = \frac{\dot{m}_{HPI,o}\left[h_{HPI} - e + v\left(\frac{\partial e}{\partial v}\right)_p\right]_o}{\dot{m}_{Brk,o}\left[h_{Brk} - e + v\left(\frac{\partial e}{\partial v}\right)_p\right]_o} \tag{6.25}$$

$$\Pi_\Gamma = \frac{q_{net,o}}{\dot{m}_{Brk,o}\left[h_{Brk} - e + v\left(\frac{\partial e}{\partial v}\right)_p\right]_o} \tag{6.26}$$

$$\Pi_\epsilon = \epsilon_o = \frac{P_o\left(\frac{\partial e}{\partial P}\right)_{v,o}}{\left[h_{Brk} - e + v\left(\frac{\partial e}{\partial v}\right)_p\right]_o} \tag{6.27}$$

Π_h is the energy flow rate ratio. It represents the ratio of the total energy change due to fluid injection to the energy change caused by the break flow. Π_Γ is the power ratio. It represents the ratio of the net heat into the system to the rate of fluid energy transport through the break. Π_ϵ is the fluid mixture dilation property group.

Equation (6.27) reveals that the fluid dilation property group couples the system intensive energy change to the intensive energy at the break. For high pressure systems venting to the ambient, the fluid properties at the break are determined at critical flow conditions.

Evaluating the RCS time constant, τ_{rcs}, and the dimensionless groups Π_m, Π_h, Π_r, Π_ε requires knowledge of the pressure scaled fluid properties and the critical mass flux. These parameters are evaluated in the bottom-up scaling analysis that follows.

6.2.1 Similarity of Pressure Trajectories in Dimensionless Phase Space

One of the goals of the test program is to operate the APEX-CE facility such that the pressure trends that evolve in APEX-CE for a given scenario would be the same for a similar scenario in Palisades when the results are plotted in dimensionless phase space. That is, plotting scenario pressure histories as P/P_o versus t/τ_{RCS}, or P/P_o versus M/M_o, would yield overlaying curves for the two facilities. This condition can be achieved by satisfying the following requirements:

1. The scenarios are initiated from the same initial condition in dimensionless phase space. In this case P^+ at $t^+=0$, is 1.
2. The rate of chance, (i.e., slope), is preserved in dimensionless phase space. This imposes the following scaling criterion:

$$\left(\frac{dP^+}{dt^+}\right)_R = 1 \qquad \textbf{(6.28)}$$

Satisfying the requirement given by equation (6.28) means preserving the dimensionless Π groups on the right hand side of the equation (6.24). If the two requirements listed above are satisfied, then the following is true:

$$\left(\frac{P}{P_o}\right)_{APEX} = \left(\frac{P}{P_o}\right)_{Pal} \qquad \textbf{(6.29)}$$

This means that the dimensionless pressure at any point along the scenario trajectory will be the same in APEX-CE and Palisades.

Figure 6.3 shows how the saturation pressures in APEX-CE would relate to the saturation pressures in Palisades. In this figure, P_o for Palisades is 6.2 MPa (900 psia) and P_o for APEX-CE is 2.0 MPa (293 psia). These pressures correspond to the turbine bypass pressure relief setpoints on the secondary side.

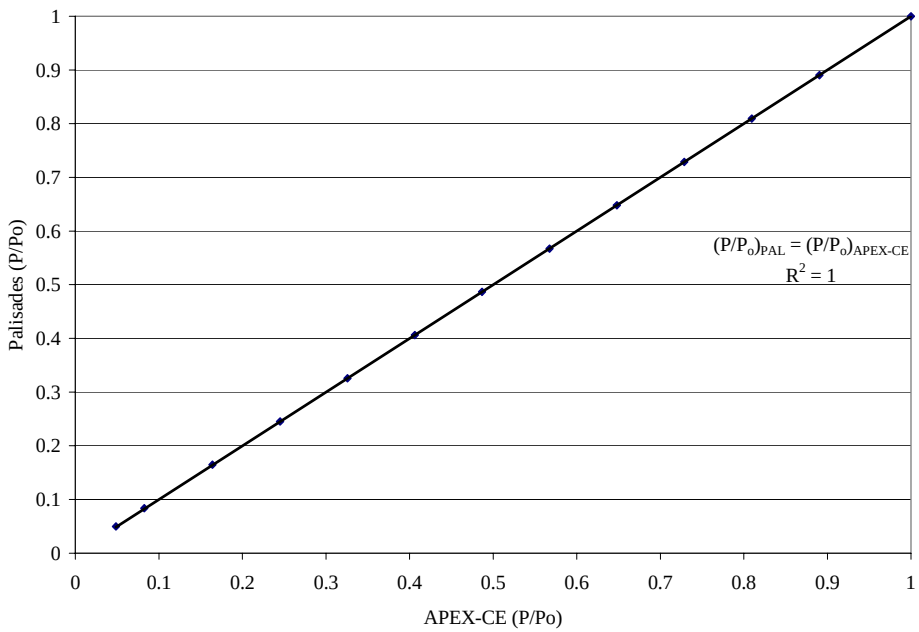

Figure 6.3 Scaling Relationship Between Palisades and APEX-CE Saturation Pressure

6.3 BOTTOM-UP SCALING DEPRESSURIZATION SCALING ANALYSIS

The objective of the bottom-up scaling analysis was to obtain the closure relations needed to evaluate the scaling ratios developed through the top-down analysis. These closure relations are dependent on fluid properties. Therefore, the first step in the bottom-up analysis was the development of the method to relate fluid properties in Palisades to those at reduced pressure in APEX-CE.

6.3.1 Self-Similarity of Fluid Properties in Phase Equilibria (P_{sat} Scaling)

The equation of state for many of the important thermodynamic properties, ψ (P), of the saturated fluid can be described by a simple power function as follows:

$$\psi = \psi_o \left(\frac{P}{P_o} \right)^{\xi} \tag{6.30}$$

where ψ_o can be evaluated at an arbitrary reference pressure, P_o, within the range of applicability of equation (6.30) and ξ is an empirically determined constant. For saturated water,

having a pressure between atmospheric and approximately 15 MPa (2175 psia), the following thermodynamic properties are well correlated by equation (6.30) as demonstrated in Figures 6.4 through 6.7.

$$\frac{Pv_{fg}}{h_{fg}} = \left(\frac{Pv_{fg}}{h_{fg}}\right)_o \left(\frac{P}{P_o}\right)^{0.11} \tag{6.31}$$

$$s_f = s_{f,o}\left(\frac{P}{P_o}\right)^{0.20} \tag{6.32}$$

$$v_g = v_{g,o}\left(\frac{P}{P_o}\right)^{-1.02} \tag{6.33}$$

$$v_{fg} = v_{fg,o}\left(\frac{P}{P_o}\right)^{-1.06} \tag{6.34}$$

The form of equation (6.30) has the special property of being “invariant” with respect to a two-parameter transformation in scale. That is, rescaling the variables such that:

$$\psi = C_1\psi^* \tag{6.35}$$

$$\psi = C_1\psi_o^* \tag{6.36}$$

$$P = C_2P^* \tag{6.37}$$

$$P = C_2P_o^* \tag{6.38}$$

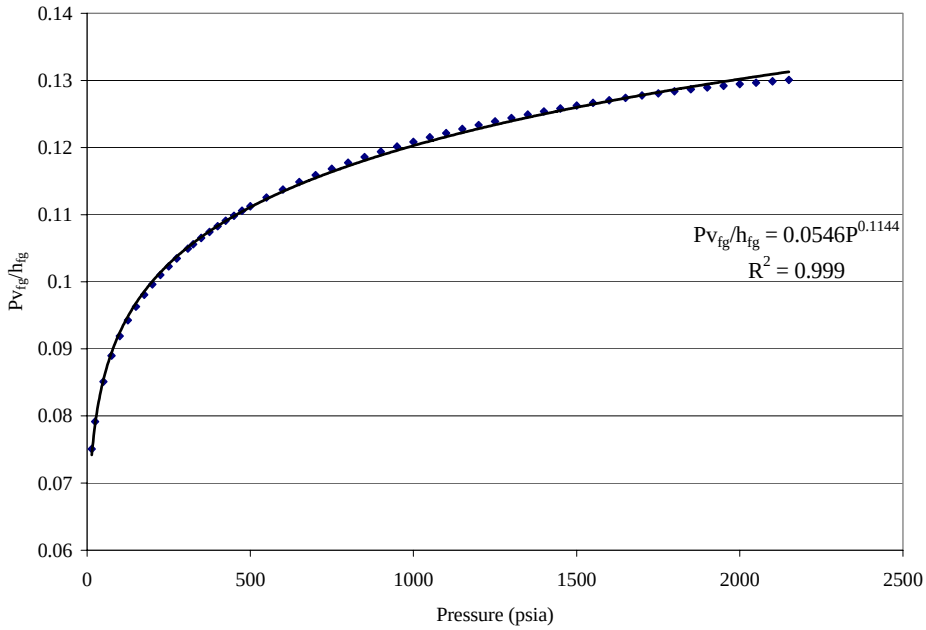

Figure 6.4 Power Law for Pv_{fg}/h_{fg} as a Function of Pressure

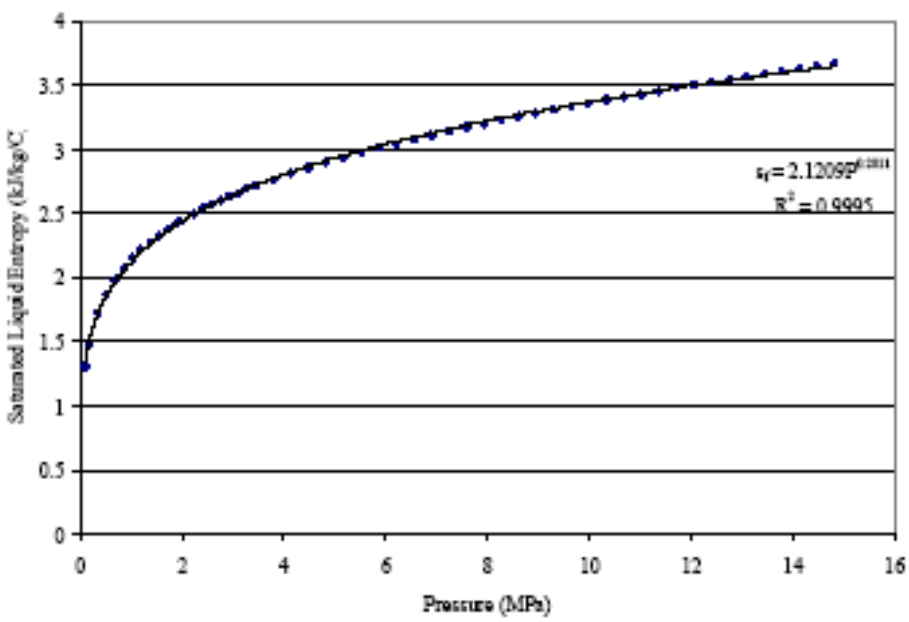

Figure 6.5 Power Law for s_f as a Function of Pressure

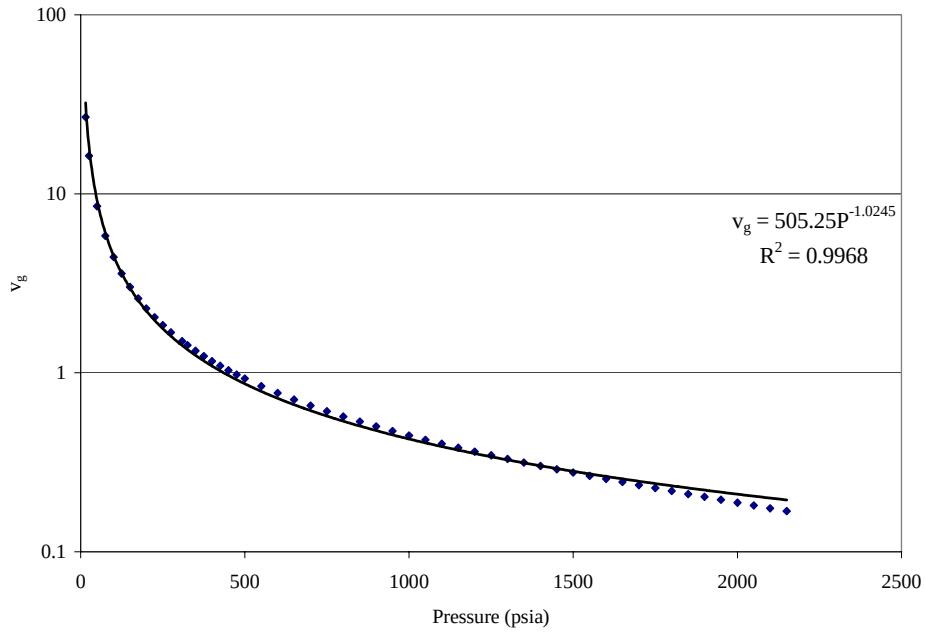

Figure 6.6 Power Law for v_g as a Function of Pressure

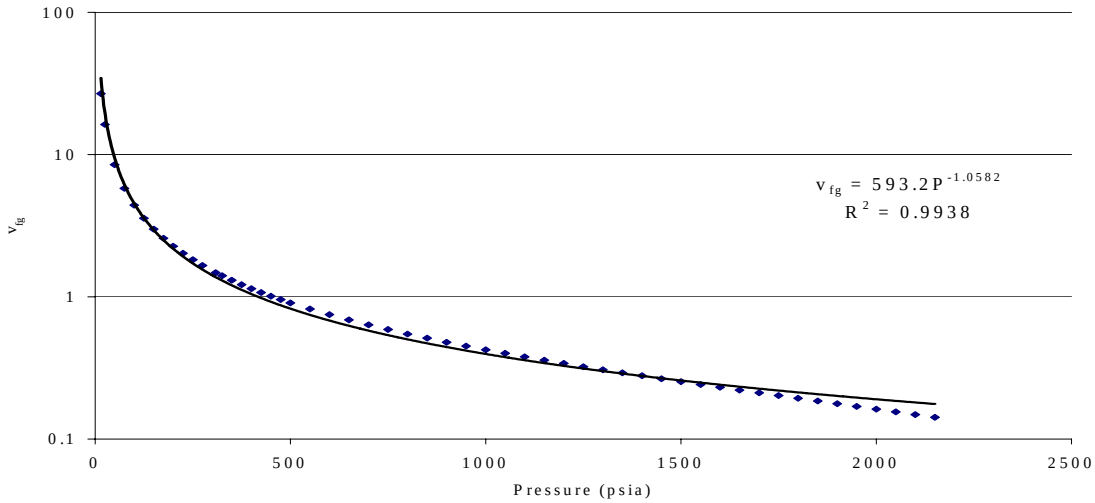

Figure 6.7 Power Law for v_{fg} as a Function of Pressure

where C_1 and C_2 are constants, and substituting these rescaled variables into equation (6.30) yields:

$$\psi^* = \psi_o^* \left(\frac{P^*}{P_o^*} \right)^{\xi} \tag{6.39}$$

The form of the equation of state remains unchanged. This type of transformation is known as a "stretching" or "similarity" transformation. The special feature of invariance with scale implies that the points and slopes of any curves in the (ψ,P) phase space can be related to corresponding points and slopes in the (ψ^*, P^*) phase space. (Bluman, 1974).[44] This type of scale invariance is known as "self-similarity." Self-similarity can be defined as a repetition of detail at descending scales.

An importance consequence of self-similarity is made readily evident by substituting pressures are preserved, then self-similarity dictates that the dimensionless fluid properties (ψ/ψ_o) will also be preserved.

6.3.2 Equations of State for Saturated Pressure and Temperature (T_{sat} Scaling)

The Clausius-Clapeyron equation is the classical differential equation that defines the slope dP/dT, for a phase equilibrium curve. It is derived assuming that the Gibb's free energies for the two-phases being considered are equal (Lay, 1990).[45] Using the saturated definition for the Gibb's free energy and relating the change in entropy to the latent heat of vaporization and the saturation temperature yields the well-known Clausius-Clapeyron equation:

$$\frac{dP}{dT} = \frac{h_{fg}}{v_{fg} T} \tag{6.40}$$

An analytical expression for an equation of state relating saturation pressure to saturation temperature can be obtained as follows:

Substituting equation (6.29) int (6.40) and rearranging yields:

$$\left(\frac{P}{P_o} \right)^{\xi - 1} dP = \left(\frac{h_{fg}}{v_{fg}} \right)_o \frac{1}{T} \, dT \tag{6.41}$$

Integrating from P_o to P_{sat} and from T_o to T_{sat} yields the desired relationship between P_{sat} and T_{sat}.

$$P_{sat}(T_{sat}) = P_o\left[1 + \xi\left(\frac{h_{fg}}{Pv_{fg}}\right)_o Ln\left(\frac{T_{sat}}{T_o}\right)\right]^{1/\xi} \qquad \textbf{(6.42)}$$

Figure 6.8 shows that equation (6.42) is quite accurate for the range of conditions examined.

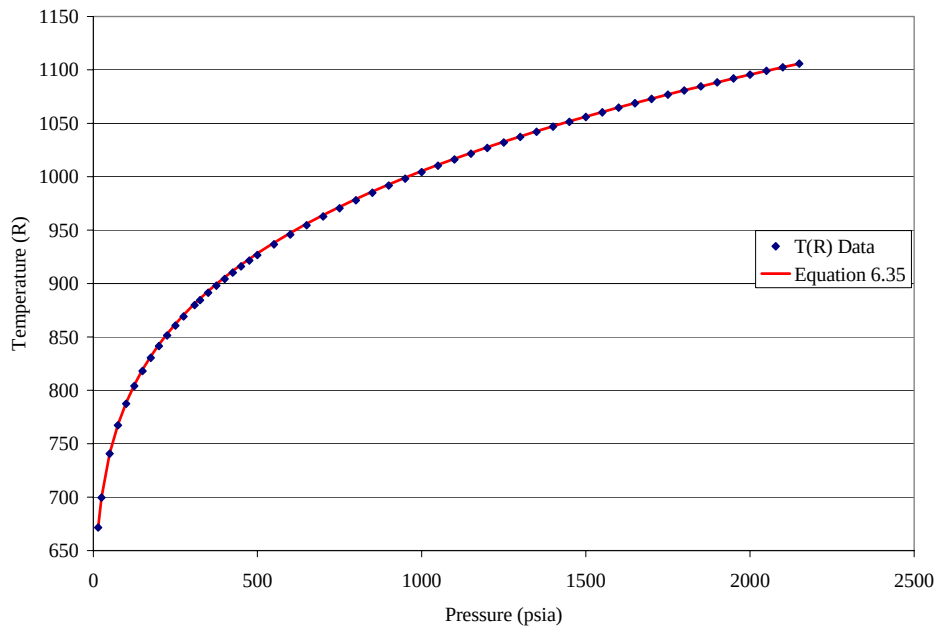

Figure 6.8 Comparison of Equation (6.42) to Steam Tables

Equation (6.42) can be rearranged to obtain saturation temperature in terms of saturation pressure. The result is:

$$T_{sat}(P_{sat}) = T_o \exp\left\{-\frac{1}{\xi}\left(\frac{Pv_{fg}}{h_{fg}}\right)_o\left[1-\left(\frac{P_{sat}}{P_o}\right)^{\xi}\right]\right\} \qquad \textbf{(6.43)}$$

This equation can be accurately approximated using the following identity:

$$\exp(x) \approx 1 + x \qquad \textbf{(6.44)}$$

for x << 1 which is applicable to the current situation. Thus equation (6.36) is approximated by:

$$T_{sat} = T_o \left\{ 1 - \frac{1}{\xi} \left(\frac{Pv_{fg}}{h_{fg}} \right)_o \left[1 - \left(\frac{P_{sat}}{P_o} \right)^{\xi} \right] \right\} \tag{6.45}$$

Rearranging equation (6.45) yields:

$$\left(\frac{h_{fg}}{Pv_{fg}} \right)_o \left[1 - \left(\frac{T_{sat}}{T_o} \right) \right] = \frac{1}{\xi} \left[1 - \left(\frac{P_{sat}}{P_o} \right)^{\xi} \right] \tag{6.46}$$

This equation in valid for both APEX-CE and Palisades for the range of saturated conditions being examined. Writing this equation for APEX-CE yields:

$$\left(\frac{h_{fgo}}{P_o v_{fgo}} \right)_{APEX} \left[1 - \left(\frac{T_{sat}}{T_o} \right)_{APEX} \right] = \frac{1}{\xi} \left[1 - \left(\frac{P_{sat}}{P_o} \right)^{\xi}_{APEX} \right] \tag{6.47}$$

and for Palisades:

$$\left(\frac{h_{fgo}}{P_o v_{fgo}} \right)_{Pal} \left[1 - \left(\frac{T_{sat}}{T_o} \right)_{Pal} \right] = \frac{1}{\xi} \left[1 - \left(\frac{P_{sat}}{P_o} \right)^{\xi}_{Pal} \right] \tag{6.48}$$

Recalling that:

$$\left(\frac{P_{sat}}{P_o} \right)_{APEX} = \left(\frac{P_{sat}}{P_o} \right)_{Pal} \tag{6.49}$$

as given by equation (6.29), it is recognized that the right hand side of equation (6.47) and (6.48) are identical. Therefore equations (6.47) and (6.48) can be set equal to obtain:

$$\left(\frac{h_{fgo}}{P_o v_{fgo}} \right)_{APEX} \left[1 - \left(\frac{T_{sat}}{T_o} \right)_{APEX} \right] = \left(\frac{h_{fgo}}{Pv_{fgo}} \right)_{PAL} \left[1 - \left(\frac{T_{sat}}{T_o} \right)_{PAL} \right] \tag{6.50}$$

Rearranging this equation yields the desired saturation temperature scaling relation:

$$\left(\frac{T_{sat}}{T_o}\right)_{Pal} = \left(\frac{h_{fgo}}{P_o v_{fgo}}\right)_R \left(\frac{T_{sat}}{T_o}\right)_{APEX} - \left[\left(\frac{h_{fgo}}{P_o v_{fgo}}\right)_R - 1\right] \tag{6.51}$$

Equation (6.51) is linear as shown in Figure 6.9 for the APEX-CE and Palisades reference temperatures (i.e., the saturation temperatures for the corresponding APEX-CE and Palisades reference pressures). Figure 6.9 compares the approximate solution given by equation (6.51) to the exact result obtained using the steam tables.

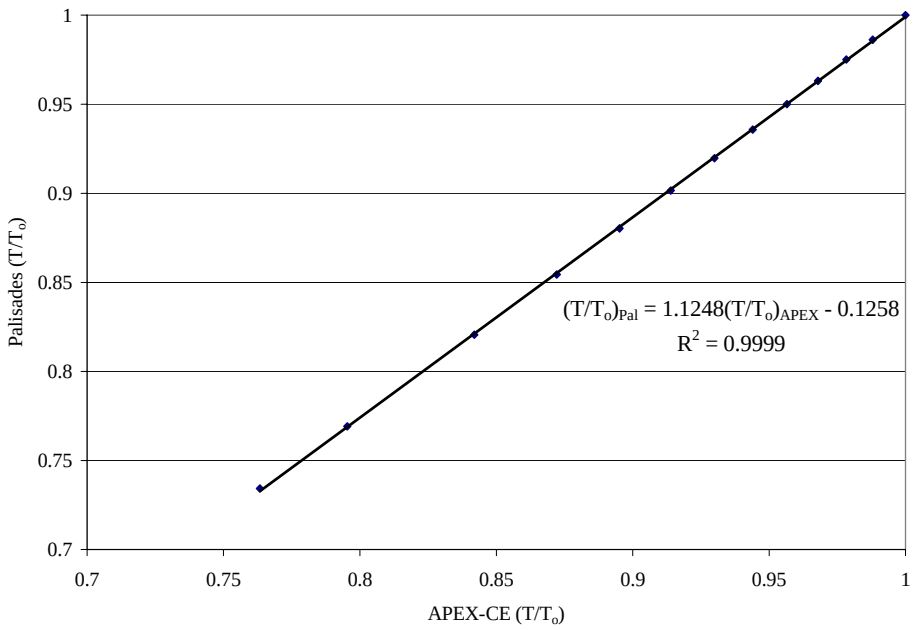

Figure 6.9 Scaling Relationship Between Palisades and APEX-CE Saturation Temperature

6.3.3 DILATION PROPERTY GROUP FOR SATURATED LIQUID-VAPOR BLOWDOWNS

This section demonstrates how the dilation property group, Π_ϵ, given by equation (6.27), is evaluated for different fluid conditions. For a two-phase fluid mixture in phase equilibrium, the following thermodynamic relations are applicable for the mixture specific internal energy and the mixture specific volume, respectively:

$$e = e_f + x e_{fg} \tag{6.52}$$

$$v = v_f + x v_{fg} \tag{6.53}$$

Eliminating the fluid mixture equilibrium quality, x, between equations (6.52) and (6.53) yields the following expression for the specific internal energy:

$$e = e_f + \frac{v - v_f}{v_{fg}} e_{fg} \tag{6.54}$$

The partial derivative of this equation with respect to specific volume, while holding pressure constant, yields:

$$\left(\frac{\partial e}{\partial v}\right)_P = \frac{e_{fg}}{v_{fg}} \tag{6.55}$$

Lastly, the latent heat of vaporization is given by:

$$h_{fg} = Pv_{fg} + e_{fg} \tag{6.56}$$

The reader is encouraged to substitute equations (6.52) through (6.46) into equation (6.27) to obtain the following expression for the saturated mixture dilation property group:

$$\Pi_\epsilon = \frac{1}{\left[v_f + x_{Brk} v_{fg}\right]} \left(\frac{Pv_{fg}}{h_{fg}}\right) \left(\frac{\partial e}{\partial P}\right)_v \tag{6.57}$$

where the equilibrium vapor quality at the break is given by x_{Brk}:

$$x_{Brk} = \frac{h_{Brk} - h_f}{h_{fg}} \tag{6.58}$$

Let us examine the pressure dependencies of the terms that comprise the fluid mixture dilation property group given by equation (6.57). The property group (Pv_{fg}/h_{fg}) has already been evaluated as shown in Figure 6.3 and found to be described by equation (6.31), a power law that exhibits self-similarity for a wide range of saturation pressures.

The last term on the RHS of equation (6.57), $(\partial e/\partial P)_v$, is a partial derivative which requires examining the change in the fluid mixture internal energy with respect to pressure *while holding the mixture specific volume, v, constant*. It should not be confused with the total specific internal energy change with respect to pressure. An adequate model for this term can be obtained by developing an expression for the mixture internal energy as a function of pressure while at constant specific volume and taking the derivative with respect to pressure. Therefore, the term $(\partial e/\partial P)_v$ shall be evaluated assuming that the system expands along a trajectory which maintains the specific

volume of the mixture at a constant value, v_o, which is the initial specific volume of the saturated mixture. That is,

$$e = e_f + e_{fg}\left(\frac{v_o - v_f}{v_{fg}}\right) \tag{6.59}$$

For the depressurization transients of interest to this analysis, the saturated mixture blowdown begins with the system nearly filled with saturated liquid with the exception of a small vapor volume located in the pressure vessel head. Since the density of the liquid phase is much greater than that of the vapor phase, the initial system vapor quality is very low and hence the initial fluid mixture specific volume is essentially the same as the saturated liquid phase specific volume. Thus the value of v_o, implemented in equation (6.59) is closely approximated by v_{fo}. Figure 6.10 shows how the mixture internal energy varies with pressure assuming a constant specific volume, $v_o = v_{fo}$, during the depressurization process. The plot has been made dimensionless to collapse the trends for a variety of initial pressures.

Note that for pressure ratios greater than ~0.5, the trend is linear; indicating that the slope, $(\partial e/\partial P)_v$, is a constant in this region. As shown in the figure, the following power law accurately ($R^2 = 0.9999$) describes the mixture specific internal energy ratio for a wide range of normalized pressures.

$$\left(\frac{e}{e_o}\right)_{v_{fo}} = \left(\frac{P}{P_o}\right)^{0.2603} \tag{6.60}$$

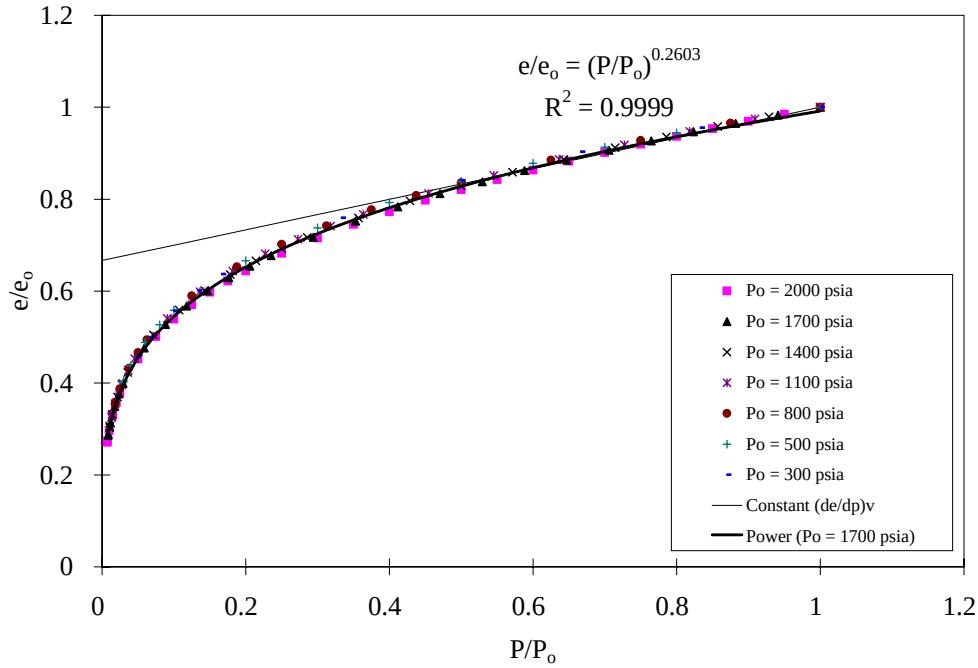

Figure 6.10 Plot of Dimensionless Mixture Specific Energy as a Function of Dimensionless Pressure

Taking the derivative of this equation with respect to pressure yields the expression for the desired partial derivative:

$$\left(\frac{\partial e}{\partial P}\right)_{v_{fo}} = 0.2603\ \frac{e_{fo}}{P}\left(\frac{P}{P_o}\right)^{0.2603} \qquad \textbf{(6.61)}$$

It should be noted that the numerical constants arising in equations (6.60) and (6.61) are particular to the case where the initial fluid mixture specific volume and specific energy are given by v_{fo} and e_{fo} respectively. Different constants are obtained at different initial vapor qualities for the saturated mixture.

Substituting equations (6.31) and (6.61) into (6.57) yields the following equation for the dilation property group.

$$\Pi_\epsilon = \frac{0.2603}{\left[v_f + x_{Brk}\, v_{fg}\right]}\left(\frac{e_f v_{fg}}{h_{fg}}\right)_o\left(\frac{P}{P_o}\right)^{-0.6257} \qquad \textbf{(6.62)}$$

Equation (6.62) can be readily evaluated for two bounding cases, saturated liquid breaks and saturated vapor breaks.

The fluid conditions for breaks located at low points in the RCS can be approximated assuming saturated liquid at the break. For these conditions, x_{Brk} would be approximately zero, and equation (6.62) would become:

Saturated Liquid Breaks:

$$\Pi_{\epsilon_f} = 0.2603 \left(\frac{e_f v_{fg}}{v_f h_{fg}} \right)_o \left(\frac{P}{P_o} \right)^{-0.6257} \tag{6.63}$$

Here it has also been assumed that v_f does not change significantly over the range of pressure of interest.

The fluid conditions for breaks located at high points in the RCS (e.g., PZR PORV) can be approximated assuming saturated vapor at the break. For these conditions, x_{Brl} would equal one and equation (6.62) would become:

Saturated Vapor Breaks:

$$\Pi_{\epsilon_g} = 0.2603 \left(\frac{e_f}{h_{fg}} \right)_o \left(\frac{P}{P_o} \right)^{0.4443} \tag{6.64}$$

To obtain this equation, use has been made of equation (6.33), the power law for the vapor specific volume.

Equations (6.62) and (6.64) are written in terms of scaling ratios as follows:

$$\left(\Pi_{\epsilon_f} \right)_R = \left(\frac{e_f v_{fg}}{v_f h_{fg}} \right)_{o,R} \tag{6.65}$$

and

$$\left(\Pi_{\epsilon_g} \right)_R = \left(\frac{e_f}{h_{fg}} \right)_{o,R} \tag{6.66}$$

where equation (6.29) has been implemented to eliminate the pressure ratios. For the reference pressure of interest to this project (APEX-CE P_o = 293 psia(P_o = 1.97825 MPa); Palisades P_o = 900 psia (P_o = 6.2036 MPa)), it was found that:

$$\left(\Pi_{\epsilon_f}\right)_R = 2.29 \tag{6.67}$$

$$\left(\Pi_{\epsilon_g}\right)_R = 0.61 \tag{6.68}$$

6.3.4 Critical Flow Models

For the blowdown cases of interest to this study, all of the break flows are assumed to be choked. This section presents two critical flow models used to estimate the break mass flow rate; a saturated vapor model and a saturated liquid model.

In general, the break mass flow rate is expressed as:

$$\dot{m}_{Brk} = C_D G_c A_{Brk} \tag{6.69}$$

where C_D is the discharge coefficient, G_c is the critical mass flux and A_{Brk} is the break flow area.

This initial critical mass flow rate for saturated steam, approximated as a perfect gas, is given by: (Moody, 1990)[46]

Saturated Vapor:

$$\dot{m}_{Brk,o} = C_D A_{Brk} \left(\frac{2}{\gamma + 1}\right)^{\frac{\gamma+1}{2(\gamma-1)}} \left[\gamma \rho_{go} P_o\right]^{1/2} \tag{6.70}$$

where C_D is the discharge coefficient, A_{Brk} is the break flow area and γ is the ratio of specific heats, which is approximately 1.33 for steam.

The transient, pressure dependent, critical mass flow rate for the steam would be:

$$\dot{m}_{Brk} = \dot{m}_{Brk,o} \left(\frac{P}{P_o}\right)^{\frac{1+\gamma}{2\gamma}} \tag{6.71}$$

Once again we find a power law, self-similar in pressure.

The models typically implemented for the case of saturated liquid choke flow are the Homogeneous Equilibrium Model or the Henry-Fauske Model.[47] An earlier study of APEX data indicated that the Henry-Fauske Model at saturated liquid conditions best fit the APEX data (Pimentel, 1996).[48]

The Henry-Fauske critical flow model for saturated liquid is given by the following set of equations:

$$G_c = \left[\left\{ \left(V_g\right)_{Brk} - v_f \right\} \frac{x_{Brk}}{(0.14)\left(s_{fg}\right)_{Brk}} \left(\frac{ds_f}{dP} \right)_{Brk} \right]^{-1/2} \tag{6.72}$$

and

$$\frac{P_{Brk}}{P} = 1 - \frac{v_f G_c^2}{2P} \tag{6.73}$$

In these equations, the parameters with the subscript "Brk" are evaluated at the break plane. All other parameters are evaluated at the system conditions. Thus, P_{Brk} is commonly known as the throat pressure and P would be the stagnation pressure. A typical value of equilibrium quality for the saturated liquid breaks observed in APEX was x_{Brk} equal to 0.03.

Taking the derivative of equation (6.32) with respect to pressure yielded the following expression for (ds_f/dP) in equation (6.72):

$$\frac{ds_f}{dP} = 0.2 \, \frac{s_{f,o}}{P} \left(\frac{P}{P_o} \right)^{0.2} \tag{6.74}$$

Equations (6.72) and (6.73) were solved iteratively to obtain the critical flow rates for saturated liquid breaks in APEX-CE and Palisades. Figure 6.11 presents the result of this analysis. Figure 6.11 indicates that the critical flow model also obeys a power law that is self-similar in pressure. That is:

$$G_c \approx G_{co} \left(\frac{P}{P_o} \right)^{0.7063} \tag{6.75}$$

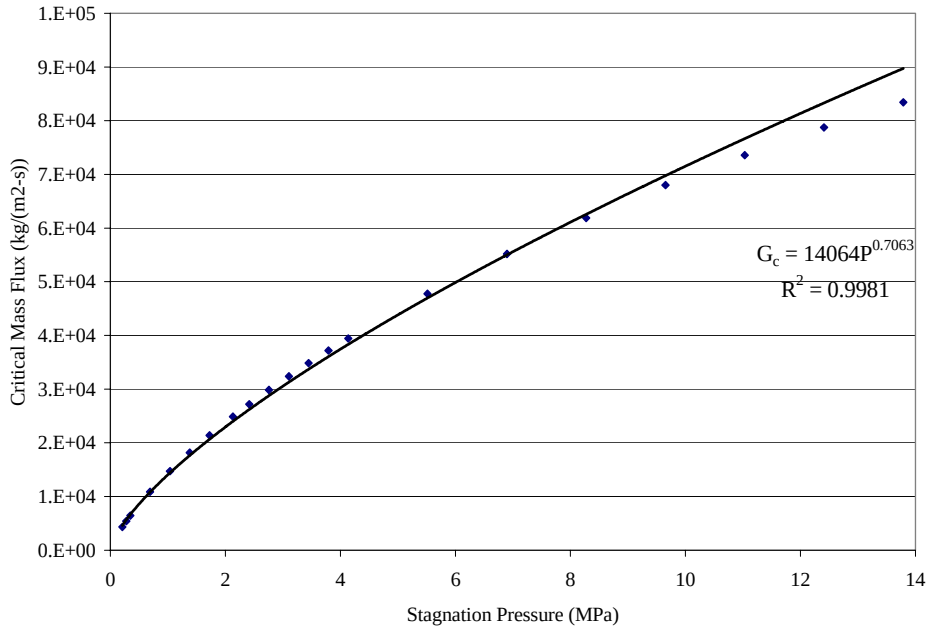

Figure 6.11 Critical Mass Flux for Saturated Liquid Breaks as Predicted by the Henry-Fauske Model ($x_{Brk} = 0.03$)

Using equation (6.69), the mass flow rate for saturated liquid breaks can be expressed as:

$$\dot{m}_{Brk} \approx \dot{m}_{Brk,o} \left(\frac{P}{P_o} \right)^{0.7063} \tag{6.76}$$

Equations (6.71) and (6.76) served as the closure relations for the top-down scaling dimensionless groups, Π_m, Π_h, Π_Γ, and the time constant τ_{RCS}.

6.4 RCS DEPRESSURIZATION AND INVENTORY SCALING CRITERIA

The goal of the SBLOCA test series is to simulate the RCS pressure decay and inventory loss for a variety of transients pertinent to PTS. Because the RCS saturation temperature is coupled to the saturation pressure, the RCS cooldown rate can also be inferred from the test data. It is desired that:

$$\left(\tau_{RCS}\right)_R = 1 \tag{6.77}$$

$$\left(\tau_{RCS}\,\frac{dM^+}{dt}\right)_R = 1 \tag{6.78}$$

$$\left(\tau_{RCS}\,\frac{dP^+}{dt}\right)_R = 1 \tag{6.79}$$

Applying these conditions to the dimensionless balance equations given by equations (6.14) and (6.24) means that the following ratios must be on the order of one.

$$\tau_{RCS,R} = \left[\frac{M_{RCS}}{\dot{m}_{Brk}}\right]_{o,R} \tag{6.80}$$

$$\Pi_{m,R} = \left(\frac{\dot{m}_{HPI,o}}{\dot{m}_{Brk,o}}\right)_R \tag{6.81}$$

$$\left(\frac{\Pi_h}{\Pi_\varepsilon}\right)_R = \left[\frac{\dot{m}_{HPI}\left[h_{HPI} - e + v\left(\frac{\partial e}{\partial v}\right)_p\right]_o}{\dot{m}_{Brk,o}\;P_o\left(\frac{\partial e}{\partial v}\right)_{v,o}}\right]_R \tag{6.82}$$

$$\left(\frac{\Pi_\Gamma}{\Pi_\varepsilon}\right)_R = \left[\frac{q_{net,o}}{\dot{m}_{Brk,o}\;P_o\left(\frac{\partial e}{\partial v}\right)_{v,o}}\right]_R \tag{6.83}$$

$$\left(\Pi_{\varepsilon}\right)_R = \left[\frac{P_o\left(\frac{\partial e}{\partial v}\right)_{v,o}}{\left[h_{Brk} - e + v\left(\frac{\partial e}{\partial v}\right)_p\right]_o}\right]_R \tag{6.84}$$

Two SBLOCA cases are considered in the analysis; the case of saturated vapor at the break and that of saturated liquid at the break.

6.4.1 Saturated Vapor Breaks

For saturated vapor breaks, such as a stuck-open pressurizer PORV, the following would be true:

$$h_{Brk} = h_g \tag{6.85}$$

Thus implementing equations (6.54) through (6.56) yields:

$$\left[h_{Brk} - e + v\left(\frac{\partial e}{\partial v}\right)_p\right]_o = \frac{v_g h_{fg}}{v_{fg}} \tag{6.86}$$

Similarly:

$$\left[h_{HPI} - e + v\left(\frac{\partial e}{\partial v}\right)_p\right]_o = \left[\frac{h_{fg} v_f}{v_{fg}} - \Delta h_{sub}\right]_o \tag{6.87}$$

The HPI subcooling is defined as h_f - h_{HPI}. Using these fluid property relations, it is now possible to evaluate equations (6.80) through (6.84).

Substituting the critical flow equation for saturated vapor, equation (6.70), into (6.80) yields.

$$\left[\frac{M_{RCS}}{A_{Brk}\left[\rho_{go} P_o\right]^{1/2}}\right]_R = 1 \tag{6.88}$$

Solving for the break area ratio yields:

$$\left(A_{Brk}\right)_R = \left(\frac{M_{RSC}}{\left[\rho_{go} P_o\right]^{1/2}}\right)_R \tag{6.89}$$

Setting equation (6.81) equal to one and rearranging yields the HPI mass flow rate scaling ratio:

$$\left(\dot{m}_{HPI,o}\right)_R = \left(A_{Brk}\left[\rho_{go}P_o\right]^{1/2}\right)_R \tag{6.90}$$

The thermal fluid mixing scaling analysis of Chapter 5 imposes constraints on the HPI mass flow rate. Substituting equations (6.61), (6.70), and (6.87) into (6.82) and setting the result equal to one yields the HPI subcooling scaling ratio:

$$\left[\frac{h_{fg}v_f}{v_{fg}} - \Delta h_{sub}\right]_{o,R} = \left[\frac{A_{Brk}\left[\rho_{go}P_o\right]^{1/2}e_{fo}}{\dot{m}_{HPI}}\right]_R \tag{6.91}$$

Substituting equation (6.61) into (6.83) and setting the result equal to one yields the power scaling ratio:

$$\left(q_{net,o}\right)_R = \left[A_{Brk}\left[\rho_{go}P_o\right]^{1/2}e_{fo}\right]_R \tag{6.92}$$

Equation (6.84) has already been evaluated for saturated vapor at the break. It is given by equation (6.66).

6.4.2 Saturated Liquid Breaks

For saturated liquid breaks, the following would be true:

$$h_{Brk} = h_f \tag{6.93}$$

Thus implementing equations (6.54) through (6.56) results in:

$$\left[h_{Brk} - e + v\left(\frac{\partial e}{\partial v}\right)_p\right]_o = \frac{v_f h_{fg}}{v_{fg}} \tag{6.94}$$

Substituting the critical flow equation for saturated liquid, equation (6.76), into (6.80) and applying the requirement of (6.77) yields:

$$\left[\frac{M_{RCS,o}}{C_D G_{co} A_{Brk}}\right]_R = 1 \tag{6.95}$$

Assuming similar discharge coefficients and rearranging yields the break flow area ratio:

$$A_{Brk,R} = \left(\frac{M_{RCS,o}}{G_{co}} \right)_R \tag{6.96}$$

Setting equation (6.81) equal to one and rearranging yields the HPI mass flow rate ratio:

$$\dot{m}_{HPI,R} = \left[G_{co} A_{Brk,o} \right]_R \tag{6.97}$$

Substituting equations (6.61), (6.75), and (6.87) into (6.82) and setting the result equal to one yields the HPI subcooling scaling ratio:

$$\left[\frac{h_{fg} v_f}{v_{fg}} - \Delta h_{sub} \right]_{o,R} = \left[\frac{G_{co} A_{Brk} e_{fo}}{\dot{m}_{HPI}} \right]_R \tag{6.98}$$

Substituting equations (6.61) and (6.75) into (6.83) and setting the result equal to one yields the power scaling ratio:

$$\left(q_{net,o} \right)_R = \left[G_{co} A_{Brk} e_{fo} \right]_R \tag{6.99}$$

Equation (6.84) has already been evaluated for saturated liquid at the break. It is given by equation (6.65).

6.4.3 Numerical Values of the Scaling Ratios and Initial Conditions

Tables 6.1 through 6.3 present the numerical values for the scaling ratios and initial conditions for the SBLOCA transients.

Table 6.1 Scaling Ratios for APEX-CE SBLOCAs

Break Area Ratio (saturated vapor)	1:77.7
Break Area Ratio (saturated liquid)	1:109.5
Core Decay Power Ratio	1:276
HPSI Flow Rate Ratio	1:276

Table 6.2 Time Constants and Π Groups for APEX-CE SBLOCAs

	Saturated Vapor Breaks	Saturated Breaks
$\tau_{RCS,R}$	1.0	1.0
$\Pi_{m,R}$	1.0	1.0
$\left(\frac{\Pi_h}{\Pi_\varepsilon}\right)_R$	1.05	1.05
$\left(\frac{\Pi_\Gamma}{\Pi_\varepsilon}\right)_R$	1.34	1.34
$(\Pi_\varepsilon)_R$	0.62	2.25

Table 6.3 Numerical Values for APEX-CE SBLOCA Initial Conditions

Parameters	Palisades	APEX-CE	Units
RCS Pressure	2060	385	psia
RCS Cold Leg Temperature	537.3	403	°F
Decay Power (6.65%)	168.4	0.610	MW
SG Pressure	770	255	psia
SG Liquid Mass	133,593	506.5	lbm
SG Vapor Mass	8,545	6.0	lbm
SG Liquid Level	31.74	6.6	ft
Hot Leg Break (Saturated Liquid)			
Break Area	1.54	0.014	in^2
Break Diameter	1.40	0.134	in
Stuck Open PZR PORV (Saturated Liquid)			
Break Area	5.774	0.074	in^2
Break Diameter	2.71	0.308	in.

6.5 SUMMARY AND CONCLUSIONS

This chapter presents the results of the SBLOCA scaling analysis. The goal was to scale the APEX-CE initial conditions and break flow areas such that the RCS depressurization rate and

corresponding cooldown rate would be preserved in dimensionless phase space. Two types of break conditions were considered; all saturated vapor at the break, such as the stuck-open pressurizer Power Operated Relief Valve (PORV) and an all saturated liquid break, which was the assumed condition for the hot leg break with charging and HPSI flow.

The scaling analysis provided the RCS initial conditions and the break flow areas. All of the Π groups, as shown in Table 6.2, were found to have values on the order of one.

An examination of the Π groups ratios indicates that for saturated vapor breaks (i.e., stuck-open PORVs) the depressurization and cooldown rate will be reasonably simulated in APEX-CE. Some distortion may occur in simulating the hot leg break because conditions at the break will likely be two-phase rather that saturated liquid as assumed in the analysis. The validity of this assumption will depend on whether the charging and HPSI flows keep the break conditions near the saturated liquid state.

7.0 STEAM GENERATOR DEPRESSURIZATION/RCS COOLDOWN SCALING ANALYSIS

The scenarios of interest to this analysis are Main Steam Line Breaks (MSLBs). Both large and small MSLBs are being considered; the largest break fluid discharge rate being limited by the steam generator flow restrictor. The opening of a break on the steam line causes a significant quantity of liquid to flash to steam on the shell side of the steam generator. The reduction in secondary side pressure produces a corresponding reduction in saturation temperature. The reduced secondary side temperature results in a cooldown of the primary loop; the rate of cooldown being dependent on the steam line break size. The primary side cooldown causes a reduction in primary side pressure. It is possible that the primary side pressure could drop below the HPSI actuation setpoint thus resulting in a further cooldown of the primary loop. Loop stagnation could occur for those scenarios which result in a trip of the primary coolant pumps (e.g., manual trip or loss of offsite power). If a MSLB occurs in one steam generator, the resulting primary loop temperature could drop below the fluid temperature on the shell side of the “intact” steam generator. Therefore the intact steam generator would become a heat source and single-phase natural circulation would be interrupted in the loops connected to the intact steam generator.

Figure 7.1 presents the scaling analysis flow diagram for secondary side depressurization. First, a top-down system level scaling analysis was performed for the Reactor Coolant System (RCS) and the Steam Generator. Use was made of the two-phase fluid depressurization rate equation developed in Section 6.1 and an energy balance was performed to obtain the equations that relate the secondary side energy loss rate to the primary side cooldown rate. This included the development of the scaling criterion for the MSLB size. A bottom-up scaling analysis was performed to describe the scaling of the local transport phenomena. The critical flow scaling information of Section 6.1 was implemented.

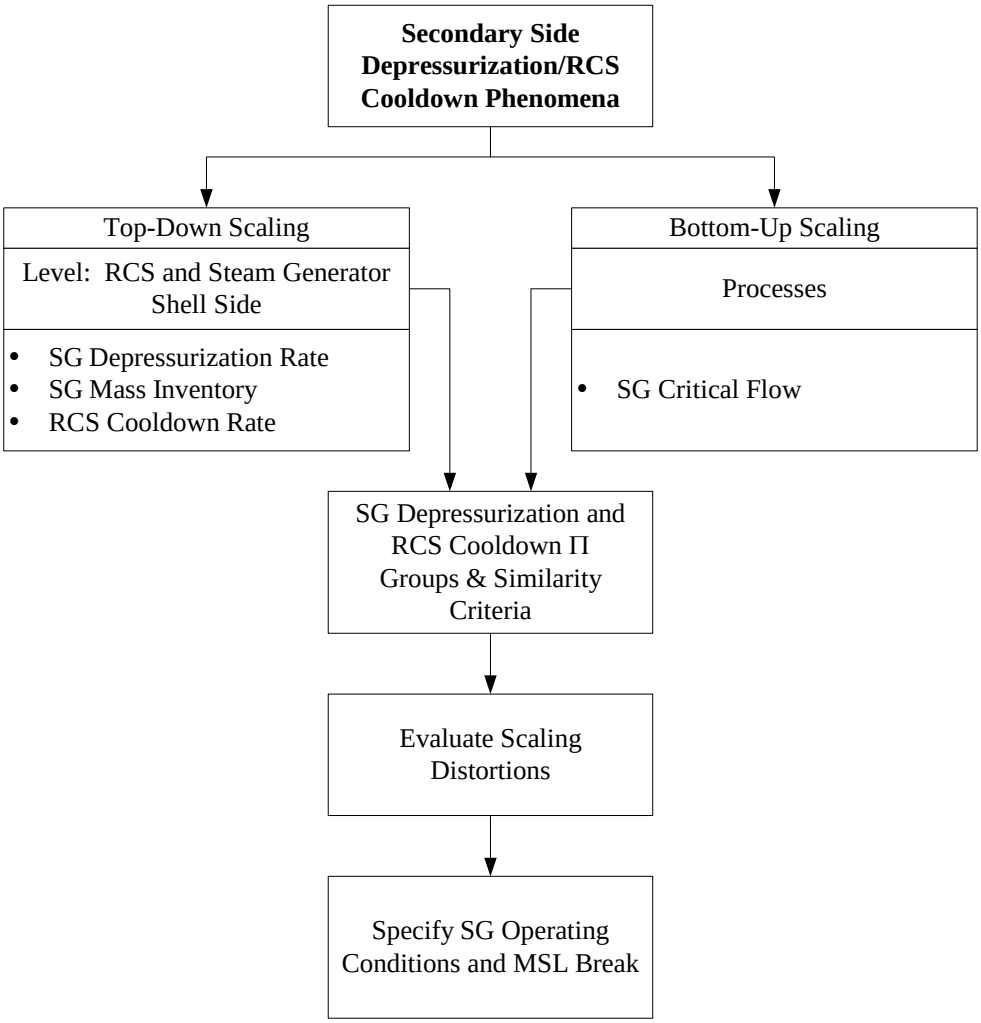

Figure 7.1 Flow Chart of the Secondary Side Depressurization Scaling Analysis

7.1 Governing Equations for Steam Generator Blowdown and RCS Cooldown

Figure 7.2 describes the steam generator and RCS control volumes considered in this analysis. The steam generator control volume was used for the depressurization analysis and the resulting blowdown energy transfer rate was used to determine the primary side cooldown rate. Two steam generators are shown. One steam generator will have a broken main steam line and the other will be considered the “intact” steam generator.

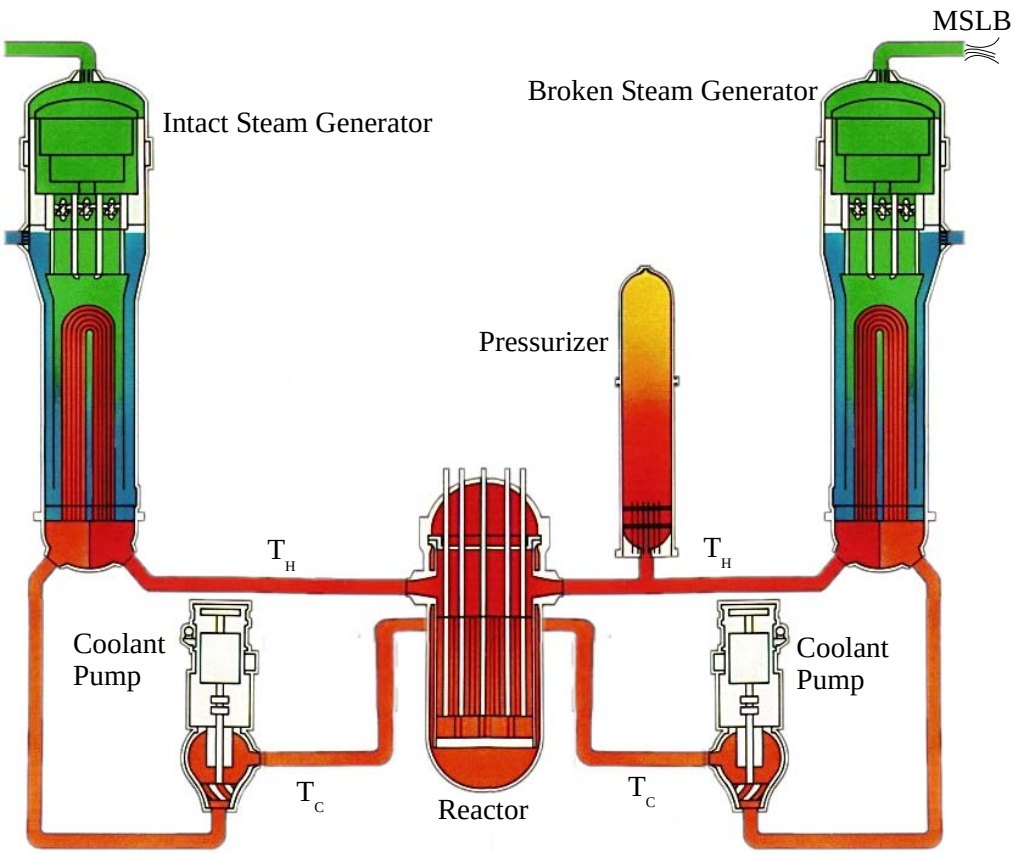

Figure 7.2 Steam Generator and RCS Control Volumes Used for MSLB Scaling

The governing mass and energy conservation equations for the RCS are as follows:

RCS Mass Conservation:

$$\frac{dM_{RCS}}{dt} = \dot{m}_{HPI} \tag{7.1}$$

RCS Energy Conservation:

$$C_v \frac{d}{dt}\left(M_{RCS}T_{RCS}\right) = \dot{m}_{HPI}h_{HPI} - q_{SG} + q_{core} \tag{7.2}$$

where it has been assumed that a positive value of q_{SG} represents heat transfer from the RCS to the steam generator and heat loss has been neglected. Expanding the time derivative on the left side of this equation and substituting the mass conversation equation yields:

$$M_{RCS} C_v \frac{dT_{RCS}}{dt} = q_{core} - q_{SG} - \dot{m}_{HPI}\left[C_v T_{RCS} - C_p T_{HPI}\right] \tag{7.3}$$

Use has also been made of the thermodynamic relation:

$$\dot{m}\Delta h = \dot{m} C_p \Delta T \tag{7.4}$$

Thus, the governing equation for the RCS cooldown is given by equation (7.3).

Taking advantage of the depressurization scaling work performed in Section 6.1, the depressurization rate equation for the steam generator is identical in form to equation (6.12). Thus for the broken steam generator:

$$\begin{aligned} M_{SG}\left(\frac{\partial e}{\partial P}\right)_v \frac{dP_{SG}}{dt} &= \dot{m}_{FW}\left[h_{FW} - e + v\left(\frac{\partial e}{\partial v}\right)_{p_SG}\right] \\ &- \dot{m}_{SLB}\left[h_{SLB} - e + v\left(\frac{\partial e}{\partial v}\right)_{p_SG}\right] + q_{SG} \end{aligned} \tag{7.5}$$

The sources of injection water to the steam generator are the Main Feedwater (MFW) and the Auxiliary Feedwater (AFW). The heat source for the steam generators is the primary coolant inside the SG u-tubes and the vent path is the main steam line break.

Adding equations (7.3) and (7.5) eliminates q_{SG} and results in the following governing equation which relates the time rate of change of SG pressure to the time rate of change of RCS average fluid temperature.

$$\begin{aligned} M_{RCS} C_v \frac{dT_{RCS}}{dt} &= -M_{SG}\left(\frac{\partial e}{\partial P}\right)_v \frac{dP_{SG}}{dt} + q_{core} - \dot{m}_{HPI}\left[C_v T_{RCS} - C_p T_{HPI}\right] \\ &+ \dot{m}_{FW}\left[h_{FW} - e + v\left(\frac{\partial e}{\partial P}\right)\right]_{SG} \\ &- \dot{m}_{SLB}\left[h_{SLB} - e + v\left(\frac{\partial e}{\partial P}\right)\right]_{SG} \end{aligned} \tag{7.6}$$

Equation (7.6) represents the governing equation for the steam generator blowdown/RCS cooldown behavior for the MSLB.

Because APEX-CE is a reduced pressure facility, the MSLB scaling was aimed at preserving the primary coolant temperature change as a function of time. That is, it was desired that:

$$\left(\frac{dT_{RCS}}{dt}\right)_{APEX} = \left(\frac{dT_{RCS}}{dt}\right)_{Pal} \tag{7.7}$$

for the experiments. Thus, the average RCS temperature changes would be preserved.

7.2 Top-Down MSLB Scaling Analysis

Equation (7.6) is expressed in dimensionless form by dividing each term by its respective initial condition. That is, the dimensionless terms are related to initial conditions by:

$$M_{RCS} = M_{RCS,o}\, M^{+}_{RCS} \tag{7.8}$$

$$\frac{dT_{RCS}}{dt} = \left[\frac{dT_{RCS}}{dt}\right]_{o} \left[\frac{dT_{RCS}}{dt}\right]^{+} \tag{7.9}$$

$$M_{SG} = M_{SG,o}\, M^{+}_{SG} \tag{7.10}$$

$$\left(\frac{\partial e}{\partial P}\right)_{v} = \left(\frac{\partial e}{\partial P}\right)_{v,o} \left(\frac{\partial e}{\partial P}\right)^{+}_{v} \tag{7.11}$$

$$P_{SG} = P_{SG,o}\, P^{+}_{SG} \tag{7.12}$$

$$q_{core} = q_{core,o}\, q^{+}_{core} \tag{7.13}$$

$$\dot{m}_{HPI} = \dot{m}_{HPI,o}\, \dot{m}^{+}_{HPI} \tag{7.14}$$

$$\left[C_v T_{RCS} - C_p T_{HPI}\right] = \left[C_v T_{RCS} - C_p T_{HPI}\right]_o \left[C_v T_{RCS} - C_p T_{HPI}\right]^+ \tag{7.15}$$

$$\dot{m}_{FW} = \dot{m}_{FW.o}\ \dot{m}_{FW}^{+} \tag{7.16}$$

$$\left[h_{FW} - e + v\left(\frac{\partial e}{\partial v}\right)_{p_SG}\right] = \left[h_{FW} - e + v\left(\frac{\partial e}{\partial v}\right)_{p_SG,o}\right]\left[h_{FW} - e + v\left(\frac{\partial e}{\partial v}\right)_{p_SG}\right]^+ \tag{7.17}$$

$$\dot{m}_{SLB} = \dot{m}_{SLB,o}\ \dot{m}_{SLB}^{+} \tag{7.18}$$

$$\left[h_{SLB} - e + v\left(\frac{\partial e}{\partial v}\right)_{p_SG}\right] = \left[h_{SLB} - e + v\left(\frac{\partial e}{\partial v}\right)_{p_SG,o}\right]\left[h_{SLB} - e + v\left(\frac{\partial e}{\partial v}\right)_{p_SG}\right]^+ \tag{7.19}$$

Substituting equations (7.8) through (7.9) into (7.6) and dividing by

$$\dot{m}_{SLB,o}\left[h_{SLB} - e + v\left(\frac{\partial e}{\partial v}\right)_{P_{SG,o}}\right]$$

yields:

$$\begin{aligned}
\Pi_{\epsilon}\ \tau_{SG}\ M_{SG}^{+}\left(\frac{\partial e}{\partial P}\right)_{v}^{+}\frac{dP_{SG}^{+}}{dt} \quad &= -\ \Pi_{\Gamma}\ M_{RCS}^{+}\left(\frac{dT_{RCS}}{dt}\right)^{+} \\
&+\ \Pi_{q}\ q_{core}^{+} - \Pi_{HPI}\ \dot{m}_{HPI}^{+}\left[C_{v}T_{RCS} - C_{p}T_{HPI}\right]^{+} \\
&-\ \Pi_{FW}\ \dot{m}_{FW}^{+}\left[h_{FW} - e + v\left(\frac{\partial e}{\partial v}\right)_{P_{SG}}\right] \\
&-\ \dot{m}_{SLB}^{+}\left[h_{SLB} - e + v\left(\frac{\partial e}{\partial v}\right)_{P_{SG}}\right]^{+}
\end{aligned} \tag{7.20}$$

where the steam generator blowdown time constant is given by:

$$\tau_{SG} = \frac{M_{SG,o}}{\dot{m}_{SLB.o}} \tag{7.21}$$

and the characteristic time ratios are given by:

$$\Pi_{\epsilon} = \left[\left(\frac{\partial e}{\partial P_{SG}} \right)_{v} \frac{P_{SG}}{\left[h_{SLB} - e + v \left(\frac{\partial e}{\partial v} \right)_{p_{SG}} \right]_{o}} \right] \tag{7.22}$$

$$\Pi_{T} = \left[\frac{M_{RCS}\, C_{v}}{\dot{m}_{SLB} \left[h_{SLB} - e + v \left(\frac{\partial e}{\partial v} \right)_{p_{SG,o}} \right]} \left(\frac{d\, T_{RCS}}{dt} \right) \right]_{o} \tag{7.23}$$

$$\Pi_{\Gamma} = \left[\frac{q_{core}}{\dot{m}_{SLB} \left[h_{SLB} - e + v \left(\frac{\partial e}{\partial v} \right)_{p_{SG}} \right]} \right]_{o} \tag{7.24}$$

$$\Pi_{HPI} = \left[\frac{\dot{m}_{HPI} \left(C_{v} T_{RCS} - C_{p} T_{HPI} \right)}{\dot{m}_{SLB} \left[h_{SLB} - e + v \left(\frac{\partial e}{\partial v} \right)_{p_{SG}} \right]} \right]_{o} \tag{7.25}$$

$$\Pi_{FW} = \left[\frac{\dot{m}_{FW} \left[h_{FW} - e + v \left(\frac{\partial e}{\partial v} \right)_{p_{SG}} \right]}{\dot{m}_{SLB} \left[h_{SLB} - e + v \left(\frac{\partial e}{\partial v} \right)_{p_{SG}} \right]} \right]_{o} \tag{7.26}$$

The dimensionless Π groups show the importance of each of the transport terms relative to the break energy transport term which is expected to dominate the process.

7.3 Bottom-Up MSLB Scaling Analysis

The objective of the bottom-up scaling analysis was to obtain the closure relations needed to evaluate the dimensionless Π groups developed in the top-down scaling analysis. Equations of state and critical flow models are needed for this purpose.

7.3.1 SG Fluid Properties

The analyses presented in Sections 6.3.1 through 6.3.3 are directly applicable. First, we seek to obtain simple expressions for the following thermodynamic property groups:

$$\left[h_{SLB} - e + v\left(\frac{\partial e}{\partial v}\right)_{p}\right]_{SG,o} \tag{7.27}$$

For the main steam line break, h_{SLB} can be reasonably approximated by h_g for saturated vapor. Furthermore, assuming saturated fluid conditions in the steam generator permits one to substitute equations (6.54) through (6.56) into (7.27) to obtain:

$$\left[h_{SLB} - e + v\left(\frac{\partial e}{\partial v}\right)_{p}\right]_{SG,o} = \left(\frac{v_g h_{fg}}{v_{fg}}\right)_{SG,o} \tag{7.28}$$

Similarly, substituting equations (6.5) through (6.56) into the following thermodynamic property group:

$$\left[h_{FW} - e + v\left(\frac{\partial e}{\partial v}\right)_{p}\right]_{SG,o} \tag{7.29}$$

yields the expression:

$$\left[h_{FW} - e + v\left(\frac{\partial e}{\partial v}\right)_{p}\right]_{SG,o} = \left[\frac{h_{fg}\, v_f}{v_{fg}} - \Delta h_{SUB}\right]_{SG,o} \tag{7.30}$$

where the feedwater subcooling Δh_{SUB} is defined as h_f - h_{FW}.

Lastly, the fluid property group given by equation (7.22) was already evaluated in Section 6.3.3. It is given by equation (6.64) for initial conditions as:

$$\Pi_{\varepsilon go} = 0.2603\ \frac{e_{f,o}}{h_{fg_o}} \tag{7.31}$$

Having obtained simple expressions for the various thermodynamic property groups, the next step in the bottom-up scaling analysis was to obtain an expression for the critical mass flow rate.

7.3.2 Steam Generator Critical Flow Model

Critical flow for the condition of saturated vapor at the break was evaluated in Section 6.3.4. Equation (6.70) is directly applicable and is given for the main steam line break as:

$$\dot{m}_{SLB,o} = C_D \, A_{SLB} \left(\frac{2}{\gamma + 1} \right)^{\frac{\gamma+1}{2(\gamma-1)}} \left[\gamma \, \rho_g \, P_{SG} \right]_o^{1/2} \tag{7.32}$$

7.4 Scaling Criteria

This section provides the scaling criteria for the MSLB transient. Using the fluid properties and critical flow model presented in the previous section, the steam generator blowdown time constant and the dimensionless Π groups given by equation (7.21) through (7.26) can be rewritten in terms of scaling ratios as follows:

$$\tau_{SG,R} = \left[\frac{M_{SG,o}}{A_{SLB} \left[\rho_{go} \, P_{SG,o} \right]^{1/2}} \right]_R \tag{7.33}$$

$$\Pi_{\epsilon,R} = \left(\frac{e_{fo}}{h_{fg,o}} \right)_R \tag{7.34}$$

$$\Pi_{T,R} = \left[\frac{M_{RCS,o} \, C_{vo} \, v_{fg,o}}{A_{SLB} \left[\rho_{g_o} \, P_{SG,o} \right]^{1/2} h_{fg,o} \, v_{g,o}} \left(\frac{d T_{RCS}}{dt} \right)_o \right]_R \tag{7.35}$$

$$\Pi_{\Gamma,R} = \left[\frac{q_{core,o} \, v_{fg,o}}{A_{SLB} \left[\rho_{go} \, P_{SG,o} \right]^{1/2} h_{fg,o} \, v_{g,o}} \right]_R \tag{7.36}$$

$$\Pi_{HPI,R} = \left[\frac{\dot{m}_{HPI,o} \left(C_v \, T_{RCS} - C_p \, T_{HPI} \right) v_{fg,o}}{A_{SLB} \left[\rho_{go} \, P_{SG,o} \right]^{1/2} h_{fg,o} \, v_{g,o}} \right]_R \tag{7.37}$$

$$\Pi_{FW,R} = \left[\frac{\dot{m}_{FW,o} \left[h_{fg} v_f - \Delta h_{SUB} \, v_{fg} \right]_o}{A_{SLB} \left[\rho_{go} \, P_{SG,o} \right]^{1/2} h_{fg,o} \, v_{g,o}} \right]_R \tag{7.38}$$

Optimally, it is desired that all of the scaling ratios given by equations (7.33) through (7.38) be on the order of one.

The goal of the MSLB is to simulate the primary side cooldown as a result of a secondary side blowdown. Because the MSLB tests being considered involve large breaks, the dominant term in the energy conservation equation will be the energy transport out of the break. Thus, the break area was selected by requiring:

$$\Pi_{T,R} = 1 \tag{7.39}$$

Substituting this requirement into equation (7.35) and rearranging yields:

$$\left(\frac{dT_{RCS}}{dt}\right)_{o,R} = \left[\frac{A_{SLB}\left[\rho_{go}P_{SG,o}\right]^{1/2}h_{fg,o}v_{g,o}}{M_{RCS,o}C_{po}v_{fg,o}}\right]_R \tag{7.40}$$

Equation (7.7) was implemented to preserve the RCS temperature transient in APEX-CE. That is:

$$\left(\frac{dT_{RCS}}{dt}\right)_{o,R} = 1 \tag{7.41}$$

Substituting equation (7.41) into equation (7.40) and solving for the break flow area ratio yields:

$$\left(A_{SLB}\right)_R = \left[\frac{M_{RCS,o}C_{v,o}v_{fg,o}}{\left[\rho_{go}P_{SG,o}\right]^{1/2}h_{fg,o}v_{g,o}}\right]_R \tag{7.42}$$

Substituting equation (7.42) into (7.33) yields:

$$\tau_{SG,R} = \left[\frac{M_{SG,o}h_{fg,o}v_{g,o}}{M_{RCS,o}C_{vo}v_{fg,o}}\right]_R \tag{7.43}$$

It is required that the blowdown time be preserved in APEX-CE. Thus:

$$\tau_{SG,R} = 1 \tag{7.44}$$

Substituting this requirement into equation (7.43) and solving for the initial steam generator mass ratio yields:

$$\left(M_{SG,o}\right)_R = \left[\frac{M_{RCS,o}\, C_{vo}\, v_{fg,o}}{h_{fg,o} v_{g,o}}\right]_R \tag{7.45}$$

Substituting equation (7.42) into (7.36)and requiring $\Pi_{\Gamma,R}$ to equal one yields the scaling criterion for the core power:

$$\left(q_{core,R}\right)_R = \left[M_{RCS,o}\, C_{v,o}\right]_R \tag{7.46}$$

Substituting equation (7.42) into (7.37) and requiring $\Pi_{HPI,R}$ to equal one yields the scaling criterion for the HPSI flow rate:

$$\left(\dot{m}_{HPI,o}\right)_R = \left[\frac{M_{RCS,o}}{\left[T_{RCS} - \left(\frac{C_p}{C_v}\right) T_{HPI}\right]_o}\right]_R \tag{7.47}$$

It is noted that local fluid mixing considerations are important in selecting a scaling criterion for $\dot{m}_{HPI}$. These were discussed in Chapter 5.

Substituting equation (7.42) into (7.38) and requiring $\Pi_{FW,R}$ to equal one yields the scaling criterion for the feedwater flow rate:

$$\dot{m}_{FW,R} = \left[\frac{M_{RCS,o}\, C_{v,o}\, v_{fg,o}}{\left[h_{fg} v_f - \Delta h_{SUB}\, v_{fg}\right]_o}\right]_R \tag{7.48}$$

7.4.1 Numerical Values of the Scaling Ratios and Initial Conditions

Tables 7.1 through 7.6 present the numerical values and initial conditions for the scaling ratios and the initial conditions for the MSLB transients as initiated from hot zero power (HZP) and full power (FP) conditions.

Table 7.1. Scaling Ratios For APEX-CE Hot Zero Power MSLBs

Steam Line Break Area Ratio	1:84.7
Steam Generator Mass Ratio	1:268.9
Core Decay Power Ratio	1:276.0
HPSI Flow Rate Ratio	1:276.0
AFW Flow Rate Ratio	1:179.5

Table 7.2 Time Constants and Π Groups for Hot Zero Power MSLBs

$\tau_{SG,R}$	1.00
$\Pi_{\varepsilon,R}$	0.61
$\Pi_{T,R}$	1.00
$\Pi_{\Gamma,R}$	0.83
$\Pi_{HPI,R}$	0.69
$\Pi_{FW,R}$	1.00

Parameters	Palisades	APEX-CE	Units	Palisades	APEX-CE	Units
RCS Pressure	14.20	2.65	MPa	2060	385	psia
Cold Leg Temperature	550.9	484.8	°K	532	413	°F
Decay Power (0.5%)	12.65	0.046	MW	11990	43.41	Btu/s
Steam Generator Pressure at HZP	6.21	1.98	MPa	900	287.0	psia
Steam Generator Liquid Mass at HZP	92435.4	343.8	kg	203783	757.9	lbm
Steam Generator Vapor Mass at HZP	3164.3	1.7	kg	6976	3.7	lbm
Steam Generator Liquid Level at HZP	9.7	2.9	m	31.74	9.7	ft
Double-Ended MSLB						
Steam Generator Flow Restrictor Area	1757.7	20.8	cm^2	272.45	3.218	in^2
Steam Generator Flow Restrictor Diameter	47.31	5.14	cm	18.63	2.02	in
1.0 ft^2 MSLB						
MSLB Area	929.0	11.0	cm^2	144	1.701	in^2
MSLB Diameter	34.39	3.74	cm	13.54	1.472	in
Stuck Open ADV						
ADV Flow Area	112.0	1.5	cm^2	17.36	0.228	in^2
ADV Diameter	11.94	1.37	cm	4.70	0.539	in

Table 7.3 Numerical Values for Initial Conditions for the Hot Zero Power MSLBs

Table 7.4 Scaling Ratios for APEX-CE Full Power MSLBs

Steam Line Break Area Ratio	1:82.9
Steam Generator Mass Ratio	1:259.6
Core Decay Power Ratio	1:276.0
HPSI Flow Rate Ratio	1:276.0
AFW Flow Rate Ratio	1:176.5

Table 7.5 Time Constants and Π Groups for Full Power MSLBs

$\tau_{SG,R}$	1.00
$\Pi_{\varepsilon,R}$	0.63
$\Pi_{T,R}$	1.00
$\Pi_{\Gamma,R}$	0.81
$\Pi_{HPI,R}$	0.65
$\Pi_{FW,R}$	1.00

Parameters	Palisades	APEX-CE	Units	Palisades	APEX-CE	Units
RCS Pressure	14.2	2.65	MPa	2060	385	psia
Cold Leg Temperature	550.9	484.8	°K	532	400	°F
Decay Power (6.65%)	168.4	0.610	MW	159612	578	Btu/s
Steam Generator Pressure at HFP	5.31	1.70	MPa	770	247.0	psia
Steam Generator Liquid Mass at HFP	60597.4	233.4	kg	133593	514.5	lbm
Steam Generator Vapor Mass at HFP	3876.0	2.6	kg	8545	5.7	lbm
Steam Generator Liquid Level at HFP	9.67	2.35	m	31.74	7.7	ft
Double-Ended MSLB						
Steam Generator Flow Restrictor Area	1757.7	21.20	cm^2	272.45	3.29	in^2
Steam Generator Flow Restrictor Diameter	47.31	5.20	cm	18.63	2.05	in
1.0 ft^2 MSLB						
MSLB Area	929.0	11.21	cm^2	144	1.74	in^2
MSLB Diameter	34.39	3.78	cm	13.54	1.49	in
Stuck Open ADV						
ADV Flow Area	112.0	1.5	cm^2	17.36	0.228	in^2
ADV Diameter	11.94	1.37	cm	4.70	0.539	in

Table 7.6 Numerical Values for Initial Conditions for the Full Power MSLBs

7.5 SUMMARY AND CONCLUSIONS

This chapter presents the results of the MSLB scaling analysis. The goal was to scale the APEX-CE initial conditions and MSLB flow area such that the RCS cooldown rate would be preserved. Two sets of initial conditions were examined; a MSLB from hot zero power conditions (~0.5% decay power) and a MSLB from full power conditions (~6.65% decay power could be achieved in APEX-CE). The scaling analysis provided the necessary steam generator initial conditions and the MSLB flow areas. All of the Π groups, as shown in Table 7.2, were found to have values on the order of one. Thus, it is expected that the MSLB transients will be reasonably simulated in APEX-CE.

Based on the Π group comparisons, some distortion is expected in the steam generator blowdown rate because of $\Pi_{\varepsilon,R}$. This results because of the reduced pressure conditions in APEX-CE. Similarly, $\Pi_{HPI,R}$ has been adjusted to preserve the mixing characteristics in the cold leg.

8.0 SUMMARY AND CONCLUSIONS

This section summarizes the results of the APEX-CE PTS scaling analysis in terms of the analysis objectives. That is, this scaling analysis was performed to:

1. To identify the characteristic geometric scale ratios for the APEX-CE Test Facility and to establish the geometric similarity between APEX-CE and the Palisades Nuclear Plant.

2. To develop the scaling basis for assuring that the following PTS thermal hydraulic phenomena could be adequately simulated in APEX-CE for various primary and secondary side transients.

   - The onset of loop stagnation
   - The onset of thermal stratification in the cold legs, and
   - Thermal fluid mixing in the cold legs and downcomer

3. To identify which of the phenomena listed in the PTS Phenomena Identification and Ranking Table (PIRT) would be adequately simulated in APEX-CE.

The results of this scaling analysis have been used to modify the existing APEX facility to produce the APEX-CE configuration and operating conditions.

8.1 GEOMETRIC SIMILARITY

The results of the scaling analysis indicate that the APEX-CE facility is geometrically similar to the Palisades Nuclear Plant for two reasons. First, there is a one-to-one correspondence of primary loop components; arranged in the same sequence and second, a comparison of the ratios of the component lengths, diameters, elevations, flow areas and volumes revealed that the geometric scale factors for each of the components were essentially constant throughout the loop. These are summarized in Table 8.1.

The reactor vessel downcomer was the only component found to have a volume scale factor that deviated significantly from the ideal value of 1:276. As a result, additional analyses were performed to assess the impact of this distortion on fluid mixing in the downcomer. REMIX calculations indicated that the larger APEX-CE downcomer still provides a reasonable simulation of the Palisades local plume mixing behavior when the data are plotted in dimensionless temperature and time scales. The REMIX analysis is presented in Chapter 5.

Table 8.1 Summary of the APEX to Palisades Scale Ratios

Geometric Parameter	**APEX-CE to Palisades Scale Ratios**
Flow Areas	~1/70
Piping Lengths	~1/4
Volumes	~1/276
Elevations	~1/3.45
Operating Parameters	
Power	1/276
Natural Circulation Mass Flow Rates	~1/276
Fluid Velocities	~1/3.66
Total RCS Power/Volume	1/1

8.2 SCALING BASIS FOR IMPORTANT THERMAL HYDRAULIC PHENOMENA

Top-down and bottom-up scaling analysis have been performed for the following transient phases:

- Single-phase fluid natural circulation
- Two-Phase fluid natural circulation
- Cold leg and downcomer fluid mixing and heat transfer
- RCS depressurization
- Steam generator depressurization/RCS cooldown

The results of these scaling analyses are summarized in the sections that follow.

8.2.1 Single-Phase Fluid Natural Circulation

Following a main steam line break with a loss of reactor coolant pumps, the primary loop flow rate is governed by single0phase fluid natural circulation. With regards to PTS modeling, it is important that the mass flow rate through the cold legs be scale such that the onset of the thermal stratification in the cold legs is properly simulated. This has been achieved by requiring that the APEX-CE test facility operate at a one-to-one time scale (i.e., isochronicity). As shown in equation (4.31), this required adjusting the primary loop loss coefficients, Π_{F1}, such that the fluid transient time around the APEX-CE loop is identical to that in the Palisades plant under single-phase fluid natural circulation conditions. Figure 4.6 compares the calculated APEX-CE core flow rates to the ideally scaled values for Palisades. The requirement of isochronicity was achieved as shown in Table 8.2.

Table 8.2 Method Used to Preserve Isochronicity in APEX-CE (*Fluid Property Similitude*)

where:

$$a_R = \frac{1}{69}$$

$$\ell_R = \frac{1}{4}$$

$$\tau_R = \left(\frac{a_c \ell^2 \Pi_{F1}}{q_{core}}\right)_R = \frac{1}{276}$$

$$\left(\Pi_{F1}\right)_R = 4$$

By requiring τ_R to equality unity, then the velocity ratio is necessarily fixed as follows:

$$u_R = \frac{\ell_R}{\tau_R} = \frac{1}{4} \qquad \textbf{(8.1)}$$

and consequently the volumetric flow ratio is:

$$Q_R = u_R a_R = \frac{1}{276} \qquad \textbf{(8.2)}$$

The fluid mixing scaling analysis performed in Chapter 5 demonstrates how the result of equation (8.2) is used to assure that the onset of cold leg thermal stratification is preserved.

8.2.2 Two-Phase Fluid Natural Circulation

Following the onset of a SBLOCA, two-phase natural circulation conditions may be established upon tripping the reactor coolant pumps. Depending on the break size, RCS pressure may remain

relatively constant for a prolonged period. Two-phase natural circulation will persist under these conditions provided that the steam generators are still available to remove heat and the steam generator tubes have not voided. It was of particular interest to this scaling analysis to determine the conditions required to interrupt two-phase natural circulation. Earlier APEX tests have demonstrated that even when the long tubes of the steam generator have stopped flowing, the short tubes will continue to provide primary loop flow; extending the "well-mixed" conditions in the downcomer.

The objective of the two-phase fluid natural circulation scaling analysis was to develop the similarity criteria needed to specify the primary loop resistance, preserve the important flow pattern transitions in the hot legs and cold legs and to preserve the onset of primary loop stagnation.

The analysis demonstrated that the transition from stratified two-phase conditions in the hot legs and cold legs will be reasonably simulated in APEX-CE, particularly when fluid property similitude exists. The Taitel-Dukler13 model was implemented to make this assessment. The values of the dimensionless ratios FrCL and FRHL were found to be approximately 0.7.

The interruption of two-phase natural circulation during a SBLOCA is tied to the transition to the onset of the reflux condensation mode of heat transfer in the steam generators. Duffey and Sursock's17 model was used to estimate the conditions for the onset of reflux condensation in both Palisades and APEX-CE. The results are given in Table 4.2. The calculations indicate that primary loop stagnation in Palisades would occur when 82% of the primary inventory still remains. Similar results, 79%, were obtained for APEX-CE. The pressurizer liquid inventory was excluded from these calculations as was done by Duffey and Sursock. The results indicate that APEX-CE can be used to simulate the onset of primary loop stagnation during an SBLOCA.

8.2.3 Cold Leg and Downcomer Thermal Fluid Mixing and Wall Heat Transfer

A detailed analysis has been performed to assess the following phenomena:

- The onset of thermal stratification in the cold legs
- The onset of buoyant backflow in HPSI line
- Global mixing and heat transfer in the cold leg and downcomer volumes
- Top-entry axisymmetric plume entrainment rate and temperature decay
- HPSI side-entry plume entrainment
- HPSI nozzle turbulence
- Downcomer planar plume entrainment and velocity
- Downcomer wall heat transfer
- REMIX calculations for APEX-CE and Palisades

1. *Onset of the Thermal Stratification in the Cold Legs and Buoyant Backflow in the HPSI Line*.

A new criterion for the onset of thermal stratification in the cold legs has been developed using a hydraulic jump analysis. The new criterion is in agreement with the stratification criterion developed by Theofanous for the cold leg and injection flow rates of interest to the present study. The key dimensionless groups, Fr_{HPI} and $Fr_{HPI/CL}$ have been preserved by design, assuring that the onset of

thermal stratification in APEX-CE and the onset of buoyant backflow in the HPSI line will be similar to that in the Palisades Plant.

2. *Global Mixing and Heat Transfer in the Cold Legs and Downcomer*.

A new control volume model was developed to predict the time-dependent mixed mean temperature at the downcomer exit. The model was assessed against the CREARE ½-scale data and shown to be in good agreement. The control volume model served as the basis for the op-down scaling analysis which provided the dimensionless time scale, t^+, and dimensionless temperature scale, ΔT^+, which characterize the mixing problem.

They are defined as follows:

$$t^+ = \frac{t}{\tau_m} \tag{8.3}$$

$$\Delta T^+ = \frac{(T_m - T_{HPI})}{(T_{L,o} - T_{HPI})} \tag{8.4}$$

and have been used to effectively collapse the existing CREARE 1/2-scale data.

3. *HPSI plume entrainment, Temperature Decay, and Turbulence*

The classic similarity solutions for buoyant jets and forced plumes developed by Roose,[31] have been used as the basis for the HPSI and downcomer plume scaling analyses. The fundamental assumptions in the analysis; Taylor's entrainment assumption, the similarity of velocity and buoyant profiles in the plume and the Gaussian profile assumption permitted integration of governing partial differential equations to yield the plume balance equation in terms of the average properties of the plume. The averaged balance equations were used to obtain the following key dimensionless groups for the HPSI plume:

$$\Pi_{QE} = \left(\frac{Q_E}{Q_{HPI}}\right)_o \tag{8.5}$$

$$Fr_{HPI} = \frac{Q_{HPI}}{a_{HPI}\left[\frac{g\Delta\rho_p D_{HPI}}{\rho_{HPI}}\right]_o} \tag{8.6}$$

$$L^{+} = \left(\frac{z_{inj}}{D_{HPI}} \right) \tag{8.7}$$

It was demonstrated previously that Fr_{HPI} was preserved in APEX-CE by design. Similarly, L^{+} was also preserved by design. It was shown that by preserving these two criteria in APEX-CE, that the plume entrainment:

$$\left(\Pi_{QE}\right)_R = 1 \tag{8.8}$$

and the plume temperature decay:

$$\left(\Delta T^{+}\right)_R = 1 \tag{8.9}$$

were automatically preserved.

It was found that both Fr_{HPI} and the injection Reynold's number, Re, could not be preserved simultaneously. The analysis shows that the APEX-CE injection line flow would be laminar while the Palisades HPSI line flow would be turbulent. The impact of this different is likely to be insignificant relative to the mixing effect in the HPSI line caused by the flow through the HPSI check valve. Separate effects tests and CFD analyses are recommended to provide insight into HPSI line mixing.

4. *Downcomer Planar Plume Entrainment and Velocity.*

The similarity solution approach for planar plumes presented by Chen and Rodi[37,38] provided the basis for this scaling analysis. Taylor's entrainment assumption, the similarity of velocity and buoyancy profiles and the Gaussian profile assumption were implemented to integrate the governing partial differential equations for a planar plume. The resulting balance equations are

$$Fr_{DC} = \frac{Q_{p,o}}{a_{p,o}\left[\frac{g\Delta\rho_p}{\rho_p} D_{CL}\right]^{1/2}} \tag{8.10}$$

expressed in terms of the average properties of the plume. The averaged balance equation were used to obtain Π_{QE} and L^{+} as previously obtained for axisymmetric plumes and Fr_{DC}; defined as:
It was found that the downcomer Froude number could not be preserved in APEX-CE during transient conditions. That is,

$$Fr_{DC} = \frac{1}{2.9} \tag{8.11}$$

Thus separate effects tests were recommended to assess plume spreading and temperature decay. A major consideration is the effect of multiple plume interaction. It is possible that nearby plumes can merge to significantly change the wall cooldown characteristics. This was observed in the IVO test facility[41] and is expected to occur in APEX-CE.

The velocity of the planar plume was scaled using Kotsovinos' equation[42] which was found to be in good agreement with the CREARE 1/2-scale data. Based on this equation, it was found that the plume residence time ratio was preserve. That is:

$$\left(\tau_p\right)_R = \left(\frac{L_{DC}}{u_p}\right)_R \approx 1 \qquad \textbf{(8.12)}$$

5. *Downcomer Wall Heat Transfer.*

The general heat conduction equation was used to obtain the key dimensionless groups for heat transfer from the downcomer wall to the cold plume. A Dittus-Boelter correlation based on a plume Reynold's number was used to predict the convection heat transfer at the boundary. The key dimensionless groups were found to be the Fourier number, the Biot number, and the Nusselt number. The analysis indicates that:

$$\left(F_o\right)_R \approx \frac{1}{2.9} \qquad \textbf{(8.13)}$$

$$\left(Bi\right)_R \approx \frac{1}{38} \qquad \textbf{(8.14)}$$

$$\left(Nu_p\right)_R \approx \frac{1}{35} \qquad \textbf{(8.15)}$$

These results indicate that the downcomer wall temperature gradients cannot be preserved in APEX-CE. The primary reason for this is that the APEX-CE reactor pressure vessel wall is very thin (~0.5 inches / 1.25 cm) compared to Palisades vessel walls (6-8 inches / 15 to 20 cm). The thermal penetration times will be much shorter in the APEX-CE. Although useful in assessing CFD codes, the APEX-CE wall temperature gradients will not be characteristic of Palisades. However, the test program may yield useful heat transfer and plume velocity data.

6. *REMIX Calculations*

The REMIX[43] computer code was used to compare the temperature decay in APEX-CE and Palisades for comparable scaled conditions. The results were plotted in terms of t^+ and ΔT^+ and

found to be in reasonable agreement. Additional effector is needed to assess the wall heat transfer models in REMIX.

8.2.4 RCS Depressurization and Cooldown Scaling Analysis

The RCS depressurization scaling analysis determined that the pressure trends that evolve in APEX-CE for a given SBLOCA scenario would be similar to the pressure trends in Palisades for the same scenario when the results are plotted in dimensionless phase space. That is, plotting pressure histories in terms of P^+ versus t^+. This condition is achieved when:

1. The scenarios are initiated from the same initial conditions in dimensionless phase space (i.e., P^+ at $t^+=0$ is 1)

2. The rate of change of the process is preserved in dimensionless phase space. That is,

$$\left(\frac{dP^+}{dt^+}\right)_R = 1 \qquad \textbf{(8.16)}$$

Satisfying these requirements permits the saturation pressure in APEX-CE to be related to Palisades by:

$$\left(\frac{P}{P_o}\right)_{APEX} = \left(\frac{P}{P_o}\right)_{PAL} \qquad \textbf{(8.17)}$$

All of the key saturation fluid properties and the critical break flow rations were found to be described by a simple power law for the range of conditions in interest to this study. That is,

$$\psi = \psi_o \left(\frac{P}{P_o}\right)^{\xi} \qquad \textbf{(8.18)}$$

This equation has the special property of being"invariant" with respect to a two-parameter transformation in scale. This characteristic of self-similarity allows all of the key fluid properties to scale with dimensionless pressure, P^+. An equation relating saturation temperature in APEX-CE to saturation temperatures in Palisades was also developed.

An examination of the Π group ratios indicates that for saturated vapor breaks (i.e., stuck open PZR PORV) the dimensionless depressurization and cooldown rates will be reasonably simulated in APEX-CE. Some distortion may occur in simulating the hot leg break because conditions at the break will likely be two-phase rather than saturated liquid as assumed in the analysis.

8.2.5 SG Depressurization/RCS Cooldown Scaling Analysis

The steam generator depressurization scaling analysis resulted in scaling criteria for selection of the main steam line break sizes and steam generator initial conditions. Two sets of initial conditions

were examined; a MSLB from hot zero power (~0.5% decay power) and a MSLB from full power conditions (~6.65% decay power could be achieved in APEX-CE). All of the Π groups were found to have values on the order of one. Thus it is expected that the MSLB transients will be reasonably simulated in APEX-CE.

8.3 Assessment of Scaling Analysis Results Relative to the PTS PIRT Tables

This section summarizes APEX-CE's ability to model the important PTS phenomena listed in Tables 2.1 and 2.2. Overall, it is expected that APEX-CE will produce results that are very similar to those expected for the proposed Palisades plant overcooling transients when plotted in terms of dimensionless groups. Tables 8.3 and 8.4 briefly summarize the results. Many of the key phenomena listed in the tables are preserved because of geometric similarity or because they are test control parameters such feedwater flow rate and decay heat.

The limitations of the APEX-CE test facility are identified in the tables. The APEX-CE reactor vessel is thin walled, therefore wall heat conduction will be much different than what would be expected for the Palisades plant. Separate analysis would be needed to assess wall heat conduction in the Palisades plant. In addition, separate effects tests will need to be performed in APEX-CE to cover the range of downcomer Nusselt numbers of interest to Palisades.

The scaling analysis has demonstrated that the primary goals of the PTS study can be accomplished in APEX-CE. That is, APEX-CE will adequately simulate:

- The onset of loop stagnation during SBLOCA and MSLBs
- The onset of thermal stratification in the cold legs,
- Thermal mixing in the cold legs and downcomer.

The steady-state and transient PTS data obtained in APEX-CE can be used to assess the existing thermal hydraulic computer codes and any new CFD codes that might be implemented in an improved PTS thermal hydraulic methodology resulting from NRC.s re-evaluation of the PTS rule (10 CFR 50.61) and its supporting guidance (RG 1.154).

Table 8.3 APEX-CE Scaling Analysis for PTS SBLOCA Phenomena

Rank	PTS Related Phenomena	Comments
1	High Pressure Safety Injection (HPSI) Flow Rate	Key Π groups preserved. $(Fr_{HPI})_R = 1$ and $(Fr_{HPI/CL})_R = 1$
2	Reactor Vessel Wall Heat Conduction	APEX-CE walls are thin. $(Fo)_R = 0.35$; $(Bi)_R = 0.03$
3	Flow Distribution in Downcomer	Preserved. APEX-CE is geometrically similar.
4	HPSI Water Source Temperature	Preserved by test design.
5	Break Flow Rate	Preserved during saturated blowdown until flow becomes unchoked.
6	HPSI Mixing in Cold Leg and Downcomer	Key Π groups preserved. $(Fr_{HPI})_R = 1$ and $(Fr_{HPI/CL})_R = 1$
7	Decay Heat	Preserved by test design.
8	Surface Heat Transfer Coefficient on Reactor Vessel Wall	Downcomer flow is low during transient; $(Nu_p)_R = 0.03$; Separate effects tests will also be performed at higher downcomer flow rates.
9	Loop Flow Upstream of Safety Injection Connection	Natural circulation loop flows preserved by adjusting loop resistance.
10	Loop Temperature Upstream of Safety Injection Connection	Core ΔT is preserved. However, APEX-CE limited to 440 °F.
11	Downcomer to Core Inlet Bypass	Preserved. APEX-CE is geometrically similar
12	Downcomer to Upper Plenum Bypass	Preserved. APEX-CE is geometrically similar
13	Upper Head Heat Transfer Coefficient under Voided Conditions	Stored energy release rate from vessel head is scaled.
14	Liquid/Steam Interface in the Upper Part of the Downcomer	APEX-CE is geometrically similar. Preserving break flow rate will preserve timing of inventory loss and level in downcomer.
15	Feedwater Temperature	Preserved by test design.
16	Feedwater Control	Preserved by test design.
17	Steam Generator Energy Exchange	Preserved by test design.
18	Timing of Manual RCP trips	Preserved by test design.
19	Loop Flow Resistance	Preserved by test design.

Table 8.4 APEX-CE Scaling Assessment for PTS MSLB Phenomena

Rank	PTS Related Phenomena	Report Section
1	Timing of Manual RCP Trips	Preserved by test design.
2	Feedwater Temperature	Preserved by test design.
3	Feedwater Control	Preserved by test design.
4	Steam Generator Energy Exchange	Preserved by test design.
5	Steam Generator Pressure Control	Preserved by test design.
6	Steam Line Break Flow Rate (or Break Size)	Preserved. Critical flow for saturated vapor is well modeled in APEX-CE.
7	Decay Heat	Preserved by test design.
8	High Pressure Safety Injection (HPSI) Flow Rate	Key Π groups preserved. $(Fr_{HPI})_R = 1$ and $(Fr_{HPI/CL})_R = 1$
9	HPSI Water Source Temperature	Preserved by test design.
10	Surface Heat Transfer Coefficient on Reactor Vessel Wall	Downcomer flow is low during transient; $(Nu_p)_R = 0.03$; Separate effects tests will also be performed at higher downcomer flow rates.
11	Loop Flow Resistance	Preserved by test design.
Rank	**PTS Related Phenomena**	**Comments**
12	Reactor Vessel Wall Heat Conduction	APEX-CE walls are thin. $(Fo)_R = 0.35$; $(Bi)_R = 0.03$;
13	Upper Head Heat Transfer Coefficient under Voided Conditions	Stored energy release rate from vessel head is scaled.
14	Stored energy release rate from vessel head is scaled.	Key Π groups preserved. $(Fr_{HPI})_R = 1$ and $(Fr_{HPI/CL})_R = 1$
15	Downcomer Upper Plenum Bypass	Preserved. APEX-CE is geometrically similar
16	Flow Distribution in Downcomer	Preserved. APEX-CE is geometrically similar
17	HPSI Buoyant Backflow Mixing	Key Π group is preserved. $(Fr_{HPI})_R = 1$
18	Fluid Mixing in Downcomer	Key Π groups are preserved. $(Fr_{HPI})_R = 1$ and $(Fr_{HPI/CL})_R = 1$. However, the APEX-CE downcomer is large relative to Palisades on a scaled basis. $(V_{DC})_R = 1/95$. Separate effects tests will also be performed at higher downcomer flow rates.

9.0 References

1. Title 10, Energy, Part 50.6, "Fracture toughness requirements for the protection against pressurized thermal shock events," *Code of Federal Regulations*, Office of Federal Register, National Archives and Records Administration, Available through Superintendent of Documents, U.S. Government Printing Office, Washington, DC 20402, January 1999.

2. U.S. Nuclear Regulatory Commission, "Format and Content of Plant-Specific Pressurized Thermal Shock Safety Analysis Reports for Pressurized Water Reactors," Regulatory Guide 1.154, January 1987.

3. Zuber, N. "Appendix D: A Hierarchical, Two-Tiered Scaling Analysis," *An Integrated Structure and Scaling Methodology for Severe Accident Technical Issue Resolution*, U.S. Nuclear Regulatory Commission, Washington, D.C. 20555, NUREG/CR-5809, November 1991.

4. Palmrose, D., *Demonstration of Pressurized Thermal Shock Thermal-Hydraulic Analysis with Uncertainty*, RELAP5/MOD3 and TRAC-PF1/MOD2 Calculations in Support of Regulatory Guide 1.154 Revisions, prepared by Scientech for the U.S. Nuclear Regulatory Commission, Washington, D.C. 20555, NUREG/CR-5452, March 1999.

5. Roth, P., Palmrose, D., Ghan, L., Fisher, J., Berta, V. And S. Naff, *A Preliminary Study of Pressurized Thermal Shock Thermal-Hydraulic Issues in the Yankee Rowe Nuclear Power Plant*, Idaho National Engineering Laboratory Letter Report, SAN-12-92, July 1992.

6. Reyes, J.N., Groome, J.T., Lafi, A.Y., Franz, S.C., Rusher, C., Strohecker, M. Wachs, D., Colpo, S. And S. Binney, Final Report of NRC AP600 Research Conducted at Oregon State University, U.S. Nuclear Regulatory Commission, NUREG/CR-6641, August 1999.

7. Pratt, Gary E., *Natural Circulation Flow Rate*, Consumers Power, Transmitted by Gary E. Jarka via Electronic Mail Communication, November 22, 1999.

8. Schroeder, M., *Fractals, Chaos, Power Laws*, W.H. Freeman and Company, 1991.

9. Reyes, J.N., *Scaling Single State Variable Catastrophe Functions: An Application to Two-Phase Natural Circulation*, Nuclear Engineering and Design 151, pp. 41-48, 1994.

10. Ishii, M., and I. Kataoka, Similarity and Scaling Criteria for LWRs Under Single-Phase and Two-Phase Natural Circulation, Argonne National Laboratory, ANL-83-32, prepared for the U.S. Nuclear Regulatory Commission, Washington, D.C. 20555, NUREG/CR-3267, March 1983.

11. Kocamustafaogullari, G., and M. Ishii, *Reduced Pressure and Fluid Scaling Laws for Two-Phase Flow Loop*, Argonne National Laboratory, ANL-86-19, prepared for the U.S. Nuclear Regulatory Commission, Washington, D.C. 20555, NUREG/CR-4585, April 1986.

12. Schwartzbeck, R.K. and G. Kocamustafaogullari, "Similarity Requirements for Two-Phase Flow Pattern Transitions," *Nuclear Engineering and Design*, 116 pp 135-147, 1989.

13. Taitel, Y., and A.E. Dukler, "A Model for Predicting Flow Regime Transitions in Horizontal and Near Horizontal Gas-Liquid Flow." *AIChE Journal*, Vol. 22, No.1, pp. 47-54, January 1976.

14. Hochreiter, L.E., FLECHT SEASET Program Final Report, EPRI NP-4112, prepared for the U.S. Nuclear Regulatory Commission, Washington, D.C. 20555, November 1985.

15. McHugh, P.R., and R.D. Hentzen. "Natural Circulation Cooling in U.S. Pressurized Water Reactors," Prepared for the U.S. Nuclear Regulatory Commission by EG&G Idaho, NUREG/CR-5769, 1992.

16. Loomis, Guy G. and Kunishira Soda. "Results of the Semiscale MOD-2A Natural Circulation Experiments," prepared for the U.S. Nuclear Regulatory Commission by EG&G Idaho, NUREG/CR-2335, 1982.

17. Duffey, R.B., and J.P. Sursock, "Natural Circulation Phenomena Relevant to Small Break and Transients," Nuclear Engineering and Design, 102, pp 115-128, 1987.

18. Zuber, N. and J.A. Findlay, "Average Volume Concentration in Two-Phase Flow Systems," ASME, Journal of Heat Transfer, 87, (1965), 453-468.

19. Theofanous, T.G., H.P. Nourbakhsh, P. Gherson, and K. Iyer, "*Decay of Buoyancy Driven Stratified Layers with Applications to Pressurized Thermal Shock (PTS)*," U.S. Nuclear Regulatory Commission, NUREG/CR-3700, May 1984.

20. Theofanous, T.G., K. Iyer, H.P. Nourbakhsh, P. Gherson, "*Buoyancy Effects of Overcooling Transients Calculated for the NRC Pressurized thermal Shock Study*," U.S. Nuclear Regulatory Commission, NUREG/CR-3702, May 1986.

21. Theofanous, T.G., and H. Yan, "*A Unified Interpretation of One-Fifth to Full Scale Thermal Mixing Experiments Related to Pressurized Thermal Shock*," U.S. Nuclear Regulatory Commission, NUREG/CR-5677, April 1991.

22. Levy, S., *An Approximate Prediction of Heat Transfer During Pressurized Thermal Shock*, SLI-8213, prepared for Brookhaven National Laboratory, June 1982.

23. Rothe, P., and G.B. Wallis, @Scaling of Thermally Driven Fluid Mixing and Heat Transfer Associated with Pressurized Thermal Shock of Reactor Vessels," *Proceedings of Joint NRC/ANS Meeting on Basic Thermal Hydraulic Mechanisms in LWR Analysis,* Bethesda, Maryland, September 14, 1982.

24. Fanning, M.W., and P.H. Rothe, *Transient Cooldown in a Model Cold Leg and Downcomer*, Prepared for the Electric Power Research Institute, Interim Report EPRI NP-3118, May 1983.

25. Valenzuela, J.A., and F.X. Dolan, *Thermal and Fluid Mixing in 1/2- Scale Test Facility,* U.S. Nuclear Regulatory Commission, NUREG/CR-3426, September 1985.

26. Harvill, R.C., *Palisades Cycle 15 Principal Plant Parameters,* EAPPD-98-001, Revision 1, Consumers Energy, Palisades Nuclear Power Plant, September 1999.

27. Mishima, K., and M. Ishii, "Theroretical Prediction of Onset of Horizontal Slug Flow," *Journal of Fluids Engineering,* Vol. 102, pp 44-445, December 1980.

28. Kordyban, E.S. and T. Ranov, "Mechanism of Slug Formation in Horizontal Two-Phase Flow," *Journal of Basic Engineering,* Transactions of the ASME, pp. 857-864, December 1970.

29. Gardner, G.C., "Onset of Slugging in Horizontal Ducts," *International Journal of Multiphase Flow,* Vol. 5, pp. 201-209, Pergamon/Elsevier, 1979.

30. Wallis, G.B. and J.E. Dobson, "The Onset of Slugging in Horizontal Stratified Air-Water Flow," *International Journal of Multiphase Flow,* Vol. 1, pp. 173-193, Pergamon/Elsevier, 1973.

31. Rouse, H., Yih, C.-S. and H. W. Humphreys, "Gravitational convection from a boundary source," *Tellus,* Vol. 4, pp. 201-210, 1952.

32. Batchelor, G.K., "Heat convection and buoyancy effects in fluids," *Quarterly Journal of the Royal Meteorological Society*, Vol. 80, pp. 339-358, 1954.

33. Morton, B.R., "Forced plumes, " *Journal of Fluid Mechanics,* Vol. 5, pp. 151-163, 1959.

34. Turner, J.S., Buoyancy Effects in Fluids, Cambridge University Press, Cambridge, 1979.

35. Morton, B.R., Taylor Sir Geoffrey and J.S. Turner, "Turbulent gravitational convection from maintained and instantaneous sources, "*Proceedings of the Royal Society,* A-234, pp.1-23, 1956.

36. Foerthamnn, E. "Turbulent Jet Expansion, " English Translation, A.C.A. TM-789, (Original Paper in German, 1934, Ing. Archiv., 5) 1934. (Reproduced in the *Encyclopedia of Fluid Mechanics, Volume 2, Dynamics of Single-Fluid Flows and Mixing,* N. P. Cheremisinoff, Editor, Gulf Publishing Company, Houston, 1986.)

37. Chen, C.J., and W. Rodi, *Vertical Turbulent Buoyant Jets - A Review of Experimental Data,* HMT, Vol 4, Pergamon Press, New York, 1980.

38. Rodi, W., *Turbulent Buoyant Jets and Plumes,* HMT, Vol. 6, Pergamon Press, New York, 1982.

39. Theofanous, T.G., Angelini, S. and H. Yan, *Universal Treatment of Plumes and Stresses for Pressurized Thermal Shock Evaluations,* U.S. Nuclear Regulatory Commission, NUREG/CR-5854, June 1992.

40. Davis, L.R., Shirazi, M.A. and D.L. Slegel, "*Measurement of Buoyant Jet Entrainment from Single and Multiple Sources, "* Journal of Heat Transfer, Transactions of the ASME, Vol. 100, August 1978.

41. Tuomisto, H., P. Mustonen, "*Thermal Mixing Tests in a Semiannular Downcomer with Interacting Flows from Cold Legs,"* U.S. Nuclear Regulatory Commission, NUREG/IA-0004, October 1986.

42. Kotsovinos, NE., *Plane Turbulent Buoyant Jets,* Ph.D. Thesis, California Institute of Technology, 1975.

43. Iyer, K., Nourbakhsh, H.P. and T.G. Theofanous., "*REMIX: A Computer Program for Temperature Transients Due to High Pressure Injection after Interruption of Natural Circulation,"* Purdue University, U.S. Nuclear Regulatory Commission, NUREG/CR-3071, May 1986.

44. Bluman, G.W., and J.D. Cole, "*Similarity Methods for Differential Equations,"* Springer-Verlag Publishers, New York, 1974.

45. Lay, J.E., "*Statistical Mechanics and Thermodynamics of Matter,"* Harper & Row, Publishers, New York, 1990.

46. Moody, F.J., "*Introduction to Unsteady Thermoflluid Mechanics,"* John Wiley & Sons Publishers, New York, 1990.

47. Henry, R.E., and H.K. Fauske, "*The Two-Phase Critical Flow at Low Qualities, Part 1 and Part 2,"* Nuclear Science and Engineering, Vol. 41, No. 1, pp. 79-98, 1970.

48. Pimentel, D.A., "*Two-Phase Fluid Break Flow Measurements and Scaling in the Advanced Plant Experiment (APEX),"* Master's Thesis, Oregon State University, 1996.

NRC FORM 335
(9-2004)
NRCMD 3.7

U.S. NUCLEAR REGULATORY COMMISSION

BIBLIOGRAPHIC DATA SHEET

(See instructions on the reverse)

1. REPORT NUMBER
(Assigned by NRC, Add Vol., Supp., Rev., and Addendum Numbers, if any.)

NUREG/CR-6731

2. TITLE AND SUBTITLE

Scaling Analysis for the OSU APEX-CE Integral System Test Facility

3. DATE REPORT PUBLISHED

MONTH	YEAR

4. FIN OR GRANT NUMBER

W6699

5. AUTHOR(S)

J. N. Reyes, Jr., D. Bessette and G. Rhee

6. TYPE OF REPORT

Technical

7. PERIOD COVERED *(Inclusive Dates)*

10/2000-11/2001

8. PERFORMING ORGANIZATION - NAME AND ADDRESS *(If NRC, provide Division, Office or Region, U.S. Nuclear Regulatory Commission, and mailing address; if contractor, provide name and mailing address.)*

Department of Nuclear Engineering, Oregon State University, 116 Radiation Cente r, Corvallis,

9. SPONSORING ORGANIZATION - NAME AND ADDRESS *(If NRC, type "Same as above"; if contractor, provide NRC Division, Office or Region, U.S. Nuclear Regulatory Commission, and mailing address.)*

U.S. Nuclear Regulatory Commission, Office of Nuclear Regulatory Research, Division of Systems Analysis and Regulatory Effectiveness, Washington, DC 20555-0001

10. SUPPLEMENTARY NOTES

D. Bessette, Project Manager

11. ABSTRACT *(200 words or less)*

This report describes the results of a two year study performed at Oregon State University to better understand and model thermal hydraulic phenomena pertinent to Pressurized Thermal Shock (PTS) in pre ssurized water reactors (PWRs. The APEX Test Facility at Oregon State University has been modified to simulate a typica l 2x4 loop Combustion Engineering nuclear plant. The new configuration, APEX-CE, has been used to perform a series of separate e ffects and integral systems overcooling tests to investigate primary loop stagnation, cold leg thermal stratification and dow ncomer cooling and heat transfer. RELAP5 calculations have been compared to the test data to assess its ability to predi ct the onset of loop stagnation and system cooldown. STAR-CD, a Computational Fluid Dynamics (CFD) code, and REMIX have be en assessed against the APEX-CE cold leg and downcomer fluid mixing data. Flow visualization studies of HPSI in jection in a transparent cold leg have also been performed. This work is part of the U.S. Nuclear Regulatory Commission's (USNRC) effort to review its existing PTS rule. The results of this new research provide valuable insights into how to revise the e xisting Palisades PTS Phenomena Identification and Ranking Tables and how to improve the thermal hydraulic methodology current ly being used to identify and assess potential PTS scenarios in PWRs.

12. KEY WORDS/DESCRIPTORS *(List words or phrases that will assist researchers in locating the report.)*

thermal hydraulic, APEX, pressurized thermal shock, combustion engineering, sca ling

13. AVAILABILITY STATEMENT

unlimited

14. SECURITY CLASSIFICATION

(This Page)

unclassified

(This Report)

unclassified

15. NUMBER OF PAGES

16. PRICE

PRINTED ON RECYCLED PAPER